A cryptic sulfur cycle driven by iron below the sulfate-methane transition zone

Dissertation zur Erlangung des Doktorgrades der Naturwissenschaften (Dr. Rer.nat)
am Fachbereich 2 (Biologie/Chemie) der Universität Bremen

von
Lars Holmkvist
Bremen 2009

Die vorliegende Arbeit wurde in der Zeit von November 2004 bis December 2009 am Max Planck Institut für Marine Mikrobiologie in Bremen angefertigt.

1. Gutachter: Prof. Dr. Bo Barker Jørgensen
2. Gutachter: Prof. Dr. Jörn Peckmann

Weitere Prüfer:
Prof. Dr. Friedrich widdel
PD Dr. Matthias Zabel
Ph.D student Martin Glas
Master student Hannah Marchant

Tag des Promotionskolloquiums: 16.12.2009

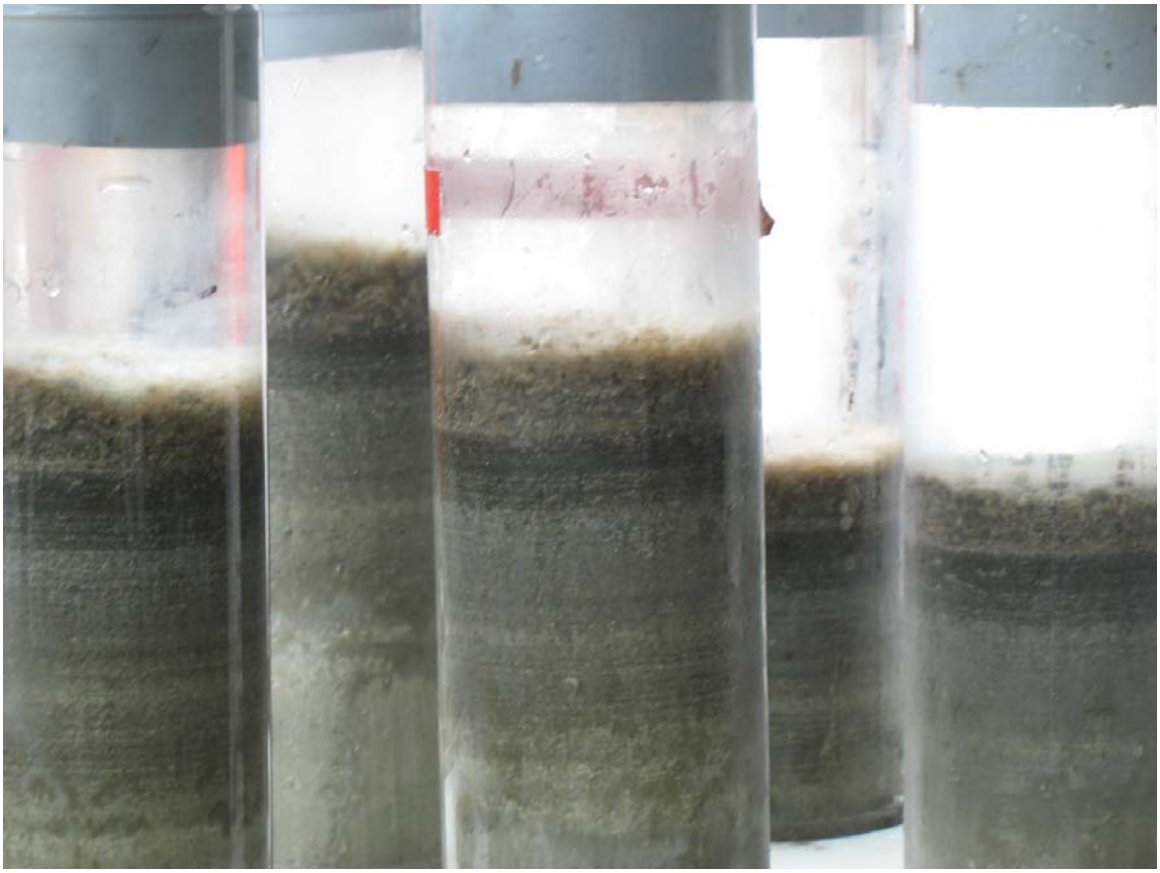

Picture of sediment cores collected during a Black Sea cruise (2007) (Photo: L. Holmkvist)

Table of contents…….….4

Acknowledgements

This Ph.D thesis deals with biogeochemical cycling of carbon, sulfur and iron compounds in marine sub-surface sediments of Aarhus Bay (Denmark), the Baltic Sea and the Black Sea, with focus on the activity and distribution of sulfate-reducing bacteria below the sulfate-methane transition zone. Besides, another project is included that deals with the release of phosphate from large sulfide-oxidizing bacteria, *Thioploca* spp., in order to study the formation of modern hydroxyapatites in an upwelling area off the Bay of Concepción (Chile).

The financial support for this thesis came from the Max Planck Society and the European Union both of which is gratefully acknowledged.

I would first of all like to thank my supervisor Prof. Bo Barker Jørgensen for accepting me as his Ph.D student and for giving me the opportunity to carry out my thesis at the Max Planck Institute in Bremen. I am very grateful to Bo for all the inspiring discussions, for helping me with correcting the manuscripts and for all the support during my time as a Ph.D student. I would also like to thank Bo and his wife, Inga, for their warm welcome to me when I first arrived to Bremen in 2004. I hope that we can continue the scientific discussions and the good friendship. I am also grateful to Dr. Timothy Ferdelman for being my supervisor and for all the help with the calculations of the sulfate reduction rates in the manuscripts. The help from Bo and Tim with all the meetings, the exiting expeditions, and their critic reading of my work together with their enthusiasm, has been a driven force and a great inspiration for me during my time as a Ph.D student.

Martina Meyer, Andrea Schipper, Thomas Max, Kirsten Imhoff, Swantje Lilienthal and Gabriele Klockgether always had time for me with assistance and good advises in the laboratory at the Max Planck Institute and for that I am very grateful. My special thanks go to Martina, Andrea and Thomas for their invaluable help in the laboratories with the analyses of sulfur and iron species.

Thanks to Jochen Nüster for introducing me to the iron geochemistry area and for help with voltametric analysis of iron. I thank Nina Knab and Christian Borowski for good discussions and help with cruise plannings. Thank you very much, Heiko Loebner, for your help with translating the summary section into german.

Without the excellent collaboration and inspiring discussion from Kyriakos Vamvakopoulos, Alexey Kamyshny, Carsten U. Schwermer, Esther T. Arning, Kathrin Küster, Joel E. Kostka, Christoph Vogt, Volker Brüchert, Jörn Peckmann and Matthias Zabel, I would not have been able to get enough information and ideas to complete the manuscripts in their present form.

Thanks to Maren Mortensen for being such a nice roommate during most of my stay in Bremen, and for keeping up the good mood during the long days in the lab. Also thanks to John Mortensen for the relaxing weekends in Bremen together with Maren. These were moments of reloading and happy days that I will never forget.

Also thanks to all the other nice people that I have meet at the MPI, MARUP and Germany in general. You have helped me to make the days go smooth and to make me feel comfortable and welcome in Germany. Thanks to Sergio, Julio, Elsabè, Ulrike, Katharina, Abdul, Julia, Phyllis, Friederike, Susanne, Anja, Nevin, Joanna, Casey and all the other nice people that I forgot to mention. Thanks to the people who joined our "MPI running club" and for all the nice sporty moments in Bürgerpark and the competitions we joined as well as the "Kohl und Pinkel fahrts".

I would also like to thank my former colleagues at DET (Dansk El & Teknik); Tommy, Søren, Eva, Tina, Rasmus, Martin etc. for employing me and enabling me to finish up my thesis while I was on work controling F24 gas stations.

Thanks to my present colleagues at the Danish Technological Institute in Aarhus; Torben, Thomas, Uffe, Ketil and Sasha, for keeping me focused on finishing the thesis and all the good advices.

Finally, I`am deeply grateful to all my Danish friends and to my family, especially my parents, for expressing their interest in my study and for their support and help along the way.
My warmest thoughts go to my dear wife, Agnete, and my lovely little son, Sigurd. Uncountable thanks to you Agnete, for your love, support and patience, and for being there for me at any time. If this work should be dedicated to anyone, it would be you.

Summary

Studies show that sulfate reduction is the quantitatively most important redox pathway in the oxidation of organic carbon within ocean margin sediments with significance for the global carbon cycle. The terminal electron acceptor, sulfate, is transported from the seawater into the sediment via diffusion and the depth distribution generally determines the extent to which sulfate reduction can take place in the sediment.

Below the sulfate zone, it was previously assumed that sulfate reduction did not occur because of the near-zero concentrations of sulfate (<50 μM) and the low content of organic carbon. Nevertheless, recent studies indicate that sulfate-reducing communities may in fact exist and be active also deep below the sulfate-methane transition in sediments on the continental shelves. For example, sulfate-reducing bacteria were found deep below the sulfate-methane transition in sediment from the Black Sea and Aarhus Bay (Denmark), by targeting the metabolic key gene, the dissimilatory (bi)sulfite reductase (dsrA). Further, sulfur isotope signatures of dissolved sulfate in marine pore waters have been used as a valuable indicator for sulfate reduction. Yet, only a few studies have actual tried to measure the *in situ* sulfate reduction rates using the $^{35}SO_4^{2-}$ radiotracer techniques within marine sub-surface sediments. Moreover, despite the geochemical evidence of sulfate reduction in sub-surface sediments, knowledge on which metabolic strategy they have in order to stay active within sub-surface sediments, as well as their role in the cycling of sulfur, iron and carbon still need to be resolved.

This Ph.D thesis deals with biogeochemical cycling of carbon, sulfur and iron compounds in marine sediments on the continental shelves in relation to the activity and distribution of sulfate-reducing bacteria below the sulfate-methane transition. The primary goal of the thesis is first to verify the activity and distribution of active sulfate-reducing sulfate reducers below the sulfate-methane transition and then to relate the sulfate reduction rates with the geochemical zonations of the sediment. After that, it will be discussed how the sulfate reducers might be able to stay active within sub-surface sediments in spite of the extremely limited access to electron donors and acceptors.

In addition to the major study, another minor project is included that aim to investigate the formation of hydroxyapatite in upwelling areas (Chile), from the release of phosphate to the pore water in sediments dominated by large sulfide-oxidizing bacteria, *Thioploca* spp.

The aim of the first report was to study sulfate reduction and sulfur-iron geochemistry in 5-6 m deep gravity cores of Holocene mud collected from the shallow Bay of Aarhus (Denmark). We wanted to understand if sulfate is generated by reoxidation of sulfide throughout the sulfate and methane zones and try to explain the abundance of active sulfate-reducers deep below the main sulfate zone from geochemical processes (i.e. oxidation of sulfide with iron oxides). We did potential sulfate reduction rate experiments, where extra sulfate and organic substrates were added to sediment sub-samples that were incubated in time serie experiments up to 48 hours. This was done in order to stimulate the sulfate-reducers and thus be able to detect the otherwise very low sulfate reduction rates within the sub-surface sediments.

Sulfate was found to penetrate down to the sulfate-methane transition zone where also the concentration of free sulfide peaked. Below the sulfate-methane transition zone, sulfide diffused down to a sulfidization front below which free iron accumulated in the pore water. Sulfate reduction rates measured by $^{35}SO_4^2$-tracer technique in the sulfate-rich sediment layers were high due to the high concentration of reactive organic matter. Within the sulfate-methane transition zone, sulfate reduction was distinctly stimulated by the anaerobic oxidation of methane. In the methane zone below, sulfate remained at "background" concentrations of <0.5 mM down to the sulfidization front and sulfate reduction decreased steeply to rates, which at 300-500 cm were 0.2-1 pmol SO_4^{2-} cm^{-3} d^{-1}, i.e. four to five orders of magnitude lower than rates near the sediment surface. The potential sulfate reduction rates were found to be 10-40-fold higher than the sulfate reduction rates estimated without extra electron donor-and acceptors added to the sediment. This demonstrated that a physiologically intact community of sulfate-reducing bacteria was present deep below the sulfate-methane transition zone.

The "background" sulfate concentration appears to be generated from the reaction of downwards diffusing sulfide with deeply buried Fe(III) species, such as poorly-reactive iron oxides or iron bound in sheet silicates. The turn-over time of sulfate increased from a 3 years at 12 cm depth to 100-1000 years down in the methane zone. Sulfate reduction in the methane zone accounted for only 0.1% of sulfate reduction in the entire sediment column and was apparently limited by the low pore water concentration of sulfate and the low availability of organic substrates. The oxidation of sulfide to sulfate in the sulfidic sediment may involve the formation of elemental sulfur or perhaps thiosulfate and the further disproportionation of a small fraction to sulfate. The net production of sulfate from the reaction of sulfide and Fe(III) to form pyrite requires an additional oxidant. This could be CO_2 which is reduced to methane and subsequently becomes re-oxidized at

the sulfate-methane transition and thereby removes excess reducing power. A cryptic sulfur cycle similar to the one described here probably occurs widespread in marine sediments, in particular along the ocean margins.

The second report describes the sediment and pore water geochemistry of long sediment cores collected in the Arkona Basin of the south-western Baltic Sea. This site contains sediment deposits of both marine and limnic origin as a result of the changing biogeochemical condition since the early history of the Baltic Sea. We observed an unusual sulfate profile deep within the limnic deposits, by which high concentrations of sulfate were present in the pore water. The presence of high sulfate concentrations within the sub-surface sediments, however, made it impossible to investigate sulfate reduction under sulfate limiting conditions. On the other hand, the extreme non-steady-state conditions of this site, has enabled us to investigate sulfate reduction and sulfidization processes across different sediment deposits.

The accumulation of sulfide in the pore water of the uppermost sediment layer and the diffusion of sulfide down into the underlying sediment lead to sulfidization and precipitation of different iron sulfide minerals. Magnetic nodules were isolated in a sulfidization front and these were found to contain iron monosulfide, greigite, pyrite as well as large crystals of elemental sulfur. A large peak in elemental sulfur was additionally found in the sulfidization front which is a sign of sulfur reoxidation processes. Our study indicated, however, that the high sulfate concentrations within the sub-surface sediment layers of the Arkona Basin were not due to oxidation of reduced sulfur species as previously assumed, but rather due to downward diffusion of sulfate during the early Holocene history of the Baltic Sea.

The third report presents data from sediment collected in the western part of the Black Sea at a water depth of 1000 m. The major objective of this study was to verify the presence of active sulfate reduction several meters below the sulfate-methane transition zone. We wanted to come up with possible explanations on how sulfate-reducing bacteria may be able to stay active within the deep limnic sub-surface sediment of the Black Sea where concentrations of sulfate and organic carbon are extremely low. The study combines activity measurements of sulfate reduction with geochemical data on sulfur and iron obtained from pore water and sediment in much the same way as the study from Aarhus Bay. Thus, potential sulfate reduction rate experiments were also performed in this study as a method to verify the presence of active sulfate-reducers below the sulfate-methane transition.

The study demonstrated that sulfate-reducing bacteria were active also several meters below the sulfate-methane transition in Black Sea sediments. The cryptic sulfate reduction below the sulfate-methane transition may be driven by sulfate produced from reoxidation of sulfur compounds in pore water and sediment with oxidized iron minerals.

The fourth report aimed to investigate the association between phosphate release, organic phosphorus mineralization, and dense communities of the filamentous sulfur bacteria, *Thioploca* spp., on the continental shelf off central Chile during the austral summer when high phytoplankton productivity and anoxic bottom water prevailed. We wanted to investigate if the large sulfur bacteria, *Thioploca*, are able to release phosphate to the pore water in concentrations high enough to enable the precipitation of hydroxyapatite.

We found that the pore water concentrations of phosphate reached 100-300 μM peak concentrations within the uppermost 0-5 cm and phosphate was lost to the overlying anoxic water column. Hence, the pore water was super-saturated with respect to hydroxyapatite but the concentration of authigenic apatite in the sediment was only a minor P-component in the sediment and most solid-phase phosphate was bound to iron. As a result, the large phosphate release was not directly related to the presence of *Thioploca* but rather the result of a high deposition and mineralization rate of fresh organic detritus. The freshly deposited phytodetritus stimulated extremely high sulfate reduction rates that supported a large *Thioploca* community of up to 100 g biomass per m^2. Effective bacterial sulfide uptake kept the sulfide concentration low, which enabled the accumulation of free iron, thus demonstrating intensive iron reduction concurrent with sulfate reduction.

Zusammenfassung

Die heutigen Forschungsergebnisse zeigen, dass die Sulfatreduktion aus quantitativer Sicht die wichtigste Redox-Reaktion in der Oxidation von organischen Karbonaten in marinen Sedimenten mit signifikanter Bedeutung für den globalen Kohlenstoffkreislauf ist.
Der terminale Elektronakzeptor Sulfat wird durch Diffusion aus dem Seewasser in die Sedimente transportiert, wobei die Tiefenverteilung des Sulfates den Umfang, in der eine Sufatreduktion stattfinden kann, bestimmt. Es wurde bisher angenommen, dass unterhalb der Sulfatzone keine Sulfatreduktion aufgrund der nahe am Nullpunkt liegenden Konzentration (unter 50 μM) und der geringen Menge an organischen Kohlenstoff möglich ist. Neuere Studien weisen aber daraufhin, dass unterhalb der Sulfate-Methan-Transitionszone Sulfatreduktionsgemeinschaften in den Sedimenten der Kontinentalhänge nicht nur existieren, sondern auch Aktivität aufweisen.
Solche Sulfat reduzierenden Bakterien wurden unterhalb der Sulfat-Methan-Transitionszone in den Sedimenten das Schwarzen Meeres und der Bucht vor Aarhus in Dänemark entdeckt. Das metabolische Schlüsselgen, die dissimilatorische (Bi-) Sulfate-Reduktase (dsrA), diente hierbei für die Sondierung. Des weiteren wurden Schwefelisotopsignaturen von gelösten Sulfaten im marinen Porenwasser als wertvoller Indikator für das Auftreten der Sulfatreduktion genutzt. Bis heute wurde nur bei wenigen Untersuchungen versucht, die *in situ* Rate für die Sulfatreduktion direkt mit der $^{35}SO_4^{2-}$ Radioaktivitätsmethode innerhalb mariner Tiefseesedimente zu messen. Trotz der geochemischen Hinweise auf eine Sulfatreduktion in tieferen Sedimenten muss darüber hinaus die Funktion solcher Organismen in den Stoffkreisläufen von Schwefel, Eisen und Kohlenstoff näher untersucht werden, um ihre Rolle komplett zu entschlüsseln.

Dieser Doktorarbeit setzt biogeochemische Kreisläufe von Kohlenstoff-, Schwefel- und Eisenverbindungen in marinen Sedimenten der Kontinentalhänge in Bezug zu der Aktivität und Verteilung von Sulfat reduzierenden Bakterien unterhalb der Sulfat-Methan-Transitionszone. Das vorrangige Ziel dieser These ist der Nachweis und die Untersuchung der Tiefenverteilung der Aktivität dieser Sulftareduzierer unterhalb der Sulfat-Methan-Transitionszone. Des Weiteren soll die Sulfatreduktionsrate in Relation zu der geochemischen Zonierung der Sedimente gesetzt werden. Im Abschluss werden mögliche Erklärungen, wie Sulfat reduzierende Bakterien in Tiefseesedimenten mit extremer Limitierung der Elektronendonoren und –akzeptoren Aktivität aufweisen könne, diskutiert.

Ergänzend zu der Hauptuntersuchung ist ein weiteres Kleinprojekt integriert mit dem Ziel, die Bildung von Apatiten durch die Freilassung von Phosphaten in das umgebende Porenwasser der Sedimente, der Dominanz der grossen Sulfat oxidierenden Bakterien *Thioploca* spp. zu zuordnen.

Das Ziel des ersten Berichtes war die Untersuchung der Sulfatreduktion und Schwefel-Eisen-Geochemie in 5 bis 6 Meter langen Schwerelotkernen, gefüllt mit Urzeitschlamm aus dem Holozän, die in der Bucht von Aarhus entnommen wurden. Wir möchten verstehen, ob Sulfat bei einer Reoxidation von Sulfiden in der Sulfat- und Methan-Zone entsteht und versuchen das Vorkommen von aktiven Sulfatreduzierern tief unterhalb dieser Zonen mit Ihren geochemischen Prozessen zu erklären. Wir führten potentielle Sulfatreduktio.nraten-Experimente mit Inkubationen von bis zu 48 Stunden durch, bei denen zusätzliches Sulfat und organische Substrate zu den Sedimentunterproben hinzugegeben wurden. Dies wurde in Einklang mit einer Stimulation der Sulfat reduzierenden Bakterien vorgenommen, die folglich über die Sulfatreduktionsrate ermittelt werden kann.

In der Sulfat-Methan-Transitionszone wurde Sulfat vorgefunden, wo ebenfalls hohe Konzentrationen von freien Sulfiden in Spitzenwerten auftraten. Unterhalb dieser Zone diffundieren die Sulfide in eine Sulfidationszone, in der freies Eisen sich im Porenwasser akkumulierte. Die mit ^{35}S-Tracer-Methode gemessenen Sulfatreduktionsraten in dem Sulfat reichen Sedimentschichten ergaben sich infolge von hohen Konzentrationen an reaktiver organischer Materie. Innerhalb der Sulfat-Methan-Transitionszone wurde die Sulfatreduktion vornehmlich durch die anaerobe Methanoxidation stimuliert. In der darunter liegenden Methanzone tritt Sulfat in einer geringen „Hintergrund"-Konzentrationen unter 0,5 mM bis zur Sulfidationszone auf und die Sulfatreduktion fällt auf Raten, von 300 bis 500 cm auf 0.2-1 pmol SO_4^{2-} cm^{-3} d^{-1}, die im Vergleich um das vier- bis fünffache geringer als die Raten der Sedimentoberfläche liegen. Die potentielle Sulfatreduktionsrate fällt mit Werten um das zehn- bis vierzigfache höher aus, als die Sulfatreduktionsraten in Sedimentproben ohne Zugabe von zusätzlichen Elektronendonoren und – akzeptoren erwarten liessen. Dies zeigt, dass eine physiologisch intakte Gemeinschaft von Sulfate reduzierenden Bakterien unterhalb der Sulfate-Methan-Transitionszone präsent ist. Die „Hintergrund"-Konzentration an Sulfat erscheint als Reaktion von Sulfiden mit tiefliegenden Eisen-(III)-Verbindungen, wie schwachreaktive Eisenoxide oder Eisenverbindungen aus Schalensilikaten, welches aufwärts diffundierte.

Die Umsatzzeit des Sulfats steigt von den 3 Jahre alten Sedimenten aus 12 cm Tiefe zu den 100 bis 1000 Jahre alten in der Methanzone. Die Sulfatreduktion der Methanzone erreicht nur 0,1 % der

Sulfatreduktion in der gesamten Sedimentsäule, was offenbar auf die Limitierung durch geringe Porenwasserkonzentrationen an Sulfat und auf die geringer Verfügbarkeit organischer Substrate zurückzuführen ist. Die Oxidation von Sulfiden zu Sulfaten in sulfidischen Sedimenten scheint die Formation von elementarem Schwefel und die weitere Disproportionierung eines geringen Anteiles zu Sulfat zur Folge zu haben.
Die Nettoproduktion von Sulfaten aus der Reaktion von Sulfiden und Eisen(III) zur Formierung von Pyrit benötigt einen weiteren Oxidant. Dies könnte Kohlendioxid sein, welchse durch Methan reduziert und anschließend in der Sulfat-Methan-Transitionszone reoxidiert wird. Dabei wird überschüssige Reduktionsenergie abgebaut. Ein verborgener Schwefelkreislauf, vergleichbar mit dem beschriebenen, kommt weit verteilt in marinen Sedimenten vor, besonders an den Ozeanrändern.

Der zweite Bericht beschreibt die Sediment- und Porenwasser-Geochemie von langen Sedimentkernen, die im Arkona-Becken der südwestlichen Ostsee gesammelt wurden.
Dieses Gebiet besitzt in der Sedimentstruktur sowohl marine als auch limnische Ablagerungen als Ergebnis des Wandels der biogeochemischen Konditionen seit der frühen Geschichte der Ostsee. Wir beobachteten ein unübliches Sulfatprofil tief in den limnischen Ablagerungen, in denen Sulfatkonzentrationen im Porenwasser auftraten. Das Vorkommen hoher Konzentrationen an Sulfat innerhalb tieferer Sedimentschichten, wie immer sie auch zustanden gekommen ist, macht die Untersuchung der Sulfatreduktion unter Sulfat limitierenden Bedingungen unmöglich. Andererseits hatten uns die extrem unbeständigen Bedingungen in diesem Gebiet die Untersuchung die Sulfatreduktion und der Sulfidationsprozesse entlang verschiedener Sedimentzusammensetzungen ermöglicht. Die Akkumulation von Sulfiden im Porenwasser oberen Sedimentschichten und die Diffusion hinunter in das darunter liegende Sediment führt zu einer Sulfidation und Ablagerung von unterschiedlichen Eisensulfidmineralien. Magnetische Knollen wurden in einer Sulfidationszone isoliert, die Eisenmonosulfid, Greigit, Pyrit sowie grosse Kristalle elementaren Schwefels beinhalteten.

Ein Höchstanteil an elementaren Schwefel wurde des Weiteren in der Sulfidationszone gefunden, was ein Anzeichen für Reoxidationsprozesse von Schwefel ist.
Unsere Untersuchungen legen nahe, dass die hohe Sulfatkonzentration in den tieferen Sedimentschichten des Arkona-Becken nicht, wie zuvor vermutet, auf eine Oxidation von reduzierten Schwefelverbindungen zurück zu führen ist, sondern vielmehr auf eine Abwärtsdiffusion des Sulfates während der früheren Geschichte der Ostsee im Holozän.

Der dritte Bericht präsentiert Daten, die aus Sedimenten des westlichen Teils des Schwarzen Meeres gesammelt wurden, die aus einer Wassertiefe von 1000 Metern entnommen wurden.

Die Zielvorgabe dieser Untersuchung war die Überprüfung einer aktiven Sulfatreduktion einige Meter unterhalb der Sulfat-Methan-Zone. Wir wollten möglichen Erläuterungen, wie Sulfat reduzierende Bakterien innerhalb von tiefen, limnischen Tiefseesedimenten des Schwarzen Meeres eine Aktivität bei geringen Konzentrationen von Sulfat und organischen Kohlenstoff aufweisen, anführen. Die Studie kombiniert Aktivitätsmessungen der Sulfatreduktion mit geochemischen Daten von Schwefel und Eisen aus dem Porenwasser und dem Sediment in der gleichen Weise wie in den Untersuchungen der Aarhus Bucht. Dabei wurden ebenso Experimente zur Ermittlung potentieller Sulfatreduktionsraten verwendet, als auch Methoden zur Prüfung der Anwesenheit aktiver Sulfatreduzierer unterhalb der Sulfat-Methan-Transitionszone. Die Untersuchung demonstriert, dass Sulfat reduzierende Bakterien mehrere Meter unterhalb dieser Zone aktiv sind. Die verborgene Sulfatreduktion scheint von Sulfaten, welche durch die Reoxidation schwefelhaltiger Verbindungen im Porenwasser und oxidierten Eisenmineralien aus dem Sediment stammen, angetrieben zu werden.

Der vierte Teil dieser Arbeit hatte sich zum Ziel gesetzt, die Assoziation zwischen Phophatfreisetzungen, organischer Phosphormineralisation und die dichtlebende Gemeinschaften der filamentösen Schwefelbakterien *Thioploca* spp. am Kontinentalhang vor dem zentralen Chile während der südlichen Sommer zu untersuchen. In dieser Zeit herrschen Bedingungen von hoher Produktion von Phytoplankton und anoxischem Oberflächenwasser. Unsere Untersuchungen sollten zeigen, dass grosse Schwefelbakterien der Gattung *Thioploca* in der Lage sind, Phosphat in solch hoher Konzentration in das Porenwasser zu entlassen, wodurch die Bildung von Hydroxyapatiten ermöglich wird.Wir konnten Porenwasserkonzentrationen an Phosphat mit Spitzenwerten von 100 bis 300 µM innerhalb der ersten fünf Zentimeter feststellen, was mit einen Mangel an Phosphat in der sich darüber befindenden anoxischen Wassersäule einhergeht.

Infolgedessen war das Porenwasser ausreichend gesättigt hinsichtlich einer möglichen Hydroxyapatit-Bildung, aber die Konzentration von autigenen Apatiten stellte nur eine geringe Menge des Phosphoranteiles im Sediment dar. Der grösste Anteil des Phosphates war mit Eisen verbunden. Als Resultat ergibt sich daraus, dass die grosse Ansammlung an Phosphat nicht direkt mit dem Vorkommen an *Thioploca* in Verbindung gebracht werden kann. Es stellt sich vielmehr als

Ergebnis einer hohen Deposition und Mineralisationsrate von frischen organischem Detritus als Ursache dar. Das frisch abgelagerte Phytodetritus stimuliert extrem hohe Sulfatreduktionsraten, welche wiederum eine grosse *Thioploca*-Gemeinschaft mit einer Biomasse von 100 g per m^2 ermöglicht. Eine effektive, bakterielle Sulfidaufnahme hält die Konzentration an Sulfid niedrig, welche die Akkumulation von freien Eisen ermöglicht. Dies demonstriert die intensive Eisenreduktion mit der gleichzeitigen Sulfatreduktion.

Introduction

Chapter 1

Major project:

A cryptic sulfur cycle driven by iron in the methane zone of marine sediments

Continental shelves and sulfate reduction

1.1.1 Continental shelves

The continental shelves are covered by terrigenous sediments, i.e.sediment derived from the erosion of rocks. The terrigenous sediment is transported to the oceans via river input, where it undergoes biological and geochemical processes and finally gets deposited on the ocean floor (Futterer 2000). About 60-70% of the sediment on the world's shelves is relict sediment deposited during the last ice age (~18000 years BP), when the sea level was ca.100-120 m lower than today (Fairbanks 1989; Pinet 1996). Sediment deposits on the shelves therefore embody the history of the continents and the oceans. The study of marine shelves is therfore the key in understanding the Earth's history and the past environmental conditions.

1.1.2 Early diagenesis and Sulfate reduction

Continental margin sediments play a major role for the global cycling of carbon. High concentrations of organic matter are deposited on shelf sediments from the water column as a result of high primary production within these areas (Field et al. 1998). The mineralization of the deposited organic matter is overall known to occur via aerobic respiration within the upper oxic sediment zone, followed by a sequence of anaerobic oxidation-reduction reactions (redox reactions) deeper in the sediment (Champ et al. 1979; Reeburgh 1983), as also illustrated in Fig. 1 and 2. However, before the different redox processes can proceed, it is important that fermentation processes first degrades the organic matter to smaller organic molecules (e.g. acetate, formate or H_2) that can serve as electron donors for the bacteria and Archaea in the sediment (Postma & Jakobsen 1996). Electron acceptors of marine pore waters (e.g. oxygen, nitrate and sulfate) often exhibit characteristic zonations with depth which may indicate the existence of the different redox reactions (Fig. 1 and 2).

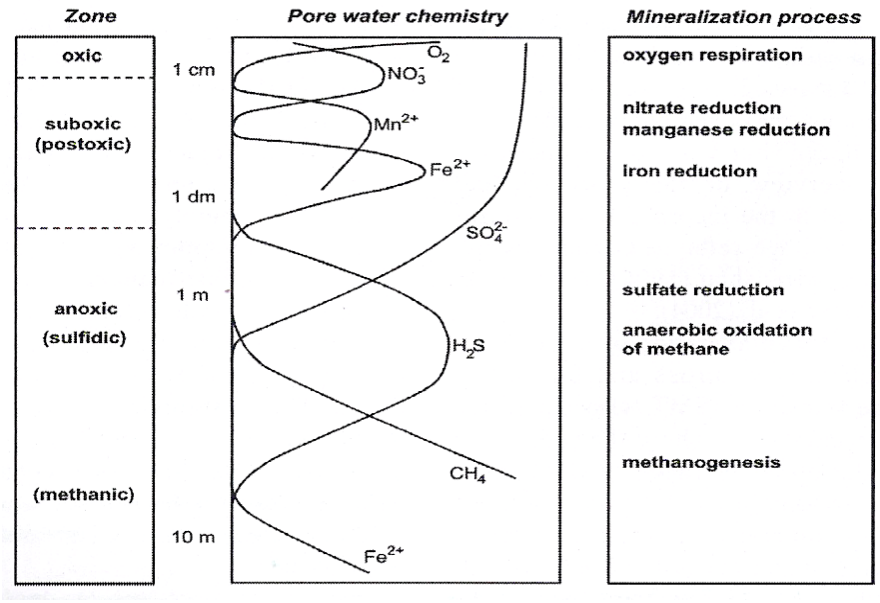

Fig. 1. Schematic representation of the biogeochemical zonation in marine sediments (after Froelich et al. (1979) and Berner (1981).

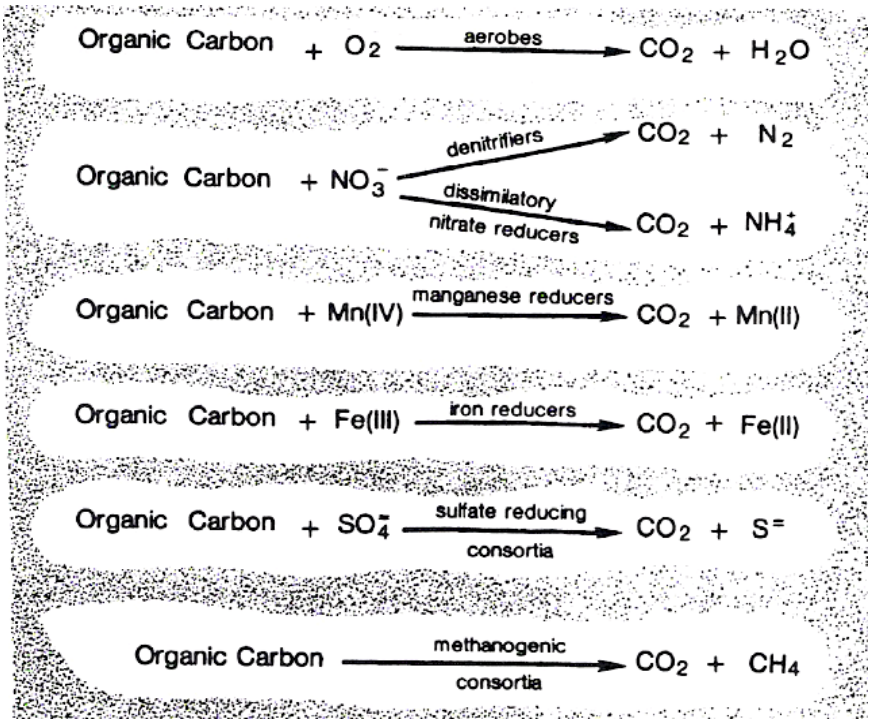

Fig. 2. Important aerobic and anaerobic mineralization processes of marine sediments. The energy yield of the reactions decreases with depth in the sediment, from aerobic oxidation of carbon close to the surface to anaerobic mineralization processes deeper in the sediment (modified after Lovley (1991).

The concentration of oxygen close to the sediment surface of continental margin sediments is often depleted due to the high deposition of organic matter. As a result, the concentrations of nitrate and iron oxides near the sediment surface are in many cases kept low (Aller 1994; Thamdrup & Canfield 1996; Kostka *et al.* 1999), and the reduction of nitrate and/or iron(oxides) is in many cases only of minor importance for the overall oxidation of carbon within the surface sediments of continental shelves. Instead, the quantitatively most important redox reactions of shelf sediments are presumably anaerobic redox pathways. For instance, studies demonstrate that sulfate reduction is the quantitatively most important redox pathway in the oxidation of organic carbon within ocean margin sediments, since it has been estimated to account for up to 25-50% of the total mineralization of organic matter (Jørgensen 1982; Reeburgh 1983; Canfield et al. 1993). Besides, more than 90% of the oceanic sulfate reduction occurs within continental shelf sediments (Jørgensen 1982) and quantification of this process by radiotracer techniques has also proved it to be an overall major pathway of carbon mineralization in marine sediments with significance for the global carbon cycle (Smith & Klug 1981; Henrichs *et al.* 1987). The sulfate reduction reaction can be written according to the overall reaction by Coleman and Raiswell (1995):

$$2CH_2O + SO_4^{2-} \rightarrow 2HCO_3^- + H_2S \qquad \text{(Eq.1)}$$

A common feature of many continental margin sediments is that bottom water sulfate penetrates several meters down into the sediment (Borowski et al. 1997). The terminal electron acceptor, sulfate, is transported from the seawater and into the sediment via diffusion and the influx of sulfate is considered to determine the extent to which sulfate reduction can take place, typically within the upper few meters of the sediment. This zone is often referred to as the sulfate zone.

1.1.3 Anaerobic oxidation of methane and sulfate reduction

The high concentrations of methane that are often observed below the sulfate zone are to a large extend the result of microbial produced methane from methanogenesis (Zehnder & Brock 1979; Claypool & Kvenvolden 1983; Heyer *et al.* 1990; Thiessen *et al.* 2006) (Fig. 1 and 2). The sediment zone below the depth where sulfate is exhausted is thus referred to as the methane zone, because the pore water concentrations of methane are high (Fig. 1). Studies from Aarhus Bay (Denmark) (Thomsen et al. 2001), the Baltic Sea (Thiessen *et al.* 2006; Laier & Jensen 2007) and

the Black Sea (Jørgensen et al. 2004), have all lfound that the methane zone is situated a few meters below the sediment surface. However, only a minor fraction of the upward diffusing methane probably escapes the sediment surface, because the methane is efficiently consumed within the sediment as first recognized by Martens and Berner (1974). The anaerobic oxidation of methane (AOM) process has now been recognized as a significant pathway of methane oxidation in marine sediments. AOM occurs mainly within a relatively narrow zone, the sulfate-methane transition zone (SMTZ), where the pore water concentrations of sulfate and methane are consumed. The AOM process is therefore most probable linked to sulfate reduction according to the following reaction proposed by Barnes and Goldberg (1976):

$$CH_4 + SO_4^{2-} \rightarrow HCO_3^- + HS^- + H_2O \qquad \text{(Eq.2)}$$

A number of geochemical and microbiological studies have tried to clarify the exact stoiechiometry of the AOM process as well as the microorganisms involved. Yet, the AOM process is up till now (2009) still poorly understood. Nonetheless, it is clear that sulfate reduction is greatly enhanced within the SMTZ and that AOM is coupled to sulfate reduction. This has been verified from several microbiological studies which show that sulfate-reducing bacteria (SRB) belonging to the *Desulfosarcina-Desulfococcus* branch of the Deltaproteobacteria, are closely associated with methanotrophic Archaea (Boetius et al. 2000; Orphan et al. 2001; Knittel et al. 2005). Further, pore water depth profiles of sulfate and sulfide from a number of marine and brackish biogeochemical studies also show that sulfate reduction is stimulated within the AOM zone. For example, in Fig. 3 it is shown that methane is depleted when it diffuses upwards into the AOM zone at a depth of acout 200 cm. Typically, methane does not accumulate until after sulfate is nearly exhausted. The sharp decline in sulfate together with the peak in sulfide of the AOM zone is also indicative of high rates of sulfate reduction. This was confirmed from $^{35}SO_4^{2-}$ radiotracer experiments in a study by Iversen and Jørgensen (1985), where sulfate reduction rates (SRR) were observed to peak within the AOM zone in sediment from the Kattegat/Skagerrak off the coast of Denmark (Fig. 4).

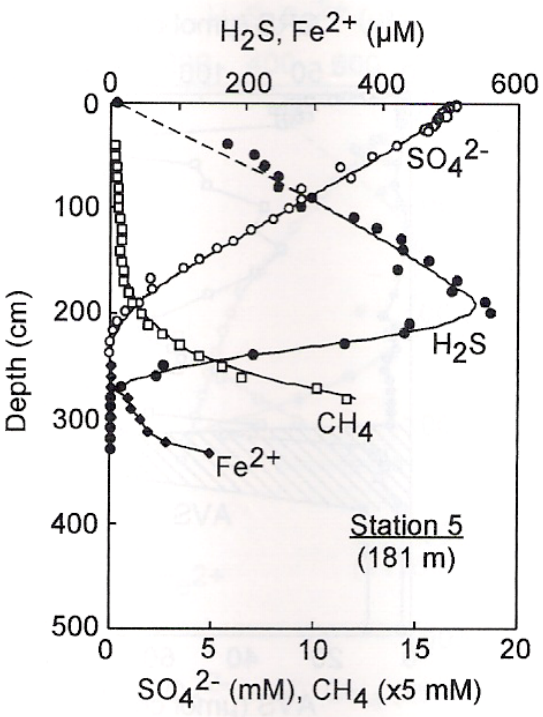

Fig. 3. Pore water depth profiles of sulfate, sulfide, methane and dissolved iron from Black Sea sediments (Jørgensen *et al.* 2004). The AOM zone is located at a depth of ca. 200 cm.

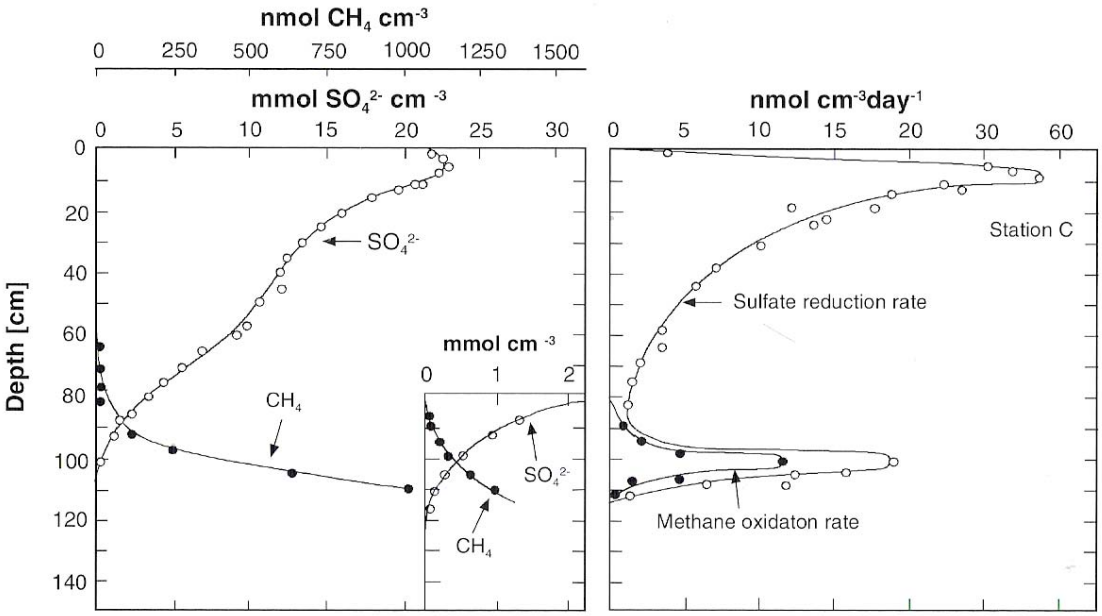

Fig. 4. SRR, methane oxidation and pore water concentrations of methane and sulfate in sediment from the Kattegat/Skagerrak off the coast of Denmark (Iversen & Jørgensen 1985).

Biogeochemistry of sulfur and iron

1.2.1 The sulfur cycle: an overview

In aquatic sediments, compounds of sulfur undergo bacterial redox transformations known as the microbial sulfur cycle. The mineralization of deposited organic matter on the shelves is to a large extent controlled by microbiological and also geochemical processes of sulfur transformations in the sediment. The marine sediments are the main sink for seawater sulfate, the dominant sulfur coumpound in seawater. The largest sink for oceanic sulfur has been argued to be the burial of sulfide minerals whereas organic sulfur compound makes up only a minor fraction (Vairavamurthy et al. 1995). The sulfur cycle is not only the reduction of sulfate to sulfide followed by reoxidation of sulfide to sulfate, but may include a combination of intermediate cycles of shunts and interactions with other element cycles (Jørgensen 1990; Thamdrup et al. 1993; Finster et al. 1998), where the oxidation states of the involved sulfur compounds occur in the range of -2 (in H_2S) to +6 (in SO_4^{2-}). Overall, the sulfide produced from sulfate reduction can be reoxidized to a variety of different sulfur intermediates such as zero-valent sulfur species (i.e. elemental sulfur, polysulfides or polythionates), thiosulfate and/or sulfite (Cline & Richards 1969; Pyzik & Sommer 1981; Dos Santos Afonso & Stumm 1992). The sulfur intermediates may then be further transformed by respiratory bacterial reduction to sulfide, bacterial or chemical oxidation, chemical precipitation (e.g. with iron minerals in pore water or sediment) or from bacterial disproportionation processes.

1.2.2 Sulfidization and pyritization

Sulfide production from sulfate reduction often leads to a pronounced overprinting and sulfidization of the sediment that is initially supplied to the seafloor. For instance, previous studies of sub-surface sediments from the Black Sea and the Baltic Sea show that sulfidization occurs from sulfide produced from AOM and/or mineralization processes of organic matter (Boettcher & Lepland 2000; Neretin *et al.* 2004). This is because accumulation of sulfide in the pore water and the subsequent diffusion downwards into the underlying sediment layers causes the precipitation of iron sulfide minerals, when sulfide reacts with different iron species in pore water and/or sediment. Sulfidization processes are, therefore, possible controlled by the diffusive flux of sulfide from above and the content of reactive iron in the underlying sediment layers as also suggested in a study by Neretin et al. (2004) from Black Sea sediments. The sediment depth where

probably the largest part of the downward diffusing sulfide reacts with iron species is regularly referred to as the diagenetic front or sulfidization front. This zone is often recognized as a distinct black band, as a result of the accumulation of iron monosulfides and the magnetic mineral greigite. The formation pathway of iron sulfides (e.g. iron monosulfides, greigite and pyrite) in sulfidization processes have generally been described in several earlier studies (Berner 1970; Pyzik & Sommer 1981; Berner 1984). Only a few studies have, however, in detail examined the biogeochemistry of pore water and sediment close to or within a sulfidization front. Nevertheless, the general assumption is that several complex oxidation processes of sulfur species occur along with pyritization processes (the formation of pyrite).

The general formation of iron-sulfide minerals (e.g. greigite and pyrite) in anoxic marine sediments have been studied thoroughly and is considered to follow a well-defined chemical formation sequence: non-crystalline iron-sulfides (FeS) $\rightarrow$ mackinawite (FeS) $\rightarrow$ greigite (ferricmagnetic iron sulfide, Fe_3S_4) $\rightarrow$ pyrite (FeS_2) (Berner 1967; Berner 1970; Sweeney & Kaplan 1973; Berner 1984). The formation of FeS in the first step is known to occur when sulfide produced from sulfate reduction reacts with dissolved iron or with reactive iron minerals in the sediment. The conversion of the metastable FeS fraction (the AVS fraction) into pyrite, however, is still largely unresolved and has been the subject of a number of studies because sedimentary pyrite represents the most important sink for seawater sulfate. Several transformation reactions of pyrite formation have been proposed. Overall, in order to convert FeS to FeS_2, an electron acceptor is required to oxidize the sulfide within the FeS moiety and the Fe/S ratio has to decrease from ca. 1:1 to 1:2 either via the addition of sulfur or from the loss of iron (Schoonen 2004). From this perspective, three possible reaction pathways in FeS_2 formation with FeS are proposed (Zopfi et al. 2004): (1) conversion of FeS via the addition of sulfur with the incorporated sulfur species acting as electron acceptors (2) conversion of FeS via the addition of sulfur with a non-sulfur compound acting as electron acceptor and (3) conversion of FeS via iron loss combined with an electron acceptor. Formation of FeS_2 according to the first reaction pathway is thought to take place when FeS reacts with elemental sulfur (S^0) or with other sulfur reactants such as for example polysulfide and colloidal sulfur species (Berner 1970; Luther III *et al.* 1991):

$$FeS + S^0, S_n^{2-} \rightarrow FeS_2 \qquad \text{(Eq.3)}$$

The second conversion mechanism (Eq.4) proposes that FeS reacts with sulfide (H_2S or HS^-) in the pore water (Rickard & Luther III 1997):

$$FeS + H_2S \rightarrow FeS_2 \qquad \text{(Eq.4)}$$

This pathway has received much attention because sulfide is often observed to be the most abundant sulfur source available in marine sediments. Besides, the electron acceptors needed in this reaction are supposed to be phases of reactive ferric iron or manganese oxides and these minerals are often found in natural systems (Aller & Rude 1988). Previous studies also suggest that the formation of FeS_2 is usually favoured under high concentrations of dissolved sulfide and reactive iron-oxide specimen in the sediment (Berner 1984; Raiswell & Berner 1985; Canfield & Berner 1987).
The third pathway (not shown) is the least investigated. However, a few studies suggest that the iron loss reaction occasionally is the most dominant process responsible for the change in the Fe/S ratio (Zopfi *et al.* 2004).

Previous studies have proposed that inorganic polysulfides plays an important role in the formation of FeS_2 or metal-polysulfide complexes in natural aquatic systems (Rickard 1975; Howarth 1979; Luther 1991; Chadwell *et al.* 1999; Luther III *et al.* 2003). Polysulfide concentrations are found to range from 60 to 100 μM in a study from The Great Marsh (Delaware, Sussex County, USA) (Boulegue *et al.* 1982; Ferdelman 1994). Besides, a study from the Great Sippewissett salt marsh (Massachusetts, USA), showed that polysulfide concentrations in marine pore waters reached 10 μM (Luther III *et al.* 1985).

The preservation of Fe_3S_4 in marine sediments is supposed to occur when the conversion of FeS to FeS_2 is incomplete. This is because Fe_3S_4 is an intermediate step in the reaction pathway of FeS_2. Hence, the preservation of Fe_3S_4 should in theory be possible under very different circumstances depending on the accessibility of different reactants or oxidants in the formation pathway of FeS_2. Previous studies have, for instance, shown that Fe_3S_4 preservation is favoured if the sediment content of reactive iron is high and/or if the content of organic matter is low (Kao *et al.* 2004). In such cases, sulfide production and accessibility is kept low as a result of lowered sulfate reduction (due to low carbon content) and because reactive iron and /or dissolved iron efficiently removes the sulfide from the pore water that is produced. This finding is also supported by Roberts and Weaver (2005), who showed that Fe_3S_4 is often associated with different

authigenetic and detrital mineral phases such as nodular and framboidal FeS_2, detrital sheet silicate grains, authigenic clays (smectite and illite), siderite and gypsum.

The non-steady-state processes that occur during the transition from one depositional situation to another, or at the interface between two sediment types, typically comprise the development of geochemical reaction fronts. These fronts can either be fixed at particular sediment horizons for a prolonged period of time or move downwards or upwards within the sediment column. Paleomagnetic and environmental magnetic studies also suggests that Fe_3S_4 is the mineral responsible for the elevated magnetic signals often found among different sediment types (Snowball & Thompson 1990; Roberts & Turner 1993; Reynolds *et al.* 1994; Oda & Torii 2004). For example, Strechie et al. (2002) studied the magnetic properties in sediment collected from the Black Sea. They found a major change in the magnetic mineral assemblages together with generally higher magnetic signals at the lacustrine to marine transition zone.

1.2.3 Iron compounds and iron reduction

The first and third most abundant transition metals in the Earth's crust is iron and manganese (Wedepohl 1995). These metals appear in a number of biogeochemical processes in marine sediments. Common oxidation states of iron and manganese in marine sediments (under circum neutral pH and anoxic conditions) are, for instance, ferrous iron (Fe^{2+}) and manganese (Mn^{2+}) which are dissolved in the pore water, whereas solid phase iron and manganese can be present as ferric iron (Fe^{3+}) and manganese oxides (MnO_2).

The occurrence of manganese and iron reduction in continental margin sediments has been demonstrated from pore water profiles of Fe^{2+} or Mn^{2+} (Ehrlich 1987; Aller 1990; Jahnke 1990). Fig. 3, for instance, shows an increase in the pore water concentrations of Fe^{2+} below the depth where sulfide is no longer present in the pore water, which is indicative of iron reduction. Microbial reduction of ferric iron is one of the most important processes that take place in aquatic sediments (Lovley 1991). Several studies have also shown that Fe-reducers are capable of coupling the reduction of crystalline Fe minerals, including oxides goethite (Roden & Zachara 1996) and magnetite (Kostka & Nealson 1995), and the silicate, smectite (Kostka et al. 1996), to energy generation. Molecular studies have indicated that microorganisms in the *Geobacteracea* family are the predominant Fe(III)-reducing microorganisms in a variety of sedimentary environments in which Fe(III) reduction is an important terminal electron acceptor process (Rooney-Varga et al. 1999; Stein et al. 2001).

Iron can in general be found in a variety of minerals such as iron sulfides, carbonates ($FeCO_3$), iron oxides or within lattice of phyllosilicates, a part of the clay fraction. The clay fraction, which consist of particles less than 2 μm in diameter are abundant and ubiquitous in soils and sediments. For example, clay minerals are the main constituents of most marine sediment and make up nearly 50% of the entire terrigeneous sediment. Clay minerals are found mostly in limnic or brackish sub-surface sediment layers. For instance, glacial varved clays were deposited in the Mecklenburg and Hanö bays as well as in the Arkona and Bornholm basins of the Baltic Sea (Kögler & Larsen 1979). The clay mineral assemblages of recent sediments in the Baltic Sea (deposited ~5500 years BP) are rather homogeneous and variations results mainly from the erosion of different glacial source deposits, with illite, smectite and kaolinite being the dominat clay minerals (Sohlenius *et al.* 1996; Gingele & Leipe 1997). Most of the oxidized iron by weight in natural sediments is associated with phyllosilicates (clay minerals) (Thamdrup 2000) and studies have shown that a significant fraction of the iron present in the lattice of phyllosilicates is redox sensitive and can undergo many redox cycles without moving or mobilizing (König et al. 1997).

1.2.4 Reactive iron towards sulfide

Reactive iron is defined as the fraction of iron that readily reacts chemically with sulfide (Berner 1970; Canfield & Berner 1987; Canfield 1989).A recent study by Poulton and Canfield (2005) reported a new extraction scheme for the separation of seven different pools of iron in marine sediments:

(1) Carbonate associated iron, including siderite and ankerite
(2) Easily reducible oxides, including ferrihydrite and lepidocrocite
(3) Reducible oxides, including goethite, hematite and akaganéite
(4) Magnetite
(5) Poorly reactive sheet silicate iron
(6) Pyrite iron
(7) Unreactive silicate iron

The reactive pools of iron (fraction 2, 3 and 5) will be discussed in the following section, since these fractions are most relevant for the reoxidation reactions of sulfide and thus for the present study. In spite of the past years interest in the development and description of iron oxide

extraction techniques, no simple methods has yet been developed that is able to precisely determine the pools and reactivity's for each of the most common iron and manganese oxides. Yet, in spite of these difficulties several chemical extraction procedures are being used which roughly makes it possibly to discriminate between the most common categories of reactive iron pools. Chemical extractions have been performed in several earlier studies to estimate the solid-phase reactive Fe(III) minerals of marine sediments (Canfield 1989; Leslie et al. 1990; Oenema 1990).Reactive iron is widely determined by reductive dissolution with dithionite, because dithionite has been demonstrated to extract a large portion of the amorphous and crystalline iron oxides (easily reducible oxides) as well as a fraction of the reactive iron silicates (Canfield 1989; Kostka & Luther 1994; Kostka & Luther 1995). The fraction of iron oxides that react with sulfide most rapidly is the easily reducible oxides (fraction 2). This fraction is extracted with 1 M HCl at room temperature (Kostka & Luther 1994). The poorly-reactive silicate iron fraction, defined as the difference between iron extracted by dithionite at room temperature and that extracted by boiling concentrated HCl (Berner 1970), is however only applied in a few studies, although the silicate bound ferrous and ferric iron is quantitatively important in marine sediments (Haese 2000). A study by Raiswell et al. (1994) tried to compare three dissolution techniques (dithionite, cold 1 M HCl and boiling 12 M HCl) for their capacity to extract iron from a variety of iron minerals, and iron-bearing sediments, as a function of different extraction times and different grain size. It was shown that all the iron oxides were quantitatively extracted by the dithionite and boiling HCl methods, but not with the cold HCl method. Besides, both HCl techniques extracted more iron from silicates than with the dithionite method.

The reaction of iron and/or manganese oxides with sulfide is among others determined by the mineralogy, crystallography and the surface property of the iron and/or manganese oxides. A number of studies have tried to determine the degree of reactivity among different iron oxide minerals towards sulfide, in order to understand the rate of pyrite formation or sulfide oxidation processes (Berner 1984; Raiswell & Berner 1985; Canfield *et al.* 1992; Raiswell *et al.* 1994; Poulton *et al.* 2004). Although the estimated reactivity's of some iron oxides (e.g. magnetite) toward sulfide may vary among different investigators, there is a general agreement that iron oxides with a lower degree of crystal order react within minutes to hours (e.g. iron (oxyhydr)oxides, ferrihydrite) whereas more ordered minerals (e.g. goethite, hematite and magnetite) reacts with sulfide on time scales of days to years (Fig. 5). The fraction of iron in sheet silicates that are often associated with clay minerals is referred to as poorly reactive iron (Fig.5), since this iron reacts with

sulfide on time scales in the order of thousand of years. However, only a few studies have overall investigated the reactivity of poorly reacting iron oxides in marine sediments.

Iron Mineral / fraction	Rate constant $\lambda[yr^{-1}]$	Half life $t_{1/2}$
Ferrihydrite [(1)]	2,200	2.8 hours
Lepidocrocite [(1)]	> 85	< 3 days
Goethite [(1)]	22	11.5 days
Hematite [(1)]	12	31 days
Magnetite [(1)]	$6.6 \cdot 10^{-3}$	105 years
Sheet silikates [(1)]	$1.0 \cdot 10^{-5}$	10,000 years
poorly-reactive Silikate fraction [(2)]	$0.29 \cdot 10^{-3}$	$2.4 \cdot 10^{6}$ years

Fig. 5. Reactivity of iron minerals towards sulfide according to [(1)] Canfield et al. (1992) and [(2)] and Raiswell and Canfield (1996). The poorly-reactive silicate fraction" was determined as: ($Fe_{HCl, boiling}$-$Fe_{Dithionite}$)/Fe_{total}

The presence of reactive iron oxides in marine sediments is argued to explain the removal of sulfide from the pore water as also discussed above. For example, studies show that iron oxides such as ferrihydrite and lepidocrocite are abundant in marine sediments (Canfield 1989; Canfield & Raiswell 1991), and their presence may explain why sulfide does not accumulate in the surface zone of sediments, even with high sulfate reduction (Canfield & Raiswell 1991; Canfield *et al.* 1992). The depth where sulfide accumulates in continental margins sediments is thus closely related to the depth of iron oxide/oxyhydroxide exhaustion (Canfield & Raiswell 1991). However, rates of sulfide formation often exceeds the burial of iron in marine sediments, and iron limitation may thus be common particularly around the continental margins (Canfield & Raiswell 1991). As a

result, sulfide often accumulates in the pore water (e.g. in the Black Sea), because of iron oxide/oxyhydroxide exhaustion and the large decrease in iron mineral reactivity towards sulfide between hematite and the next most reactive iron phase such as magnetite or sheet silicates (Fig. 5). Sheet silicates are particularly poorly reactive towards sulfide compared to rates of sulfide production and sulfide would thus accumulate and not be retained. Diagenetic models based on pore water concentrations of sulfate, sulfide and solid phase iron contents in sediments from the Peru margin suggest that the poorly-reactive iron fraction is only sulfidized on a million year time scale (Raiswell & Canfield 1996).

1.2.5 Pathways of sulfide oxidation

Oxidation of sulfide is known to occur within the oxic zone of marine sediments by oxygen. For instance, 90 % of the sulfide produced by sulfate reduction in coastal sediments is typically reoxidized (Jørgensen 1982) and gross sulfate reduction may in some instances be underestimated by a factor of up to 5 in the oxidized zone of the sediment (Moeslund et al. 1994; Fossing 1995). However, there are several indicators that sulfide is oxidized completely to sulfate also in the absence of oxygen (or nitrate) in marine and limnic sediments. On the basis of studies of the depth distributions of inorganic sulfur transformations in sediments, it has been concluded that sulfide oxidation can take place also within the anoxic zone of marine sediments (Howarth 1984; Jørgensen 1988), even under strong reducing conditions (Jørgensen 1988; Fossing & Jørgensen 1990). For example, only 4 to 32 % of the sulfide produced from sulfate reduction within the upper 2 m of the sediment, in the area between the Baltic Sea and the North Sea, was permanently buried as FeS_2 while the rest was reoxidized (Jørgensen et al. 1990). Reoxidation of sulfide, chemically or biologically, has generally been observed to result in the production of a number of other sulfur intermediates such as zerovalent sulfur (elemental sulfur, polysulfides or polythionates), thiosulfate ($S_2O_3^{2-}$) and sulfite (SO_3^{2-}) (Cline & Richards 1969; Pyzik & Sommer 1981) as also described above. However, many of these sulfide oxidation processes are still not completely understood.

Anoxic reoxidation of sulfide has been experimentally demonstrated from both marine and freshwater localities, by adding $^{35}SO_4^{2-}$ tracer to anoxic nitrate-free sediments (Fossing & Jørgensen 1990; Jørgensen 1990; Jørgensen & Bak 1991; Elsgaard & Jørgensen 1992). Still however, the electron acceptors in the reducing sediment layers have not been quantitatively identified, but probably include oxidized manganese and iron minerals (Aller *et al.* 1986; Aller & Rude 1988; Jørgensen 1988; King 1990). Fig. 6 shows a generalized picture of possible reoxidation

processes of sulfide in marine sediment. In this figure, sulfide production can occur either from the degradation of organic matter, methane oxidation, or from sulfur disproportionation of elemental sulfur. The produced sulfide is then reoxidized by means of iron oxides which result in the formation of elemental sulfur and ferrous iron that can out-precipitate sulfide and/or result in the formation of pyrite. If oxygen is available, pyrite can be reoxidized back to sulfate, and manganese (Mn^{2+}) is oxidized to manganese oxides (MnO_2) (Fig. 6).

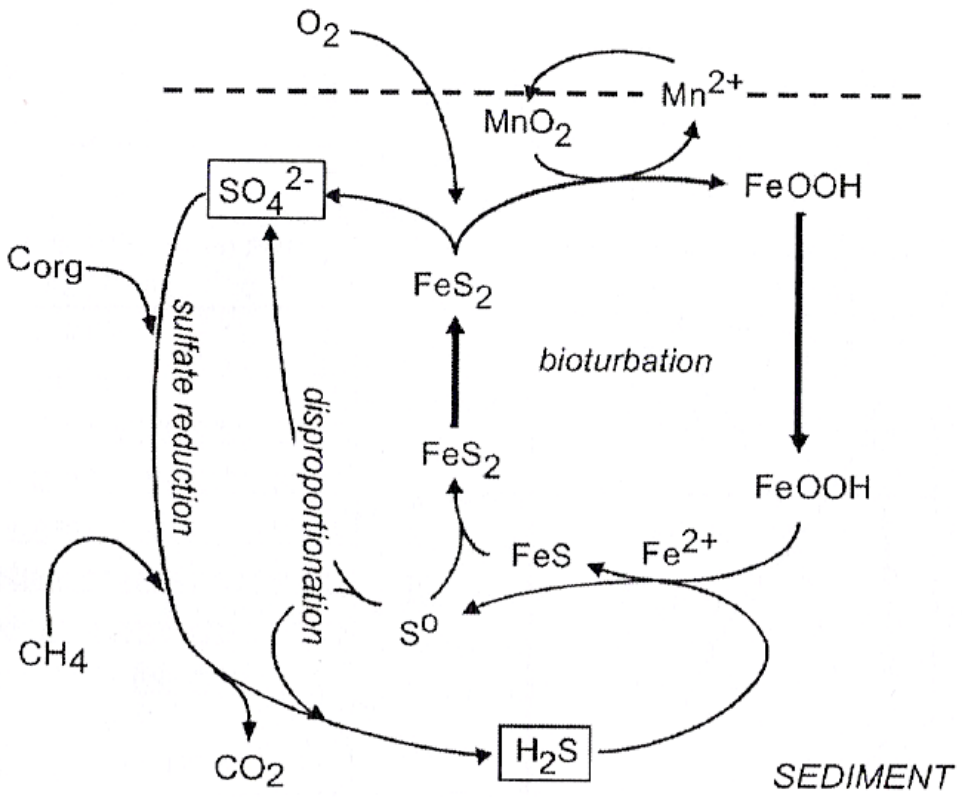

Fig 6. A generalized picture of the sulfur cycle (from Jørgensen and Nelson (2004)

However, recent studies on sulfide reoxidation processes imply that Fig. 6 is too general to explain all of the sulfide reoxidation processes that occur within sub-surface sediments, where molecular oxygen is absent. For example, a number of studies demonstrate the existence of disproportionation processes within sub-surface sediments that may play a significant role in the cycling of sulfur in aquatic systems (Canfield et al. 1998). A study by Thamdrup and Finster (1993), for instance, showed that marine enrichment cultures in sediment collected from Aarhus Bay (Denmark) were able to biologically transform elemental sulfur into sulfide and sulfate when

elemental sulfur and iron oxides were added to the medium. Disproportionation takes place in the presence of iron oxides, because the metals maintain sulfide concentrations low enough for elemental disproportionation to be exergonic (Thamdrup *et al.* 1993). The observed production of sulfide and sulfate was explained from microbial disproportionation of elemental sulfur according to the following reaction by Thamdrup et al. (1993):

$$4\ S^0 + 4H_2O \rightarrow 3H_2S + SO_4^{2-} + 2H^+ \qquad \text{(Eq.5)}$$

Disproportionation of intermediate oxidation products of sulfide is additionally recognized as an important process in the reoxidation of sulfide to sulfate (Thamdrup *et al.* 1993; Canfield & Thamdrup 1994; Habicht & Canfield 2001). Bacteria conducting thiosulfate and sulfite disproportionation were first described in a study by Bak and Pfennig (1987). In fact, thiosulfate has been found to be one of the most important product of sulfide oxidation in sediments, so its further transformations are therefore key reactions in the sulfur cycle (Jørgensen 1990; Jørgensen 1990). The disproportionation of thiosulfate may produce isotopic fractionations contributing to the depletion of sedimentary sulfides in ^{34}S as proposed by Jørgensen (1990). Further, cycles of fractionation accompanying the bacterial disproportionation of elemental sulfur, followed by sulfide oxidation, has overall been suggested to generate large ^{34}S depletions of many marine sulfides (Canfield & Thamdrup 1994).
The reoxidation of sulfide by means of iron and manganese oxides, respectively, has been shown in several studies according to the following reactions:

$$H_2S + 4H^+ + 2FeOOH \rightarrow S^0 + 2Fe^{2+} + 4H_2O \text{ (Sørensen 1982)} \qquad \text{(Eq.6)}$$

$$H_2S + 2H^+ + MnO_2 \rightarrow Mn^{2+} + S^0 + 2H_2O \text{ (Burdige \& Nealson 1986)} \qquad \text{(Eq.7)}$$

The addition of Mn(IV) to anoxic sulfide-containing sediments has been demonstrated to result in the production of sulfate, which thereby suggest that Mn(IV) is able to reoxidize sulfide (Aller & Rude 1988; King 1990). However, this was not the case when Fe(III) was added to sulfide-containing sediment (Aller & Rude 1988; King 1990; Elsgaard & Jørgensen 1992). Evidence for Fe(III) and Mn(IV) reduction by sulfide in marine sediments is that although sulfate reduction continuously produces sulfide in the suboxic zone, the concentrations are kept low (<1μM) (Sørensen & Jørgensen 1987; Canfield 1989; Bak & Pfennig 1991).

The reoxidization of sulfde with iron and/or manganese oxides, may thus explain the accumulation of elemental sulfur in marine sediments since significant amounts of elemental sulfur are found within sub-oxic zones of both marine and freshwater sediments (Smith & Klug 1981; Troelsen & Joergensen 1982; Thode-Andersen & Jørgensen 1989). In situ, however, elemental sulfur is likely rapidly cycled (e.g. via disproportionation) and is for this reason normally found in rather low concentrations (1 to 20 μmol cm^{-3}) (Thode-Andersen & Jørgensen 1989).

The reoxidation of iron sulfide has been demonstrated in chemical experiments, where FeS_2 and FeS are oxidized by MnO_2 but not with NO_3^- or amorphous Fe(III) oxide (Schippers & Jørgensen 2001). Further, Aller and Rude (1988) described the complete oxidation of solid phase acid volatile sulfide (AVS) to sulfate by manganese oxide in marine sediment according to the overall reaction:

$$FeS + 4MnO_2 + 8H^+ \rightarrow Fe^{2+} + SO_4^{2-} + 4Mn^{2+} + 4H_2O \quad \text{(Eq.8)}$$

The oxidation of FeS_2 in a MnO_2 rich marine sediment was also shown in a study by Schippers and Jørgensen (2001) using $^{55}FeS_2$ as an isotopically labelled tracer. The reaction products of FeS_2 oxidation in this study indicated that FeS_2 was oxidized via the "thiosulfate-mechanism"and FeS via the "polysulfide-mechanism" according to the overall reaction proposed by Schippers and Sand (1999):

$$FeS_2 + 7.5MnO2 + 11H^+ \rightarrow Fe(OH)_3 + 2SO_4^{2-} + 7.5Mn^{2+} + 4H_2O \quad \text{(Eq.9)}$$

$$FeS + 1.5MnO_2 + 3H^+ \rightarrow Fe(OH)_3 + S^0 + 1.5Mn^{2+} \quad \text{(Eq.10)}$$

Studies also shows that FeS and FeS_2 oxidation with Fe(III) and Mn(IV) may lead to the production of elemental sulfur (Moses *et al.* 1987; Aller & Rude 1988; Schippers & Jørgensen 2001). The oxidation of FeS_2 is demonstrated to be a complex chemical process that involves a Fe(II)/Fe(III)-shuttle in the pore fluid between the mineral surfaces of FeS_2 and manganese oxides (Schippers & Jørgensen 2001).

Sulfate reduction and sulfate reducers in sub-surface sediments

1.3.1 Microbial activity in sub-surface sediments

The microbial degradation of organic matter deposited upon the shelf sediments occurs over time scales ranging from hours to millions of year. This is because some organic compounds are more easily degraded by the microbial communities than others. Thus, organic compounds that are more difficult to degrade tend to accumulate in the sediment over time and the microbial activity with depth is for this reason often much reduced. Little is known about the microbiology of underlying sediments, although around 70% of the Earth's surface is marine, which can be more than a kilometre deep. However, despite the geochemical evidence of microbial life in deeper sediments, their significance has not yet been fully established (Sinclair & Ghiorse 1989). Presumably, the microbial life within the deep biosphere must have a profound effect on deep-sediment diagenetic processes, and their presence considerably extends the biosphere (Parkes et al. 1994).

So far, studies have revealed that sub-surface habitats contain a great variety of microbial life within deep and old sediments (Parkes *et al.* 1994; Pedersen 2000; Coolen *et al.* 2002; D´Hondt *et al.* 2004). In general, the estimated depth distributions of bacterial activity within sub-surface sediments suggest that the bacterial populations are located in relation to geochemical changes in the sediment (Parkes *et al.* 1994). However, conditions become more extreme for life in the sub-surface sediment layer as a consequence of less efficient electron acceptors, nutrient limitation, limited porosity/permability and increasing pressure. Numerous microscopic acridine orange direct counts (AODC) conducted on sediment cores several hundreds meters below the sediment surface, reveals that the number of bacteria within sub-surface sediments are surprisingly high (Parkes *et al.* 1994; Parkes *et al.* 2000). In fact, Whitman et al. (1998) suggest that the sub-seafloor may harbour over half of all prokaryotic cells on Earth. However, since the AODC technique cannot discriminate between dead and alive cells (Kepner & Pratt 1994), the goal of some molecular studies have been to estimate the number of active cells within sub-surface sediments. Some of these studies have, for example, used molecular techniques such as fluorescence in situ hybridization (CARD-FISH) (Schippers et al. 2005; Teske 2005), 16S eRNA gene clone libaries (Sørensen 2004) and quantitative real-time PCR (Q-PCR) (Schippers *et al.* 2005; Schippers & Neretin 2006) and demonstrated that also active cells may be present within the sub-surface sediments.

1.3.2 Sulfate reduction in sub-surface sediments

Studies show that where sulfate is abundant i.e. within the sulfate zone the rate of microbial sulfate reduction is controlled primarily by the temperature and the availability of degradable organic matter (Westrich & Berner 1988). However, the concentrations of sulfate and organic carbon often both decrease with depth and reaches almost near-zero values below the sulfate zone. Thus, the aim of a few recent studies has been to search for active SRB below the sulfate zone. Although sulfate-reducing bacteria in marine sediments do not belong to the most abundant group of bacteria even in those with high rates of sulfate reduction (Llobet-Brossa *et al.* 2002), changes in the sulfate-reducing community are likely to appear if the appropriate detection method is chosen.

Sulfur isotope signatures of dissolved sulfate in marine pore water have been used as a valuable indicator for the occurrence of microbial sulfate reduction and previous studies have thus be able to confirm the presence of sulfate reduction also deep below the sulfate zone (Jørgensen 1979; Boettcher et al. 2000; Boettcher et al. 2004). In addition, an investigation from the tidal flat of the island of Spiekeroog (Germany) showed that sulfate reduction occurred 2 m below the sediment surface with low rates in the range of 0.01–0.3 μmol cm^{-3} d^{-1} (Wilms et al. 2006). From Aarhus Bay (Denmark) sediment, Thomsen et al. (2001) demonstrated the presence of active sulfate-reducing - and methanogenic communities in a 6 m long sediment core deep below the SMTZ. Studies from Black Sea sediments have also shown the occurrence of active sulfate-reducing communities deep below the SMTZ, by targeting their metabolic key gene, the dissimilatory (bi)sulfite reductase (dsrA) (Leloup et al. 2007). They showed that the SRB were predominant in the sulfate zone, but occurred also in the methane zone within limnic deposits.

The specific *per* cell respiration rate of the SRB has been determined by comparing the viable cell counts with measured SRR. This was done in a study by Sahm and co-workers (1999), who investigated the structure of sulfate-reducing bacteria using slot-blot hybridization of rRNA, in relation to the sulfate reduction rates along a vertical profile of a coastal marine sediment within the upper sediment layers of Aarhus Bay (Denmark). The estimated cellular SRR determined from this study were between 0.01 and 0.09 fmol SO_4^{2-} $cell^{-1}$ day^{-1}. The estimated rates were below the rates obtained for pure cultures (0.2-50 fmol SO_4^{2-} $cell^{-1}$ day^{-1}) growing exponentially at near optimal temperature with surplus of substrates.

Recent studies indicate that sulfate-reducers have a more versatile metabolism than previously thought and different metabolic strategies may help them to sustain life within sub-surface sediments (Habicht et al. 2005). For instance, if sulfate is scarce, the sulfate reducing bacteria may use sulfite, thiosulfate, or elemental sulfur either as alternative electron acceptors or for disproportionation of sulfur compounds in their anaerobic energy metabolism (Bak & Cypionka 1987; Bak & Pfennig 1987; Lovley & Phillips 1994). Besides, some sulfate reducing bacteria may be able to ferment (Widdel & Hansen 1992), reduce poorly crystalline Fe(III) oxides (Coleman et al. 1993) or perhaps live in a consortium with methanogenic archaea as within the AOM zone. The existence of different terminal accepting redox reactions in separate zones is, at least for Fe(III) and sulfate reduction, perhaps less strict as pointed out above and studies suggest that the sulfate and iron reducers compete for available substrates in sub-surface sediments (Kao et al. 2004). Further, thermodynamic calculations of conditions for equilibrium between Fe(III) and sulfate reduction indicate that, depending on the stability of the iron oxide, simultaneous reduction of Fe(III) and sulfate is thermodynamically possible under a wide range of sedimentary conditions and sulfate reduction may even occur before Fe(III) reduction (Postma & Jakobsen 1996). Sediments rich in Fe^{2+} have proven to reduce sulfate as well, as indicated by radiotracer sulfate reduction measurements (Canfield 1989; Jacobsen & Postma 1994).

The availability of sulfate within sub-surface sediment supposedly depends on the downward influx of sulfate from above and sulfate producing processes. As described above, reoxidation of different sulfur species (e.g. sulfide and elemental sulfur) may lead to the release of sulfate and the sulfate limited communities of sulfate-reducers within the sub-surface sediment therefore probably depends on these processes as also suggested in Leloup et al. (2007). A few studies have suggested the ferrous iron (Fe^{2+}) can be oxidized chemically and biologically to ferric iron (Nealson 1983; Mandernack & Tebo 1993). The interaction of manganese oxides with ferrous iron is probably an important mechanism for ferric iron formation according to the following reaction by Myers and Nealson (1988):

$$2Fe^{2+} + MnO_2 + 4H_2O \rightarrow Mn^{2+} + 2Fe(OH)_3 + 2H^+ \qquad \text{(Eq.11)}$$

However, since there is no oxidation of reduced sulfur forms by Fe(III) to generate sulfate (Lovley & Phillips 1987; Aller & Rude 1988; King 1990), disproportionation may play an important role in the reoxidation of sulfur intermediated to sulfate, as described above.

Aim of the thesis and sampling sites

1.4.1 Aim of the thesis

The main focus of the present Ph.D work is biogeochemical cycling of different sulfur and iron spices below the SMTZ in marine sediments of the continental shelves. In particular, the aim of the study is to verify and investigate the presence of active SRB below the SMTZ and try to understand and explain how these microorganisms are distributed relative to the chemical zonation of the sediment, and thereby be able to investigate how they are able to stay active in sediment zones where sulfate reaches near-zero concentrations.

Thus, the goal has been to obtain geochemical pore water and sediment data of different sulfur and iron compounds as well as precise estimates of low SRR. This was important, since we wanted to carry out a detailed comparison of the geochemical data with the SRR in order to investigate if SRB are dependent on or stimulated by sediment processes that releases sulfate to the pore water, i.e. chemical reoxidation of sulfur species by means of iron oxides.

Geochemical analysis and SRR experiments were performed on long gravity cores and Rumohr Lot cores collected at St. “M1” within Aarhus Bay, at St. “9” in the Black Sea and at St. “A6” in the Arkona Basin of the Baltic Sea. These sites were chosen because earlier studies shows the existence of a SMTZ and/or the presence of interesting sediment transitions zones which suits our biogeochemical study of sulfate reduction within sub-surface sediments.
The expectedly low rates of sulfate reduction below the SMTZ were measured as potential SRR. The potential sulfate reduction rate measurements, which is a relatively new developed technique, was performed by adding extra sulfate and substrates to the sediment in anoxic glass syringes before the addition of 35-sulfate tracer. The idea behind potential sulfate reduction rate measurements was to try and tune up the in situ metabolic rate of the sulfat-reducing communities thus be able to detect the low rates. Further, the measurements of sulfate at low pore water concentrations (<0.5mM) and the analysis of different iron minerals was of great importance to the project.

1.4.2 The Bay of Aarhus

Aarhus Bay is an open Bay on the east coast of Jutland (Denmark) with a water depth of 10-20 m. Most of the Aarhus Bay deposits consist of Holocene mud which are partly modified by glacial deformations and covered by tills related to the Weichselian ice age (Houmark-Nielsen 1987; Pedersen & Petersen 1997). Deglaciation of the region started about 18 cal. ka BP, when the glacier margin followed the west coast of Sweden (Houmark-Nielsen 2003). The fading isostatic effect and the ongoing eustatic sea level rise resulted in a relative rise in the sea level and thus a rise in the sea level in the region of Aarhus Bay where the Littorina Sea transgression flooded the northern entrance to the Great Belt about 9.5 cal. ka BP (Jensen et al. 2004) with an initial brackish estuarine phase. In Aarhus Bay, marine transgressive sand and basin mud represent the Littorina Sea sediments, deposited until present time (Jensen & Bennike 2009).

The central basin of Aarhus Bay is a flat area dominated by mud whereas incised channels with mixed sediments characterise the north-western part just outside the city Aarhus and the south-eastern entrances to the bay, south of Helgenæs (Jensen & Bennike 2009). A study by Jensen and Bennike (2009) demonstrated that Aarhus Bay consist of 6 different sediment layers: the early Holocene freshwater/peat unit (lake sediment), Marine unit 1 (the initial Littorina Trangression deposits, 8.7-8.0 cal. ka BP), Marine unit 2 (clay-mud, 7.1-6.1 cal. ka BP) and Marine unit 3 (varies from stiff clay-mud to soft sandy-mud, 3-0.6 cal. ka BP).

Shallow methane-gas depth-contour was carried out in a study by Jensen and Bennike (2009) in order to establish the general Late Weichselian and Holocene stratigraphy and to map the gas related acoustic blanking. They showed that the shallow gas accumulations are related to the Holocene organic deposits, mainly the marine mud and sandy mud. The accumulation of methane in Aarhus Bay occurs a few meters below the sediment surface as a consequence of AOM, in which depth sulfate reduction is stimulated. In general, sulfate reduction within Aarhus Bay plays an important role of total carbon mineralization with estimated percentages up to 44% as calculated per m^2 of the seafloor (Fossing et al. 1992).

1.4.3 The Baltic Sea

The Baltic Sea is at present time the largest brackish water body on the Earth surface. It is divided into three main basins, and one of these, the Arkona Basin, is located in the Western part of the Baltic Sea (Sohlenius *et al.* 1996). Gravity cores for the present study were collected within the Arkona Basin of the Baltic Sea in order to study sulfur oxidation processes across the

different sediment deposits and be able to explain the high accumulation of sulfate in the pore water deep below the sediment surface that was discovered in a study by Thiessen et al. (2006).

The sediment stratigraphy of this area has been shown to contain deposits of both limnic and brackish/marine origin (Neumann 1981; Björck 1995; Moros *et al.* 2002; Thiessen *et al.* 2006). The different sediment deposits are considered to reflect fluctuations in salinity and water-level changes within the Baltic Sea since the last deglaciation for about 13 -14 ky BP (Björck 1995; Andrèn *et al.* 2000; Moros *et al.* 2002). The salinities has in general decreased in the surface waters since the start of the present marine stage at 7.7 ky BP, from about 13‰ during the early stage to the present day value of 8‰ (Bloomquist 1977). Consequently, due to the fluctuation in salinity since the start of the marine stage it is likely that the biogeochemical processes across the different sediment deposits of the Baltic Sea are subject to non-steady-state conditions. For example, variations in the diffusion pattern of sulfate from the bottom water into the sediment are likely to have affected the rates of sulfate reduction in different ways as well as the degree of sulfidization within the sediment.

1.4.4 The Black Sea

The Black Sea is the largest anoxic basin in the world. Major characteristics of this environment are the partly anoxic and sulfidic water column (Neretin et al. 2006). Consequently, there is neither oxygen nor nitrate present within the sediment and sulfate thus constitutes the main electron acceptor. Hence, mineralization of organic matter occurs mainly via sulfate reduction within the upper 2-4 m of the sediment, below which depth methanogenesis occurs (Jørgensen *et al.* 2004). Presumably, the sulfur cycle plays overall an important role in the sediment biogeochemistry in Black Sea sediments, because sulfate can penetrate a few meters down through the different sediment layers of both brackish and limnic origin (Jørgensen *et al.* 2004).

We sampled two very long (~10 m) gravity cores in the Paleo-Dniepr area of the western Black Sea in order to perform geochemical analysis of sulfur and iron compounds as well as SRR and PSRR measurements and be able to relate the depth distribution of active sulfate-reducers to the chemical zonation. Earlier studies by Neretin et al. (2004), Jørgensen et al. (2004), Leloup et al. (2007) and Knab et al. (2008) have all investigated the biogeochemistry of the western Black Sea, which thus enabled us to compare the obtained result to similar studies.

Chapter 2

Minor project:
Phosphorous release and biogeochemistry of large sulfur bacteria

2.1 Hydroxyapatite formation and large sulfur bacteria

The formation of hydroxyapatite, i.e. precipitation of francolite $[Ca, Na, Mg]_{10}[PO_4]_{6-x}[CO_3]_xF_y[F, OH]_2$), is a major sink in the global phosphorous budget of marine sediments (Ruttenberg 1992). Since phosphorous is an essential nutrient for algal growth in the ocean, it is important to understand how hydroxyapatite is formed. However, although hydroxyapatite on the ocean floor has been well studied, the concentrating mechanisms leading to supersaturation and preciitaion have not yet been identified.

Modern formation of hydroxyapatite occurs mainly along ocean margins with strong upwelling such as on the continental shelf off Namibia or off Chile and Peru as well as the Arabian Sea (Föllmi 1996; Schenau *et al.* 2000). Interestingly, these areas are also the habitats for population of large, nitratestoring sulfur bacteria, *Beggiatoa* and *Thioploca* spp. (Schulz & Jørgensen 2001). Consequently, a functional connection between these sulfur bacteria and the formation of hydroxyapatite could exist, especially because abundant microfossils resembling large filamentous sulfur bacteria have been found embedded in deposits containing hydroxyapatite of the Monterey formation (Williams & Reimers 1983). Recently, Schulz and Schulz (2005) discovered that large sulfur bacteria (*Thiomargarita*)store polyphosphate in high concentrations within their cells. Thus, these bacteria could potentially produce steep phosphate peaks in anoxic sediments leading to the rapid precipitation of hydroxyapatite.

2.2 Aim of the study

The basis for the "*Thioploca* project" was the study by Schulz and Schulz (2005) that motivated us to combine microbiological studies of *Thioploca* spp. present off the coast of Chile with geochemical studies to better understand the recent and past influence of *Thiomargarita* and other large sulfur bacteria on the modern formation of hydroxyapatite.

Publications

Chapter 3

A cryptic sulfur cycle driven by iron in the methane zone of marine sediment (Aarhus Bay, Denmark)

Lars Holmkvist[a, b]*, Timothy G. Ferdelman[a] and Bo Barker Jørgensen[a,c]

[a]Department of Biogeochemisty, Max-Planck Institute for Marine Microbiology, Celsiusstr. 1, 28359 Bremen, Germany

[b]Chemistry and Water Technology, Danish Technological Institute, Kongsvang Allé 29, 8000 Aarhus C, Denmark

[c]Center for Geomicrobiology, Department of Biological Sciences, University of Aarhus, Ny Munkegade, Bld. 1535, 8000 Aarhus C, Denmark

Keywords: Sulfate reduction; potential sulfate reduction rates; sulfur-iron geochemistry; sulfide reoxidation, Aarhus Bay

* Corresponding author.

E-mail address: LHT@teknologisk.dk, Tel.: +45 72 20 23 95

Abstract

Sulfate reduction and sulfur-iron geochemistry were studied in 5-6 m deep gravity cores of Holocene mud from Aarhus Bay (Denmark). A goal was to understand whether sulfate is generated by reoxidation of sulfide throughout the sulfate and methane zones, which might explain the abundance of active sulfate reducers deep below the main sulfate zone. Sulfate penetrated down to 130 cm where methane started to build up and where the concentration of free sulfide peaked at 5.5 mM. Below this sulfate-methane transition, sulfide diffused downwards to a sulfidization front at 520 cm depth, below which free iron accumulated in the pore water. Sulfate reduction rates measured by ^{35}S-tracer incubations in the sulfate zone were high due to high concentrations of reactive organic matter. Within the sulfate-methane transition, sulfate reduction was distinctly stimulated by the anaerobic oxidation of methane. In the methane zone below, sulfate remained at positive "background" concentrations of <0.5 mM down to the sulfidization front. Sulfate reduction decreased steeply to rates which at 300-500 cm depth were 0.2-1 pmol SO_4^{2-} cm^{-3} d^{-1}, i.e. four to five orders of magnitude lower than rates measured near the sediment surface. The turn-over time of sulfate increased from 3 years at 12 cm depth to 100-1000 years down in the methane zone. Sulfate reduction in the methane zone accounted for only 0.1% of sulfate reduction in the entire sediment column and was apparently limited by the low pore water concentration of sulfate and the low availability of organic substrates. Amendment of the sediment with both sulfate and organic substrates immediately caused a 10-40-fold higher, "potential sulfate reduction" which showed that a physiologically intact community of sulfate reducing-bacteria was present. The "background" sulfate concentration appears to be generated from the reaction of downwards diffusing sulfide with deeply buried Fe(III) species, such as poorly-reactive iron oxides or iron bound in sheet silicates. The oxidation of sulfide to sulfate in the sulfidic sediment may involve the formation of elemental sulfur and the further disproportionation of a small fraction to sulfate. The net production of sulfate

from the reaction of sulfide and Fe(III) to form pyrite requires an additional oxidant. This could be CO_2 which is reduced to methane and subsequently becomes re-oxidized at the sulfate-methane transition and thereby removes excess reducing power. A cryptic sulfur cycle similar to the one described here probably occurs widespread in marine sediments, in particular along the ocean margins.

1. INTRODUCTION

Marine sediments have a vertical zonation of the predominant terminal mineralization processes by which buried organic matter becomes mineralized and oxidized to CO_2. A depth sequence is generally observed of zones where oxygen, nitrate, Mn(IV), Fe(III) and sulfate are consumed as the terminal electron acceptors through geochemical oxidation reactions or through microbial respiration pathways (Berner, 1981; Froelich et al., 1979). The extension of these reaction zones depends on the deposition rate of organic matter and is more constrained to the upper sediment strata on the continental shelf than in the deep sea. It is well known that the reactions are mixed in a spatially and temporally complex manner within the oxic and suboxic zones where burrowing and bioirrigating fauna creates a complex, three-dimensional chemical environment (Fossing et al., 2000).

In sub-surface continental shelf sediments molecular diffusion of sulfate down into the sediment mostly controls the vertical zonation of sulfate reduction and methanogenesis. The sulfate-methane transition zone (SMTZ) marks the depth where sulfate becomes depleted and methanogenesis takes over as the terminal process of organic matter mineralization (Iversen and Jørgensen, 1985). Within the SMTZ, sulfate reduction is driven mostly by anaerobic oxidation of methane (AOM), which diffuses upwards from the deeper sulfate-depleted sediment (Barnes and Goldberg, 1976). These biogeochemical processes all depend on microbial catalysis and their zonation should therefore be reflected in the zonation of the predominant microbial communities. Recent data on the relative distribution of sulfate-reducing bacteria (SRB) in Black Sea and Aarhus Bay sediments shows that SRB may constitute just as high a proportion of the total bacterial numbers within the methane zone as in the sulfate zone (Leloup et al., 2006; Leloup et al., 2009). It was not clear from those data, however, whether the (SRB) were actively reducing sulfate within

the methane zone or whether their abundance was due to other types of metabolism, such as sulfur disproportionation, iron reduction, or fermentation. Sulfate was detected throughout the methane zone at concentrations of a few hundred μM. This was considered to be a "background" concentration that might either be an artifact or might be below a threshold concentration required for sulfate reduction to occur (Leloup et al., 2006).

Those microbiological observations inspired us to explore the potential for sulfate reduction deep below the SMTZ and to test whether sulfate-reducing bacteria might be able to maintain an active respiratory metabolism in spite of μM concentrations of sulfate in the pore water. The Aarhus Bay, located at the transition between the Baltic Sea and the North Sea, appeared to be a promising site for such a study. The Aarhus Bay (Denmark) is a shallow semi-enclosed basin with a deep Holocene mud deposit overlying late glacial till and post-glacial clay (Jensen and Bennike, 2008). Earlier studies in Aarhus Bay had shown that AOM takes place within the SMTZ a few meters below the sediment surface (Dale et al., 2008; Thomsen et al., 2001). Our present study indicated that sulfide produced from sulfate reduction within the SMTZ diffuses both upwards and downwards and causes a pronounced sulfidization front deep within the methane zone. It appears that the deep sediment still contains iron oxides that may chemically oxidize sulfide in the pore water. This oxidation of sulfide could potentially lead to the production of sulfate that could in turn be used by the sulfate-reducing bacteria in the methane zone. Hence, our working hypothesis was that the presence of active sulfate reducers below the SMTZ in Aarhus Bay may be enabled by an ongoing production of sulfate in the otherwise sulfate-depleted environment. We present here the biogeochemical evidence. In separate publications, the distribution and diversity of sulfate-reducing bacteria and evidence of their active gene expression in sub-surface Aarhus Bay sediment are presented (Kostka et al., in prep; Leloup et al., 2009).

2. MATERIAL AND METHODS

2.1. Sediment sampling

Sediment cores were taken by a large gravity corer (6 m steel barrel with a 12 cm diameter polyvinyl-chloride inner core liner and a core catcher) and Rumohr-type gravity corer (1 m long, 10 cm diameter polycarbonate barrel, with no core catcher). Cores were taken at Station M1 (St. M1) in the central part of Aarhus Bay (Denmark) (56°07.058 ' N and 10°20.865' E, Fig. 1) at a water depth of 15 m, during a research cruise in March 2007 on the MS *Henry*. Four gravity cores were taken with lengths of 4.7 to 5.5 m. Three Rumohr cores were taken with lengths up to 70 cm in order to obtain undisturbed surface sediment and thereby to estimate the loss of surface sediment in the gravity cores. The loss of surface sediment (10-30 cm) was estimated by aligning the sulfate reduction rates or the pore water sulfate concentrations at the top of the gravity cores with those in the Rumohr cores. Whole Rumohr cores were brought back to the laboratory in the core liner, whereas gravity cores were split into 1 m sections onboard MS *Henry* and stored at near *in situ* temperature (~8°C) until processed. Magnetic susceptibility, pore water extraction, solid phase sampling and sulfate reduction rate measurements was performed on the longest gravity core. The potential sulfate reduction rate measurements were done on two separate gravity cores and the fourth core was used to collect mussel shells for ^{14}C age determination.

2.2. Pore water extraction

Rhizone soil moisture samplers (Rhizosphere Research Products, Wageningen, Netherlands) were used for the extraction of pore water in the Rumohr and gravity cores. The rhizones consist of a 5 or 10 cm long inert porous polymer tube with a pore size of 0.1 μm through which pore fluid is extracted by vacuum created by disposable 10 mL syringes. Pore water for

sulfate, sulfide and dissolved iron was extracted from the longest gravity core after gently pushing the rhizones into pre-drilled holes in the core liner at 10 cm depth intervals. Pore water was similarly extracted from the Rumohr cores at 5 cm depth intervals. By comparison with pore water squeezing under N_2, we found the rhizone extraction to yield higher and more consistent and reproducible data for reactive pore water species such as H_2S or Fe^{2+}.

Pore water samples for sulfate and sulfide were fixed by mixing 1 mL of pore water with 0.25 mL 1% zinc acetate. Pore water for determination of dissolved iron was preserved by acidifying 1 mL pore water with 0.1 mL 10% HCl. In order to test whether auto-oxidation of sulfide occurred during the pore water extraction and thereby affected the sulfate data we extracted pore water under strict anoxic conditions inside an anaerobic glove box at 60 cm depth intervals at 270-410 cm depth in another gravity core. The extracted pore water was immediately acidified with 0.1 mL 10% HCl and outgassed with N_2 in order to remove H_2S. The low sulfate concentrations measured within the methane zone of the sediment by this careful approach did not differ significantly from sulfate data obtained without the anaerobic glove box.

2.3. Pore water analyses

Sulfate was analyzed by non-suppressed ion chromatography (100 µl injection volume, Waters, column IC-Pak^{TM}, 50 × 4.6 mm). The eluent was 1 mM isophthalate buffer in 10% methanol, adjusted to pH 4.5 with saturated sodium borohydrate, and the flow rate was 1.0 ml min^{-1}. Hydrogen sulfide (sum of H_2S and HS^-, in the following called "H_2S") was determined spectrophotometrically at 670 nm (Shimadzu UV 1202) on zinc-preserved pore water samples by the methylene blue method (Cline, 1969). Dissolved iron was measured according to Stookey (1970) with Ferrozine (1 g L^{-1} in 50 mM HEPES buffer, pH 7) spectrophotometrically at 562 nm (Shimadzu UV 1202).

2.4. Solid phase sampling

The longest gravity core was kept unopened and scanned for magnetic susceptibility (MS) and further processed within two days after sampling. Sediment sub-samples for iron and sulfur analysis as well as sulfate reduction rates were collected in between the depths where pore water was extracted in order to minimize sample oxidation. Porosity and density samples were taken with 10 mL cut-off syringes at 20 cm depth intervals. Sediment for the analysis of sulfur, iron and carbon were collected at 10 cm depth intervals and stored in gas-tight plastic bags (iron and carbon samples) or in plastic tubes with zinc acetate dihydrate (20% w/v) (sulfur samples) and immediately frozen at -20°C. Samples for sulfate reduction rate measurements were taken at 10 cm depth intervals with butyl rubber stoppered glass tubes (5 cm^3) and kept at *in situ* temperature.

2.5. Solid phase analyses

Magnetic susceptibility was measured on the longest, whole gravity core with a Bartington Instruments MS2 meter, equipped with a MS2C sensor, at a scan rate of 1 cm min^{-1}. The water content in the sediment was determined from the weight loss after drying at 60°C until constant weight and sediment density as the wet weight per cm^{-3}. Solid phase iron was extracted from sub-samples of frozen sediment in a cold 0.5 M HCl solution for 1 h on a rotary shaker. The extracted Fe(II) was then determined in HCl extracts by the Ferrozine method (Stookey, 1970). Extracted Fe(III) was determined as the difference between total iron (Fe(II) + Fe(III)), extracted with Ferrozine + 1% w/v hydroxylamine hydrochloride, and the Fe(II). Total iron in the bulk sediment was extracted from freeze dried sub-samples by boiling in 12.5 M HCl for 1 min according to Berner (1970) and Raiswell *et al*. (1988). The extracted total iron was determined with Ferrozine + 1% w/v hydroxylamine hydrochloride. Total reactive iron in the sediment was extracted with

dithionite-citrate-acetic acid according to Canfield (1989) and determined with Ferrozine + 1% w/v hydroxylamine hydrochloride. Solid manganese oxides (Mn(IV)) were determined using flame atomic absorption spectrometry (Perkin Elmer, Atomic Absorption Spectrometer 3110) in the supernatant from the dithionite extracts

Freeze dried sediment for the determination of total organic carbon (TOC) was pre-treated with HCl, dried again, and analyzed on a CNS analyzer (Fisons^{TM} Na 1500 elemental analyzer). AVS (acid volatile sulfide = dissolved sulfide + iron monosulfides) and CRS (Chromium Reducible Sulfur = pyrite + elemental sulfur) were determined by the two step acidic Cr-II method (Fossing and Jørgensen, 1989). The volatilized and trapped sulfide was determined spectrophotometrically at 670 nm (Shimadzu UV 1202) by the methylene blue method (Cline, 1969).

2.6. Sulfate reduction rates (SRR)

Triplicate samples of 5 cm^3 were carefully collected in butyl rubber stoppered glass tubes for the measurement of SRR. Sampling was done at 3 cm depth intervals down to 55 cm and 10 cm depth intervals below that depth, alternating with the depths of pore water extraction. The glass tubes were injected with 5 µl carrier-free $^{35}SO_4^{2-}$ tracer (~500 kBq per 5 cm^3) and incubated for 24 h at *in situ* temperature. Sulfate reduction was stopped by mixing the sample with 10 ml cold zinc acetate (20% w/v) and freezing. The samples were later treated by cold chromium distillation after Kallmeyer *et al*. (2004) and SRR were calculated according to Jørgensen (1978):

$$SRR = [sulfate] \times (^{35}S\text{-}CRS/^{35}S\text{-}sulfate) \times (1.06/t)\ pmol\ cm^{-3}\ d^{-1} \qquad \text{(Eq. 1)}$$

where [sulfate] is the sulfate concentration in pmol per cm^3 of wet sediment, ^{35}S-CRS is the radioactivity of total reduced sulfur at the end of incubation, ^{35}S-sulfate is the initial radioactivity of

sulfate added to the experiment, 1.06 is a correction factor for the expected isotope discrimination against ^{35}S-sulfate versus the bulk ^{32}S-sulfate by the sulfate-reducing bacteria, and t is the incubation time measured in days. We use here the unit pmol SO_4^{2-} (1 pmol = 10^{-12} mol) rather than nmol SO_4^{2-} (1 nmol = 10^{-9} mol) because of the predominance of SRR in the pmol cm^{-3} d^{-1} range. This unit has proven to be practical to describe sub-seafloor rates of microbial processes (e.g. Parkes et al. (2005)).

It is important for the SRR measurements at very low pore water sulfate concentration that the injection of carrier-free ^{35}S-sulfate does not increase the sulfate concentration significantly. We calculated that the applied injection of 500 kBq $^{35}SO_4^{2-}$ into 5 mL sediment adds only 2 nM sulfate to the pore water.

In the deeper, methanogenic part of the sediment, beneath the main sulfate zone, we determined "potential sulfate reduction rates" (P-SRR) in similar 5 cm^3 samples. In the nearly sulfate-depleted sediment at 165-540 cm depth, sediment samples from two independent gravity cores (referred to as GC A and B, respectively) were injected under N_2 with stock solutions of non-radioactive sulfate (1 mM final concentration) and organic substrates (100 µM final concentrations of propionate, acetate, lactate and formate). The samples were then pre-incubated for 12 h during which sulfate and substrates diffused out to reach a uniform distribution in the sediment. Subsequently, 10 µl of carrier-free $^{35}SO_4^{2-}$ tracer (~800 kBq) was injected into each sample.
A time series experiment with five 12 h incubations starting at 0, 12, 24, 36 and 48 h was done with triplicate samples of 5 cm^3 sediment for each time point. The incubations were stopped by mixing the sample into 10 ml cold zinc acetate (20% w/v) and treating as described above.

2.7. ^{14}C age determinations

Shells of the bivalve, *Cerastoderma lamarcki,* from 460 cm sediment depth were used for ^{14}C age determination at the Poznan Radiocarbon Laboratory (Poland). The shells were cleaned with H_2O_2 (15-30%) to remove organic coatings, then quickly etched with 0.5 M HCl to remove the outer carbonate layer, and again treated with H_2O_2. The remaining carbonate was leached with conc. H_3PO_4 in a vacuum line. The sample CO_2 was reduced with H_2 over 2 mg of Fe powder as a catalyst and the resulting carbon/iron mixture was pressed into a pellet in the target holder as described by Czernik and Goslar (2001). The content of ^{14}C was measured in an accelerator mass spectrometer (Compact Carbon AMS) by comparing the simultaneously collected ^{14}C, ^{13}C and ^{12}C beams of each sample with those of oxalic acid standard CO_2 and coal background material (Goslar et al., 2004). Conventional ^{14}C ages were calculated with a $\delta^{13}C$ correction for isotopic fractionation according to Stuiver and Polach (1977) and based on the $^{13}C/^{12}C$ ratio measured simultaneously with the $^{14}C/^{12}C$ ratio.

2.8. Modelling of pore water data

The modelling software, PROFILE, of Berg et al. (1998) was applied to the measured pore water data to calculate net rates of production or consumption of sulfate, sulfide, and dissolved iron. This one-dimensional numerical modelling program first divides the sediment into an arbitrary number of equidistant zones, each with a constant process rate, whereby an objective selection of the simplest process rate distribution is provided which optimally reproduces the measured concentration profiles. The criterion for optimal fit is to minimize the sum of squared deviations (SSE) from the data for each zone with different numbers of equally spaced zones. The model provides F tests for different fits and suggests the minimal number of zones that provide an optimal fit. The model ensures continuity between zones and thus provides also fluxes of the solutes.

Sulfate. Boundary conditions were: concentration at 50 cm = 12.10 mM and flux at 540 cm = 0.00 mmol m^{-2} d^{-1}. The molecular diffusion coefficient, $D(SO_4^{2-})$, used was 6.36 10^{-6} cm^2 s^{-1}. All diffusion coefficients were taken from Table 3.1 in Schulz and Zabel (2000) and recalculated to 8ºC, which is the annual mean temperature in Aarhus Bay and at the SMTZ (Dale et al., 2008).

Sulfide (H_2S+HS^-). Boundary conditions were: concentration at 2.5 cm = 0.00 mM and flux at 570 cm = 0.00 mmol m^{-2} d^{-1}. The molecular diffusion coefficient, $D(H_2S/HS^-)$, used was 11.9 10^{-6} cm^2 s^{-1}, taking into account the degree of dissociation at an estimated sediment pH of 7.4.

Iron (Fe^{2+}). Boundary conditions were: concentration at 500 cm = 0.00 mM and concentration at 560 cm = 0.235 mM. The molecular diffusion coefficient, $D(Fe^{2+})$, used was 4.26 10^{-6} cm^2 s^{-1}.

3. RESULTS

3.1. Sediment description

The cored sediment showed a distinct stratigraphy, which reflected changes in the depositional environment through the Holocene (Fig. 2). The TOC content decreased with depth from about 3% dry weight in the upper 150 cm to a minimum of 0.8% at 230 cm (Fig. 2). Below that depth, the concentration gradually increased again. The TOC minimum marks the transition from an underlying brackish-marine Unit 1 to marine Units 2-3 according to the stratigraphy described by Jensen and Bennike (2008).

By a combination of shallow seismic profiles, visual inspection of sediment cores, biostratigraphy of mollusc shells, and radiocarbon dating, Jensen and Bennike (2008) identified a vertical series of post-glacial deposits in the central Aarhus Bay. The lowermost and oldest deposit is poorly sorted glacial till, above which a late-glacial ice-lake clay and silt deposit of up to 10 m thickness is found. The upper three sediment units, which are included in our cores, are related to the Holocene transgression and were deposited under shifting hydrography and salinity. This shift is evident from the molluscs which were identified from the different layers in our cores. In the marine Unit 1, below 230 cm, the brackish bivalve, *Cerastoderma lamarcki*, was common and indicated lower salinity than today. By ^{14}C-dating, the age of a *C. lamarcki* shell collected at 460 cm depth was found to be 8.3 cal. ka BP. This age falls into the age interval of 8.7-8.0 cal. ka BP determined for Unit 1 by Jensen and Bennike (2008). There was a sharp, probably erosional, boundary to the marine mud deposits of the overlying Units 2-3 at 230 cm depth. In Units 2-3 the diversity of mollusc shells was characteristic of marine conditions and included *Aporrhais pespelecani, Littorina obtusata, Hiatella striata, Mytilus edulis and Scrobicularia plana.* Two radiocarbon age determinations in Unit 2 yielded ages of 6.1 and 7.1 cal. ka BP (Jensen and

Bennike, 2008). The resulting mean sedimentation rate of Units 2-3 is thus ca 0.3 mm per year. This is lower, also when sediment compaction is taken into account, than the modern sedimentation rate of ~0.6 mm per year determined for the same area of Aarhus Bay through the ^{210}Pb method (Fossing et al., 2004).

Visual inspection of the gravity cores showed a grey sediment color throughout most of the core interrupted at 490-580 cm depth in Unit 1 by a diffuse band of very dark grey sediment with mm-size black spots (Fig. 2). This dark band represented the modern sulfidization front as determined by later chemical analyses. The dark color was due to amorphous iron sulfides and the spots were nuclei of greigite (Fe_3S_4) formation. The SMTZ occurred in the middle of Unit 2-3, but lacked visible imprint. Free gas developed upon core retrieval in the deeper part of the gravity cores due to methane super-saturation.

The porosity decreased roughly linearly with depth in the interval 90-560 cm according to the equation: Porosity = 0.77 – 0.0002 × depth (cm). According to an earlier study of the grain size distribution at the same site, the sediment includes 20% fine sand, 22% silt, and 55% clay (Pejrup et al., 1996).

3.2. Pore water profiles of sulfate, sulfide, iron and manganese

Figure 3a and b present the pore water profiles of sulfate, free sulfide, and dissolved iron. The main sulfate zone extended down to about 130 cm depth where sulfate dropped to 0.5 mM (Fig. 3a). Between 130 cm and 300 cm, sulfate fluctuated with a decreasing depth trend (see data in Fig. 3a with expanded concentration scale). Below 300 cm, the concentration decreased continuously from 0.4 mM to below the detection limit of 0.04 mM at 530 cm. Sulfate concentrations at 500-530 cm depth were just at the detection limit of the ion chromatographic technique used and an indirect concentration estimate was therefore made (see under 3.4.). Free sulfide was present in the pore

water from ca 5 cm below the sediment surface and down to 500 cm depth with a peak concentration of 5.6 mM sulfide at 130 cm (Fig. 3b). Free sulfide could not be detected (<0.005 mM) below 500 cm depth where a steep gradient of dissolved iron started which reached 0.25 mM at 560 cm (Fig. 3b). Pore water concentrations of dissolved manganese were low throughout the core. Concentrations dropped from >5 μM in the upper sediment layers to below detection (<1 μM) at 60 cm depth, remained below detection through the peak of free sulfide, and increased again gradually to 7 μM between 200 and 540 cm depth (data not shown).

3.3. Iron, manganese and sulfur geochemistry

The magnetic susceptibility increased from 2×10^{-5} SI units at the sediment surface to 20×10^{-5} SI at 550 cm depth (Fig. 4a). Total iron increased from 40 μmol cm^{-3} at 45 cm to 290 μmol cm^{-3} at 575 cm (Fig. 4b). Reactive iron remained low, <8 μmol cm^{-3}, within the upper 375 cm and increased to ca 50 μmol cm^{-3} below 500 cm depth (Fig. 4b). Ferric iron was low within the upper 275 cm below which concentrations fluctuated between 0 and 12 μmol cm^{-3} (Fig. 4c). Ferric iron increased steeply below 530 cm similar to dissolved iron in the pore water. The maximum concentration measured was 36 μmol cm^{-3} at 575 cm depth. Manganese oxide was low, about 0.4 μmol cm^{-3} down to 200 cm, below which concentrations increased to 4-6 μmol cm^{-3} (Fig. 4d). The maximum concentration of manganese oxides was 7 μmol cm^{-3} at 455 cm depth. The concentration of acid volatile sulfide (AVS) was 1-2 μmol cm^{-3} down to 170 cm depth, <1 μmol cm^{-3} from 175 to 480 cm, and increased steeply below 480 cm to reach nearly 6 μmol cm^{-3} at 575 cm (Fig. 4e). The concentration of chromium reducible sulfide (CRS) was generally high, 100-300 μmol cm^{-3}, with a broad maximum between 100 and 400 cm (Fig. 4f). The CRS concentration had a sharp peak, 305 μmol cm^{-3}, at exactly 535 cm depth. From that very depth, we collected magnetic minerals using a handheld magnet and found that the ferri-magnetic iron-sulfur mineral, greigite (Fe_3S_4), was

present, corresponding to black spots and grains noted by visual core inspection. Greigite is extracted by the two-step acidic Cr-II reduction method along with other iron sulfides, whereby about 2/3 of the gregite is extracted in the AVS fraction and 1/3 in the CRS fraction (Cornwell and Morse, 1987).

3.4. Experimentally measured sulfate reduction rates (SRR)

The SRR data are separated into two graphs with three different scales in order to better describe the rates within the different depth intervals (Fig. 5a and b). The SRR of the Rumohr core peaked with a maximum rate of 38000 pmol cm^{-3} d^{-1} at 4.5 cm depth (Fig. 5a). Below the maximum, the SRR dropped steeply to 100 pmol cm^{-3} d^{-1} at 50 cm depth. The SRR within the 75 to 250 cm depth interval of the gravity core were two orders of magnitude lower than the rates near the surface and decreased with depth from 90 to 0.3 pmol cm^{-3} d^{-1} (Fig. 5a). The sulfate concentration decreased steeply within this interval and reached <0.5 mM at a depth of 130 cm (Fig. 3a). At 130 cm depth there was a peak in SRR with a maximum rate of 150 pmol cm^{-3} d^{-1}. Although methane was not measured in the gravity core, previous studies from Aarhus Bay showed that the bottom of the sulfate zone is also the transition to the methane zone (Dale et al., 2008; Thomsen et al., 2001). The peak of SRR thus occurred within the SMTZ where sulfate reduction was enhanced by AOM. The concentration of free sulfide peaked right at this depth (Fig. 3b).

The SRR deeper than 250 cm were nearly four orders of magnitude lower than the rates near the surface (Fig. 5b) varying between 0.2 and 1.4 pmol cm^{-3} d^{-1}. Just below 500 cm depth, where the measured pore water sulfate concentration dropped below the detection limit, the SRR showed increased values that were most probably due to an overestimated sulfate concentration as the detection limit was approached. Incubations with ^{35}S-sulfate were made also below 530 cm but SRR are not plotted because the sulfate concentrations were too low to be detected (<40 μM).

The depth distribution of SRR is primarily controlled by the availability of degradable organic matter, which decreases over many orders of magnitude with depth and age in the sediment. In order to show this general decrease, we plotted all the experimentally measured SRR as a function of depth in a double-log plot (Fig. 6a). For the calculation of the log-log linear regression, we omitted SRR data from a) the upper 10 cm of the surface sediment where other processes such as oxygen respiration or iron reduction replace SRR as the most important terminal oxidation pathways, b) within the AOM zone where methane diffusing up from the deeper sediment adds a peak to the SRR, and c) below 495 cm depth where the SRR become inaccurate, and most probably overestimated, due to sulfate concentrations near the detection limit.

Fig. 6a shows that the log-log relation between SRR and sediment depth follows a linear trend:

$$\log \text{SRR (pmol cm}^{-3}\text{ d}^{-1}) = -3.07 \times \log \text{depth (cm)} + 7.58; (r^2 = 0.99) \quad \text{(Eq. 2)}$$

or

$$\text{SRR (pmol cm}^{-3}\text{ d}^{-1}) = 38 \times 10^6 \times (\text{depth (cm)})^{-3.07} \quad \text{(Eq. 2a)}$$

A comparison between the distributions of pore water sulfate and sulfate reduction rate, expressed by the log-log linear correlation (Eq. 2a and Fig. 6a), allows a calculation of sulfate turn-over time at different sediment depths. Fig. 6b shows in a semi-logarithmic plot the turn-over time of pore water sulfate from 12 to 500 cm sediment depth. In the upper part of the sediment the calculated turn-over time increased from 3 years at 12 cm to 100 years at 50 cm depth. Below 50 cm the turn-over time varied between 100 and 1000 years with the longest turn-over time between 300 and 400 cm. As the sulfate concentration dropped from 200 μM at 400 cm to much lower values the turn-over time decreased again with depth.

As the general trend of SRR vs. depth followed a power law function (Eq. 2a), we used Equation 2 to calculate hypothetical sulfate concentrations in the deepest depth range where the sulfate concentrations had dropped below our detection limit. By this indirect, and admittedly unconventional approach, we assumed that the observed log-log decrease of SRR versus depth would continue down below 500 cm, where the measured sulfate data became uncertain. Thus, we turned around Equation 1, which calculates SRR, and used the fraction of ^{35}S-sulfate reduced to ^{35}S-CRS to calculate sulfate concentrations instead, assuming that the SRR versus depth trend could be correctly described by Equation 2, also below 500 cm depth:

$$[\text{sulfate}] = \text{SRR} \times (^{35}\text{S-sulfate} / ^{35}\text{S-CRS}) \times (t/1.06) \text{ pmol cm}^{-3} \quad \text{(Eq. 3)}$$

In Equation 3 we thus knew the SRR, the ^{35}S-sulfate and ^{35}S-CRS, and the t. By this approach, we were able to estimate the concentrations of sulfate below 500 cm depth, i.e. below the detection limit of our ion chromatographic technique, as deep as the experimental ^{35}S-sulfate measurements had been done. The resulting sulfate concentrations exhibited a decrease with depth from ca 500 µM around 300 cm depth down to concentrations less than 4 µM below 500 cm (Fig. 7a and insert). The decreasing trend in the estimated concentrations of sulfate generally matched the decreasing trend of sulfate concentrations measured in the pore water down to the depth where sulfate could no longer be detected (Fig. 7a). In order to present the depth distribution of the measured and estimated sulfate concentrations down to the lowest values, a sulfate versus depth trend was also presented using a logarithmic concentration scale (Fig. 7b). The trend curve in this graph is drawn to illustrate that, below 400 cm, the measured and estimated concentrations of sulfate decreased more steeply than above this zone. This graph also shows that, provided a continued power law relation between SRR and depth, the sulfate concentration apparently dropped

below 1 μM at a depth of 530 cm. However, in the case that the lowest sulfate concentrations caused lower SRR below 500 cm depth than the rates extrapolated from the power law relation, then the calculated sulfate concentrations would be somewhat higher than shown in Fig. 7.

3.5. Potential sulfate reduction rates (P-SRR)

Sulfate reduction rates were measured in the gravity core after amendment of the sediment with sulfate and a mixture of carbon sources (propionate, acetate, lactate and formate) injected into the sediment sub-samples 12 hours before radiotracer injection. During this pre-incubation, sulfate and carbon sources diffused out into the sediment to reach a mean concentration of 1 mM and 0.1 mM, respectively. Fig. 8a and b present the P-SRR measured in gravity cores A and B together with the measured pore water concentrations of sulfate. Highest P-SRR were measured just below the main sulfate zone, at 200-300 cm (compare Fig. 8a and Fig. 3a). The P-SRR were much higher than the SRR at all depths below the main sulfate zone. The P-SRR were mostly in the range of 5-30 pmol cm^{-3} d^{-1} below 300 cm depth, whereas the un-amended SRR were mostly between 0.3 and 1 pmol cm^{-3} d^{-1}. This shows that, under *in situ* conditions, the respiration rate of sulfate-reducing microorganisms was strongly limited by low sulfate and/or low electron donor availability. It is interesting that particularly high P-SRR were measured at 538 cm which corresponds to the sulfidization front where upwards diffusing free iron met downwards diffusing sulfide (cf. Fig. 3b). In contrast to the SRR measurements, the P-SRR do not have the uncertainty of inaccurate determination of low sulfate concentration at this depth so that the peak is a real value.

The time course experiments showed that P-SRR started right away from the first incubation period after the injection of ^{35}S tracer to the sediment, indicating that there was no growth involved during the experiments. Based on experience from other sediments, the 0.5-2 days

incubation times used were too short to allow significant change of the sulfate-reducing community through growth at this temperature (e.g. Robador et al., in review).

3.6. Modelled rates of sulfate reduction, sulfide oxidation and iron flux

SRR were not only determined by the ^{35}S tracer method but were also calculated by reaction-transport modelling from the pore water sulfate distribution in the gravity core. We separated the results from the Rumohr core and the gravity core and used an upper boundary at 50 cm sediment depth for the calculated depth-integrations in order not to include bioirrigated sediment in the modelled rates. The H_2S peak, located at 130 cm depth within the SMTZ, marked the "watershed" for the H_2S fluxes which was directed both upwards and downwards (Fig. 3b). We used, however, 165 cm depth as a second boundary for the depth-integrated budgets as 165 cm marks the transition from modelled net H_2S production above to net H_2S consumption below. Thus, below 165 cm free sulfide diffused downwards under continuous net consumption and only a part of it reached the sulfidization front at 540 cm depth (Fig. 3b).

The depth-integrated data are calculated as rates per unit area (mmol m^{-2} d^{-1}) and are summarized in Table 1, which distinguishes gross rates, as provided by measured ^{35}S-tracer SRR and net rates, as provided by the modelled SRR and H_2S turnover data.

Both measured and modelled SRR demonstrated a steep decrease in microbial activity between the surface and subsurface sediment. The measured gross rate of sulfate reduction, integrated over the upper 0-50 cm of the sediment (1. in Table 1), was 4.68 mmol m^{-2} d^{-1}. The total net SRR below 50 cm was 0.67 mmol m^{-2} d^{-1} down to 165 cm depth and 0.005 mmol m^{-2} d^{-1} from 165 cm and down to 540 cm (2. and 3. in Table 1) where sulfate dropped below the detection limit (Fig. 3a). Although the gross SRR in the 165-540 cm depth interval was extremely low, it was still possible to detect the activity by ^{35}S tracer measurements. The experimentally determined rates for

the 165-540 cm interval added up to 0.004 mmol m^{-2} d^{-1} (4. in Table 1), i.e. nearly the same as the modelled rates.

The gross rates of H_2S production are assumed to be the same as the measured gross rates of sulfate reduction. The modelled net rates of H_2S production added up to 0.36 mmol m^{-2} d^{-1} in the 50-165 cm depth interval. This was 53% of the modelled net sulfate reduction and was close to the total upwards flux of H_2S (0.34 mmol m^{-2} d^{-1}) across the 50 cm depth horizon (5. and 6. in Table 1). The difference between net sulfate reduction and net sulfide production, 0.67-0.36 = 0.31 mmol m^{-2} d^{-1} (7. in Table 1) is due to loss of free sulfide within the depth interval by reaction and binding with oxidized iron species and possibly other minor reactions such as sulfidization of organic matter.

Below 165 cm depth the H_2S diffused downwards under further reaction with iron species. Given the low net SRR of 0.005 mmol m^{-2} d^{-1} below 165 cm depth, the rate of H_2S production was correspondingly low. The net consumption of H_2S in the 165-540 cm depth interval was 0.114 mmol m^{-2} d^{-1} (8. in Table 1). Less than 10% of this (0.012 mmol m^{-2} d^{-1}) was consumed directly at the sulfidization front (Fig. 3B). This, however, was still slightly higher that the Fe^{2+} flux of 0.007 mmol m^{-2} d^{-1} that diffused up to the front from the deep non-sulfidic sediment below (9. in Table 1). The sulfidization front was thus not completely maintained by the opposed fluxes of H_2S and Fe^{2+}, but was also a front of slow, downwards progressing sulfidization of solid-phase iron minerals.

4. DISCUSSION

4.1. Sulfate background in the methane zone

The Aarhus Bay data showed a general zonation of sulfate and sulfide which is typical of organic-rich and iron-rich ocean margin sediments. Sulfate dropped rather steeply with depth below the sea floor, from the seawater concentration of 22 mM, typical for this slightly brackish region at the entrance to the Baltic Sea, to <1 mM at 110-130 cm depth. Interestingly, just beneath the main sulfate zone the sulfate concentration did not immediately fall below our detection limit (ca 40 μM). Instead, a detectable background concentration remained down through the entire depth interval containing free sulfide (Fig. 3a), far down into the sediment characterized by high methane concentration. The background concentration of sulfate was not just a constant "blank value", but showed systematic depth variation. It was 0.5-1 mM at 120-200 cm, near the peak in free sulfide concentration. Below 200-300 cm it decreased gradually with depth and fell below our detection limit at 500 cm depth. The ^{35}S-tracer experiments indicated that sulfate was apparently available even deeper than 500 cm.

There are several possible explanations for the sulfate background in the methane zone:

A) The background could be an analytical artifact due to chemical or biological oxidation of free sulfide during the time between coring and sulfate measurement. This would be consistent with the positive correlation between the concentrations of background sulfate and of free sulfide below 130 cm depth (Fig. 3a and b). It would not be consistent with an oxidation of solid-phase reactive sulfides since there is an inverse correlation between background sulfate and acid volatile sulfide (Fig. 3a and 4e). We tried to carefully control each step between coring and sulfate measurement in order to exclude such possible artifacts. Gravity cores were sectioned and kept upright in the core liners on the ship and during transport to avoid air contact with the outside of the

sediment core. The sampling of pore water using rhizons inserted into the middle of the core took place on the day of coring, and pore water was immediately fixed with Zn-acetate and frozen to prevent sulfide oxidation. The first extracted pore water was always discarded as it had been in contact with air. In additional tests we extracted pore water under strict anoxic conditions within an anaerobic glove box to clarify whether auto-oxidation of sulfide with oxygen occurred during the extraction of pore water in open air. The results showed no difference between the concentrations of sulfate extracted in open air and sulfate extracted under controlled anoxic conditions and indicated that oxidation of sulfide did not explain the sulfate data.

B) The sulfate could be passively diffusing down into the methane zone and be turning over only very slowly because it was not being consumed effectively by sulfate-reducing microorganisms. If the sulfate concentration was below a physiological threshold for uptake and respiration the sulfate background would be biologically unavailable. Ingvorsen et al. (1984) observed such a threshold of 2-6 μM SO_4^{2-} in a chemostat culture of marine sulfate-reducing bacteria, *Desulfobacter postgatei,* grown under acetate limitation, and a threshold of 10-20 μM SO_4^{2-} when grown under sulfate limitation. Fresh-water strains of sulfate-reducing bacteria, which are adapted to low sulfate concentration, have much higher sulfate affinity with half-saturation concentrations of sulfate uptake, Km, down to 5 μM in batch culture (Ingvorsen and Jørgensen, 1984) and expectedly much lower threshold concentrations. Thus, the measured sulfate background was higher than threshold concentrations that might be implied from pure culture studies for sulfate-reducing bacteria adapted to low sulfate concentrations. Furthermore, the observation that the sulfate concentration apparently dropped to concentrations <4 μM beneath 500 cm (Fig. 7a and 7b) speaks against an unavailable threshold concentration of 0.1-0.5 mM. A concentration minimum between 200 and 300 cm depth seemed to preclude that the deep sulfate background was fed by

diffusion from above. Alternatively, the minimum could be the result of a non-steady state sulfate distribution.

C) The sulfate could be generated *in situ* down in the methane zone, most probably by reaction between free sulfide and oxidized iron or other potential oxidants in the sediment. Since the Holocene mud in the upper methane zone was deposited several thousand years ago, the buried oxidized iron must have survived high concentrations of free sulfide over this time scale. Such resistance to reaction with sulfide is characteristic of Fe(III) bound in clay minerals and possibly of hematite, Fe_2O_3 (Canfield et al., 1992). The possible mechanisms of such a sulfate generation will be discussed in the following.

4.2. Deep sulfate formation by sulfide oxidation

The distribution of H_2S in marine pore waters is generally controlled by the balance between its formation from sulfate reduction and removal by reaction with iron oxides or with organic matter in the sediment (Canfield, 1989; Canfield et al., 1992). Our data show that sulfide produced within the SMTZ diffused downwards into the brackish-marine sediment layer where it reacted with different iron compounds that still remained reactive several thousand years after burial. This reaction with iron is indicated by the drop in H_2S concentration below the SMTZ (Fig. 3b) and the presence of oxidized and reactive iron species below 250-350 cm depth (Fig. 4b and c). The iron oxides in the sub-surface, therefore, constituted a deep barrier that effectively bound and partly oxidized the downward diffusing sulfide. The immediate products of chemical reaction between sulfide and Fe(III) species are different sulfur intermediates such as zero-valent sulfur (e.g. elemental sulfur and polysulfides), thiosulfate or sulfite (Dos Santos Afonso and Stumm, 1992; Pyzik and Sommer, 1981; Zopfi et al., 2004). In the presence of Fe(III), sulfide tends to remain at intermediate oxidation states and forms pyrite, whereas in the presence of manganese oxides,

sulfide may be oxidized all the way to sulfate (Aller and Rude, 1988; Burdige and Nealson, 1986; Schippers et al., 2001; Yao and Millero, 1996). Sulfate may, however, apparently also be produced from the oxidation of pyrite with Fe(III) (Bottrell et al., 2000), while several sulfate-reducing bacteria can catalyze the oxidation of elemental sulfur to sulfate using Mn(IV) (Lovley and Phillips, 1994).

Bacterial disproportionation of elemental sulfur coupled with binding and oxidation of the generated sulfide by oxidized iron or manganese may lead to the production of sulfate in marine sediments (Thamdrup et al., 1993). Disproportionating bacteria are widespread and abundant in anoxic sediments (Finster et al., 1998; Thamdrup et al., 1993) and disproportionation processes are important in the sulfur cycle of both limnic and marine sediments (Jørgensen and Bak, 1991). It is thus very likely that elemental sulfur and other intermediates are produced within the sub-surface sediments of Aarhus Bay as a result of sulfide oxidation with Fe(III) and/or manganese oxides. Studies from the Black Sea and the Baltic Sea have shown that zero-valent sulfur may accumulate to concentrations exceeding 40 μM and 1 mM, respectively, especially where the free sulfide concentrations are high (Holmkvist *et al*., in prep).

The content of Fe(III)-bearing minerals increased below the SMTZ and the total iron content increased continuously down through the sediment column (Fig. 4b and c). Consequently, Fe(III) may play an important role for the reoxidation of sulfur species. The distribution of extracted iron species in the sediment suggests that Fe(III) in easily reducible iron oxides (e.g. ferrihydrite, goethite or hematite) pri80marily occurred below 500 cm, as indicated by the sharp increase in the content of ferric iron (Fig. 4c). As a result of the high pore water concentrations of sulfide down to 500 cm, easily reducible iron oxides were largely depleted down to that depth, below which the sediment was apparently rich in reactive iron oxide minerals. The fraction of poorly-reactive iron oxides and/or iron bound in sheet silicates is defined as the difference between the total iron and the

reactive iron fraction (Fig. 4b). This fraction made up by far the largest part of the reducible iron oxides within the sub-surface sediments of Aarhus Bay. Apparently, the deeper marine-brackish sediment of Marine Unit I contained a range of different poorly-reactive iron oxides and iron associated with clay minerals.

Oxidized manganese generally reacts faster with sulfide than oxidized iron, which tends to enhance its importance for sulfide oxidation relative to iron in the uppermost part of the sediment (Thamdrup et al., 1994). The measured MnO_2 concentrations were, accordingly, low down to 200 cm and also below that depth much lower than the concentrations of Fe(III). Since the role of manganese for sulfide oxidation depends not only on reactivity but also on the buried quantity, MnO_2 probably played only a minor role for the reoxidation of reduced sulfur species within the sub-surface sediment.

The downward diffusing sulfide generated a sulfidization front as it reacted with deeper iron species in the pore water and sediment. The position of the sulfidization front was indicated by the sharp interface between H_2S and Fe^{2+} in the pore water and by the steep increase in FeS (AVS) concentration at 500 cm depth. The increase in total iron, reactive iron, and ferric iron around this depth showed that sulfide reacted with a range of different iron species within the sulfidization front. The reactions between pore water sulfide and iron species resulted in the formation of a sequence of iron-sulfide minerals, including amorphous iron sulfides (FeS), greigite (ferricmagnetic iron sulfide, Fe_3S_4), and pyrite (FeS_2) (Berner, 1970; Berner, 1984; Sweeney and Kaplan, 1973). Greigite was visible as mm to sub-mm size grains, each surrounded by a few mm wide dark halo of FeS. The greigite zone occurred in a dark grey band of the sediment and the presence of the paramagnetic mineral was evident from the peak of magnetic susceptibility at 500-550 cm (Fig. 2 and 4a)

The binding of sulfide as different iron sulfides, and the cryptic formation and turnover of sulfate below the main sulfate zone, must depend on the burial rate of Fe(III) minerals with the ability to react over a time scale of several thousand years in the Holocene mud deposit. If we assume steady state, the burial rate of iron can be estimated from the sedimentation rate (0.3 mm per year) and the concentration gradient of solid phase iron. With respect to the reactive iron and the ferric iron, however, their concentrations in the gravity core were near zero down to 360 cm and 260 cm depth, respectively. This could imply that there is currently near-zero burial of reactive iron down into the sulfidic methane zone. Since modelling of pore water sulfide showed that there is indeed a net removal of sulfide below 165 cm and down to 540 cm, the progressing sulfidization of buried iron minerals is apparently not in steady state. The mean net consumption of sulfide in the depth interval 165-540 cm was 0.114 mmol m^{-2} d^{-1} (8. in Table 1) corresponding to 30 pmol H_2S cm^{-3} d^{-1}. For comparison, the reactive iron content in the lower part of this depth interval was 50 µmol cm^{-3} (Fig. 4 b), which could potentially bind 25 µmol H_2S cm^{-3}, corresponding to ca 3000 years of calculated sulfide consumption. Due to the apparent non-steady state of these processes it is difficult to develop a more accurate budget. Yet, the comparison of a) sulfide binding capacity by buried reactive iron, b) the ca 6000 year age of the sediment, and c) the modelled net consumption rate of sulfide indicates agreement within a factor of two.

4.3. Redox balance of deep sulfate formation

The observation of potential and active sulfate reduction deep down in the methane zone implies a continuous source of sulfate, presumably from sulfide oxidation with Fe(III). We discuss here a set of possible - and generally well established - reactions between sulfide and oxidized iron that lead to the formation of pyrite and a transient formation of sulfate. These reactions were proposed and discussed in detail by Robert A. Berner (1967; Berner, 1970) and others already many

years ago. However, in order to understand the potential for a cryptic sulfate formation through sulfide reaction with deeply buried oxidized iron it is necessary to reconsider the redox balance. It should be noted up front that the formation of pyrite from H_2S implies a net sulfide oxidation from the oxidation step of -2 to a mean oxidation step of -1 and that there is no net formation of sulfate by these reactions alone. An additional oxidant is required.

As an example of a reactive iron species, FeOOH is used in the following equations. Other Fe(III) species, such as magnetite (Fe_3O_4) or Fe(III) bound in sheet silicates, yield a similar net redox balance and are reactive on a more relevant time scale of hundreds to many thousands of years (Canfield et al., 1992). The net result is independent of whether the sulfide oxidation intermediate is elemental sulfur, S^0, or thiosulfate, $S_2O_3^{2-}$ or another sulfur species. Elemental sulfur is a common product of H_2S oxidation by metals (Burdige and Nealson, 1986; Pyzik and Sommer, 1981) and S^0 disproportionation to H_2S and SO_4^{2-} has been demonstrated in coastal marine sediments similar to those in Aarhus Bay (Canfield and Thamdrup, 1996). However, S^0 disproportionation is not exergonic under the high H_2S concentrations found throughout the upper methane zone so that other sulfur intermediates, such as thiosulfate, which is also disproportionated in marine sediments, may play the same role (Jørgensen and Bak, 1991).

H_2S oxidation by FeOOH to $S_2O_3^{2-}$ (Eq. 4) results in a concomitant liberation of Fe^{2+}. The $S_2O_3^{2-}$ may then be disproportionated (Eq. 5) whereby the sulfane atom is reduced to H_2S while the sulfonate atom is oxidized to SO_4^{2-}. The liberated Fe^{2+} may react with further H_2S (letters of equations relate to Fig. 9):

(A) $2\ H_2S + 8\ FeOOH + 14\ H^+ \rightarrow S_2O_3^{2-} + 8\ Fe^{2+} + 13\ H_2O$ (Eq. 4)

(B) $S_2O_3^{2-} + H_2O \rightarrow H_2S + SO_4^{2-}$ (Eq. 5)

(C) $8\ H_2S + 8Fe^{2+} \rightarrow 8\ FeS + 16\ H^+$ (Eq. 6)

Since FeS is not the main end product of reaction, but is present in the sulfide zone at 100-1000-fold lower concentration than FeS_2 (Fig. 4e), a further reaction of FeS to pyrite must take place. We propose here, as one possible pathway, the Wächtershäuser reaction whereby H_2S is oxidized with the concomitant formation of molecular hydrogen (Eq. 7) (Drobner et al., 1990; Rickard, 1997):

(D) $8\ H_2S + 8\ FeS \rightarrow 8\ FeS_2 + 8\ H_2$ (Eq. 7)

The sum equation for reactions 4 to 7 is indicated below by a roman numeral in order to distinguish it from the individual reaction steps. The net reaction with SO_4^{2-} and FeS_2 as end products is then:

$17\ H_2S + 8\ FeOOH \rightarrow SO_4^{2-} + 8\ FeS_2 + 8\ H_2 + 12\ H_2O + 2\ H^+$ (Sum Eq. I)

The reducing power from H_2S, here in the form of H_2, does not accumulate but may be used by sulfate-reducing bacteria:

$SO_4^{2-} + 4\ H_2 + 2\ H^+ \rightarrow H_2S + 4\ H_2O$ (Eq. 8)

The sum of Equations 4 to 8 then describes a reaction with FeS_2 only as the product:

$16\ H_2S + 8\ FeOOH \rightarrow 8\ FeS_2 + 4\ H_2 + 16\ H_2O$ (Sum Eq. II)

By complete conversion of H_2S and Fe(III) to pyrite there is thus no free sulfate left but instead an excess of H_2, which might potentially consume further SO_4^{2-}, beyond that which was formed by disproportionation. Alternatively, the excess H_2 could be consumed by the reduction of Fe(III), but this would result in a net release of Fe^{2+}, which does not accumulate in the sulfide zone. The Fe^{2+} would instead react with H_2S and, thus, a complete conversion of H_2S into FeS_2, only by reaction with Fe(III), is not possible without an additional mechanism to remove excess reducing power. Alternatively, a part of the Fe^{2+} formed (Eq. 4) could precipitate as authigenic siderite ($FeCO_3$) and thereby store the reducing equivalents in the solid phase. This would enable more sulfate to form through the recycling of H_2S from disproportionation (Eq. 5) with further reaction with oxidized iron (Eq. 4). Siderite is, however, generally sub-saturated and does not accumulate in pyritic sediments with high sulfide concentrations and non-detectable (<20μM) Fe^{2+} concentrations (Berner, 1964; Postma, 1982).

Since we are considering cryptic sulfate formation down in the methane zone, the H_2 may alternatively be consumed by methanogenic archaea, which are anyhow present and active in the methane zone and may therefore compete with the sulfate reducers for H_2 at the low sulfate concentration. Thereby, the reducing power is stored in a diffusible product, CH_4, which we know builds up to a high concentration gradient and diffuses upwards to be oxidized in the SMTZ at ca 130 cm sediment depth:

(E) $4H_2 + CO_2 \rightarrow CH_4 + H_2O$ (Eq. 9)

Reaction with FeS_2 and methane as the only end products would then be the sum of Equations II and 9:

$$16\ H_2S + 8\ FeOOH + CO_2 \rightarrow 8\ FeS_2 + CH_4 + 18\ H_2O \qquad \text{(Sum Eq. III)}$$

By the reaction of sulfide with Fe(III) through Equation (III), there would be no net sulfate accumulation, but a low background concentration of sulfate could exist. Furthermore, an intermediate sulfate reduction could occur at a rate of 1 SO_4^{2-} reduced per 16 H_2S bound in pyrite according to Sum Eq. I. If a larger fraction of the H_2 would be consumed by methanogenic archaea according to Eq. 9, then sulfate accumulation could indeed take place. The intermediate sulfate reduction would be diminished accordingly because the reducing power would go into CO_2 reduction instead of SO_4^{2-} reduction.

These results were in principle realized by Robert A. Berner (Berner, 1967; 1970) already before Günther Wächtershäuser (1988) proposed the reaction of Eq. 7 and David Rickard (1997) later proposed it to be a functioning pathway under temperatures and chemical conditions prevailing in marine sediments. The reaction was proposed by Berner in order to explain the net oxidation of sulfide and net formation of pyrite implied from geochemical studies of marine sediments. In order to explain the excess reducing power in Sum Eq. II, Berner (1970) proposed that S^0 might be formed by sulfide oxidation with molecular oxygen at the sediment surface and then be mixed down into the sediment. Although this would provide the additional oxidant required, it is not a plausible explanation for the sulfate formation proposed here since the primary oxic zone penetrates only a few mm-cm down from the overlying seawater and since transport in the deep sulfidized methane zone is clearly by molecular diffusion. Meysman and Middelburg (2005), using a similar set of equations, re-iterated the problem, and suggested that many diagenetic models are necessarily "leaky" with respect to either S^0 or H_2.

The Sum Equation I shows that the transient formation of sulfate corresponds to only 1/17, corresponding to 6%, of the free sulfide which reacts with Fe(III). Although no net sulfate

production results from the proposed reaction sequences, unless methanogenesis takes over part of the H_2 otherwise used by sulfate reduction, the proposed reactions may still explain the positive correlation between SO_4^{2-} and H_2S concentrations. Modelling of the SO_4^{2-} profile between 165 and 540 cm depth (Fig. 3a) showed a mean net SRR of 1.3 pmol cm^{-3} d^{-1}, while the gross SRR, measured by ^{35}S tracer experiments, decreased down through this depth interval from 13 pmol cm^{-3} d^{-1} at 165 cm to 2 pmol cm^{-3} d^{-1} at 525 cm (Fig. 5a and b). The mean net H_2S consumption in the same interval, calculated from modelling of the H_2S profile below 165 cm depth, was much higher, 30 pmol cm^{-3} d^{-1}. This comparison shows, in accordance with the discussion above, that the sulfate turnover constitutes only a small fraction of the total sulfide turnover. Thus, a reaction rate between H_2S and Fe(III) of 30 pmol cm^{-3} d^{-1} could lead to a sulfate reduction of ca. 2 pmol SO_4^{2-} cm^{-3} d^{-1} according to Sum Eq. I, which is similar to the modelled SRR

In conclusion, a network of reactions may explain a complete conversion of sulfide to pyrite. Since the binding of H_2S in FeS_2 is associated with a partial oxidation from -2 to -1, there must be redox balance between the amount of H_2S bound and the amount of Fe(III) reduced. This invariably leads to an excess of Fe^{2+}, which binds free H_2S as FeS. If part of the H_2 reacts with CO_2 and is removed by CH_4 diffusing up to the SMTZ, then the sulfide oxidation can go quantitatively to FeS_2. Some H_2S diffuses downwards and out of the sulfidized methane zone to react at the sulfidization front. This removal of H_2S, however, does not change the redox balance but only the amount of iron sulfides formed.

The proposed gradual transition from sulfate reduction to methanogenesis below the SMTZ has implications for the overall regulation of SRR with depth and age in the sediment. The depth relation was described by a power function (log-log linear function in Fig. 6a) with an exponent of -3. The exponent implies a steeper decrease in SRR than the general exponent of -1 found for organic matter reactivity versus age in marine systems (Middelburg, 1989). A steeper decrease than

-1 has been observed also in other marine sediments by ^{35}S-sulfate reduction measurements (Jørgensen and Parkes, submitted; Lettmann et al., in prep., Kallmeyer et al., in prep.). In the Aarhus Bay sediment, SRR probably accounted for a gradually decreasing fraction of the organic matter mineralization with depth below the SMTZ where methanogenesis gradually took over, a transition which would result in the more negative exponent observed. A drop in the slope of the log SRR vs. log depth at the transition into the methane zone was expected but was not distinct (Fig. 6A).

4.4. Sulfate-reducing bacteria below the SMTZ

Our experimental measurements of actual and potential sulfate reduction demonstrate the presence of active sulfate-reducing bacteria several meters below the SMTZ. This is in accordance with the direct demonstration, using DNA based techniques, of relatively high SRB abundance throughout the methane zone (Leloup et al., 2009). The data of Leloup et al. (2009) were obtained from a gravity core taken in Aarhus Bay close to the coring site of the present study. Real-time PCR quantification was done of the 16S rRNA gene of all bacteria and of *dsrAB*, dissimilatory (bi)sulfite reductase, a key gene of all SRB. The results obtained, (without the use of ethidium azide (EMA) to exclude damaged cells), showed that the SRB comprised in average 13% of the total bacterial cells in the sulfate zone, 22% in the SMTZ, and 8% in the methane zone. DGGE analyses, based on the amplification of the *dsrA* gene (400 bp), showed that the richness of sulfate-reducing bacteria did not change with depth through the geochemical zones, but that the clustering of gene sequences was related to the particular zone. A full-length clone library of the *dsrAB* gene (1900 bp) showed that the SRB in the upper sulfate zone were related mostly to the *Desulfobacteraceae*, while sequences deep in the sulfate zone, in the SMTZ, and in the methane zone were mostly gram-positive SRB

(Leloup et al., 2009). It is not clear in which way the latter SRB may be adapted to the environmental conditions in these zones of low availability of sulfate and electron donor.

We were able to stimulate the activity of SRB in the methane zone many-fold by the addition of sulfate and organic substrates to the sediment (Fig. 8). The much higher potential SRR compared to the un-amended SRR shows that the communities of SRB below the SMTZ were limited by the low concentrations of sulfate and/or organic substrate but had the ability, within hours, to step up their metabolic rate once this limitation was alleviated. We propose that these SRB were indeed living by sulfate reduction rather than surviving by a fermentative metabolism or by metal reduction. The low background values of sulfate beneath the SMTZ thus reflect a dynamic equilibrium between production and consumption of sulfate, and the *in situ* respiration of the SRB is coupled to the rate of sulfate release to the pore water and perhaps to a low diffusive flux of sulfate from above.

The depth distribution of SRB in the Aarhus Bay sediment can be directly compared to the depth distribution of SRR (Leloup et al., 2009). Since the SRB were quantified in a different core than the SRR, although at the same site, we used the generalized power law function for the SRR data (Equation 2) for this comparison and calculated the mean sulfate reduction rates per cell. Fig. 10 shows that these cell-specific SRR dropped more than two orders of magnitude, from 0.08 fmol $cell^{-1}$ d^{-1} at 10 cm depth to about 0.0003 fmol $cell^{-1}$ d^{-1} in the methane zone at 300 cm depth. The former rate is typical for SRB in near-surface sediments of bays and fjords (Ravenschlag et al., 2000; Sahm et al., 1999), while the latter rate approaches the extremely low cell-specific rates calculated for deep sub-surface sediments (Jørgensen and D´Hondt, 2006). From this we conclude that already below one meter sediment depth, with a sediment age of a few thousand years, the cellular metabolism of the sulfate-reducing bacteria was maintained at a level typical for the deep biosphere. Such a low metabolic rate may enable mean division times of the SRB cells on the order

of a hundred years or more (cf. Jørgensen & D´Hondt (2006)) which is comparable to the similarly long turnover times of sulfate.

5. CONCLUSIONS

It has been repeatedly observed in ocean margin sediments that H_2S in the pore water peaks at the SMTZ and drops in concentration below the SMTZ. Fewer studies have demonstrated that H_2S drops all the way to zero concentration deep down in the methane zone where a band of iron sulfide may mark a sulfidization front. The drop in H_2S is generally explained by reaction with deeply buried Fe(III) that leads to more oxidized states of sulfur. The formation of sulfate from these reactions has generally not been implied, however, probably because the detection of a low background concentration of sulfate could also be an artifact due to sediment and pore water handling. We propose that the sulfate formation in Aarhus Bay is not an artifact, but that a cryptic sulfur cycle exists which involves both the formation and reduction of sulfate at trace concentration. We also propose that Aarhus Bay is not unique in this respect but that a similar recycling of sulfate occurs widespread in sub-surface marine sediments, concurrent with sulfate reduction and methanogenesis, although the background concentration of sulfate in the methane zone is usually lower that reported here. Our recent study of the same phenomenon in Black Sea sediment has shown similar low background concentrations of sulfate and similar abundant communities of SRB below the SMTZ (Holmkvist et al., in prep.) (Leloup et al., 2007).

It is striking that the Fe(III)-driven sulfate formation is detected down in the methane zone rather than in the sulfate zone where the high sulfate concentration obscures its formation. It is also interesting that the formation and diffusion loss of methane in that zone may facilitate the complete pyrite formation by removing excess reducing power and even facilitate the formation of excess sulfate. Modelling of the pore water profiles of sulfate and sulfide showed that the net sulfide production was only half of the net sulfate reduction. A continuous partial reoxidation of produced sulfide with Fe(III) and binding in pyrite thus took place not only in the methane zone but also

throughout the sulfate zone. A small fraction of this reoxidation may go all the way to sulfate, thereby enhancing the difference between the measured gross sulfate reduction rates and the modelled net sulfate reduction rates (cf. Table 2). Although sulfate reduction could be detected down in the methane zone, it was probably a small fraction of the ongoing methanogenesis and corresponded to only 0.1% of the total sulfate reduction in the sulfate zone.

Acknowledgements— We thank Thomas Max for assistance with solid phase analysis of TOC, Vera Lukies from the Center for Marine Environmental Sciences (MARUM) in Bremen (Germany) for assistance with magnetic susceptibility measurements, and Tomasz Goslar at the Poznan Radiocarbon Laboratory (Poland) for the C-14 age analyses. We thank Preben G. Sørensen, Kristian B. Laursen, Nina Knab and the captain and crew of the MS *Henry* for the successful sampling. Finally, we thank Marc Alperin and Hans Røy for stimulating discussions. This study was financially supported by the Max Planck Society and by the EU 5th FP project, METROL.

REFERENCES

Aller R. C. and Rude P. D. (1988) Complete oxidation of solid phase sulfides by manganese and bacteria in anoxic marine sediments. *Geochim Cosmochim Ac* **52**, 751-765.

Barnes R. O. and Goldberg E. D. (1976) Methane production and consumption in anoxic marine sediments. *Geol.*, 297-300.

Berg P., Risgaard-Petersen N., and Rysgaard S. (1998) Interpretation of measured concentration profiles in sediment pore water. *Limnol Oceanogr* **43**, 1500-1510.

Berner R. A. (1964) Stability fields of iron minerals in anaerobic marine sediments. *The Journal of Geology* **72**, 826-34.

Berner R. A. (1967) Thermodynamic stability of sedimentary iron sulfides. *Amer. J. Sci.* **265**, 773-785.

Berner R. A. (1970) Sedimentary pyrite formation. *Amer. J. Sci.* **268**, 1-23.

Berner R. A. (1981) A new geochemical classification of sedimentary environments. *J. Sedimentary Petrology* **51**, 359-365.

Berner R. A. (1984) Sedimentary pyrite formation: An update. *Geochim Cosmochim Ac* **48**, 605-615.

Bottrell S. H., Parkes R. J., Cragg B. A., and Raiswell R. (2000) Isotopic evidence for anoxic pyrite oxidation and stimulation of bacterial sulphate reduction in marine sediments. *Journal of the Geological Society* **157**, 711-714.

Burdige D. J. and Nealson K. H. (1986) Chemical and microbiological studies of sulfide-mediated manganese reduction. *Geochemical J.* **4**, 361-387.

Canfield D. E. (1989) Reactive iron in marine sediments. *Geochimica et Cosmochimica Acta* **53**, 619-632.

Canfield D. E., Raiswell R., and Bottrell S. (1992) The reactivity of sedimentary iron minerals toward sulfide. *Am J Sci* **292**, 659-683.

Canfield D. E. and Thamdrup B. (1996) Fate of elemental sulfur in an intertidal sediment. *FEMS Microbiology Ecology* **19**, 95-103.

Cline J. D. (1969) Spectrophotometric determination of hydrogen sulfide in natural waters. *Limnol Oceanogr* **14**, 454-458.

Cornwell J. C. and Morse J. W. (1987) The Characterization of Iron Sulfide Minerals in Anoxic Marine-Sediments. *Mar Chem* **22**, 193-206.

Czernik J. and Goslar T. (2001) Preparation of graphite targets in the Gliwice Radiocarbon Laboratory for AMS 14C dating. *Radiocarbon* **43**, 283-291.

Dale A. W., Aguilera D. R., Regnier P., Fossing H., Knab N. J., and Jørgensen B. B. (2008) Seasonal dynamics of the depth and rate of anaerobic oxidation of methane in Aarhus Bay (Denmark) sediments. *Geochim Cosmochim Acta* **72**, 2880-2894.

Dos Santos Afonso M. and Stumm W. (1992) The reductive dissolution of iron (III) (hydr) oxides by hydrogen sulfide. *Langmuir* **8**, 1671-1676.

Drobner E., Huber H., Waechtershaeuser G., Rose D., and Stetter K. O. (1990) Pyrite formation linked with hydrogen evolution under anaerobic conditions. *Nature* **346**, 742-744.

Finster K., Liesack W., and Thamdrup B. (1998) Elemental sulfur and thiosulfate disproportionation by Desulfocapsa sulfoexigens sp. nov., a new anaerobic bacterium isolated from marine surface sediment. *Applied and Environmental Microbiology* **64**, 119-125.

Fossing H. and Jørgensen B. B. (1989) Measurement of bacterial sulfate reduction in sediments: Evaluation of a single-step chromium reduction method. *Biogeochemistry* **8**, 205-222.

Fossing H., Ferdelman T. G., and Berg P. (2000) Sulfate reduction and methane oxidation in continental margin sediments influenced by irregation (South-East Atlantic off Namibia). *Geochim Cosmochim Ac* **64**, 897-910.

Fossing H., Berg P., Thamdrup B., Rysgaard S., Munk Soerensen H., and Nielsen K. (2004) A model set-up for an oxygen and nutrient flux model for Aarhus Bay (Denmark), pp. 65. National Environmental Research Institute, Ministry of the Envrionment, Denmark.

Froelich P. N., Klinkhammer G. P., Bender M. L., Luedtke N. A., Heath G. R., Cullen D., Dauphin P., Hammond D., and Hartman B. (1979) Early oxidation of organic matter in pelatic sediments of the eastern equatorial Atlantic: Suboxic diagenesis. *Geochim Cosmochim Ac* **43**, 1075-1090.

Goslar T., Czernik J., and Goslar E. (2004) Low-energy 14C AMS in Poznan Radiocarbon Laboratory, Poland. *Nuclear Instruments and Methods* **223**, 5-11.

Ingvorsen K. and Jørgensen B. B. (1984) Kinetics of sulfate uptake by freshwater and marine species of Desulfovibrio. *Arch. Microbiol.* **139**, 61-66.

Ingvorsen K., Zehnder A. J. B., and Jørgensen B. B. (1984) Kinetics of sulfate and acetate uptake by Desulfobacter postgatei. *Appl. Environ. Microbiol.* **47**, 403-408.

Iversen N. and Jørgensen B. B. (1985) Anaerobic methane oxidation rates at the sulfate-methane transition in marine sediments from Kattegat and Skagerrak (Denmark). *Limnol. Oceanogr.* **30**, 944-955.

Jensen J. B. and Bennike O. (2008) Geological setting as background for methane distribution in Holocene mud deposits, Århus Bay, Denmark. *Continental Shelf Res.*

Jørgensen B. B. (1978) A comparison of methods for the quantification of bacterial sulfate reduction in coastal marine sediments. III. Estimation from chemical and bacteriological field data. *Geomicrobiology Journal* **1**, 49-64.

Jørgensen B. B. and Bak F. (1991) Pathways and microbiology of thiosulfate transformations and sulfate reduction in a marine sediment (Kattegat, Denmark). *Applied and Environmental Microbiology* **57**, 847-856.

Jørgensen B. B. and D´Hondt S. (2006) A starving majority deep beneath the seafloor. *Science* **314**, 932-934.

Kallmeyer J., Ferdelman T. G., Weber A., Fossing H., and Jørgensen B. B. (2004) A cold chromium distillation procedure for radiolabeled sulfide applied to sulfate reduction measurements. *Limnol Oceanogr: Methods* **2**, 171-180.

Leloup J., Quillet L., Berthe T., and Petit F. (2006) Diversity of the dsrAB (dissimilatory sulfite reductase) gene sequences retrieved from two contrasting mudflats of the Seine estuary, France. *Fems Microbiology Ecology* **55**, 230-238.

Leloup J., Loy A., Knab N. J., Borowski C., Wagner M., and Jørgensen B. B. (2007) Diversity and abundance of sulfate-reducing microorganisms in the sulfate and methane zones of a marine sediment, Black Sea. *Environ Microbiol* **9**, 131-142.

Leloup J., Fossing H., Kohls K., Holmkvist L., Borowski C., and Jørgensen B. B. (2009) Sulfate-reducing bacteria in marine sediment (Aarhus Bay, Denmark): abundance and diversity related to geochemical zonation. *Environ Microbiol* **11**, 1278 - 1291.

Lovley D. R. and Phillips E. J. P. (1994) Novel Processes for Anaerobic Sulfate Production from Elemental Sulfur by Sulfate-Reducing Bacteria. *Applied and Environmental Microbiology* **60**, 2394-2399.

Meysman F. J. R. and Middelburg J. J. (2005) Acid-volatile sulfide (AVS) - A comment. *Mar Chem* **97**, 206-212.

Middelburg J. J. (1989) A simple rate model for organic matter decomposition in marine sediments. *Geochim Cosmochim Ac* **53**, 1577-1581.

Parkes R. J., Webster G., Cragg B. A., Weightman A. J., Newberry C. J., Ferdelman T. G., Kallmeyer J., Jørgensen B. B., Aiello I. W., and Fry J. C. (2005) Deep sub-seafloor prokaryotes stimulated at interfaces over geological time. *Nature* **436**, 390-394.

Pejrup M., Valeur J., and Jensen A. (1996) Vertical fluxes of particulate matter in Aarhus Bight, Denmark. *Continental Shelf Res.* **16**, 1047-1064.

Postma D. (1982) Pyrite and siderite formation in brackish and freshwater swamp sediments. *Am. J. Sci.* **282**, 1151-1183.

Pyzik A. J. and Sommer S. E. (1981) Sedimentary iron monosulfides: kinetics and mechanism of formation. *Geochim Cosmochim Ac* **45**, 687-698.

Raiswell R., Buckley F., Berner R. A., and Anderson T. F. (1988) Degree of pyritization of iron as a paleoenvironmental indicator of botom water oxygenation. *Journal of Sedimentary Petrology* **58**, 812-819.

Ravenschlag K., Sahm K., Knoblauch C., Jørgensen B. B., and Amann R. (2000) Community structure, cellular rRNA content, and activity of sulfate-reducing bacteria in marine Arctic sediments. *Applied and Environmental Microbiology* **66**, 3592-3602.

Reeburgh W. S. (1976) Methane consumption in Cariaco trench waters and sediments. *Earth Planet Sc Lett* **28**, 337-344.

Rickard D. (1997) Kinetics of pyrite formation by the H2S oxidation of iron (II) monosulfide in aqueous solutions between 25 and 125 degrees Celsius: The rate equation. *Geochimica et Cosmochimica Acta* **61**, 115-134.

Rickard D. T. and Luther III G. W. (1997) Kinetics of pyrite formation by the H2S oxidation of iron (II) monosulfide in aqueous solutions between 25 and 125 degrees Celsius: The mechanism. *Geochemica et Cosmochimica Acta* **61**, 135-147.

Sahm K., MacGregor B. J., Joergensen B. B., and Stahl D. A. (1999) Sulphate reduction and vertical distribution of sulphate-reducing bacteria quantified by rRNA slot-blot hybridization in a coastal marine sediment. *Environ Microbiol* **1**, 65-74.

Schippers A., Jozsa P. G., Kovacs Z. M., Jelea M., and Sand W. (2001) Large-scale experiments for microbiological evaluation of measures for safeguarding sulfidic mine waste. *Waste Management* **21**, 139-146.

Schulz H. and Zabel M. (2000) Marine Geochemistry. In Marine Geochemistry.Heidelberg *Springer* pp.

Stookey L. L. (1970) Ferrozine - a new spectrophotometric reagent for iron. *Anal Chem* **42**, 779-781.

Stuiver M. and Polach H. (1977) Discussion: reporting of 14C data. *Radiocarbon* **19**, 355-363.

Sweeney R. E. and Kaplan I. R. (1973) Pyrite framboid formation: Laboratory synthesis and marine sediments. *Economic Geol.* **68**, 618-634.

Thamdrup B., Finster K., Hansen J. W., and Bak F. (1993) Bacterial disproportionation of elemental sulfur coupled to chemical reduction of iron or manganese. *Applied and Environmental Mecorbiology* **59**, 101-108.

Thamdrup B., Fossing H., and Jørgensen B. B. (1994) Manganese, iron, and sulfur cycling in a coastal marine sediment, Aarhus Bay, Denmark. *Geochim Cosmochim Ac* **58**, 5115-5129.

Thomsen T. R., Finster K., and Ramsing N. B. (2001) Biogeochemical and molecular signatures of anaerobic methane oxidation in a marine sediment. *Applied and Environmental Microbiology* **67**, 1646-1656.

Waechtershaeuser G. (1988) Before enzymes and templates: Theory of surface metabolism. *Microbiological Reviews* **52**, 452-484.

Yao W. S. and Millero F. J. (1996) Oxidation of hydrogen sulfide by hydrous Fe(III) oxides in seawater. *Mar Chem* **52**, 1-16.

Zopfi J., Ferdelman T. G., and Fossing H. (2004) Distribution and fate of sulfur intermediates-sulfite, tetrathionate, thiosulfate, and elemental sulfur-in marine sediments. In Distribution and fate of sulfur intermediates-sulfite, tetrathionate, thiosulfate, and elemental sulfur-in marine sediments (ed. J. P. Amend, K. J. Edwards, and T. W. Lyons).Colorado *The Geological Society of America* pp.1-205.

Table 1. Depth-integrated process rates. Gross rates were measured experimentally by ^{35}S, net rates were modelled from pore water data.

No.	Process and depth interval	Rate
1.	SRR, gross, 0-50 cm	4.68 mmol m^{-2} d^{-1}
2.	SRR, net, 50-165 cm	0.67 mmol m^{-2} d^{-1}
3.	SRR, net, 165-540 cm	0.005 mmol m^{-2} d^{-1}
4.	SRR, gross, 165-540 cm	0.004 mmol m^{-2} d^{-1}
5.	H_2S net production, 50-165 cm	0.36 mmol m^{-2} d^{-1}
6.	H_2S net production vs. net SRR, 50-165 cm	53%
7.	SRR – H_2S net production, 50-165 cm	0.31 mmol m^{-2} d^{-1}
8.	H_2S net consumption, 165-540 cm	-0.114 mmol m^{-2} d^{-1}
9.	Fe^{2+} flux up to sulfidization front	0.007 mmol m^{-2} d^{-1}

Figure legends

Fig. 1

Map of the study area, Aarhus Bay in Denmark, with location of coring site "M1".

Fig. 2

Total organic carbon (% dry weight) and stratigraphy of the sediment.

Fig. 3

Pore water concentrations of (a) sulfate (with the same data below 130 cm plotted on two different scales), and (b) free sulfide and dissolved iron. RC = data from Rumohr Corer; GC = data from Gravity Corer.

Fig. 4

(a) Magnetic susceptibility ($\chi \times 10^{-5}$, SI units), (b) total iron and total reactive iron, (c) ferric iron, (d) manganese oxides, (e) Acid Volatile Sulfide (AVS) and (f) Chromium Reducible Sulfur (CRS).

Fig. 5

Sulfate reduction rates measured experimentally using $^{35}SO_4^{2-}$. (a) 0-75 cm depth from Rumohr corer (RC), 45-250 cm depth from gravity corer (GC), and (b) 250-520 cm depth from gravity corer. Note the different scales for SRR. In frame (b) the "SRR inaccurate" indicates that the sulfate concentrations used for these calculations were at the detection limit and were expectedly over-estimated. Error bars show standard deviation of triplicate measurements.

Fig. 6

(a) Log-log plot of ^{35}S-sulfate reduction rates from the Rumohr Corer (open circles) and the gravity corer (closed circles) versus depth. The line shows the linear regression of the log-log data. Encircled data points were not included in the linear regression. The log-log plot is inserted into the graph with measured pore water concentrations of sulfate (same as Fig. 3a) from the Rumohr Corer (open circles) and the gravity corer, (b) semi-log plot of calculated sulfate turnover times versus depth.

Fig. 7

(a) Measured and estimated sulfate concentrations below 300 cm (see text for explanation) and (b) semi-log plot of measured and estimated sulfate concentrations with trend line drawn.

Fig. 8

Potential sulfate reduction rates and sulfate concentrations. (a) 0-700 cm depth, (b) 250-700 cm depth. Error bars show standard deviation of triplicate measurements.

Fig. 9

Conceptual diagram of the cryptic sulfur cycle driven by iron in the methane zone of marine sediment. Reactions between Fe(III) and sulfide, combined with sulfur disproportionation, enable a quantitative conversion of sulfide to pyrite. The intermediate formation of sulfate and removal of excess reducing power may be driven by the formation of methane and by its reoxidation at the sulfate-methane transition. Encircled capital letters refer to equations presented in the text.

Fig. 10

Rates of sulfate reduction per cell, using the SRR data from the linear correlation in Fig. 6a. Numbers of sulfate-reducing bacteria were determined by quantitative PCR (method without EMA) of the key gene for dissimilatory sulfate reduction, *dsrAB* (Leloup et al., 2009)

Figure 1

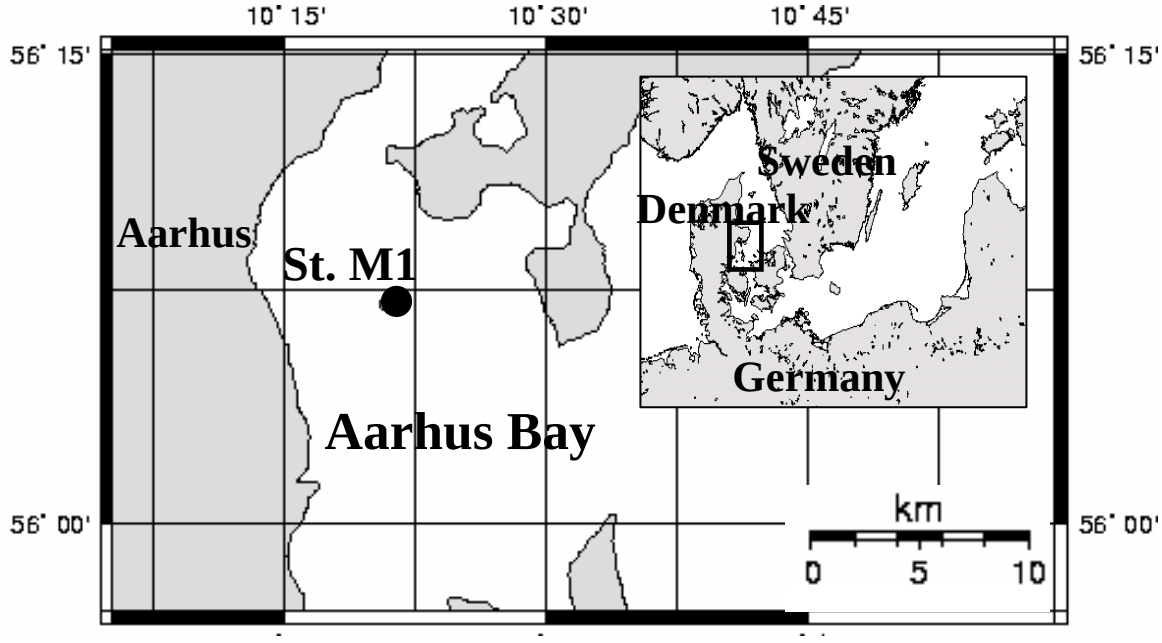
10° 15'
10° 30'
10° 45'
56° 15'
56° 15'
Aarhus
St. M1
Aarhus Bay
Sweden
Denmark
Germany
km
0
5
10
56° 00'
56° 00'

Fig. 2

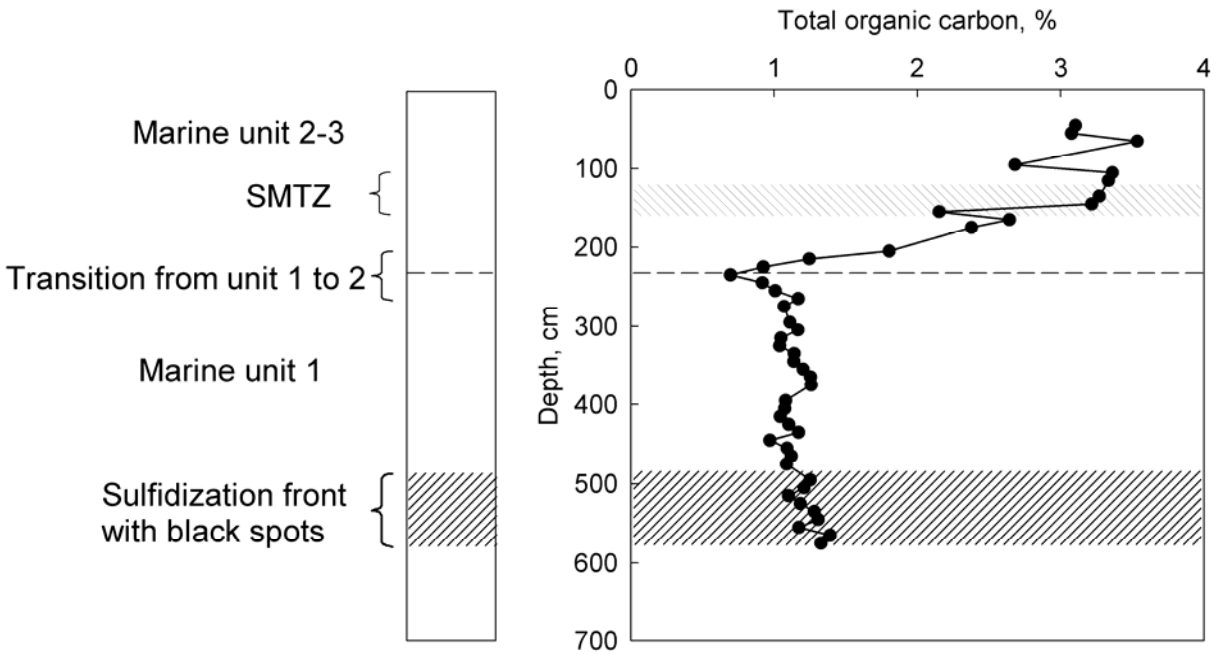
Marine unit 2-3
SMTZ
Transition from unit 1 to 2
Marine unit 1
Sulfidization front
with black spots
Total organic carbon, %
0
1
2
3
4
Depth, cm
0
100
200
300
400
500
600
700

Fig. 3

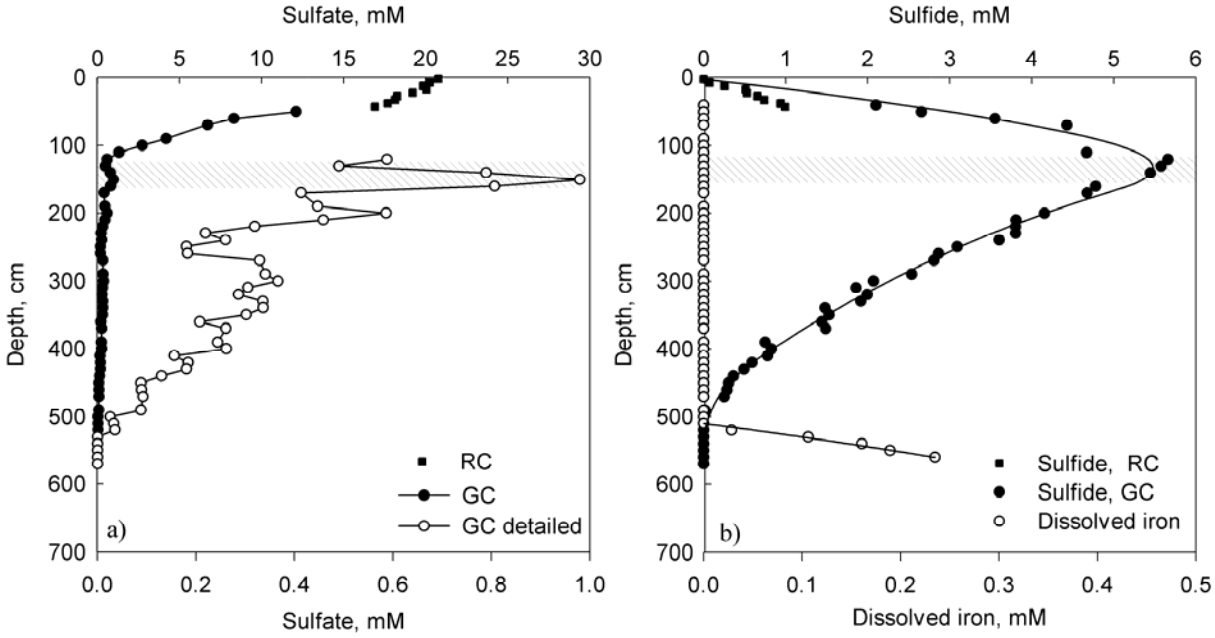
Sulfate, mM
Depth, cm
RC
GC
GC detailed
a)
Sulfide, mM
Sulfide, RC
Sulfide, GC
Dissolved iron
b)
Dissolved iron, mM

Fig. 4

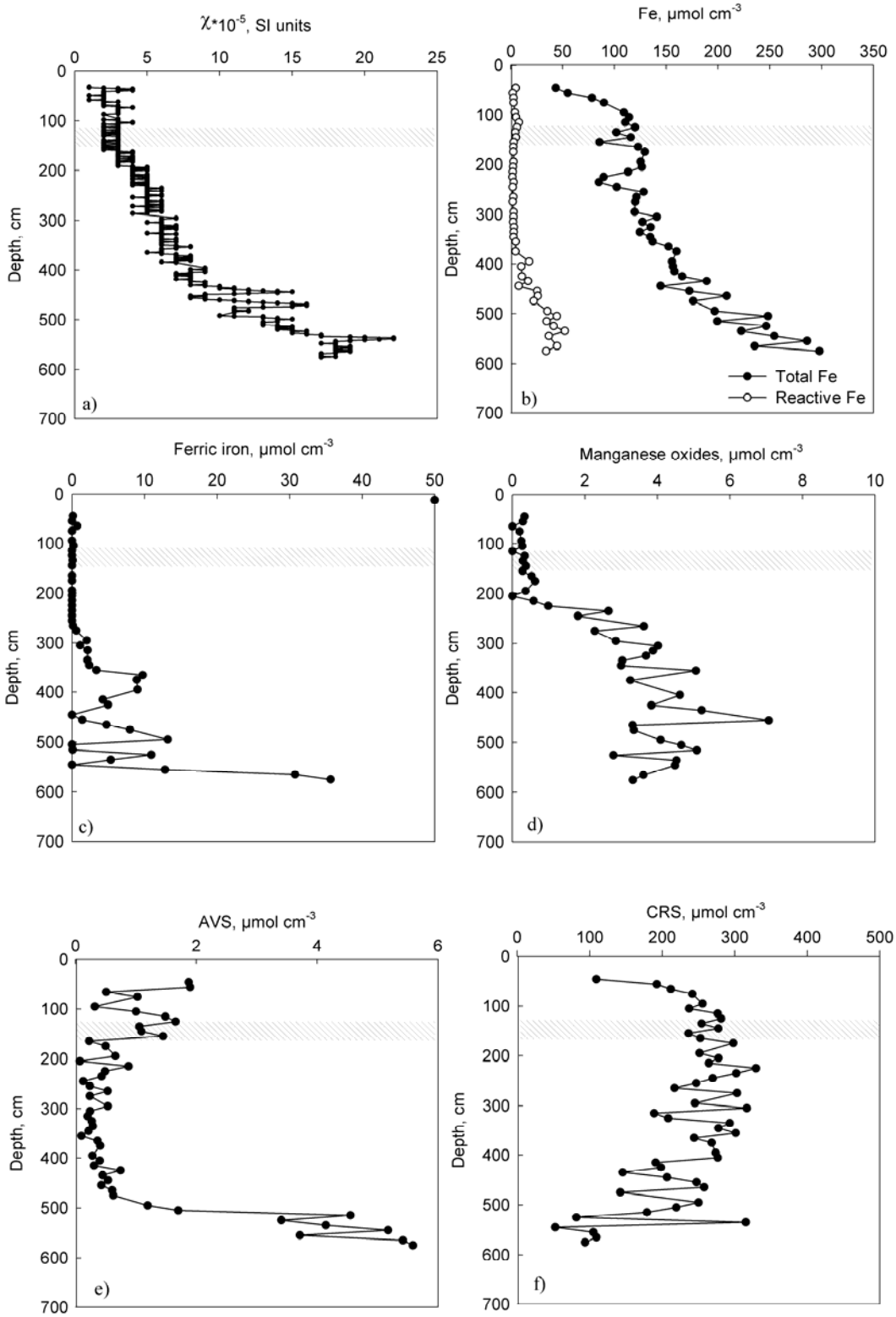
χ*10-5, SI units
Depth, cm
a)
Fe, μmol cm-3
Total Fe
Reactive Fe
b)
Ferric iron, μmol cm-3
c)
Manganese oxides, μmol cm-3
d)
AVS, μmol cm-3
e)
CRS, μmol cm-3
f)

Fig. 5

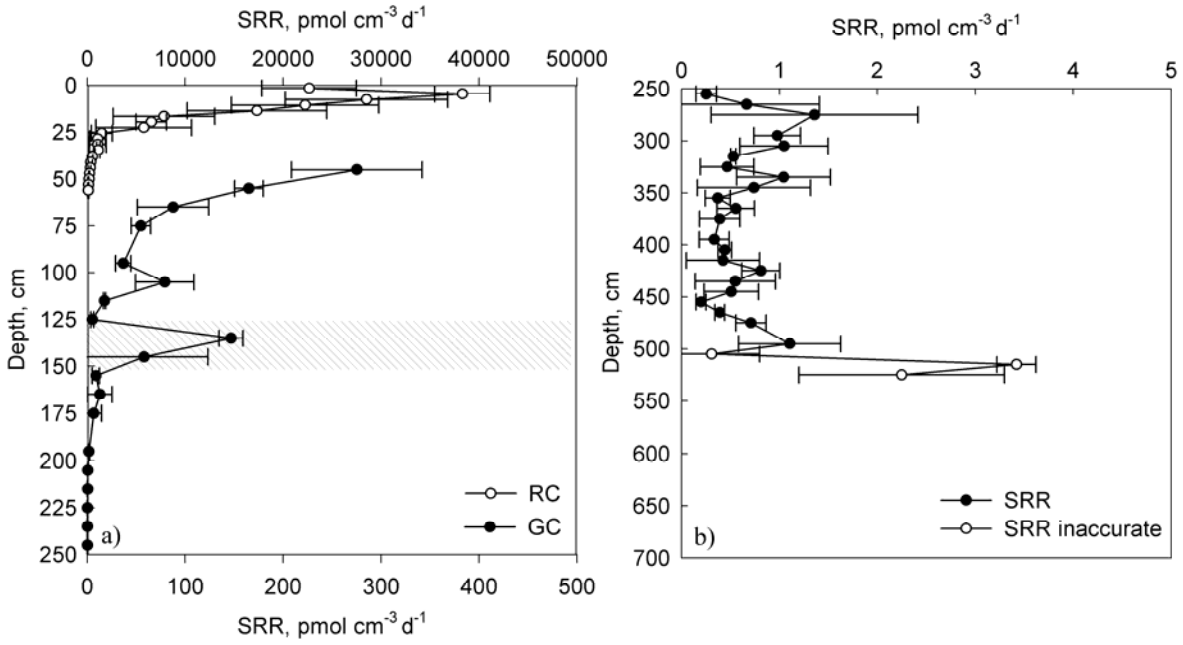
SRR, pmol cm-3 d-1
Depth, cm
RC
GC
a)
SRR, pmol cm-3 d-1
SRR
SRR inaccurate
b)

Fig.

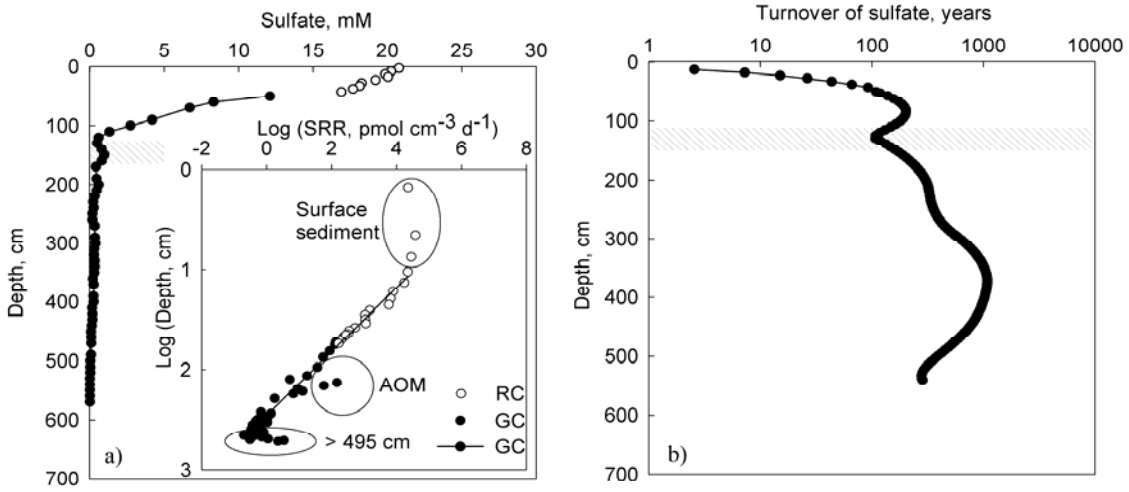
Sulfate, mM
Depth, cm
Log (SRR, pmol cm-3 d-1)
Log (Depth, cm)
Surface sediment
AOM
> 495 cm
RC
GC
GC
a)
Turnover of sulfate, years
b)

6

Fig. 7

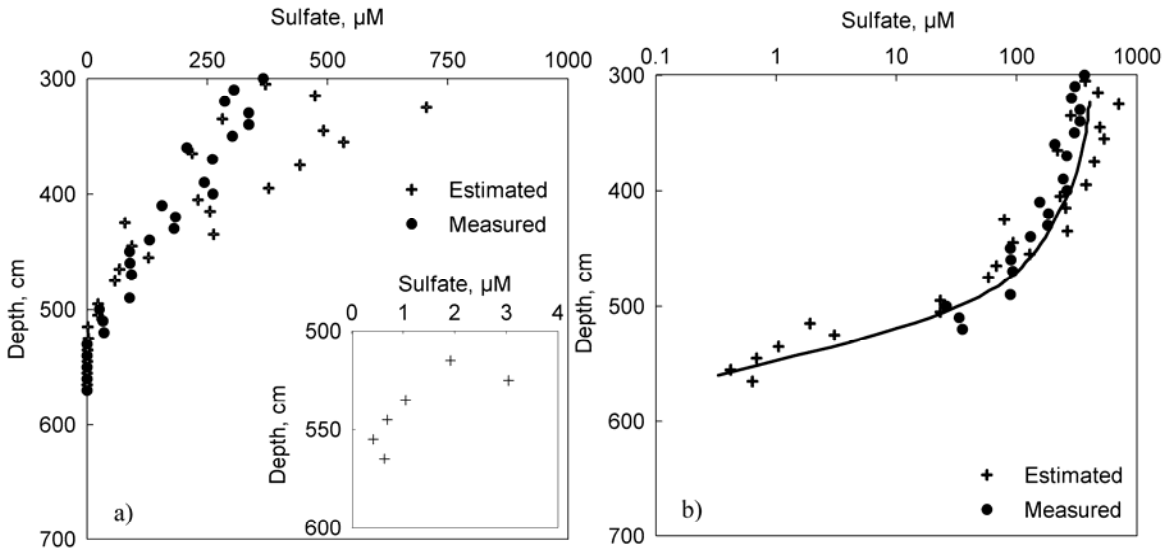
Sulfate, μM
0
250
500
750
1000
300
400
500
600
700
Depth, cm
Estimated
Measured
a)
Sulfate, μM
0
1
2
3
4
500
550
600
Depth, cm
Sulfate, μM
0.1
1
10
100
1000
300
400
500
600
700
Depth, cm
Estimated
Measured
b)

Fig. 8

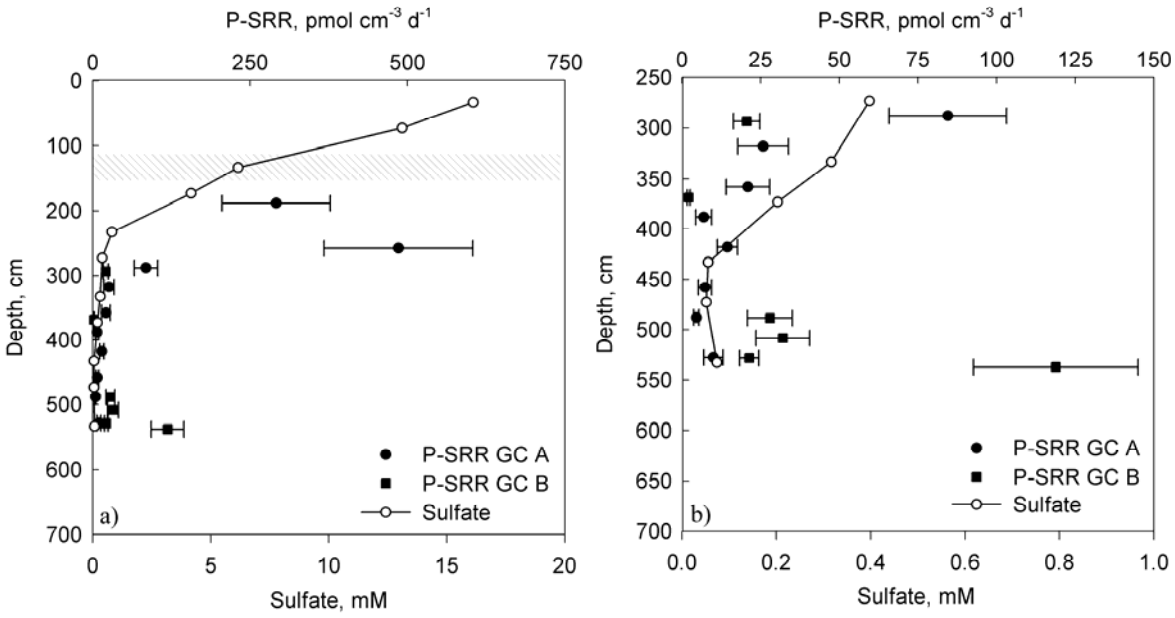
P-SRR, pmol cm-3 d-1
Depth, cm
Sulfate, mM
P-SRR GC A
P-SRR GC B
Sulfate
a)
b)

Fig. 9

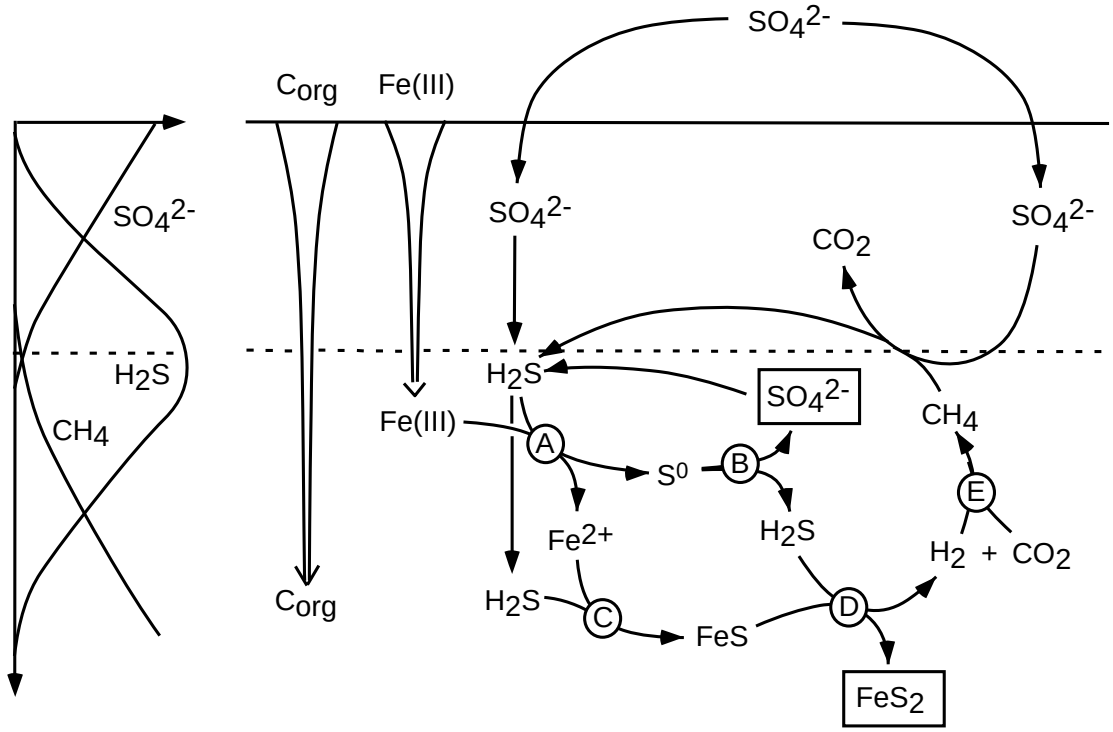
SO4 2-
Corg
Fe(III)
SO4 2-
SO4 2-
CO2
SO4 2-
H2S
CH4
H2S
SO4 2-
CH4
Fe(III)
A
S0
B
E
Fe2+
H2S
H2 + CO2
Corg
H2S
C
FeS
D
FeS2

Fig. 10

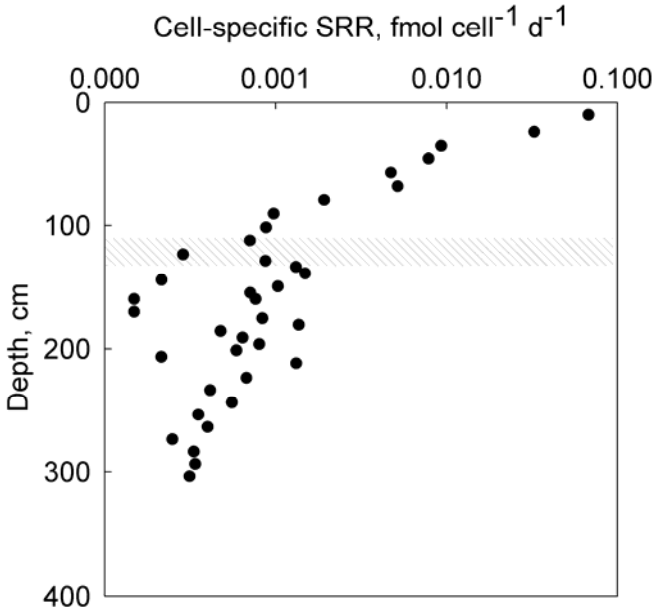
Cell-specific SRR, fmol cell^{-1} d^{-1}
0.000
0.001
0.010
0.100
0
100
200
300
400
Depth, cm

Chapter 4

Sulfur and iron diagenesis in post-glacial limnic and brackish sediments of the Arkona Basin (Baltic Sea)

Lars Holmkvist*[a], Kyriakos Vamvakopoulos[a], Alexey Kamyshny, Jr.[a,c], Volker Brüchert[a,d], Tim Ferdelman[a] and Bo Barker Jørgensen[a,e]

[a]Biogeochemisty Group, Max-Planck Institute for Marine Microbiology, Celsiusstrasse 1, 28359 Bremen, Germany

[b]Chemistry and Water Technology, Danish Technological Institute, Kongsvang Allé 29, 8000 Aarhus C, Denmark

[c]Department of Geology and Earth System Science, Interdisciplinary Center, University of Maryland, College Park, MD 20742, USA

[d]Department of Geology and Geochemistry, Stockholm University, Svante Arrhenius Väg 8c, 10691 Stockholm, Sweden

[e]Center for Geomicrobiology, Department of Biological Sciences, University of Aarhus, Ny Munkegade, Bld. 1535, 8000 Århus C, Denmark

Keywords: Sulfate reduction; iron reduction; sulfide oxidation; stable sulfur isotopes; oxygen isotopes

* Corresponding author.

E-mail address: LHT@teknologisk.dk, Tel.: +45 72 20 23 95

Abstract

Diagenetic changes of sulfur and iron species were studied across the different sedimentary units in 3-m long sediment cores from the Arkona Basin, SW Baltic Sea. Analyses of pore water profiles were combined with sedimentological and mineralogical analyses of the cores. The data show that the modern sediments of the Arkona Basin are subject to non-steady-state diffusion and diagenesis. Sulfide accumulates in the pore water of the Holocene sediment layer and diffuses down into the late glacial deposits where buried iron minerals are sulfidized and lead to the precipitation of different iron sulfide minerals. A peak in magnetic susceptibility at the sulfidization front is due to a high concentration of ≤1 mm-sized grains of greigite and other minerals embedded in a black band of the sediment. The sulfidization front of deep Fe(III) minerals and formation of pyrite are accompanied by steep gradients of free sulfide and polysulfides. Our study suggests an explanation for an unusual sulfate profile in the pore water by which high concentrations of sulfate are present within the deep limnic deposits. Oxygen and sulfur isotope data indicate that the high sulfate concentrations at depth are not due to reoxidation of reduced sulfur species but rather due to a downward diffusion of sulfate which took place during the late glacial history of the Baltic Sea and which has turned to an upwards leakage of sulfate in modern time.

1. INTRODUCTION

The reduction of pore water sulfate to sulfide by dissimilatory sulfate reduction is the dominant pathway of anaerobic organic carbon oxidation in ocean margin sediments . Sulfate reduction often leads to a pronounced overprinting of the sediment geochemistry through sulfidization of the buried minerals and of the organic material initially supplied to the seafloor. The sulfidization is driven by sulfide formed both during mineralization of buried organic matter and during anaerobic oxidation of methane diffusing up from deeper, sulfate-depleted deposits . The accumulation of sulfide in the pore water and the diffusion of sulfide down into the underlying, methanogenic sediment lead to the precipitation of iron sulfide minerals. The degree of sulfidization is, thus, generally controlled by the diffusive flux of sulfide from above and by the concentration of reactive iron in the underlying sediment layers (Neretin et al., 2004).

The distinct depth where the downward diffusing free sulfide reacts with iron species in the sediment is referred to as the diagenetic front or the sulfidization front. This horizon is often recognized as a distinct black band due to a high content of iron monosulfides and of the magnetic mineral greigite, Fe_3S_4. The formation of iron sulfide minerals (e.g. iron monosulfides, greigite, and pyrite) during sulfidization have been described in many earlier studies (Berner, 1970; Berner, 1984; Pyzik and Sommer, 1981). The general observation is that several complex oxidation processes of sulfur species occur along with the pyritization process. The downwards diffusing sulfide is ultimately bound by iron and partly oxidized when it reacts with iron oxides at the sulfidization front . The products of sulfide oxidation include different sulfur intermediates such as zero-valent sulfur (e.g. S^0 and polysulfides), thiosulfate, and sulfite (Zopfi et al., 2004), all of which may undergo disproportionation to sulfide and sulfate. Through repeated partial oxidation to S^0 and disproportionation to sulfide and sulfate, reduced sulfur species can be oxidized all the way back to sulfate in the presence of iron or manganese oxides (Aller and Rude, 1988; Burdige and Nealson,

1986; Yao and Millero, 1996). The distribution of sulfide in marine pore waters is thus strongly controlled by reactive iron species in the sediment (Canfield, 1989; Canfield et al., 1992). Disproportionation of intermediate oxidation products of sulfide is an important process in the reoxidation of sulfide to sulfate (Thamdrup et al., 1993; Thamdrup et al., 1994).

The Baltic Sea is the largest brackish water body on Earth and has three main basins (Sohlenius et al., 1996), of which the Arkona Basin is located in the southwestern part of the Baltic Sea (Fig. 1). Stratigraphic analysis of the late glacial to Holocene sediments show alternating limnic and brackish/marine deposits (Neumann, 1981). The changes in salinity are caused by the retreat of the Fennoscandian ice sheet and the changes in water-level and connection to the ocean following the last glaciation, 13 -14,000 yr BP . The sediments in the Arkona Basin have consequently been subject to non-steady-state deposition and diagenesis. In particular, changing concentrations of sulfate in the seawater since the last glaciation have strongly altered the diffusion flux and depth of sulfate penetration in the sediment. Such changes have affected the rates of sulfate reduction and the degree of sulfidization within the sediment. If a particular environmental situation was maintained for a sufficient length of time, a new steady state situation became established which may be apparent from the geochemical zonation even today.

The present study aims to understand the causes of the geochemical alterations of sulfur and iron species across the different sedimentary units within the Arkona Basin. The study combines pore water profiles and sedimentological or mineralogical analyses of sediment cores. The data suggest that the modern sediments of the Arkona Basin are subject to non-steady-state diffusion and diagenesis. We present a possible explanation for an unusual sulfate profile in the pore water by which high concentrations of sulfate is present within the deep limnic deposits. Our results indicate that the high sulfate concentrations are not due to oxidation of reduced sulfur species but rather due to downward diffusion of sulfate during the early Holocene history of the Baltic Sea.

2. MATERIAL AND METHODS

2.1. Sampling and site description

The present study is based on two gravity cores (GC A and B) taken during a research cruise of the F/S Heincke during September 8-13, 2006, as part of the EU FP5 project METROL. Cores were collected at Station "A6" (54° 59.24 ' N and 13° 39.86 ' E) in the Arkona Basin of the western Baltic Sea at a water depth of 45 m (Fig. 1). The position of this station is identical to that of Station 201311 described by Moros et al. (2002). A depth correction was made from the pore water concentration profiles of sulfate and sulfide in GC A and B. This correction demonstrated that 5-10 cm more surface sediment had been lost in GC A during gravity coring compared to GC B.

2.2. Core processing

Methane samples were taken immediately after retrieval of the first gravity core (GC A) by transferring 3 cm^3 of sediment into 20 ml serum vials with 6 ml Milli-Q water. Samples for methane were collected at 20 cm depth intervals throughout the core through small windows cut into the side of the core liner with a vibrating saw. Samples for porosity and density were similarly taken with 10 ml cut-off syringes at the same depths as methane. Rhizone soil moisture samplers (Rhizosphere Research Products, Wageningen, The Netherlands) were used for the extraction of pore water. The rhizones consists of an inert porous polymer tube with a length of 5 cm and a pore size of 0.1 µm, through which pore fluid is extracted by vacuum created with disposable 10-ml syringes connected to the Rhizone. Pore water for sulfate and sulfide measurements in GC A was extracted from the core liner windows and fixed with 2% zinc acetate. Bottom water samples were collected from separate cores taken by a multiple corer and diluted with 2% zinc acetate for later determination of sulfate and sulfide. Gravity cores and sub-samples were stored at 4°C until processed.

The cores were processed within two weeks after sampling. The GC A core was first scanned for magnetic susceptibility. Then, pore water was extracted with 10-cm long Rhizones in the GC B core by gently pushing them into predrilled holes at 5 cm depth intervals along the core. The first ~0.5 ml of extracted pore water was discarded to limit oxidation by oxygen. Pore water samples for the later determination of sulfate and sulfide were prepared by mixing ~1 ml of pore water with 250 µL 1% zinc acetate. Samples for dissolved iron were preserved by acidifying ~1 ml pore water with 100 µL 10% HCl. These samples were collected at the same depths as for sulfate and sulfide in the upper 30 cm and for every 15 cm at 30-205 cm depth. At those depths, non-acidified pore water samples were also taken for analysis of polysulfide zero-valent sulfur species (ZVS). At least 5-6 ml of pore water was required from each depth in order to detect the ZVS species. The pore water for ZVS analysis was transferred into anoxic vials immediately after extraction and analyzed within a few hours to prevent oxidation by oxygen. Solid phase sub-samples were taken from the GC B at all depths where pore water was extracted. Sediment sub-samples were collected both in plastic bags and plastic tubes containing zinc acetate (20% w/v) and immediately frozen at -20°C for later analysis of iron, sulfur and carbon.

2.3. Pore water analyses

Methane in the headspace of the 20 ml serum vials was analyzed on a gas chromatograph (5890A, Hewlett Packard) equipped with a packed stainless steel Porapak-Q column (6 feet, 0.125 inch, 80/100 mesh, Aglient Technology) and a flame ionization detector. Helium was used as a carrier gas at a flow rate of 30 ml min^{-1}. Sulfate and chloride were analysed by non-suppressed ion chromatography (100 µl injection volume, Waters, column IC-Pak^{TM}, 50 × 4.6 mm). The eluent was

1 mM isophthalate buffer in 10% methanol, adjusted to pH 4.5 with saturated Na borohydrate, and the flow rate was 1.0 ml min^{-1}. Hydrogen sulfide (H_2S and HS^-) was determined spectrophotometrically at 670 nm (Shimadzu UV 1202) on zinc-preserved pore water and bottom water samples by the methylene blue method (Cline, 1969). Dissolved iron was measured according to Stookey (1970) with Ferrozine (1 g L^{-1} in 50 mM HEPES buffer, pH 7) spectrophotometrically at 562 nm (Shimadzu UV 1202).

The analysis of zero valent sulfur (ZVS) species included solid sulfur (S_8), colloidal sulfur (S^0), polysulfides (S_n^{2-}), and polythionates ($S_nO_6^{2-}$). The pH value of each pore water sample was measured with a pH electrode before the analysis and the value was used later for ZVS concentration calculations. A newly developed protocol for detection of ZVS species was based on four steps (Kamyshny et al., 2006): (1) The detection of inorganic polysulfides by fast single-phase derivatization with methyl trifluoromethanesulfonate (Kamyshny et al., 2006), (2) detection of the sum of colloidal S^0 and polysulfide ZVS and polythionate ZVS (n>3) with hydrogen cyanide derivatization, followed by HPLC analysis of thiocyanate (Rong et al., 2005), (3) detection of the sum of polysulfide ZVS, colloidal S^0 and solid sulfur by treatment with zinc chloride followed by extraction with chloroform, and (4) the detection of polythionates (n = 4-6) by HPLC (Kamyshny et al. Submitted). The concentration of polysulfide ZVS was calculated as the sum of all ZVS species detected after derivatization with methyl triflate. The concentration of colloidal ZVS was calculated as the difference between results from the cyanolysis analysis and the concentration of polysulfide ZVS. Finally, the concentration of solid sulfur was calculated as the difference between the chloroform extraction analysis and results from the cyanolysis analysis.

2.4. Solid phase analyses

Whole-core magnetic susceptibility measurement was performed with a Bartington Instruments MS2 meter equipped with a MS2C sensor using a scan rate of 1 cm min^{-1}. The sediment density was determined as the wet weight per cm^{-3}. The pore water content was determined from the weight loss after drying at 60°C until constant weight. Total organic carbon (TOC) and total sulfur (TS) were determined in freeze dried sediment that was pretreated with HCl, dried again, and analyzed on a CNS analyzer (Fisons^{TM} Na 1500 elemental analyzer). AVS (acid volatile sulfide = dissolved sulfide + Fe monosulfide) and CRS (Cr-reducible S = FeS_2 + S^0) were determined using the two step acidic Cr-II method (Fossing and Jørgensen, 1989). The volatilized and trapped sulfide was determined spectrophotometrically at 670 nm (Shimadzu UV 1202) by the methylene blue method of Cline (1969). Total zero-valent sulfur was extracted from zinc acetate preserved sediment samples in 10 ml pure methanol on a rotary shaker for at least 16 h according to Zopfi et al. (2004). Total zero-valent sulfur was separated on an HPLC with a Zorbax ODS column (125 × 4 mm, 5 µm; Knauer, Germany) with methanol as the eluent (1 ml min^{-1}) and determined from the adsorption at 265 nm. Solid phase ferric iron (Fe(III)) was extracted from sub-samples of the frozen sediment in a 0.5 M HCl solution for 1 h on a rotary shaker. Fe(II) was determined in the supernatant of the HCl extracts by the Ferrozine method (Stookey, 1970). Fe(III) was calculated as the difference between the total iron (Fe(II) + Fe(III)), determined with Ferrozine + 1% (w(v) hydroxylamine hydrochloride), and the Fe(II). Total reactive iron in the sediment was extracted with dithionite-citrate-acetic acid according to Canfield (1989) and determined with Ferrozine + 1% (w/v hydroxylamine hydrochloride). Solid manganese oxides (Mn(IV)) were measured on the supernatant of the dithionite-extracts by flame atomic absorption spectrometry (Perkin Elmer, Atomic Absorption Spectrometer 3110).

X-ray diffraction analysis (XRD) was performed on dried and homogenized sediment samples from all investigated depths in the GC B core. XRD analysis was done on a Philips X'Pert Pro multipurpose diffractometer equipped with a Cu-tube, a fixed divergence slit of ¼°, a 16 sample changer, a secondary monochromator, and a X'Celerator detector system. The sample measurement was completed by a continuous scan from 3 – 85° 2θ, with a calculated step size of 0.016° 2θ (calculated time per step was 100 seconds). The identification of different minerals was done with the Philips software X'Pert HighScore™, which, besides the mineral identification, gives a semi-quantitative value for each identified mineral on the basis of Relative Intensity Ratio (R.I.R)-values. The R.I.R.-values were calculated as the ratio of the most intense impulse of a specific mineral to pure corundum (I/Ic) according to the "matrix-flushing method" (Chung, 1974). Finally, full quantification was done using the full-pattern quantification software QUAX (Vogt et al., 2002).

2.5. Magnetic nodules

Single magnetic nodules were collected at 68 cm sediment depth in GC B using a handheld magnet. The nodules were immediately embedded in a methacrylate resin, trimmed with a diamond band saw, and polished with an Al_2O_3 paraffin suspension. Prior to scanning electron microscopy (SEM), the surface of the polished nodules was coated with carbon to avoid charging effects. The surface morphology and texture were recorded by conventional backscattered electron and secondary electron imagery. Specific elements inside the nodules were identified using energy dispersive x-ray analysis (EDS) (Oxford INCA 300).

2.6. Sulfur and oxygen isotopes

Sulfur and oxygen isotopes in sulfate, and sulfur isotopes in free and acid volatile sulfide and pyrite were determined on the zinc acetate preserved pore water samples and on the CRS fraction of GC B using a Thermo Delta Plus isotope ratio mass spectrometer coupled to a Eurovector elemental analyzer via a Conflo II interface. Pore water sulfate was precipitated as barium sulfate by the addition of 5% barium chloride solution. The barium sulfate precipitate was collected by filtration through a 0.45 µm HA-filter and the precipitate was combusted to sulfur dioxide, catalyzed by vanadium oxide. Zinc sulfide (ZnS) obtained from AVS and CRS distillation and porewater dissolved sulfide was filtered through a 45 µm HA-filter. The filters were immersed overnight in a 5% silver nitrate solution to convert ZnS to Ag_2S. The precipitate was dried at 35°C, mixed with a fivefold excess of vanadium pentoxide and analyzed on the mass spectrometer as described above. The isotope composition is reported in the standard delta notation relative to Vienna Canyon Diablo Troilite (VCDT). Precision and accuracy were tested by running two internal lab standards of precipitated North Sea seawater ($\delta^{34}S$ = 21.0‰ vs. VCDT and IAEA Standard S2 after every 10^{th} sample. Precision of replicate analyses was ± 0.4‰.

2.7. Modelling of pore water data

The modelling software, PROFILE, of Berg et al. (1998) was applied to the measured pore water data to calculate net rates of production or consumption of dissolved sulfide and dissolved iron. This one-dimensional numerical modelling program first divides the sediment into an arbitrary number of equidistant zones, each with a constant process rate, whereby an objective selection of the simplest process rate distribution that optimally reproduces the measured concentration profiles is provided. The criterion for optimal fit is to minimize the sum of squared deviations (SSE) from the data for each zone with different numbers of equally spaced zones. The model provides F tests

for different fits and suggests the minimal number of zones that provide an optimal fit. The model ensures continuity between zones and thus provides also fluxes of the solutes. The boundary conditions were:

Sulfide (H_2S+HS^-): Boundary conditions were concentration at 67.5 cm = 0.00 mM and flux at 67.5 cm = 0.00 mmol m^{-2} d^{-1}. The molecular diffusion coefficient, $D(H_2S/HS^-) = 11.9 \times 10^{-6}$ cm^2 s^{-1}, was calculated from the degree of dissociation at a pH of 7.4.

Iron (Fe^{2+}): Boundary conditions were concentration at 52.5 cm = 0.00 mM and concentration at 257.5 cm = 0.346 mM. The molecular diffusion coefficient was: $D(Fe^{2+}) = 4.26 \times 10^{-6}$ cm^2 s^{-1}.

3. RESULTS

Four sedimentary units were identified between the surface and 3 m depth according to color, sand layers, and other parameters. The different sediment layers are here described as Units I to IV in accordance with the stratigraphy described from the central Baltic Sea by Böttcher and Lepland and from the southern Baltic Sea by Moros et al. (2002) (Fig. 2).

Unit I: 285 - 78 cm depth. The Baltic Ice Lake, deposited >11,600 cal yr BP. Lacustrine reddish-brown clay with a sand layer at 130 cm depth which probably marks the Billingen-1 drainage (Moros et al., 2002). TOC values were <1 wt % with high values of total inorganic carbon (TIC) increasing with depth (Moros et al., 2002) (data not shown).

Unit II: 78 - 70 cm depth. The Yoldia Sea and Yoldia Lake, deposited ca. 11,600 to 10,600 cal yr BP. Lacustrine/brackish reddish-brown clay with a thick sand layer at 78 cm which probably marks the transition from the Yoldia Lake to the Baltic Ice Lake (Billingen-2 drainage) (Moros et al., 2002). TOC values were 0.7 wt %.

Unit III: 70 - 45 cm depth. From the Ancylus Lake, deposited ca 10,600 - 6,500 cal yr BP. Greyish lacustrine clay with a sand layer at 70 cm depth which probably marks the transition from the Ancylus to the Yoldia Lake, reddish-brown clay at 70 - 68 cm depth, and black spots at 68 - 45 cm depth. Magnetic nodules of sub-mm to mm size were observed at the boundary between grey and reddish-brown sediment at 68 cm. TOC values were 0.6 - 2 wt %.

Unit IV: 45 - 0 cm depth. Holocene mud from the modern Littorina period, 6,500 – 0 cal yr BP. Marine/brackish olive-black mud with a strong smell of sulfide. TOC values were 3-6 wt %.

3.1. Geochemistry of carbon, sulfur and iron

Total organic carbon was high, 5-6% dry weight, in the most recent Holocene mud and decreased with depth to reach a constant low level of ca 0.7% from the lower part of Unit III (Fig. 2). TS was around 2% dry weight in Unit IV and decreased to <0.2% from the lower part of Unit III.

The sulfate concentration showed an unusual distribution as it decreased from 13 mM in the brackish bottom water to a minimum of 4 mM at 22-28 cm depth below which it increased steadily to 6-7 mM at 250 cm (Fig. 3a). The concentration of chloride dropped steeply from 318 mM in the bottom water to around 250 mM throughout the subsurface sediment (Fig. 3a). Free sulfide was present from the sediment surface to the bottom of Unit III with maximum concentrations of 1 mM (Fig. 3b). Dissolved iron was not detected in the sulfide zone but increased from the bottom of this zone at the grayish to reddish-brown sediment transition in Unit III (Fig. 3b). Dissolved iron reached 300 - 400 μM within the non-sulfidized limnic sediment of Unit I. The concentration of methane varied around 5 μM with no clear depth trend and did not exceed 10 μM at any depth (data not shown).

Modeling of the pore water sulfide and iron profiles provided estimates of the depth-integrated net production or consumption of sulfide and dissolved iron (Fig. 3b). According to the modeled solute distributions, production of sulfide took place in the 0-22 and 22-45 cm depth intervals at depth-integrated rates of 0.49 and 0.22 mmol m^{-2} d^{-1}, respectively (data not shown). A net consumption of sulfide of 0.22 mmol m^{-2} d-1 was estimated for the 45-67 cm depth interval. The total production of dissolved iron in the 52-250 cm depth interval was estimated to 0.0054 mmol m^{-2} d^{-1} and the total flux up to 52 cm was -0.0058 mmol m^{-2} d^{-1} (data not shown). A comparison of the flux estimates for sulfide and dissolved iron showed that the downwards flux of sulfide towards the sulfidization front (Unit III) was 35-fold higher than the upwards flux of dissolved iron. Dissolved

manganese increased slightly with depth but remained <30 μM throughout the core, except for a stray high value at 57 cm (data not shown).

The highest concentrations of individual polysulfide ZVS species occurred in Unit IV (Fig. 3c). Relative concentrations of individual polysulfides followed the pattern described by Kamyshny et al. (2004; 2007) for polysulfide solutions at equilibrium with S^0 under moderately alkaline conditions, ($[S_5^{2-}]>[S_6^{2-}]\geq[S_4^{2-}]>[S_7^{2-}]$). The sum of all the polysulfide ZVS species resulted in a peak concentration of 71 μM at 12.5 cm depth (Fig. 3d) which largely matched the depth profile of sulfide. This implies that polysulfide ZVS species were in equilibrium with sulfide in the pore water (Kamyshny et al., 2003).

The magnetic susceptibility was low in the highly sulfidic Unit IV and increased with depth to reach a high and distinct peak of 76×10^{-5} SI at the transition between Unit III and II (Fig. 4a). This peak was due to ≤1 mm size magnetic nodules which were abundant at the transition from gray to reddish-brown sediment at 68 cm depth. The magnetic susceptibility was relatively high, 25-30 × 10^{-5} SI, throughout the iron-rich, orange to brown colored limnic sediment of Unit I.

Total reactive iron was low, ca 100 μmol cm^{-3}, in the brackish sediment of Units IV and III and increased to nearly 1000 μmol cm^{-3} in the limnic Unit I (Fig. 4b). Total Fe(III) determined by HCl extraction was also low in Unit IV and increased down through Unit III (Fig. 4c). The concentration of Mn(IV) was low throughout Units IV to II and higher in Unit I (Fig. 4d).

The AVS concentration dropped steeply with depth from 4 μmol cm^{-3} at the sediment surface to 0.1 μmol cm^{-3} at 22 cm depth. It remained low through the rest of the core with the exception of a sharp peak at the bottom of Unit III (Fig. 4e). High concentrations of chromium reducible sulfur (CRS, mainly FeS_2) were found in Units IV and III (Fig. 4e). CRS was low through most of Units II and I with elevated values in the upper part of Unit I. The concentration of total zero-valent sulfur decreased from 0.6 to 0.1 μmol cm^{-3} between the sediment surface and 25 cm depth (Fig. 4f). There

was a second large peak in total zero-valent sulfur within Unit III with a maximum concentration of 0.8 μmol cm^{-3}. In Unit I the concentration of total zero-valent sulfur did not exceed 0.05 μmol cm^{-3}.

3.2. Magnetic nodules

Magnetic nodules, extracted by a magnet, were found in the transition of gray to reddish-brown sediment (Unit III to II) where also a sharp peak of magnetic susceptibility was detected. The nodules had circular, elliptical, or irregular elongated shapes and varied in size from a few tens of μm to several mm across. Surface scans of whole, intact nodules with SEM revealed that some nodules were covered by framboidal pyrite. The EDS analyses showed that the interior of the magnetic nodules was heterogeneous and contained iron, sulfur, silicate, barium, aluminum and magnesium. Furthermore, traces of potassium, calcium, manganese and phosphorus were found. From the ratios of sulfur and iron we were able to identify iron monosulfide (FeS), greigite (Fe_3S_4) and pyrite (FeS_2) in most of the nodules. Furthermore, we were able to identify five different types of mineral associations in the magnetic nodules: (1) nodules that consisted of mostly iron and sulfur minerals such as Fe_3S_4 and FeS_2 (Fig. 5a), (2) nodules containing iron sulfide minerals in close association with large silicate minerals (data not shown), (3) barite nodules with silicate enclosures (Fig. 5b), (4) iron sulfide nodules composed of minor granules (Fig. 5c-d), and (5) iron sulfide nodules that contained crystal-like structures of sulfur (Fig. 5e-h).

3.3. X-ray diffraction

XRD analyses were done to describe the most abundant minerals, in particular those containing Fe(III). The largest heterogeneity and the highest diversity of minerals were found in Unit III. In Unit IV, on the contrary, the number of different minerals was lowest. Silicate containing minerals such as quartz (subclass tectosilicate) and albite (feldspar) were the most

abundant minerals in nearly all of the investigated sediment samples. FeS_2 was detected only in Units IV and III whereas different types of Fe(III) containing silicates were found in Units I-III. For example, Fe(III)-bearing phyllosilicates such as illite, clinochlore, zinnwaldite and licate were found together with inosilicates such as magnesio-arfvedsonite, hastingsite and riebeckite in Unit III. Only the Fe(III) containing phyllosilicates, clinochlore and cronstedtiteesides, were found in Units I-II. Other interesting Fe(III)-bearing minerals, such as the hydrated phosphates, koninckite and beraunite, were observed in Units I-II.

3.4. Stable sulfur and oxygen isotopes

Fig. 6a-d presents results from the analyses of sulfur and oxygen isotopes. The bottom water value of $\delta^{34}S_{sulfate}$ was +21‰ (Fig. 6a), similar to the mean value of modern seawater. The pore water values of $\delta^{34}S_{sulfate}$ increased sharply just below the sediment surface where the first pore water value at 17 cm was +69‰ (Fig. 6a). There was a broad maximum of $\delta^{34}S_{sulfate}$ which extended from Unit IV to I with highest values of +74‰. Below this peak, $\delta^{34}S_{sulfate}$ decreased gradually to ca +50‰ at the bottom of the core.

The bottom water $\delta^{18}O_{sulfate}$ was +9‰, comparable to the mean value of modern seawater (Blake et al., 2006) (Fig. 6b). There was a steep subsurface increase in the pore water value of $\delta^{18}O_{sulfate}$ to 22‰ at 17 cm depth. The pore water $\delta^{18}O_{sulfate}$ remained between +22 and +24‰ throughout the rest of the core. However, a few of the data points within Unit II to III were very low, +5 to +8‰, probably due to contamination from water bound in clay or salt minerals accompanying the $BaSO_4$ precipitate. The isotopic signature of dissolved sulfide could be measured only in Unit IV (Fig. 6c). The $\delta^{34}S_{sulfide}$ increased steadily from -3 to +2‰ between 5 and 40 cm depth (Fig. 6c). The $\delta^{34}S_{CRS}$ decreased from -29 to -40‰ between 2 and 42 cm depth in Unit IV and

then increased from -40 to -11‰ through Unit III at 42 to 62 cm (Fig. 6d). In Unit I the $\delta^{34}S_{CRS}$ decreased slightly to ca -20‰.

4. DISCUSSION

4.1. Sulfate reduction

Sulfate reduction took place at high rates in the Holocene mud of Unit IV as indicated by the sharp decrease in pore water sulfate just below the sediment surface and by the broad peak in free sulfide (Fig. 3a-b). The high sulfate reduction rates implied for Unit IV are consistent with the high organic carbon concentration (Fig. 2). They are also consistent with high sulfate reduction rates measured experimentally with $^{35}SO_4^{2-}$ tracer in similar sediments from other areas of the Baltic Sea (Knab et al., 2008; Thamdrup et al., 1994).

The steep drop in the concentrations of sulfate near the sediment surface is accompanied by a drop in chloride. Yet, the sulfate/chloride ratio also showed a steep decrease, from 0.033 to 0.020 molar ratios over the top 10 cm depth interval (data not shown). This corresponds to a 40% depletion of the pore water sulfate relative to Baltic Seawater concentration and demonstrates that sulfate is being consumed by sulfate reduction in addition to the dilution with low-salinity pore water. Below 5 cm depth, chloride remained constant down to 250 cm depth. The sulfate concentration as well as the sulfate/chloride ratio increased again very gradually below a minimum in Unit IV. This indicates that sulfate reduction rates are low below Unit IV and that sulfate diffuses upwards from higher concentrations in Unit I.

A previous study in the Arkona Basin showed similarly that the concentration of sulfate in the pore water increases with depth from Unit III to Unit I (Thiessen, 2005). This increase was explained as the result of a) seawater contamination, b) sulfide oxidation during coring, sampling and storage, or c) in situ oxidation of downward diffusing sulfide. We have here observed a similar unusual sulfate profile after careful handling of two independent gravity cores and are confident that we can at least exclude the two first explanations. We propose that the sulfate profiles are correct and are due to, d) the glacial to post-glacial history of salinity, sedimentation, and sulfate reduction.

During the late-glacial melting period large amounts of organic-poor silt and clay were deposited in the Baltic Ice Lake (Unit I). The first intrusion of seawater into the Baltic occurred during the Yoldia Sea stage (10.0-9.5 kyr BP) where the salinity reached ~10‰ . At that time, the activity of sulfate reduction within the limnic Yoldia and Baltic Ice Lake sediments was probably very low due to the low organic content and thus allowed diffusion of sulfate deep down into the sediment. The barite nodules observed in our study suggest that sulfate precipitation with barium in the downwards progressing sulfate front may have occurred at some time during this stage. Only after the deposition of organic-rich mud in the Littorina sediment started about 6,500 cal yr BP, sulfate reduction also gradually increased as a result of the higher sedimentation of organic detritus and the higher sulfate concentration of the water column. Sulfate may have continued to diffuse down into the deep late-glacial deposits during the early Littorina stage, however, because the Holocene layer was still too thin to deplete sulfate to a minimum lower than the concentration deeper in the sediment. Only much later did the Unit IV mud grow to a thickness that reversed the sulfate gradient and led to the upwards flux of sulfate which is observed today.

4.2. Iron reduction and iron minerals

While Unit IV is dominated by sulfate reduction, the presence of active iron reduction below Unit III is indicated by the accumulation of dissolved iron (Fig. 3b). Our data show the presence of reducible iron oxides which may be used by the iron-reducing bacterial communities. Thus, the concentrations of reactive iron and Fe(III) increased strongly with depth from the bottom of Unit III and down through units II and I (Fig. 4b-d). These iron species probably entered the Baltic Sea during the erosion of different glacial source deposits and via river discharge (Gingele and Leipe, 1997). The reddish-brown color of the sediment below 68 cm indicates the presence of hematite (Moros et al., 2002). The high concentration of reactive iron extracted below Unit IV (Fig. 4b),

accordingly, suggests the presence of goethite and hematite. Both of these iron minerals are extracted with dithionite (Canfield, 1988; Kostka and Luther, 1994), whereas easily reducible iron oxides (e.g. ferihydrite) are mainly extracted with HCl (Chou and Zhou, 1983; Kostka and Luther, 1994). The XRD analysis also revealed the presence of Fe(III)-bearing minerals within Units I-III but indicated, on the other hand, that the content of hematite is low in all sediment units (it should be taken into account that only minerals of high concentration are likely to be detected with the XRD probe).

4.3. Sulfur and oxygen isotopes

The isotopic composition of sulfate, $\delta^{34}S_{sulfate}$, was a mirror image of the sulfate concentration and supported the conclusion that the sulfate minimum in Unit IV is due to ongoing bacterial sulfate reduction (Fig. 6a). The $\delta^{34}S_{sulfate}$ maximum of +74‰ at 25 cm depth is extremely high considering that only 40% of the sulfate was depleted due to sulfate reduction. The $\delta^{34}S_{sulfide}$ increased only slightly, from -3 to +2‰, down through Unit IV (Fig. 6b) and, thus, the isotopic difference between coexisting sulfate and sulfide reached 72‰ at the bottom of Unit IV. This strongly exceeds the isotopic fractionation observed during sulfate reduction in pure cultures (Detmers et al., 2001) and is also in the high range of values observed in most near-surface marine sediments. The strong fractionation occurs here in sediment with high sulfate reduction rates and high sulfide concentration, both of which are generally associated with less sulfur isotope fractionation (Habicht and Canfield, 1997). We propose that the large isotopic difference between sulfate and free sulfide may be a result of sulfide reoxidation due to reaction with the large amounts of buried Fe(III). When this reoxidation is coupled to disproportionation of elemental sulfur or other intermediate oxidation products, an additional isotopic fractionation may occur (Canfield and Thamdrup, 1994).

The high $\delta^{34}S_{sulfate}$ values were not the result of anaerobic oxidation of methane , because the sulfate concentration did not drop below 40% of the relative seawater value, and methane concentrations remained low, around 5 μM. The gradual decrease in $\delta^{34}S_{sulfate}$ below the peak and down through units III to I is probably due to a passive diffusion equilibration between the sulfate minimum in Unit IV and the deeper sulfate reservoir with a $\delta^{34}S_{sulfate}$ near that of seawater. In spite of the relatively low degree of sulfate depletion, the oxygen isotope composition in sulfate indicated strong enrichment of ^{18}O in the sulfate. At the sediment surface the $\delta^{18}O_{sulfate}$ was 9.5‰, typical for seawater sulfate. From 20 cm and downwards, $\delta^{18}O_{sulfate}$ values were around 23‰, i.e. 13‰ more positive than in sulfate of the overlying seawater (Fig. 6b). This indicates that the sulfate pool has undergone significant bacterial sulfate reduction, both within the Holocene mud of Unit IV and in the deep limnic deposit of Unit I (Böttcher and Lepland, 2000; Brunner et al., 2005). A number of data points dropped out from this trend, probably due to oxygen-containing impurities in the precipitated $BaSO_4$.

The $\delta^{34}S_{CRS}$ data in units I, II, and III are more difficult to interpret in terms of an active involvement of pyrite in recent sulfur cycling. The $\delta^{34}S$ data from the deeper units are better explained as the product of sulfur diagenesis during the deposition of these units. The $\delta^{34}S_{CRS}$ decreased down through Unit IV, from -29 to -41‰, and must have been formed from sulfide more depleted in ^{34}S than the present pore water sulfide of -3 to +2‰. The decrease in $\delta^{34}S_{CRS}$ down through Unit IV could be due to a higher degree of in situ sulfide reoxidation and disproportionation as the early Holocene mud layer was thinner and less sulfidic. Alternatively, the Arkona Basin could have been less eutrophic and affected by dysoxia in the past. A stronger bioirrigation of the pore water by a richer bottom fauna may thereby have prevented the strong ^{34}S-enrichment in sulfate and resulted in isotopically lighter sulfide. Down through Unit III, where the modern sulfidization front is located, there is apparently a transition from the marine pyrite formed under

excess sulfate and highly depleted in ^{34}S, to the limnic sulfide in Unit I, formed under sulfate limitation during the late-glacial period and therefore less depleted in ^{34}S. A study by Böttcher and Lepland from the central Baltic Sea observed a similar increase in the $\delta^{34}S$ values of total sulfur (mainly pyrite) within Unit III. This increase was explained by mixing of downward diffusing sulfur species with initial, syngenetic sulfur in Ancylus Lake sediments or by a reservoir effect. The modest depletion of sulfate observed in our study seems, however, to exclude a reservoir effect as the cause for the increase in $\delta^{34}S$ values of the CRS.

4.4. Sulfidization and formation of iron sulfide minerals

The color change from gray to reddish-brown within Unit III is likely the result of progressing diagenesis rather than a change in the quality of the deposited sediment (Moros et al., 2002). The color change marks the lower boundary of the downward diffusing sulfide which is produced within Unit IV and reacts with dissolved iron and iron minerals in the underlying sediment. At this sulfidization front a band of greigite (Fe_3S_4) nodules occurs, coinciding with a sharp peak in FeS (Fig. 4e). It also coincides with the steepest gradient in FeS_2. Since the rate of FeS_2 accumulation is the product of its gradient and the sedimentation rate, this is also the depth where the highest rate of pyritization takes place. The strong shift towards ^{34}S-enrichment of CRS at this depth also supports this interpretation. The greigite is probably an intermediate in the sequence of reactions that lead from FeS to FeS_2. Earlier studies have shown that Fe_3S_4 formation in marine sediments is favoured by a high concentration of reactive iron and low organic matter content (Kao et al., 2004). Besides, a study by Wang and Morse (1995) showed that formation of pyrite in the laboratory under conditions approximating those in anoxic sediments was most rapid in the presence of Fe_3S_4. At the sulfidization front the conditions of high iron and low sulfide are

combined with high fluxes of both iron and sulfide. Yet, at the sulfidization front free sulfide and free iron in the pore water meet and react at very low concentration (Fig. 3b).

The SEM and EDS analyses have helped us identify the micro-textures and mineral types within the magnetic nodules containing Fe_3S_4. Our study shows that greigite rather than magnetite is the main mineral responsible for the peak in magnetic susceptibility, a phenomenon often observed in marine sediments (Neretin et al., 2004). The content of Fe_3S_4 in each nodule was not quantified but scans of several nodules indicated that Fe_3S_4 makes up only a minor fraction of the total amount of minerals present in each nodule. This is in accordance with Roberts and Weaver (2005), who found that Fe_3S_4 is often associated with a range of different authigenic and detrital mineral phases such as nodular and framboidal FeS_2, detrital sheet silicates, authigenic clays (smectite and illite), siderite, and gypsum. We found that Fe_3S_4 within each nodule was associated mainly with different iron and sulfur minerals (e.g. S^0, FeS and FeS_2). This finding also suggest that Fe_3S_4 may be formed during pyrite formation in the reaction sequence from FeS to FeS_2 as proposed in several earlier studies (Berner, 1967; Berner, 1970; Berner, 1984; Sweeney and Kaplan, 1973).

The pathways of conversion of metastable FeS (the AVS fraction) into FeS_2 are still largely unresolved and have been the subject of a number of studies in which several transformation reactions were proposed (Rickard and Morse, 2005). The equilibrium of polysulfides with sulfide and solid sulfur has been investigated intensively over the past 50 years (Giggenbach, 1972; Maronny, 1959; Teder, 1971; Wagman et al., 1968). However, no other studies have, to our knowledge, compared depth profiles of individual polysulfides with the distribution of FeS_2 in marine sediment. The decrease in the concentration of polysulfides and the increase in FeS and FeS_2 within Unit III, suggest that FeS_2 formation occurs by reaction with polysulfides as first proposed by Berner (1970) and Luther (1991). The calculated fluxes of sulfide and dissolved iron obtained

from the PROFILE modelling showed that the downward flux of sulfide within the sulfidization front (Unit III) was much larger than the upward flux of dissolved iron.

The formation of FeS (mackinawite) from aqueous solutions of dissolved iron and sulfide at low temperatures is well-known and described by Rickard (1995). Presumably, FeS formation in the Arkona Basin occurs both when sulfide and dissolved iron react in a 1:1 stoichiometry and when solid phase iron is reduced by reaction with free sulfide. Indeed, our model calculations indicate that a large part of the sulfide reacts with solid phase iron minerals rather than with dissolved iron.

Our data show the existence of FeS_2 deep within the limnic sediment, especially in the 72.5 to 142.5 cm depth interval of Unit I-II. Presumably, the formation of FeS_2 within the different sediment deposits of the Arkona Basin has varied since the early history of the Baltic Sea under changing biogeochemical conditions. For instance, the inflow of more saline water over the limnic sediment deposits during the Yoldia Sea stage could have caused elevated rates of sulfate reduction and thereby a higher production FeS_2 if organic carbon was available.

4.5. Oxidation of sulfur species

The present study demonstrates that much of the sulfide oxidation in this Baltic Sea sediment takes place sub-surface, below the oxic and oxidized surface zones. A similar observation was made by Böttcher and Lepland from a study in the central Baltic Sea. Fe(III) and Mn(IV) below Unit IV most probably constitute an efficient barrier which oxidizes and binds the downward diffusing sulfide. The increasing content of reactive iron and Fe(III) within the Ancylus sediment layer (Unit III) is not only due to a change in the deposition of iron minerals during the late glacial to Holocene but is rather a diagenetic overprinting as Fe(III) is converted to pyrite when it reacts with sulfide from the organic-rich Holocene mud. The high concentration of total zero-valent sulfur is most likely the result of sulfide oxidation as earlier studies have shown that sulfide oxidation with Fe(III)

and Mn(IV) leads to the production of elemental S^0 (Burdige and Nealson, 1986; Pyzik and Sommer, 1981; Steudel, 1996; Yao and Millero, 1996). Also the oxidation of FeS and FeS_2 with Fe(III) and/or Mn(IV) may lead to the production of S^0 (Aller and Rude, 1988; Moses et al., 1987; Schippers and Jørgensen, 2001). The oxidation of FeS_2 by Mn(IV) apparently involves a Fe^{2+}/Fe^{3+} - shuttle between the mineral surfaces of FeS_2 and manganese oxide (Schippers and Jørgensen, 2001). In the Arkona Basin, Fe(III) is probably the most important oxidant for sulfide since the concentration of Fe(III) is up to 30-fold larger than that of Mn(IV). Yet, the high concentration of dissolved manganese in Unit III suggests that also Mn(IV) is involved in the oxidation/reduction reactions. S^0 and other intermediates of sulfide oxidation may be oxidized all the way back to sulfate through disproportionation reactions, thereby enabling an internal sulfur cycle within the sediment.

5. SUMMARY

Our data show that the sediment biogeochemistry in the Arkona Basin has been subject to non-steady-state processes. In particular, changing concentrations of sulfate in the seawater since the last glaciation may have altered the diffusion flux and depth of sulfate penetration into the sediment. We propose an explanation for the unusual sulfate profile in the pore water by which high concentrations of sulfate is present within the deep limnic deposits. Our study indicates that the deep high sulfate concentrations are not due to oxidation of reduced sulfur species but rather due to downward diffusion of sulfate during the early Holocene history of the Baltic Sea. The increase in reactive iron and Fe(III) together with the distinct peak in total zero-valent sulfur within the Ancylus sediment layer (Unit III) suggest that reoxidation of different sulfur species (H_2S, FeS and FeS_2) occurs across this sediment unit in the Arkona Basin.

ACKNOWLEDGEMENTS

We thank Martina Meyer, Thomas Max, Andrea Schipper, Kirsten Imhoff and Antje Vossmeyer for helpful assistance in the laboratory with mass spectrometry and geochemical analyses of sulfur speciation. We are grateful to Christoph Vogt from the Department of Geology at the University of Bremen (Germany) for stimulating discussions and for help with the XRD analyses. We thank Benjamin Brunner at the MPI in Bremen for helpful discussions on the isotope data. Finally, we would like to thank the captain and crew of the F/S Heincke for a successful expedition. This study was financially supported by the Max Planck Society.

REFERENCES

Aller R. C. and Rude P. D. (1988) Complete oxidation of solid phase sulfides by manganese and bacteria in anoxic marine sediments. *Geochim Cosmochim Ac* **52**, 751-765.

Berg P., Risgaard-Petersen N., and Rysgaard S. (1998) Interpretation of measured concentration profiles in sediment pore water. *Limnol Oceanogr* **43**, 1500-1510.

Berner R. A. (1967) Thermodynamic stability of sedimentary iron sulfides. *Amer. J. Sci.* **265**, 773-785.

Berner R. A. (1970) Sedimentary pyrite formation. *Amer. J. Sci.* **268**, 1-23.

Berner R. A. (1984) Sedimentary pyrite formation: An update. *Geochim Cosmochim Ac* **48**, 605-615.

Blake R. E., Surkov A. V., Böttcher M. E., Ferdelman T. G., and Jørgensen B. B. (2006) Oxygen isotope composition of dissolved sulfate in deep-sea sediments: Eastern equatorial Pacific Ocean. In Oxygen isotope composition of dissolved sulfate in deep-sea sediments: Eastern equatorial Pacific Ocean (ed. B. B. Jørgensen, S. D´Hondt, and D. J. Miller).(Also available at http://www-odp.tamu.edu/publications) *Ocean Drilling Program* pp.1-24.

Böttcher M. E. and Lepland A. (2000) Biogeochemistry of sulfur in a sediment core from the west-central Baltic Sea: Evidence from stable isotopes and pyrite textures. *J Marine Syst* **25**, 299-312.

Brunner B., Bernasconi S. M., Kleikemper J., and Schroth M. H. (2005) A model for oxygen and sulfur isotope fractionation in sulfate during bacterial sulfate reduction processes. *Geochim Cosmochim Acta* **69**, 4773-4785.

Burdige D. J. and Nealson K. H. (1986) Chemical and microbiological studies of sulfide-mediated manganese reduction. *Geochemical J.* **4**, 361-387.

Canfield D. E. (1988) Sulfate reduction and the diagenesis of iron in anoxic marine sediments. Ph.D. Thesis, Yale University.

Canfield D. E. (1989) Reactive iron in marine sediments. *Geochim Cosmochim Acta* **53**, 619-632.

Canfield D. E., Raiswell R., and Bottrell S. (1992) The reactivity of sedimentary iron minerals toward sulfide. *Am J Sci* **292**, 659-683.

Canfield D. E. and Thamdrup B. (1994) The production of S-34-depleted sulfide during bacterial disproportionation of elemental sulfur. *Science* **266**, 1973-1975.

Chou T. and Zhou L. (1983) Extraction techniques for selective dissolution of amorphous iron oxides from soils and sediments. *Soil Science Society American Journal* **47**, 225-232.

Chung F. H. (1974) Quantitative interpretation of X-ray diffraction patterns, I. Matrix-flushing method of quantitative multicomponent analysis. *Journal of Applied Crystallography* **7**, 513 - 519.

Cline J. D. (1969) Spectrophotometric determination of hydrogen sulfide in natural waters. *Limnol Oceanogr* **14**, 454-458.

Detmers J., Bruechert V., Habicht K. S., and Kuever J. (2001) Diversity of sulfur isotope fractinations by sulfate-reducing prokaryotes. *Applied and Environmental Microbiology* **67**, 888-894.

Fossing H. and Jørgensen B. B. (1989) Measurement of bacterial sulfate reduction in sediments: Evaluation of a single-step chromium reduction method. *Biogeochemistry* **8**, 205-222.

Giggenbach W. (1972) Optical spectra and equilibrium distrubution of polysulfide ions in aqueous solutions at 20°C. *Inorganic Chemistry* **11**, 1201-1207.

Gingele F. X. and Leipe T. (1997) Clay mineral assemblages in the western Baltic Sea: recent distribution and relation to sedimentary units. *Mar Geol* **140**, 97-115.

Habicht K. and Canfield D. E. (1997) Sulfur isotope fractionation during bacterial sulfate reduction in organic-rich sediments.

Kamyshny A., Goifman A., Gun J., Rizkov D., and Lev O. (2003) Kinetics of disproportionation of inorganic polysulfides in undersaturated aqueous solutions at environmentally relevant conditions. *Aquatic Geochemistry* **9**, 291-304.

Kamyshny A., Goifman A., Gun J., Rizkov D., and Lev O. (2004) Equilibrium distribution of polysulfide ions in aqueous solutions at 25°C: a new approach for the study of polysulfides equilibria. *Environ Sci Technol* **38**, 6633-6644.

Kamyshny A., Ekeltchik I., Gun J., and Lev O. (2006) Method for the determination of inorganic polysulfide distribution in aqatic systems. *Anal Chem* **78**, 2359-2400.

Kamyshny A., Gun J., Rizkov D., Voitsekovski T., and Lev O. (2007) Equilibrium distribution of polysulfide ions in aqueous solutions at different temperatures by rapid single phase derivazation. *Environmental Science & Technology* **41**, 6633-6644.

Kao S. J., Horng C. S., Roberts A. P., and Liu K. K. (2004) Carbon-sulfur-iron relationships in sedimentary rocks from southwestern Taiwan: influence of geochemical environment on greigite and pyrrhotite formation. *Chem Geol* **203**, 153-168.

Knab N. J., Dale A. W., Lettmann K., Fossing H., and Jørgensen B. B. (2008) Thermodynamic and kinetic control on anaerobic oxidation of methane in marine sediments. *Geochim Cosmochim Acta* **72**, 3746-3757.

Kostka J. E. and Luther G. W. (1994) Partitioning and speciation of solid-phase iron in salt-marsh sediments. *Geochim Cosmochim Ac* **58**, 1701-1710.

Luther III G. W. (1991) Pyrite synthesis via polysulfide compounds. *Geochimica et Cosmochimia Acta* **55**, 2839-2849.

Maronny G. (1959) Constantes de dissotiation de l`hydrogene sulfure. *Electrochimica Acta* **1**, 58-69.

Moros M., Lemke W., Kuijpers A., Endler R., Jensen J. B., Bennike O., and Gingele F. (2002) Regressions and transgressions of the Baltic basin reflected by a new high-resolution deglacial and postglacial lithostratigraphy for Arkona Basin sediments (western Baltic Sea). *Boreas* **31**, 151-162.

Moses C. O., Nordstrom D. K., Herman J. S., and Mills A. L. (1987) Aqueous pyrite oxidation by dissolved oxygen and by ferric iron. *Geochim Cosmochim Ac* **51**, 1561-1571.

Neretin L. N., Böttcher M. E., Jørgensen B. B., Volkov I. I., Lueschen H., and Hilgenfeldt K. (2004) Pyritization processes and greigite formation in the advancing sulfidization front in the upper pleistocene sediments of the Black Sea. *Geochim Cosmochim Ac* **68**, 2081-2093.

Neumann G. (1981) Lagerungsverhältnisse spät- und postglazialer Sedimente im Arkona-Becken. Ph.D. Thesis, Institut für Meereskunde, Warnemünde, Germany. *unpublished*.

Pyzik A. J. and Sommer S. E. (1981) Sedimentary iron monosulfides: kinetics and mechanism of formation. *Geochim Cosmochim Ac* **45**, 687-698.

Rickard D. (1995) Kinetics of FeS precipitation: Part 1. Compeeting reaction mechanisms. *Geochim Cosmochim Acta* **59**, 4367-4380.

Rickard D. and Morse J. W. (2005) Acid volatile sulfide (AVS). *Mar Chem* **97**, 141-197.

Roberts A. P. and Weaver R. (2005) Multiple mechanisms of remagnetization involving sedimentary greigite (Fe_3S_4). *Earth Planet Sc Lett* **231**, 263-277.

Rong L., Lim L. W., and Takeuchi T. (2005) Determination of iodide and thiocyanate in seawater by liquid chromatography with poly(ethylene glycol) stationary phase. *Chromatographia* **61**, 371-374.

Schippers A. and Jørgensen B. B. (2001) Oxidation of pyrite and iron sulfide by manganese dioxide in marine sediments. *Geochim Cosmochim Ac* **65**, 915-922.

Sohlenius G., Sternbeck J., Andren E., and Westman P. (1996) Holocene history of the Baltic Sea as recorded in a sediment core from the Gotland Deep. *Mar Geol* **134**, 183-201.

Steudel R. (1996) Mechanism for the formation of elemental sulfur from aqueous sulfide in chemical and microbiological desulfurization processes. *Ind Eng Chem Res* **35**, 1417-1423.

Stookey L. L. (1970) Ferrozine - a new spectrophotometric reagent for iron. *Anal Chem* **42**, 779-781.

Sweeney R. E. and Kaplan I. R. (1973) Pyrite framboid formation: Laboratory synthesis and marine sediments. *Economic Geol.* **68**, 618-634.

Teder A. (1971) The equilibrium between elementary sulfur and aqueous polysulfide solution. *Acta Chemica Scandinavica* **25**, 1722-1728.

Thamdrup B., Finster K., Hansen J. W., and Bak F. (1993) Bacterial disproportionation of elemental sulfur coupled to chemical reduction of iron or manganese. *Applied and Environmental Mecorbiology* **59**, 101-108.

Thamdrup B., Fossing H., and Jørgensen B. B. (1994) Manganese, iron, and sulfur cycling in a coastal marine sediment, Aarhus Bay, Denmark. *Geochim Cosmochim Ac* **58**, 5115-5129.

Thiessen O. (2005) Bacterial methane formation and distribution in marine environments: case studies from Arkona Basin (Western Baltic Sea) and hotspots in the Central south Pacific. Ph.D. Thesis, University of Christian-Albrechts Kiel.

Vogt C., Lauterjung J., and Fischer R. X. (2002) Investigation of the clay fraction (<2 μm) of the clay mineral society reference clays. *Clays and Clay Minerals* **50**, 388-400.

Wagman D. D., Evans W. H., Parker V. B., Halow I., Bailey S. M., and Schum R. H. (1968) Selected values of chemical thermodynamic properties. *Natl. Bur. stand. US Goverment Office, Washington, DC., Tech. Note*, 270-3.

Wang Q. and Morse J. W. (1995) Pyrite formation under conditions approximating those in anoxic sediments I. Pathway and morphology. *Mar Chem* **52**, 99-121.

Yao W. S. and Millero F. J. (1996) Oxidation of hydrogen sulfide by hydrous Fe(III) oxides in seawater. *Mar Chem* **52**, 1-16.

Zopfi J., Ferdelman T. G., and Fossing H. (2004) Distribution and fate of sulfur intermediates-sulfite, tetrathionate, thiosulfate, and elemental sulfur-in marine sediments. In Distribution and fate of sulfur intermediates-sulfite, tetrathionate, thiosulfate, and elemental sulfur-in marine sediments (ed. J. P. Amend, K. J. Edwards, and T. W. Lyons).Colorado *The Geological Society of America* pp.1-205.

Figure Legends

Fig. 1. Map of the study area, Arkona Basin in the Western Baltic Sea, with location of coring site "A6".

Fig. 2. Total organic carbon and total sulfur (% dry weight) distributions at Station A6. The sedimentary Units I-VI are indicated.

Fig. 3. Pore water concentrations of (a) sulfate and chloride, (b) sulfide and dissolved iron as well as modeled concentrations (lines), (c) individual zero-valent sulfur species, and (d) sulfide and total polysulfide zero-valent sulfur.

Fig. 4. Depth distributions of (a) magnetic susceptibility, (b) total reactive iron, (c) ferric iron, (d) manganese oxides, (e) AVS and CRS, and (f) total zero-valent sulfur.

Fig. 5. Scanning electron micrographs of sliced magnetic nodules from the depth of peak magnetic susceptibility. (a) Surface scan of sliced nodule that consists mostly of iron-sulfide minerals. EDS analysis revealed the presence of Fe_3S_4 in the center and FeS_2 in the periphery of the nodule. (b) Surface scan of a sliced barite nodule. The light gray area is barite whereas the dark area consisted of silicate. (c) Surface scans of a sliced nodule with a very heterogeneous interior which probably was a conglomerate of smaller nodules. (d) Magnification of the lower region of the nodule in Fig. 5c. EDS analysis of the dark inner area revealed FeS while the light-gray area was FeS_2. (e) Magnification of the lower region of a sliced iron-sulfide nodule (small picture in the top right corner). The gray crystal-like structures in the middle of the nodule are rich in sulfur. (f) SEM

image of a large sulfur crystal. (g) The same image as in Fig. 5g but showing sulfur in green. (h) The same image as in Fig. 5g but showing iron in red.

Fig. 6

Sulfur and oxygen isotopic compositions of sulfate, sulfide and pyrite versus depth. (a) Isotopic composition of $\delta^{34}S_{sulfate}$ (‰ vs. VCDT) in pore water. (b) Isotopic signal of $\delta^{18}O_{sulfate}$ (‰ vs. VSMOW) in pore water. (c) Isotopic composition of $\delta^{34}S_{\sum sulfide}$ (‰ vs. VCDT) in pore water. (d) Isotopic composition of $\delta^{34}S_{CRS}$ (‰ vs. VCDT) in CRS (pyrite). The different sedimentary units are marked as Units I-VI.

Fig. 1

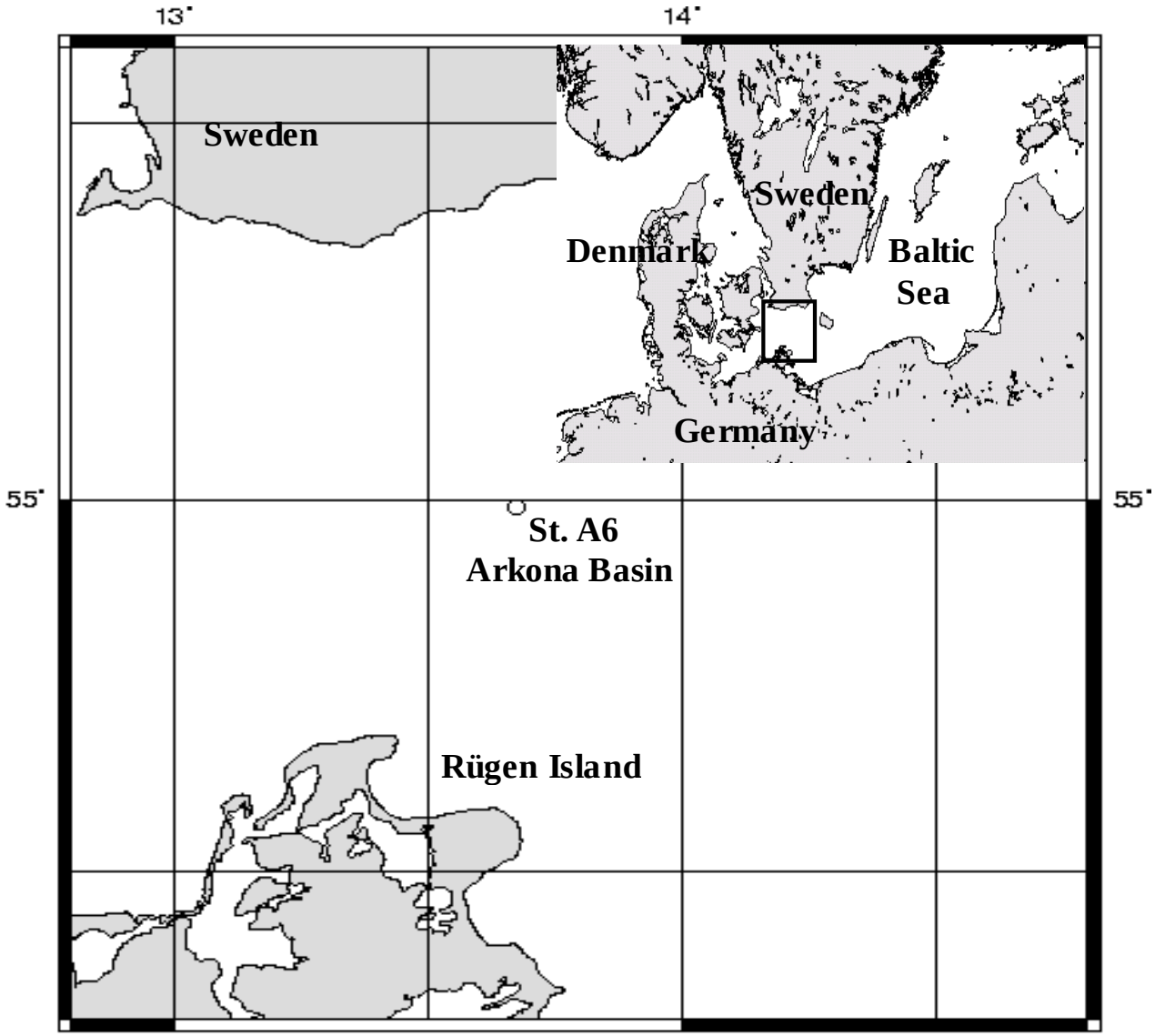
13°
14°
Sweden
Sweden
Denmark
Baltic
Sea
Germany
55°
55°
St. A6
Arkona Basin
Rügen Island

Fig. 2

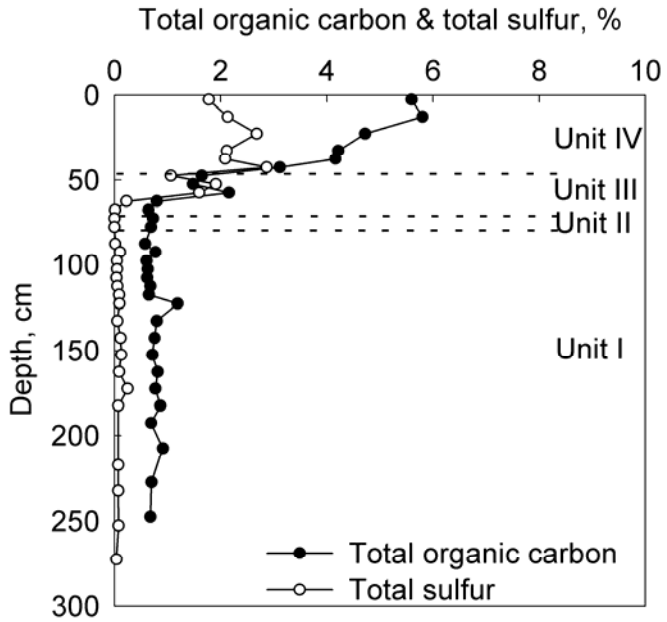
Total organic carbon & total sulfur, %
0
2
4
6
8
10
0
50
100
150
200
250
300
Depth, cm
Unit IV
Unit III
Unit II
Unit I
Total organic carbon
Total sulfur

Fig. 3

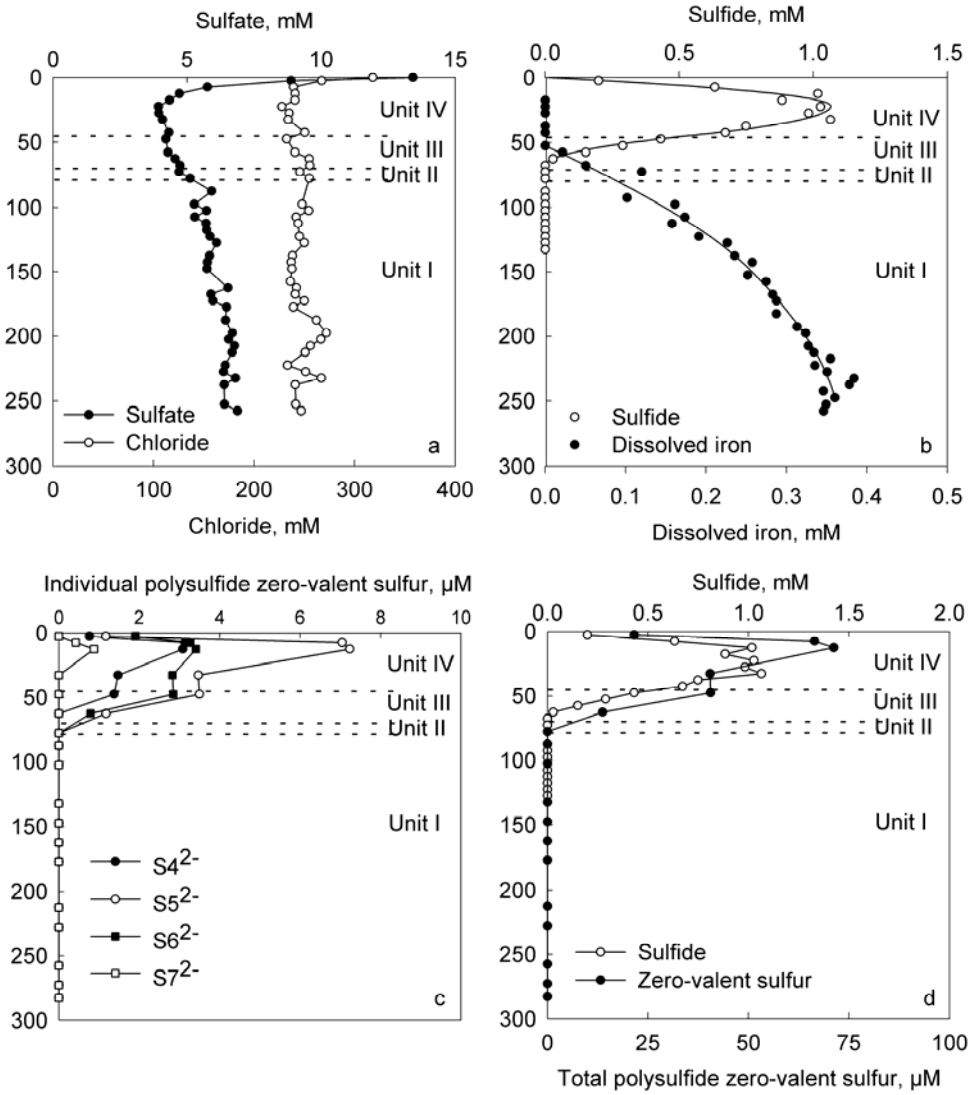
Sulfate, mM
Unit IV
Unit III
Unit II
Unit I
Sulfate
Chloride
a
Chloride, mM
Sulfide, mM
Sulfide
Dissolved iron
b
Dissolved iron, mM
Individual polysulfide zero-valent sulfur, μM
S4 2-
S5 2-
S6 2-
S7 2-
c
Sulfide, mM
Zero-valent sulfur
d
Total polysulfide zero-valent sulfur, μM

Fig. 4

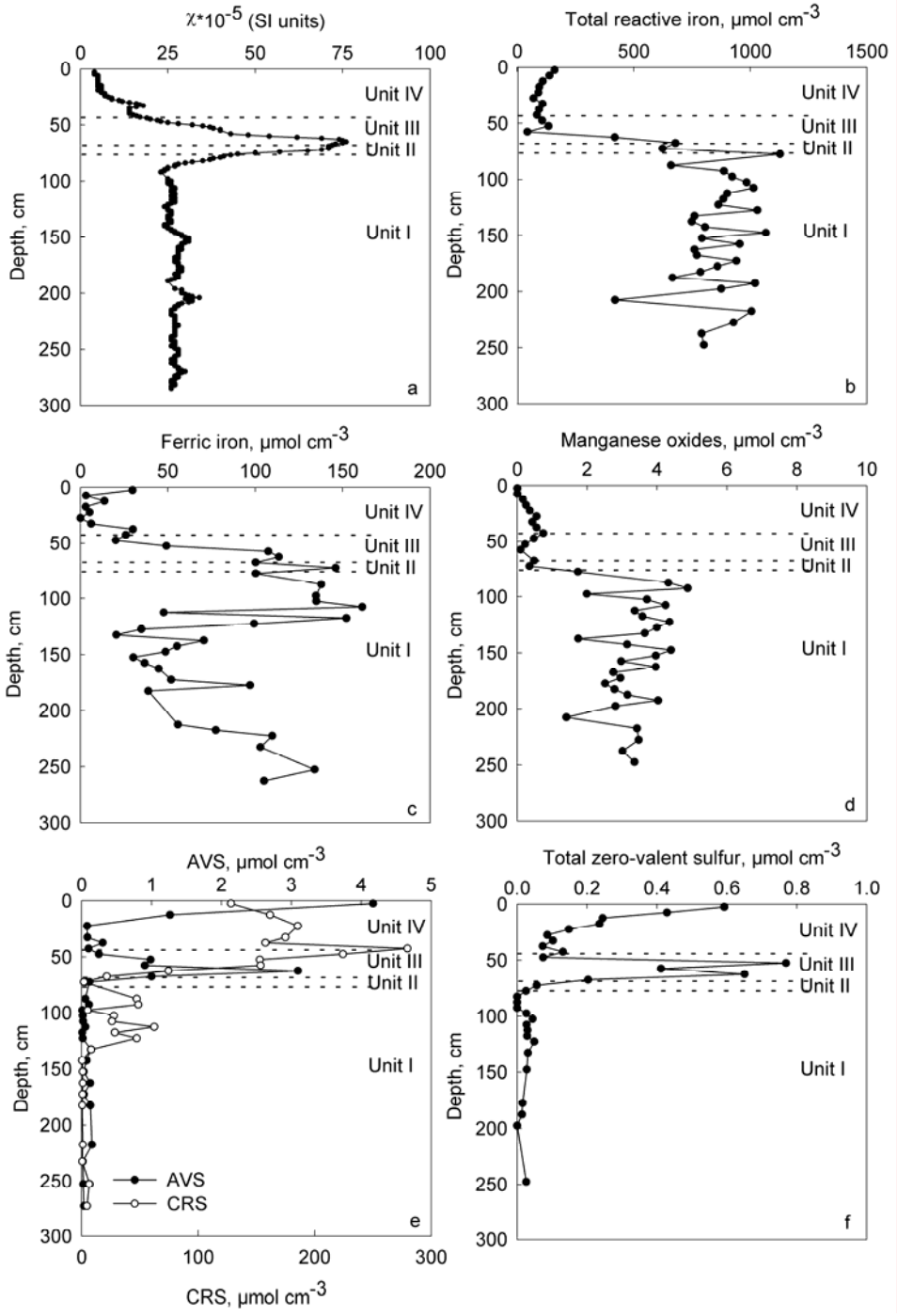
χ*10-5 (SI units)
Total reactive iron, μmol cm-3
Ferric iron, μmol cm-3
Manganese oxides, μmol cm-3
AVS, μmol cm-3
Total zero-valent sulfur, μmol cm-3
Depth, cm
Unit IV
Unit III
Unit II
Unit I
AVS
CRS
CRS, μmol cm-3
a
b
c
d
e
f

Fig. 5

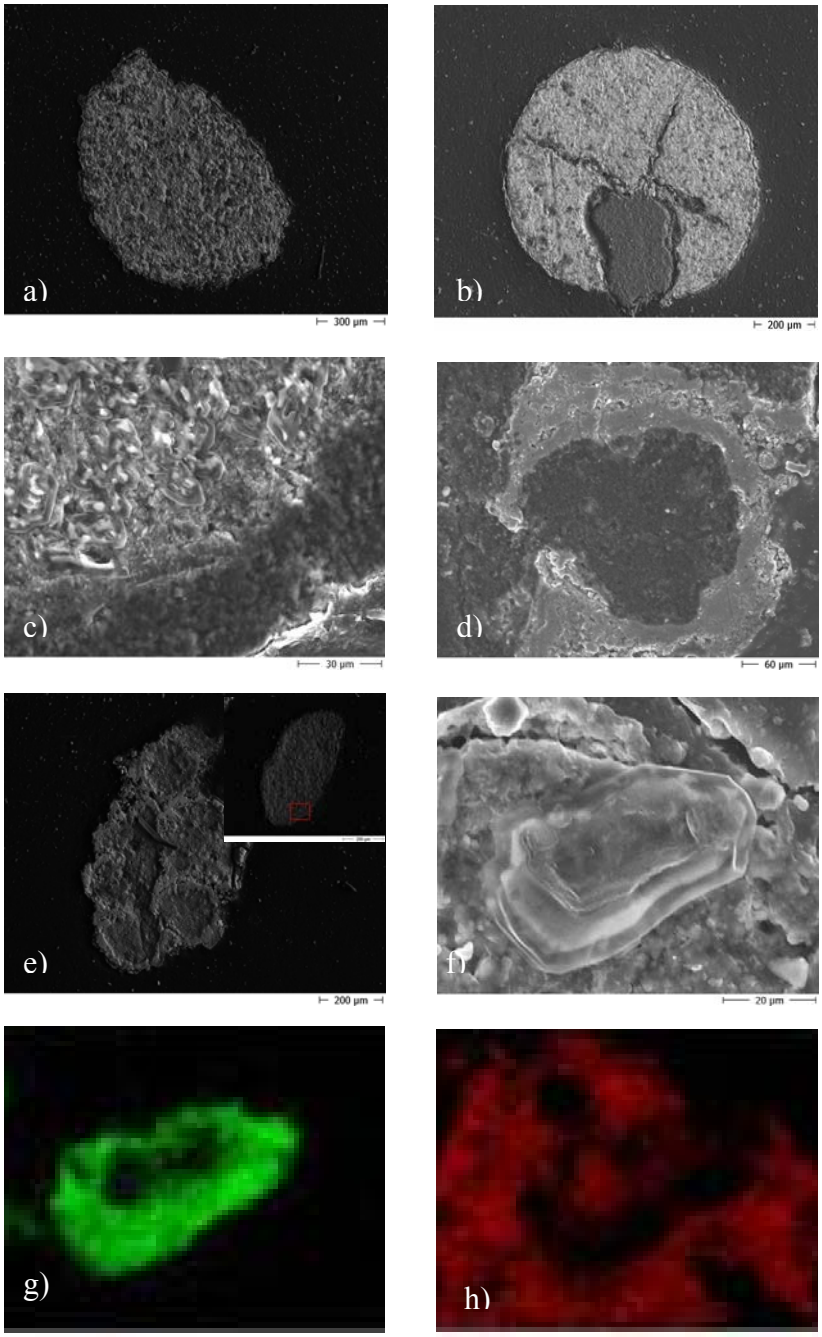

Fig. 6

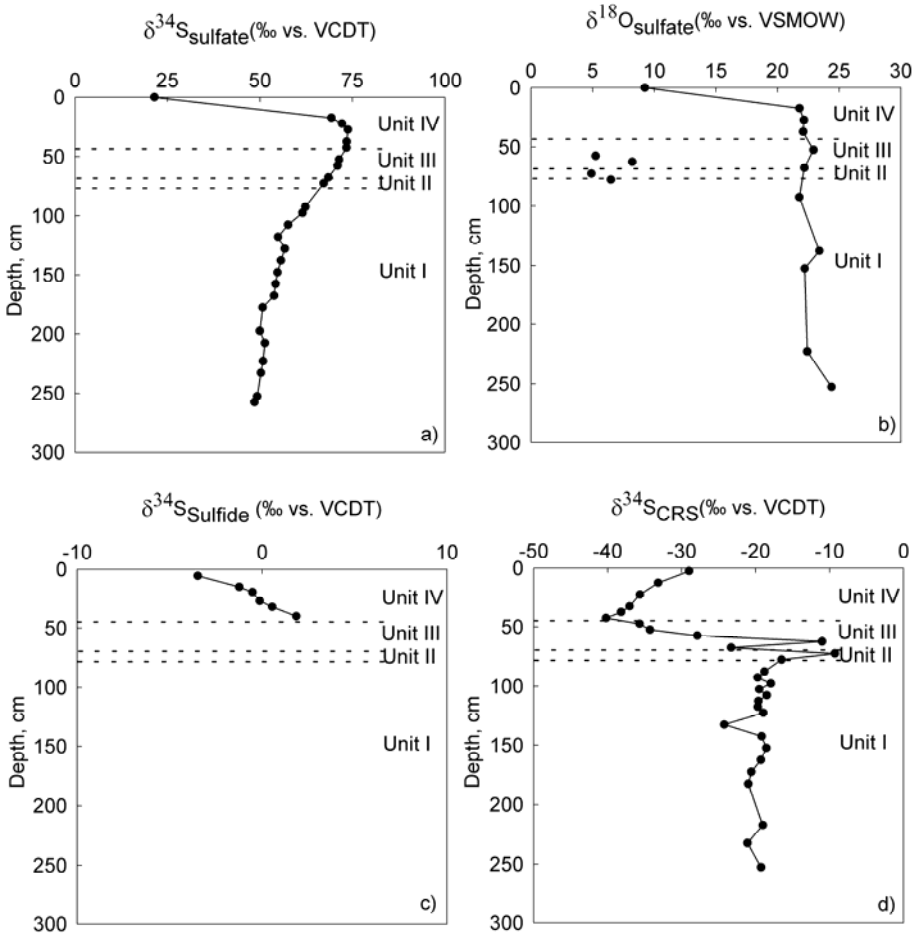
δ34Ssulfate(‰ vs. VCDT)
δ18Osulfate(‰ vs. VSMOW)
δ34SSulfide (‰ vs. VCDT)
δ34SCRS(‰ vs. VCDT)
Depth, cm
Unit IV
Unit III
Unit II
Unit I
a)
b)
c)
d)

Chapter 5

Sulfate reduction below the sulfate-methane transition in Black Sea sediments

Lars Holmkvist[a,b]*, Alexey Kamyshny, Jr.[a,c], Christoph Vogt[d], Kyriakos Vamvakopoulos[a], Timothy G. Ferdelman[a] and Bo Barker Jørgensen[a,e]

[a]Biogeochemisty Group, Max-Planck Institute for Marine Microbiology, Celsiusstrasse 1, 28359 Bremen, Germany

[b]Chemistry and Water Technology, Danish Technological Institute, Kongsvang Allé 29, 8000 Aarhus C, Denmark

[c]Department of Geology and Earth System Science, Interdisciplinary Center, University of Maryland, College Park, MD 20742, USA

[d]Fachbereich Geowissenschaften, Universität Bremen, Klagenfurter Str., 28359 Bremen, Germany

[e]Center for Geomicrobiology, Department of Biological Sciences, Aarhus University, Ny Munkegade, Bld. 1535, 8000 Århus C, Denmark

Keywords: Black Sea; sulfate reduction; potential sulfate reduction; reoxidation, sulfur species

* Corresponding author.

E-mail address: LHT@teknologisk.dk Tel.: +45 72 70 23 95

Abstract

A sudden increase in salinity about 7,000 years ago caused a shift in the deposited sediments of the Black Sea from limnic to brackish-marine. Due to the large anoxic deep water basin and the relatively high concentration of sulfate, organic matter is mineralized primarily through sulfate reduction in modern Black Sea sediments. Earlier studies have shown that sulfate-reducing bacteria are abundant within the limnic sub-surface sediment in spite of extremely low concentrations of sulfate and organic carbon. A main objective of the present study was therefore to understand the depth distribution of sulfate reduction across the different sediment units, even deep below the sulfate-methane transition. The study combined experimental measurements of sulfate reduction using ^{35}S radiotracer with analyses of sulfur and iron geochemistry in pore water and sediment. Potential sulfate reduction rates were measured with ^{35}S in sediment samples that were amended with sulfate and organic substrates and incubated in time-series up to 48 hours. Sulfate reduction could thereby be detected and quantified at depths where concentrations of sulfate were otherwise too low to enable calculation of the rates. The results demonstrate that sulfate-reducing bacteria are active several meters below the sulfate-methane transition in Black Sea sediments. The cryptic sulfate reduction below the sulfate-methane transition may be driven by sulfate produced from reoxidation of sulfur compounds in pore water and sediment with oxidized iron minerals.

1. Introduction

The environmental conditions of the Black Sea, the largest anoxic basin on Earth, have changed strongly during the past 25,000 years. The first evidence of seawater intrusion through the Bosporus into the post-glacial lake comprising the Black Sea dates back to about 9,800 yr B.P. (Arthur and Dean, 1998; Jones and Gagnon, 1994). A permanent rise in salinity occurred only a few thousand years later, however, when seawater entered and marine conditions were established. At least three different sedimentary units have been recognized to be deposited in slope and deep-sea sediments over the past 25,000 years (Ross and Degens, 1974). Unit 1 is a carbonate-rich microlaminated sediment deposited under anoxic marine conditions within the last 3,000 years, following the invasion of planktonic coccolithophorids, *Emiliania huxleyi*. Unit 2 is an organic-rich microlaminated sediment deposited under anoxic marine conditions between 3,000 and 7,000 yr B.P. Unit 3 consists of alternating light and dark lutite, an organic-poor limnic sediment type of clay or silt with grain size less than 1/16 mm, deposited before 7,000 yr B.P. under oxic limnic conditions. These Pleistocene deposits of limnic origin are found throughout the modern Black Sea below a sediment depth of about one meter (Hay et al., 1991).

Sulfate reduction within Unit I-II of the modern Black Sea plays a dominant role in the benthic mineralization of organic carbon. The process is enhanced by anoxic and sulfidic bottom water conditions while its depth in the seabed appears to be limited by downward diffusion of sulfate into the upper sediment layers. Sulfate reduction rates (SRR) peak in the sulfate-methane transition (SMT) where the activity of sulfate-reducing bacteria (SRB) is stimulated by anaerobic oxidation of methane (AOM) (Knab

et al., 2008). The high SRR within the SMT leads to an enhanced production of sulfide, which here shows peak concentration in the pore water and diffuses upwards and downwards in the sediment (Neretin et al., 2004). The downward diffusing sulfide reacts with iron species in the sediment below and forms a distinct diagenetic sulfidization front. This front is often recognized as a black band due to a high content of iron monosulfides (FeS) and greigite (Fe_3S_4) (Berner, 1970; Berner, 1984; Neretin et al., 2004; Pyzik and Sommer, 1981). Different oxidation processes of sulfur species takes place in the sulfidization front that lead to an overall pyritization. The products of sulfide oxidation include different intermediates such as zero-valent sulfur (ZVS) species (i.e. elemental sulfur and polysulfides), thiosulfate, and sulfite (Zopfi et al., 2004), all of which may undergo disproportionation to sulfide and sulfate (Thamdrup et al., 1993; Thamdrup et al., 1994).

Only a few studies have addressed the potential for sulfate reduction below the SMT in marine sediments. The experimental measurement of deep sulfate reduction is hindered by the low concentrations of sulfate (<50 μM) in the pore water. Thus, the activity and role of sulfate-reducing communities detected below the SMT is not known. It is possible that the SRB deep in the sediment have an important impact on the cycling of carbon, sulfur and iron. It was recently shown that sulfate-reducing communities are present several meters below the SMT in Black Sea sediments (Leloup et al., 2007). This was demonstrated by quantitative PCR targeting their metabolic key gene, the dissimilatory (bi)sulfite reductase (dsrA). However, it is not clear how the SRB make a living below the SMT. Many sulfate-reducing prokaryotes have a versatile metabolism which apparently enables them to adapt to the extreme conditions of sub-surface

sediments with low availability of electron donors and acceptors. For instance, pure culture studies of the sulfate-reducing archaea, *Archaeoglobus fulgidus*, show an ability to shift the metabolic pathway to different carbon sources when grown under different levels of sulfate (0.3-14 mM) (Habicht et al., 2005). Other explanations for the presence of active sulfate reducers beneath the SMT could be the ability to ferment (Widdel and Hansen, 1992) or to reduce poorly crystalline Fe(III) oxides (Coleman et al., 1993).

By combining activity measurements of SRR with geochemical data on sulfur and iron, we studied the activity and depth distribution of active SRB below the SMT. The results demonstrate the presence of active SRB several meters below the sulfate zone in post-glacial limnic sediments of the Black Sea. We present a possible explanation for the presence of active SRB by which sulfate is produced in the methane zone from oxidation of reduced sulfur compounds with iron minerals.

2. Materials and methods

2.1. Sampling and site description

The present study is based on two gravity cores (GC A and B) and a multi-corer core (MUC) taken during research cruise M75/5 of the RV METEOR in the Black Sea from May 11th to June 6th 2007. Cores were collected at Station 9 (44°39.08'N, 32°1.00'E) in the Dniepr paleodelta in the northwestern part of the Black Sea at a water depth of 1000 m. The position of this station is identical to Station "P824GC" described by Knab et al. (2008) and Station P12 described by Leloup et al. (2007). Absolute depth correction of the GC A and B cores relative to the sediment surface was not possible because sulfate was not measured in the MUC. Instead, a depth correction between the GC A and B cores was made by overlaying the two pore water concentration profiles of sulfide. This correction demonstrated that only about 5 cm more sediment had been lost from the surface during coring of GC A as compared to GC B. However, the penetration depth of sulfide was quite different between the A and B cores since the location of the black band differed (see Fig. 5 B and C).

2.2. Core processing

Immediately after retrieval of the first gravity core (GC A) methane samples were taken at 80-100 cm depth intervals through small windows cut into the side of the core liner with a vibrating saw. Sediment samples of 3 cm^3 were transferred into 20 ml serum vials with 6 ml Milli-Q water, closed with a butyl rubber stopper, and crimp sealed.

The GC A and B cores as well as the MUC cores were processed in a 4°C cold room on board the METEOR within a few days after retrieval. Rhizone soil moisture samplers (Rhizosphere Research Products, Wageningen, Netherlands) were used for the extraction of pore water. The rhizones consist of an inert porous polymer tube with a length of 10 cm and a pore size of 0.1 µm, through which pore fluid is extracted by vacuum created with disposable 10 ml syringes connected to the Rhizone. Pore water for sulfate and sulfide measurements in GC A were extracted from pre-drilled holes at 10 cm depth intervals and fixed with 250 µL 2 wt. % zinc acetate. The first ~0.5 ml of extracted pore water was discarded to limit oxidation by oxygen. Samples for dissolved iron were collected at the same depths as for sulfate and preserved by acidifying ~1 ml pore water with 100 µL 10% HCl. Pore water samples for analysis of zero-valent sulfur (ZVS) in polysulfide species were extracted in between the sulfate and sulfide pore water samples at 30-60 cm depth intervals within the upper 500 cm of the sediment and at a depth of 775 cm. At least 5-6 ml of pore water was required from each depth in order to detect the ZVS species. The pore water for ZVS analysis was transferred into anoxic vials immediately after extraction and analyzed within a few hours to prevent oxidation by oxygen.

Pore water was extracted from GC B with 10 cm long Rhizones by gently pushing them into predrilled holes at 5 cm depth intervals along the core. Pore water samples for the later determination of sulfate, sulfide and dissolved iron were prepared as with the GC A core.

Solid phase sub-samples were taken from the GC A and B cores at 10 cm and 5 cm depth intervals, respectively, in between the depths where pore water was

extracted. Sediment sub-samples were collected both in plastic bags and plastic centrifuge tubes containing 10 ml of zinc acetate (20% w/v) and immediately frozen at -20°C for later analysis of iron, sulfur and carbon. Within two weeks after sampling, sediment sub-samples from the GC A core were scanned for magnetic susceptibility and all other sub-samples from both GC A and B were analyzed for carbon, sulfur and iron speciation.

2.3. Pore water analyses

Methane in the headspace of the 20 ml serum vials was analyzed on a gas chromatograph (5890A, Hewlett Packard) equipped with a packed stainless steel Porapak-Q column (6 feet, 0.125 inch, 80/100 mesh, Aglient Technology) and a flame ionization detector. Helium was used as a carrier gas at a flow rate of 30 ml min^{-1}. Sulfate was analysed by non-suppressed ion chromatography (100 µl injection volume, Waters, column IC-Pak^{TM}, 50 × 4.6 mm) (Ferdelman et al., 1997). The eluent was 1 mM isophthalate buffer in 10% methanol, adjusted to pH 4.5 with saturated Na borohydrate and the flow rate was 1.0 ml min^{-1}. Hydrogen sulfide (H_2S and HS^-) was determined spectrophotometrically at 670 nm (Shimadzu UV 1202) on zinc-preserved pore water and bottom water samples by the methylene blue method (Cline, 1969). Dissolved iron was measured according to Stookey (1970) with Ferrozine (1 g L^{-1} in 50 mM HEPES buffer, pH 7) spectrophotometrically at 562 nm (Shimadzu UV 1202). Dissolved manganese in the pore water (Mn^{2+}) was determined by flame atomic absorption spectrometry (Perkin Elmer, Atomic Absorption Spectrometer 3110).

The analysis of zerovalent sulfur (ZVS) species included solid sulfur (S_8), colloidal sulfur (S^0), polysulfides (S_n^{2-}) and polythionates ($S_nO_6^{2-}$). The pH of each pore water sample was measured with a pH electrode before the analysis and the value was used later for ZVS concentration calculations. A newly developed protocol for detection of ZVS species was based on four steps (Kamyshny et al., 2009a; Rong et al., 2005): (1) The detection of inorganic polysulfides by fast single-phase derivatization with methyl trifluoromethanesulfonate (Kamyshny et al., 2006), (2) detection of the sum of colloidal S^0 and polysulfide ZVS and polythionate ZVS (n>3) with hydrogen cyanide derivatization, followed by HPLC analysis of thiocyanate, (3) detection of the sum of polysulfide ZVS, colloidal S^0 and solid sulfur by treatment with zinc chloride followed by extraction with chloroform, and (4) the detection of polythionates (n = 4-6) by HPLC (Kamyshny et al., 2009b) . The concentration of polysulfide ZVS was calculated as the sum of all ZVS species detected after derivatization with methyl triflate. The concentration of colloidal ZVS was calculated as the difference between results from the cyanolysis and the concentration of polysulfide ZVS. Finally, the concentration of dispersed solid sulfur was calculated as the difference between the chloroform extraction and results from the cyanolysis.

2.4. Solid phase analyses

Sediment sub-samples were placed in a Bartington Instruments MS2 meter equipped with a MS2C sensor and scanned for magnetic susceptibility using a scan rate of 1 cm min^{-1}. The sediment density was determined as the wet weight per cm^3. The water content in the sediment was determined from the weight loss after drying at 60°C

until constant weight and sediment density as the wet weight per cm^3. Total organic carbon (TOC) was determined in freeze dried sediment that was pretreated with HCl, dried again, and analyzed on a CNS analyzer (Fisons^{TM} Na 1500 elemental analyzer). AVS (acid volatile sulfide = dissolved sulfide + Fe monosulfide) and CRS (Cr-reducible S = pyrite + elemental sulfur) were determined using the two step acidic Cr-II method (Fossing and Jørgensen, 1989). The volatilized and trapped sulfide was determined spectrophotometrically at 670 nm (Shimadzu UV 1202) by the methylene blue method of Cline (1969). Total zero-valent sulfur (ZVS) was extracted from zinc acetate preserved sediment samples in 10 ml pure methanol on a rotary shaker for at least 16 h according to Zopfi et al. (2004). Total ZVS was separated on an HPLC with a Zorbax ODS column (125 × 4 mm, 5 μm; Knauer, Germany) with methanol as the eluent (1 ml min^{-1}) and determined from the adsorption at 265 nm.

Solid phase ferric iron (Fe(III)) was extracted from sub-samples of the frozen sediment in a 0.5 M HCl solution for 1 h on a rotary shaker. Fe(II) was determined in the supernatant of the HCl extracts by the Ferrozine method (Stookey, 1970). Fe(III) was calculated as the difference between the total iron (Fe(II) + Fe(III)), determined with Ferrozine + 1% (w(v) hydroxylamine hydrochloride), and the Fe(II). Reactive iron (towards sulfide) in the sediment was extracted with dithionite-citrate-acetic acid according to Canfield (1989) and determined with Ferrozine + 1% (w/v hydroxylamine hydrochloride). The content of total iron in the sediment was extracted from freeze dried sub-samples in a boiling HCl solution (12.5 M) for a period of 1 min according to Berner (1970) and Raiswell et al. (1988). The extracted Fe(II) from this method was determined with Ferrozine + 1% (w(v) hydroxylamine hydrochloride). Solid manganese oxides

(Mn(IV)) were measured on the supernatant of the dithionite-extracts by flame atomic absorption spectrometry (Perkin Elmer, Atomic Absorption Spectrometer 3110).

2.5. Sulfate reduction

Sulfate reduction rates (SRR, Equation 1) in the MUC core were determined using the whole-core $^{35}SO_4^{2-}$ incubation method (Jørgensen, 1978). The MUC was injected with radiotracer (~300 kBq per injection) at 1 and 2 cm depth intervals and the injected core was incubated for 24 h at ca. 4°C. Sulfate reduction was terminated by sectioning the sediment cores, fixing the sections with 20 mL of 20% (w/v) zinc acetate, and freezing. A measured sulfate concentration of 16.5 mM was used for calculating the SRR in the MUC.

For the measurement of SRR in GC A, triplicate samples of 5 cm^3 were carefully collected in butyl rubber stoppered glass tubes. Sampling was done at 10 cm depth intervals, alternating with the depths of pore water extraction. The glass tubes were injected with 5 µl carrier-free $^{35}SO_4^{2-}$ tracer (~300 kb per 5 cm^3) and incubated for 24 h at ca. 4°C. The process was stopped by mixing the sample with 10 ml cold zinc acetate (20% w/v) and freezing. All samples were treated by cold chromium distillation after Kallmeyer et al. (2004) and SRR were calculated according to Jørgensen (1978):

$$SRR = [sulfate] \times (^{35}S\text{-}CRS/^{35}S\text{-}sulfate) \times 1.06/t \text{ pmol cm}^{-3} \text{ d}^{-1} \quad \text{(Eq. 1)}$$

where [sulfate] is the sulfate concentration in pmol per cm^3 of wet sediment (1 pmol = 10^{-12} mol), ^{35}S-CRS is the radioactivity of total reduced sulfur at the end of incubation, ^{35}S-

sulfate is the initial radioactivity of sulfate added to the experiment, 1.06 is a correction factor for the expected isotope discrimination against ^{35}S-sulfate versus the bulk ^{32}S-sulfate by the SRB, and incubation time, t, is measured in days.

In the deeper, methanogenic part of the sediment, beneath the main sulfate zone, we determined "potential sulfate reduction rates" (P-SRR) in similar 5 cm^3 samples. In this sulfate-depleted sediment below 300 cm depth, sediment samples were injected under N_2 with non-radioactive sulfate (2 mM final concentration) and organic substrates (100 µM final concentrations of propionate, acetate, lactate and formate) and then pre-incubated for 12 h. Subsequently, 10 µl carrier-free $^{35}SO_4^{2-}$ tracer (~600 kb) was injected into each sample. A five point time series experiment with incubations stopped after 0, 12, 24, 36 and 48 h was done with triplicate samples of 5 cm^3 sediment for each time point. The incubations were stopped by adding the sample into 10 ml cold zinc acetate (20% w/v) and treating as described above.

2.6. X-ray diffraction pattern analyses (XRD)

Samples for XRD analyses of mineral phases were collected from the GC A core at 30, 103, 163, 246, 316, 345 and 410 cm depths. Dried bulk samples were carefully ground to a fine powder (<20µm particle size) and prepared with a Philips back-loading system. X-ray diffractograms were measured on a Philips X'Pert Pro multipurpose diffractometer equipped with a Cu-tube (k_α 1.541, 45 kV, 40 mA), a fixed divergence slit of ¼°, a sample changer, a secondary monochromator, and a X'Celerator detector system. The measurements were done as a continuous scan from 3º to 85° 2θ, with a calculated step size of 0.016° 2θ (calculated time per step was 100 seconds). Mineral

identification was done using the Philips software X'Pert HighScore™, which, besides the mineral identification, gives a semi-quantitative value for each identified mineral on the basis of Relative Intensity Ratio (RIR-values). The RIR-values are calculated as the ratio between the strongest signal from a specific mineral phase to the strongest signal from pure corundum (I/Ic), referred to as the "matrix-flushing method" after Chung (1974). In addition, mineral identification was checked with the freeware MacDiff 4.5 (Petschick et al., 1996). Full quantification was done using the full-pattern quantification software QUAX (Vogt et al., 2002).

2.7. Magnetic nodules

Sediment for the study of magnetic nodules was sampled during an earlier Black Sea cruise (METROL cruise 2004) at St. "P824GC" that was the same sample station as St. 9. Single magnetic nodules were collected from the sulfidization front at 388 cm depth using a handheld magnet. The nodules were immediately embedded in a methacrylate resin, trimmed with a diamond band saw, and polished with an Al_2O_3 paraffin suspension. Prior to scanning electron microscopy (SEM), the surface of the polished nodules was coated with carbon to avoid charging effects. The surface morphology and texture were recorded by conventional backscattered electron and secondary electron imagery. Specific elements inside the nodules were identified using energy dispersive X-ray analysis (EDS) (Oxford INCA 300).

3. Results

3.1. Sediment stratigraphy

Sediments from below the Black Sea chemocline consist of limnic clay, deposited before 7,500 yr BP, and overlain by microlaminated, organic-rich sapropel and modern marine coccolith ooze (Calvert and Karlin, 1991; Ross et al., 1970). We identified four sedimentary units between the top of the GC cores and a depth of 8 m according to color, sand layers and organic carbon content. In GC A these units were recognized as Unit I, IIa, IIb and III according to the stratigraphy defined during earlier studies (Neretin et al., 2004) (Fig. 1). Note, however, that the description of the different depth zones of the GC cores is of uncorrected depths because absolute depth correction of the GC cores and the MUC could not be made, as described above. Based on our previous experience in the Black Sea, 10-30 cm of sediment was probably lost from the surface during GC coring.

Unit I: 0 - 30 cm depth. Laminated marine coccolith ooze deposited under anoxic conditions. Some of this upper layer was lost during GC coring. TOC values were 5-6 wt %.

Unit IIa: 30-65 cm depth. Brown, marine sapropel deposited under anoxic conditions. TOC values were 7.5-15 wt %.

Unit IIb: 65- 326 cm depth. Grayish sediment of both brackish and limnic origin deposited under oxic conditions. A black band was found at 304-323 cm depth, below which a sand layer of about 3 cm thickness extended down to 326 cm. TOC values were 0.5-5 wt %.

Unit III: 326-757 cm depth. Reddish-brown limnic clay deposited under oxic

conditions. The sediment was unaffected by the sulfidization process. TOC values were <1 wt %.

The TOC content was high, 5-15 % dry weight, within the recent marine coccolith ooze and sapropelic layers (Unit I and IIa). It decreased steeply with depth (<5%) in the underlying limnic Units IIb and III (Fig. 1). TOC peaked twice within Unit IIb with values reaching 5 % at 148 cm and 1.4 % at 306 cm, most probably because of differences in the deposition of organic material or perhaps due to turbidities from the upper shelf. TOC remained below 0.5% throughout Unit III in which it decreased gradually from 0.48 to 0.33 % between 325 and 650 cm depth.

The depth and thickness of the black band and of the sand layer differ slightly between the GC A and B core. In GC B, the black band was located at 359-371 cm depth. The porosity of the GC A core decreased roughly linearly with depth in the interval 15-752 cm according to the equation:

$$\text{Porosity} = 0.825 - 0.0005 \times \text{depth (cm)} \qquad \text{(Eq. 2)}$$

3.2. Pore water chemistry

Pore water concentrations of sulfate, methane, sulfide and dissolved iron in core GC A are presented in Fig. 2 A-B. The sulfate concentration decreased from 12 mM at the top of the core (Unit I) to 0.1 mM at 230 cm, and further to below the detection limit of 0.01 mM at 400 cm (Fig. 2 A). From 250 cm depth, where the sulfate concentration had dropped below 50 μM, it could no longer be calibrated accurately

although it still generated visible peaks on the ion chromatograms. Between 250 cm and 400 cm the low concentrations of sulfate showed a very gradual decrease with depth. Methane increased below 100 cm and reached 3.4 mM at 700 cm (Fig. 2 A). Methane had probably out-gassed below a depth of about 250 cm upon core recovery and below 400 cm the sediment was observed to crack. The sulfate-methane transition (SMT), where anaerobic oxidation of methane occurs, was situated at 100-200 cm depth.

Free sulfide was present from the top of the core and down to 321 cm depth in Unit IIb (Fig. 2 B). Sulfide showed a minor peak within the Unit I-IIa layers and a large distinct peak within the SMT with a maximum concentration of 4 mM. Dissolved iron was not detected in the sulfide zone but increased downwards from the black band in Unit IIb (Fig. 2 B). Within the non-sulfidized limnic sediment of Unit III, the concentrations of dissolved iron were generally in the range of 2-4 mM. Dissolved manganese generally remained <10 μM throughout the core but peaked within Unit I and exhibited an increase with depth down to the upper part of Unit III (data not shown).

Peak concentrations of individual polysulfide ZVS species occurred in Unit IIb (Fig. 2 C). Our calculations revealed that individual polysulfides were not in equilibrium with elemental sulfur under moderately alkaline conditions as would have been expected according to Kamyshny et al. (2004). The sum of polysulfide ZVS species peaked at 158 cm depth with highest concentrations reaching 44 μM (Fig. 2 D). The depth of this peak largely matched the peak in sulfide, suggesting that polysulfide ZVS species were in equilibrium with sulfide in the pore water . Concentrations of ZVS species below the sulfidization front were too low to be detected.

3.3. Sediment geochemistry

Two distinct peaks in magnetic susceptibility were observed, a minor peak within the organic rich Unit IIa and a large peak within the black band of Unit IIb, with maximum values reaching 68×10^{-5} and 203×10^{-5} SI units, respectively (Fig. 3 A). The large peak in Unit IIb coincided with abundant magnetic nodules observed in the black band. Magnetic susceptibility was relatively high, $11\text{-}12 \times 10^{-5}$ SI, throughout the iron-rich and brown colored limnic sediment of Unit III.

Total iron in Unit I-IIb peaked around 100 cm depth with highest concentration of 170 μmol cm^{-3} (Fig 3 B). Total iron increased within the limnic Unit III and reached concentrations of 400-500 μmol cm^{-3}. Reactive iron was low (<10 μmol cm^{-3}) within the sulfidic Unit I-IIb and increased sharply to about 100 μmol cm^{-3} in Unit III (Fig. 3 B). Fe(III) determined by HCl extraction was generally low within the upper Unit I-IIb and increased in Unit III to values reaching 7 μmol cm^{-3} at 405 cm, below which the concentration decreased again (Fig. 3 C). Sediment of Unit III was less reduced as the concentrations of reactive iron (Fig. 3 B) and Fe(III) (Fig. 3C) increased. The concentration of Mn(IV) from the dithionite extracts was low throughout the core (Fig. 3 D). Mn(IV) peaked twice in Unit IIb with maximum concentrations of 6 and 5 μmol cm^{-3} at 148 and 276 cm, respectively.

The concentration of total ZVS in the sediment was generally low (<5 μmol cm^{-3}) except for a sharp peak situated right within the black band with a maximum concentration of 16 μmol cm^{-3} (Fig. 3 E). There was a minor peak in AVS concentration within Unit IIa below which the concentration stayed relatively constant, <10 μmol cm^{-3}, down to the black band where there was a distinct peak with a maximum concentration of

35.5 μmol cm^{-3} at 316 cm (Fig. 3 F). Within Unit III, AVS remained low (<1 μmol cm^{-3}) throughout the rest of the core. High concentrations of chromium reducible sulfur (CRS, mainly FeS_2) were found in Units I-IIb (ca. 100-300 μmol S cm^{-3}) whereas CRS was low (<10 μmol S cm^{-3}) through the non-sulfidized Unit III (Fig. 3 F).

3.4. Magnetic nodules

Magnetic nodules collected in the black band within Unit IIb of GC A varied in size but were typically <500 μm. Surface scans of cut and polished nodules (collected in 2004) by SEM and EDS analysis showed that they had a heterogeneous interior consisting mainly of iron and sulfur. From the atomic ratios, we identified iron monosulfide (FeS), greigite (Fe_3S_4), and pyrite (FeS_2) in most of the nodules studied. As an example, the nodule presented in Fig. 4 had a core of FeS_2 surrounded by Fe_3S_4. However, a general pattern in the distribution of various iron sulfide minerals within the investigated nodules was not found.

3.5. X-ray diffraction (XRD)

XRD analysis was performed on sediment collected from each of the different sediment units in order to identify Fe(III)-bearing minerals. It should be noted, however, that the individual minerals recognized with the XRD method show statistical distributions of minerals only. Thus, the percentage values of individual minerals identified are not an accurate measure of their quantity.

We detected iron oxides, goethite and hematite, only in the non-sulfidized limnic Unit III below a depth of 300 cm (i.e. below the sulfidization front) where they

reached 1 % dry wt. at 410 cm (data not shown). There was a great variety of silicate minerals found throughout the sediment core of which some contained Fe(III) (data not shown). These were mainly of the subclasses phyllosilicates (sheet silicates) and cyclosilicates. The largest fraction of the phyllosilicates was made up by the sum of illite and micas, ranging from 11 to 36 % dry wt, whereas other individual phyllosilicates did not exceed 6% dry wt). The different cyclosilicates did not show any particular trend with depth except that the sum of illite and micas, montmorillonites and smectites, as well as kaolinite and biotite all increased in concentration below the SMT (data not shown).

3.6. Sulfate reduction

The SRR data are separated into two graphs with different scales in order to better describe the rates within the different depth intervals of the upper 400 cm (Fig. 5 A and B). Note that the depths of the SRR for the MUC core are given relative to the sediment surface while depths for the GC A core are given relative to the core top and should therefore be shifted down, probably by 10-20 cm, to be aligned with the MUC data).

The highest SRR in the MUC reached 38,000 pmol cm^{-3} d^{-1} (or 38 nmol cm^{-3} d^{-1}; 1 pmol = 10^{-12} mol) at 0.5 cm (Unit I), below which depth there was a steady decrease down to 230 pmol cm^{-3} d^{-1} at 24 cm (Fig. 5 A). In GC A, SRR generally decreased with depth but peaked in the SMT with a mean rate of 410 pmol cm^{-3} d^{-1} at 123 cm (Unit IIb, Fig. 5 A). The SRR within the 200-400 cm depth interval decreased steeply and generally followed the decreasing trend of sulfate in the pore water. The SRR data below 250 cm are, however, somewhat inaccurate as the sulfate concentration

approached the detection limit of our ion chromatographic technique. Below 400 cm, sulfate could not be detected and the SRR could therefore not be calculated.

We measured potential sulfate reduction rates, P-SRR, at 300-800 cm depth in GC B in the deepest part of Unit IIb and within the limnic Unit III (Fig. 5 C) in order to test whether active SRB were present also within the deeper sulfate-depleted parts of the sediment. (Note that the depth of the black band differs slightly between the GC A and B cores, as described above). The P-SRR was 4-9 pmol cm^{-3} d^{-1} in the lower part of Unit IIb with a peak of 20 pmol cm^{-3} d^{-1} at 365 cm depth in the black band (Unit IIb, Fig. 5 C). In Unit III, P-SRR increased from 4 pmol cm^{-3} d^{-1} at 400-500 cm to 15-24 pmol cm^{-3} d^{-1} at a depth of 600-700 cm (Fig. 5 C).

Based on these results, our study demonstrates that active SRB must be present in the limnic Unit III where the concentration of sulfate was below detection. The combined time course of P-SRR from all depths within the 325-725 cm depth interval showed that P-SRR started right away from the first incubation period and that the summed rates remained of the same magnitude (data not shown). This suggests that the size of the SRB communities did not change during the 48 h time course experiments.

The depth distribution of SRR within the sulfate zone is generally controlled by the availability of degradable organic matter which decreases over many orders of magnitude with depth and age in the sediment. In order to show this we plotted all the experimentally measured SRR (MUC and GC A data), except for the inaccurate SRR below 250 cm, as a function of depth in a double-log plot (Fig. 5 D). (Note that the depths of the SRR in the GC A core relative to the MUC are not correct since it was not possible to make an absolute depth correction). The plot shows that a linear regression

analysis could be made for all the SRR data down to the SMT zone where AOM occurred. The SRR from within and below the SMT are thus not included in the linear regression since sulfate reduction in this zone is primarily AOM driven. The linear regression showed that the SRR decreased with depth in the sediment according to the following equation: $\text{Log}(\text{SRR}) = -1.2544 \times \text{Log}(Z) + 4.5951$, where Z is depth in the sediment (cm). Below the SMT, the SRR seems to decrease even steeper than above if a linear regression had been made.

4. Discussion

4.1. Sulfate reduction

In a study by Jørgensen et al. (2001), modelling of SRR within the upper two meters of a Black Sea sediment resulted in average rates of around 100 pmol cm^{-3} d^{-1}. The average SRR in GC A of the upper two meters (Fig. 5A) were 260 pmol cm^{-3} d^{-1} and thus slightly above the model results. The SRR within and above the SMT (Unit I-IIb) are in general comparable to the high SRR measured experimentally with $^{35}SO_4^{2-}$ tracer in sediments from the same area of the Black Sea (Knab et al., 2008). The steep decrease in sulfate and the broad peak in sulfide in Unit IIb point to a stimulated sulfate reduction due to anaerobic oxidation of methane within the SMT (Fig. 2 A and B). This was also demonstrated by the local peak in SRR at 123 cm (Fig. 5 A) and the depletion of methane in the SMT (100-200 cm depth interval) (Fig. 2 A). The minor peak in sulfide in Unit I (Fig. 2 B) and the high SRR in this zone (Fig. 5 A) are on the other hand consistent with the high content of organic carbon near the sediment surface (Fig. 1). It is not clear whether the near-surface H_2S peak is a transient phenomenon or an artifact. If not, then the H_2S minimum at the Unit IIa/IIb transition at 65 cm depth should indicate a strong H_2S sink right at that depth which is not consistent with, for example, the depth distribution of reactive iron.

The P-SRR experiments were used to detect bacteria with the ability to reduce sulfate in the deep methanogenic sediment of limnic origin, where the concentration of sulfate was too low to calculate in situ SRR directly from radiotracer experiments. Since the SRR and P-SRR estimates were obtained under different

experimental conditions, these rates are not directly comparable. In the P-SRR experiments, the SRB were stimulated by the addition of sulfate and organic substrates in order to analyze the metabolic capacity of the existing SRB community. Given the rather short incubation times and the constant level of SRR over time, it is unlikely that the SRB community grew during the P-SRR experiments. There was reduction of sulfate at relatively high rates during the first half hour immediately after the injection of $^{35}SO_4^{2-}$, which indicates that the community already possessed the physiological capacity for dissimilatory sulfate reduction. We found that the mean P-SRR from the GC B core at 0.5, 1, 1.5 and 2 days after injection of ^{35}S tracer was 610, 390, 360, and 155 pmol cm^{-3} d^{-1}, respectively (data not shown).

In contrast to P-SRR measurements, SRR are determined under in situ conditions where the availability of substrates was limiting. The P-SRR below 300 cm depth were accordingly much higher than the SRR (Fig. 5 B and C). The data show that SRB were not limited to the upper sediment layers, which are rich in sulfate, but that they also maintained the capacity for sulfate reduction deep beneath the SMT and even beneath the sulfidization front. These data support the observations by Leloup et al. (2007), who quantified the SRB communities in deep sediment cores from the same site by Q-PCR targeting their metabolic key gene, dissimilatory (bi)sulfite reductase (dsrA). The authors showed that SRB occurred throughout the methane zone at 200-500 cm depth in numbers of 0.8-1.5 $\times$ 10^6 cells g^{-1}. The proportion of SRB relative to the total microbial cell number was even as high in the methane zone as in the sulfate zone, namely 5-10%. Our study now shows that SRB in the methane zone are capable of performing sulfate reduction when provided with appropriate substrates.

When SRR were calculated using the measured concentrations of sulfate in the pore water, the rates reached zero below 400 cm. However, we now speculate that the SRR do not quite decrease to zero but that the sulfate concentration in the pore water below 400 cm was simply too low to enable proper calculations of the SRR. It therefore seems likely that sulfate reduction occurs also in the methane zone within the limnic Pleistocene sediment (Unit III). For future studies of sulfate reduction within sub-surface sediments it is thus crucial that analytical methods are used which can accurately detect sulfate also below 50 μM.

4.2. Geochemistry of sulfur and iron

As a result of high SRR, reduced sulfur species (i.e. sulfide, polysulfides, elemental sulfur, AVS and CRS) were present at high concentrations within the upper marine Units I-IIb. In contrast, concentrations of reduced sulfur species were low in the limnic Unit III (Fig. 2 B, Fig. 3 E and F), where a steep gradient of dissolved iron demonstrates active iron reduction (Fig. 2 B). The distribution of reducible iron oxides (Fig. 3 B, C and D) showed that these were abundantly available for iron-reducing microorganisms from the top of Unit III and down. XRD analyses below the sulfidization front also confirmed the presence of iron oxides as well as Fe(III)-bearing clay minerals in this sediment unit (data not shown).

The black band in Unit IIb marked the lower boundary of downward diffusing sulfide produced within the SMT. At the transition to Unit III or just within this unit the downward diffusing sulfide reacted with iron minerals and with dissolved iron diffusing upwards from the deeper sediment. It is not clear why the sulfidization front

occurred exactly at the 3-5 cm thick sand layer marking the transition between Unit III and IIb. There might be a lateral pore fluid transport associated with this permeable horizon which locks the sulfide-iron interface at this position. The coincidence may also be due to a shift in geochemistry, e.g. to a step-up in total iron with a high capacity to react with sulfide (Fig. 3 B).

A sharp peak in magnetic susceptibility occurred within the black band and coincided with peaks in AVS and CRS (Fig. 3A and F). Although the black color of sediments may not be a simple indicator of AVS (Rickard and Morse, 2005), it seems reasonable to assume that, in this Black Sea sediment, the black color of the sulfidization front was due to AVS (Fig. 3F). We found numerous greigite nodules within the black band and the presence of this paramagnetic iron-sulfur mineral explained the magnetic susceptibility data (Fig.3 A). SEM and EDS analyses of nodules collected with a magnet demonstrated that these contained both greigite (Fe_3S_4) and pyrite (FeS_2) (Fig. 4). The content of Fe_3S_4 in each nodule was not quantified, but scans of several nodules indicated that Fe_3S_4 makes up only a fraction of the total amount of minerals present in each nodule. This is in accordance with a study from the Baltic Sea where similar magnetic nodules were collected at the transition of two sedimentary units (Holmkvist et al., 2009, in prep).

The Fe_3S_4 may be an intermediate in the sequence of reactions leading from FeS to FeS_2. However, the formation of FeS_2 from the metastable FeS fraction (the AVS fraction) has not been completely resolved. Our study shows that sulfur intermediates were abundant within Unit IIb where the formation of FeS_2 could occur via either

polysulfides (Berner, 1970; Luther, 1991), elemental sulfur (Berner, 1970), or sulfide in the pore water (Rickard and Luther Iii, 1997).

The finding of a deep sulfidization front where sulfide produced within the SMT is trapped at depth has been observed also in other continental shelf sediments such as the Angola Basin (Pruysers, 1998), the Baltic Sea (Boesen and Postma, 1988), and the Bay of Aarhus (Denmark) (Holmkvist et al., 2009, in prep). Below the sulfidization front iron sulfides (FeS and FeS_2, Fig. 3 F) occurred at low concentration, which indicates that sulfide production had occurred. This is consistent with the finding of active sulfate reducers in the limnic sediment layers, but it may also be the result of iron sulfide formation during the earlier history of the Black Sea, at the time when the limnic deposit was formed.

4.3. Deep production of sulfate and active SRB below the SMT

One of the aims of the present study was to demonstrate whether SRB below the SMT do indeed reduce sulfate and to explain their presence within sub-surface sediments in terms of the availability of electron donors- and acceptors. The SRR measurements showed that SRB, which are present several meters below the SMT (Leloup et al., 2007), are indeed actively reducing sulfate. The P-SRR data showed that their capacity for sulfate reduction in the 326-395 cm depth interval is 3-140-fold higher than the in situ rates and probably relatively even higher deeper in the limnic Unit III (Fig. 5 C). The in situ activity is thus highly constrained by the low concentration and reactivity of TOC and possibly also by the low sulfate concentration.

Sulfate dropped steeply with depth from 12 mM at the GC core top to about 0.01 mM at 400 cm, below which sulfate could no longer be detected. We suggest that the measured low concentrations of sulfate below the SMT were not just "background" concentrations although the concentrations below 250 were inaccurate. As discussed in a comparable study from Aarhus Bay (Holmkvist et al. 2009, in prep), at least three possible explanations may be proposed for the low background concentrations of sulfate in the methane zone:

a) The background could be a handling artifact due to chemical or biological oxidation of free sulfide during the time between coring and sulfate measurement. However, the storage, sampling and analysis of the cores were done very carefully in order to minimize sample oxidation and exclude such possible artifacts. For example, gravity cores were sectioned and kept upright in the core liners on the ship and during transport to avoid air contact at the outside of the sediment core. The sampling of pore water using rhizons inserted into the middle of the core took place on the day of coring which should not have allowed sufficient time for diffusion of oxygen and sulfate from the core periphery to the centre. The first extracted pore water was always discarded as it had been in contact with air and pore water was immediately fixed with zinc acetate to prevent sulfide oxidation. It is therefore most probable that there was no significant oxidation of sulfide during the pore water extraction, which could have affected the extracted sulfate data. This was also demonstrated in the study from Aarhus Bay, where pore water was extracted under strict anoxic conditions inside an anaerobic glove box in order to test whether auto-oxidation of sulfide occurred during the extraction in open air. This experiment showed that there was no significant difference between the low

concentrations of sulfate extracted in open air with those extracted under controlled anoxic conditions.

b) The sulfate could be a biologically unavailable background or even be passively diffusing down into the methane zone, because it was not being consumed by sulfate-reducing microorganisms. The sulfate background could be biologically unavailable because the concentration was below a physiological threshold for uptake and respiration. However, the fact that the sulfate concentration did drop to undetectable concentration beneath 400 cm speaks against the hypothesis of an untouchable threshold concentration. Besides, it also seems unlikely that the background sulfate was fed continuously by diffusion from above since there was a concentration drop beneath the SMT at 200-300 cm depth (Fig. 5B).

c) The sulfate could be generated in situ down in the methane zone by reaction between free sulfide or iron sulfide minerals with oxidized iron buried with the sediment. We propose that this is indeed the main explanation for the measured low sulfate concentrations, as discussed in further detail by Holmkvist et al. (in prep).

The iron oxides within the non-sulfidized Unit III (Fig. 3 B, C and D) constitute an efficient barrier which oxidizes and traps the downward diffusing sulfide at the sulfidization front as described above. The parallel decrease in sulfide and sulfate above the sulfidization front suggests a close association between the formation of sulfate and in situ reoxidation of sulfide. From the XRD analyses we found that hematite and goethite were present below the sulfidization front. This was consistent with an increase in reactive iron below the sulfidization front (Fig. 3 B) since the dithionite method extracts hematite and goethite (Kostka and Luther, 1994).

The cryptic formation of sulfate within the methane zone is, however, not simple to explain based on reactions between free sulfide and solid-phase Fe(III). Based on earlier considerations on pyrite formation from sulfide and Fe(III) reactions (Berner, 1967; Berner, 1970; Drobner et al., 1990; Rickard, 1997), disproportionation of intermediate sulfur species to sulfide and sulfate (Canfield and Thamdrup, 1996), and a removal of excess reducing power in the form of H_2 by methanogenic archaea, the study from Aarhus Bay proposed a revised redox balance of the reactions between sulfide and oxidized iron we propose the following net equation (Eq. 3) (Holmkvist et al. 2009, in prep):

$$16\ H_2S + 8\ FeOOH \rightarrow 8\ FeS_2 + 4\ H_2 + 16\ H_2O \qquad \text{(Eq. 3)}$$

In the set of reactions behind this net equation, a transient formation of sulfate (but no overall net production of sulfate) could occur by the partial oxidation of sulfide with iron oxides and subsequent disproportionation of the intermediate sulfur species to sulfate. The iron oxy-hydroxide chosen as an example for the proposed reaction (Equation 5) is goethite (FeOOH). However, other less reactive Fe(III)-containing minerals such as sheet silicates detected with XRD are more likely to be responsible.

The transient production of sulfate could stimulate and maintain active SRB within the methane zone. In the Black Sea sediments, elemental sulfur (a fraction of the total sum of ZVS in Fig. 3 E) may form when sulfide is oxidized chemically by metals according to well known oxidation reactions described by Burdige and Nealson (1986)

and Pyzik and Sommer (1981). Oxidation of sulfide (or other sulfur intermediates) seems to be particularly intensive at the sulfidization front as indicated by the large peak in total ZVS (Fig. 3 E). This finding is in agreement with the increasing content of easily reducible iron oxides down through the sulfidization front (reactive iron in Fig. 3 B). Further, the presence of ZVS species, ranging from 0.2-2 μmol cm^{-3}, in sediment extending from the SMT and down to the sulfidization front (Fig. 4 E) supports our expectancy of Fe(III) driven sulfide oxidation.

It is an interesting observation that active SRB were found also within the limnic sediment of Unit III (Fig. 5 C), although sulfate and sulfide were not detected in the pore water. We suspect that the SRB present in Unit III reduce sulfate also in situ since the radioactive ^{35}S counts in the TRIS fraction from the SRR samples were significantly above the blank values (data not shown). It therefore seems likely that sulfate was present below the sulfidization front, but concentrations were too low to be detected (<50μM), and that the sulfide produced from sulfate reduction was removed immediately from the pore water due to reaction with Fe(III).

ZVS species could not be detected below a depth of 345 cm. This indicates that only a very limited reoxidation of free sulfide occurs in Unit III and that rapid removal of ZVS via disproportionation prevented accumulation. Reoxidation of free sulfide according to equation 5 may not be the only explanation for the production of sulfate below the sulfidization front, however. Reoxidation of iron sulfide minerals, such as FeS or FeS_2 (the AVS and CRS fraction, respectively, Fig. 3 F) to elemental sulfur and subsequent disproportionation, might also lead to a sub-surface production of sulfate in Unit III. The reoxidation of iron sulfide minerals with iron oxide minerals has been

proposed from several previous studies (Burdige and Nealson, 1986; Pyzik and Sommer, 1981; Steudel, 1996; Yao and Millero, 1996).

The oxidation of FeS_2 could also be due to deeply buried Mn(IV). This reaction between two solid mineral phases has been suggested to involve an Fe(II)/Fe(III)-shuttle between the mineral surfaces of FeS_2 and manganese oxides (Aller and Rude, 1988; Moses et al., 1987; Schippers and Jørgensen, 2001). In Black Sea sediments, Fe(III) and MnO_2 were extracted from the sediment below the SMT in equal quantities (Fig. 3 C and D). However, the fraction of poorly-reactive iron oxides and/or iron silicates, defined as the difference between the content of total iron and reactive iron fraction (Fig. 4 B), made up by far the largest fraction of iron oxides which potentially could re-oxidize sulfur compounds in the sediment. The predominant role of iron was also indicated by the high amount clay minerals by which some may contain Fe(III) detected in Unit III by XRD (data not shown).

The P-SRR in Unit III increased with depth (Fig. 5 C) and showed a high potential for sulfate reduction of the microbial community. The SRB living down in the methane zone are apparently adapted to low concentrations of sulfate and must have high affinity to sulfate at low concentrations. Ingvorsen and Jørgensen (1984) found that fresh-water strains of SRB grown in batch culture were able to sustain growth at sulfate concentrations down to 5 μM. Perhaps the SRB within Unit III originate from fresh-water strains from the time when the Black Sea was still a lake. Alternatively, it may well be that marine sulfate-reducing bacteria develop high sulfate affinity when growing under limiting sulfate concentrations.

Conclusions

The potential sulfate reduction data from the present study show for the first time that SRB present several meters below the SMT in Black Sea sediment are apparently active sulfate reducers. We propose that there is an ongoing cryptic sulfur cycle in the deep methane-rich sediment by which Fe(III) and Mn(IV) minerals oxidize sulfide or other reduced sulfur species in pore water and sediment. The immediate oxidation products are sulfur species of intermediate oxidation steps, such as elemental sulfur. Through disproportionation reactions these may be partly oxidized to sulfate, which serves as electron acceptor for the sulfate-reducing bacteria.

Acknowledgement

We thank Martina Meyer, Thomas Max, Andrea Schipper and Kirsten Imhoff at the Max Planck Institute for Marine Microbiology for assistance in the laboratory with analyses of sulfur speciation. We thank Nina Knab (University of Southern California, USA) for sampling the sediment used to study the magnetic nodules and Vera Lukies from the Center for Marine Environmental Sciences (MARUM in Bremen, Germany) for assistance with magnetic susceptibility measurements. XRD analyses were performed by the research group Crystallography, Dept. of Geosciences, University of Bremen. We are grateful to Christian Borowski from the MPI for planning and leading the M75/5 METEOR cruise. Finally, we thank the captain and crew of the RV METEOR for a successful expedition. This study was financially supported by the Max Planck Society.

References

Aller R. C. and Rude P. D. (1988) Complete oxidation of solid phase sulfides by manganese and bacteria in anoxic marine sediments. *Geochim Cosmochim Ac* **52**, 751-765.

Arthur M. A. and Dean W. E. (1998) Organic-matter production and preservation and evolution of anoxia in the Holocene Black Sea. *Paleoceanography* **13**, 395-411.

Berner R. A. (1967) Diagenesis of iron sulfide in recent marine sediments. *Estuaries*, 268-272.

Berner R. A. (1970) Sedimentary pyrite formation. *Amer. J. Sci.* **268**, 1-23.

Berner R. A. (1984) Sedimentary pyrite formation: An update. *Geochim Cosmochim Ac* **48**, 605-615.

Boesen C. and Postma D. (1988) Pyrite formation in anoxic environments of the Baltic. *Am J Sci* **288**, 575-603.

Burdige D. J. and Nealson K. H. (1986) Chemical and microbiological studies of sulfide-mediated manganese reduction. *Geochemical J.* **4**, 361-387.

Calvert S. E. and Karlin R. E. (1991) Relationships between sulphur, organic carbon, and iron in the modern sediments of the Black Sea. *Geochim Cosmochim Ac* **55**, 2483-2490.

Canfield D. E. (1989) Reactive iron in marine sediments. *Geochim Cosmochim Acta* **53**, 619-632.

Canfield D. E. and Thamdrup B. (1996) Fate of elemental sulfur in an intertidal sediment. *FEMS Microbiology Ecology* **19**, 95-103.

Chung F. H. (1974) Quantitative interpretation of X-ray diffraction patterns, I. Matrix-flushing method of quantitative multicomponent analysis. *Journal of Applied Crystallography* **7**, 513 - 519.

Cline J. D. (1969) Spectrophotometric determination of hydrogen sulfide in natural waters. *Limnol Oceanogr* **14**, 454-458.

Coleman M. L., Hedrick D. B., Lovley D. R., White D. C., and Pye K. (1993) Reduction of Fe(III) in sediments by sulphate-reducing bacteria. *Nature* **361**, 436-438.

Drobner E., Huber H., Waechtershaeuser G., Rose D., and Stetter K. O. (1990) Pyrite formation linked with hydrogen evolution under anaerobic conditions. *Nature* **346**, 742-744.

Ferdelman T. G., Lee C., Pantoja S., Harder J., Bebout B. M., and Fossing H. (1997) Sulfate reduction and methanogenesis in a Thioploca-dominated sediment off the coast of Chile. *Geochim Cosmochim Ac* **61**, 3065-3079.

Fossing H. and Jørgensen B. B. (1989) Measurement of bacterial sulfate reduction in sediments: Evaluation of a single-step chromium reduction method. *Biogeochemistry* **8**, 205-222.

Habicht K. S., Salling L., Thamdrup B., and Canfield D. E. (2005) Effect of low sulfate concentrations on lactate oxidation and isotope fractionation during sulfate reduction by *Archaeoglobus fulgidus* strain Z. *Appl Environ Microbiol* **71**, 3770-3777.

Hay B. J., Arthur M. A., Dean W. E., Neff E. D., and Honjo S. (1991) Sediment Deposition in the Late Holocene Abyssal Black-Sea with Climatic and Chronological Implications. *Deep-Sea Res* **38**, S1211-S1235.

Ingvorsen K. and Jørgensen B. B. (1984) Kinetics of sulfate uptake by freshwater and marine species of Desulfovibrio. *Arch. Microbiol.* **139**, 61-66.

Jones G. and Gagnon A. (1994) Radiocarbon chronology of Black Sea sediments. *Deep - Sea Research I* **41**, 531-557.

Jørgensen B. B. (1978) A comparison of methods for the quantification of bacterial sulfate reduction in coastal marine sediments. III. Estimation from chemical and bacteriological field data. *Geomicrobiology Journal* **1**, 49-64.

Jørgensen B. B., Weber A., and Zopfi J. (2001) Sulfate reduction and anaerobic methane oxidation in Black Sea sediments. *Deep-Sea Research I* **48**, 2097-2120.

Kallmeyer J., Ferdelman T. G., Weber A., Fossing H., and Jørgensen B. B. (2004) A cold chromium distillation procedure for radiolabeled sulfide applied to sulfate reduction measurements. *Limnol Oceanogr: Methods* **2**, 171-180.

Kamyshny A., Goifman A., Gun J., Rizkov D., and Lev O. (2004) Equilibrium distribution of polysulfide ions in aqueous solutions at 25°C: a new approach for the study of polysulfides equilibria. *Environ Sci Technol* **38**, 6633-6644.

Kamyshny A., Ekeltchik I., Gun J., and Lev O. (2006) Method for the determination of inorganic polysulfide distribution in aqatic systems. *Anal Chem* **78**, 2359-2400.

Kamyshny A., Borkenstein C. G., and Ferdelman T. G. (2009a) Protocol for Quantitative Detection of Elemental Sulfur and Polysulfide Zero-Valency Sulfur Distribution in Natural Aquatic Samples. *Geostandards and Geoanalytical Research* **33**.

Kamyshny J. A. (2009b) Improved Cyanolysis Protocol for Detection of Zero-valent Sulfur in Natural Aquatic Systems. *Limnology and Oceanograph: Methods* **7**, 442 - 448.

Knab N. J., Cragg B. A., Hornibrook E. R. C., Holmkvist L., Borowski C., Parkes R. J., and Jørgensen B. B. (2008) Regulation of anaerobic methane oxidation in sediments of the Black Sea. *Biogeosciences Discussions* **5**, 2305–2341.

Kostka J. E. and Luther G. W. (1994) Partitioning and speciation of solid-phase iron in salt-marsh sediments. *Geochim Cosmochim Ac* **58**, 1701-1710.

Leloup J., Loy A., Knab N. J., Borowski C., Wagner M., and Jørgensen B. B. (2007) Diversity and abundance of sulfate-reducing microorganisms in the sulfate and methane zones of a marine sediment, Black Sea. *Environ Microbiol* **9**, 131-142.

Luther G. W. (1991) Pyrite synthesis via polysulfide compounds. *Geochimica et Cosmochimia Acta* **55**, 2839-2849.

Moses C. O., Nordstrom D. K., Herman J. S., and Mills A. L. (1987) Aqueous pyrite oxidation by dissolved oxygen and by ferric iron. *Geochim Cosmochim Ac* **51**, 1561-1571.

Neretin L. N., Böttcher M. E., Jørgensen B. B., Volkov I. I., Lueschen H., and Hilgenfeldt K. (2004) Pyritization processes and greigite formation in the advancing sulfidization front in the upper pleistocene sediments of the Black Sea. *Geochim Cosmochim Ac* **68**, 2081-2093.

Petschick R., Kuhn G., and Gingele F. (1996) Clay mineral distribution in surface sediments of the South Atlantic: sources, transport, and relation to oceanography. *Mar Geol* **130**, 203-229.

Pruysers P. A. (1998) Early diagenetic processes in sediments of the Angola Basin, eastern South Atlantic. Ph.D. thesis, Universiteit Utrecht.

Pyzik A. J. and Sommer S. E. (1981) Sedimentary iron monosulfides: kinetics and mechanism of formation. *Geochim Cosmochim Ac* **45**, 687-698.

Raiswell R., Buckley F., Berner R. A., and Anderson T. F. (1988) Degree of pyritization of iron as a paleoenvironmental indicator of botom water oxygenation. *Journal of Sedimentary Petrology* **58**, 812-819.

Rickard D. (1997) Kinetics of pyrite formation by the H2S oxidation of iron (II) monosulfide in aqueous solutions between 25 and 125 degrees Celsius: The rate equation. *Geochimica et Cosmochimica Acta* **61**, 115-134.

Rickard D. and Morse J. W. (2005) Acid volatile sulfide (AVS). *Mar Chem* **97**, 141-197.

Rickard D. T. and Luther III G. W. (1997) Kinetics of pyrite formation by the H2S oxidation of iron (II) monosulfide in aqueous solutions between 25 and 125 degrees Celsius: The mechanism. *Geochemica et Cosmochimica Acta* **61**, 135-147.

Rong L., Lim L. W., and Takeuchi T. (2005) Determination of iodide and thiocyanate in seawater by liquid chromatography with poly(ethylene glycol) stationary phase. *Chromatographia* **61**, 371-374.

Ross D. A., Degens E. T., and Macllvaine J. (1970) Black Sea: recent sedimentary history. *Science* **170**, 163-165.

Ross D. A. and Degens E. T. (1974) Recent sediments of Black Sea. *Amer. Assoc. Petrol. Geol.* **20**, 183-199.

Schippers A. and Jørgensen B. B. (2001) Oxidation of pyrite and iron sulfide by manganese dioxide in marine sediments. *Geochim Cosmochim Ac* **65**, 915-922.

Steudel R. (1996) Mechanism for the formation of elemental sulfur from aqueous sulfide in chemical and microbiological desulfurization processes. *Ind Eng Chem Res* **35**, 1417-1423.

Stookey L. L. (1970) Ferrozine - a new spectrophotometric reagent for iron. *Anal Chem* **42**, 779-781.

Thamdrup B., Finster K., Hansen J. W., and Bak F. (1993) Bacterial disproportionation of elemental sulfur coupled to chemical reduction of iron or manganese. *Applied and Environmental Mecorbiology* **59**, 101-108.

Thamdrup B., Fossing H., and Jørgensen B. B. (1994) Manganese, iron, and sulfur cycling in a coastal marine sediment, Aarhus Bay, Denmark. *Geochim Cosmochim Ac* **58**, 5115-5129.

Vogt C., Lauterjung J., and Fischer R. X. (2002) Investigation of the clay fraction (<2 μm) of the clay mineral society reference clays. *Clays and Clay Minerals* **50**, 388-400.

Widdel F. and Hansen T. (1992) The dissimilatory sulfate-and sulfur-reducing bacteria. In *The Prokaryotes* (ed. A. Balows, H. Trüper, M. Dworkin, W. Harder, and K. H. Schleifer), pp. 583-624. Springer-Verlag.

Yao W. S. and Millero F. J. (1996) Oxidation of hydrogen sulfide by hydrous Fe(III) oxides in seawater. *Mar Chem* **52**, 1-16.

Zopfi J., Ferdelman T. G., and Fossing H. (2004) Distribution and fate of sulfur intermediates-sulfite, tetrathionate, thiosulfate, and elemental sulfur-in marine sediments. In Distribution and fate of sulfur intermediates-sulfite, tetrathionate, thiosulfate, and elemental sulfur-in marine sediments (ed. J. P. Amend, K. J.

Edwards, and T. W. Lyons).Colorado *The Geological Society of America* pp.1-205.

Figure legends

Fig. 1

Total organic carbon (% dry weight) distribution at St. 9. The different sedimentary units (Units I-III) are indicated.

Fig. 2

Pore water concentrations of (A) sulfate, sulfide, dissolved iron and methane, (B) sulfate, sulfide and dissolved iron within the black band and the sand layer, (C) sulfide and individual and sum of zero-valent sulfur species.

Fig. 3

Depth distributions of (A) magnetic susceptibility, (B) reactive iron, (C) ferric iron, (D) manganese oxides, (E) AVS and CRS, and (F) total zerovalent sulfur.

Fig. 4

Scanning electron micrographs of sliced magnetic nodules from the depth of peak magnetic susceptibility at 388 cm. (A) Surface scan of sliced nodule that consists mostly of iron-sulfide minerals. EDS analysis revealed the presence of FeS_2 in the center and Fe_3S_4 in light-gray periphery of the nodule. (B) The same image as in Fig. 4 A, but showing iron in red from EDS analysis. (C) The same image as in Fig. 4 A, but showing sulfur in green from EDS analysis.

Fig. 5

Sulfate reduction rates (SRR) measured experimentally using $^{35}SO_4^{2-}$ from (A) 0-200 cm depth of the MUC (open circles, upper scale) and GC A (closed circles, lower scale) and (B) 200-400 cm depth in GC A only. The shaded area illustrates the sulfidization front with a sand layer at the bottom. Error bars show standard deviation of triplicate measurements. (C) Potential sulfate reduction rates (P-SRR) measured experimentally using $^{35}SO_4^{2-}$ at 300-800 cm depth. (D) Log-log plot of sulfate reduction rates vs. depth in MUC (open circles) and GC A (closed circles). Linear regression line of the log-log data above the AOM is shown. Selected data points from within and below the zone where AOM occurred were not included in the linear regression.

Fig. 1

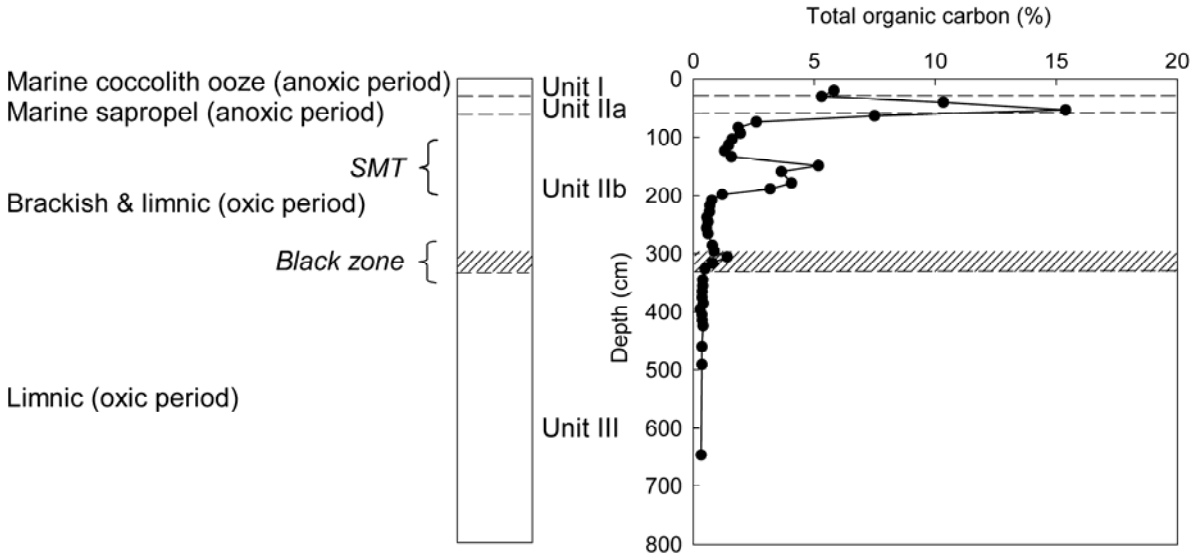
Total organic carbon (%)
0
5
10
15
20
Marine coccolith ooze (anoxic period)
Marine sapropel (anoxic period)
SMT
Brackish & limnic (oxic period)
Black zone
Limnic (oxic period)
Unit I
Unit IIa
Unit IIb
Unit III
Depth (cm)
0
100
200
300
400
500
600
700
800

Fig. 2

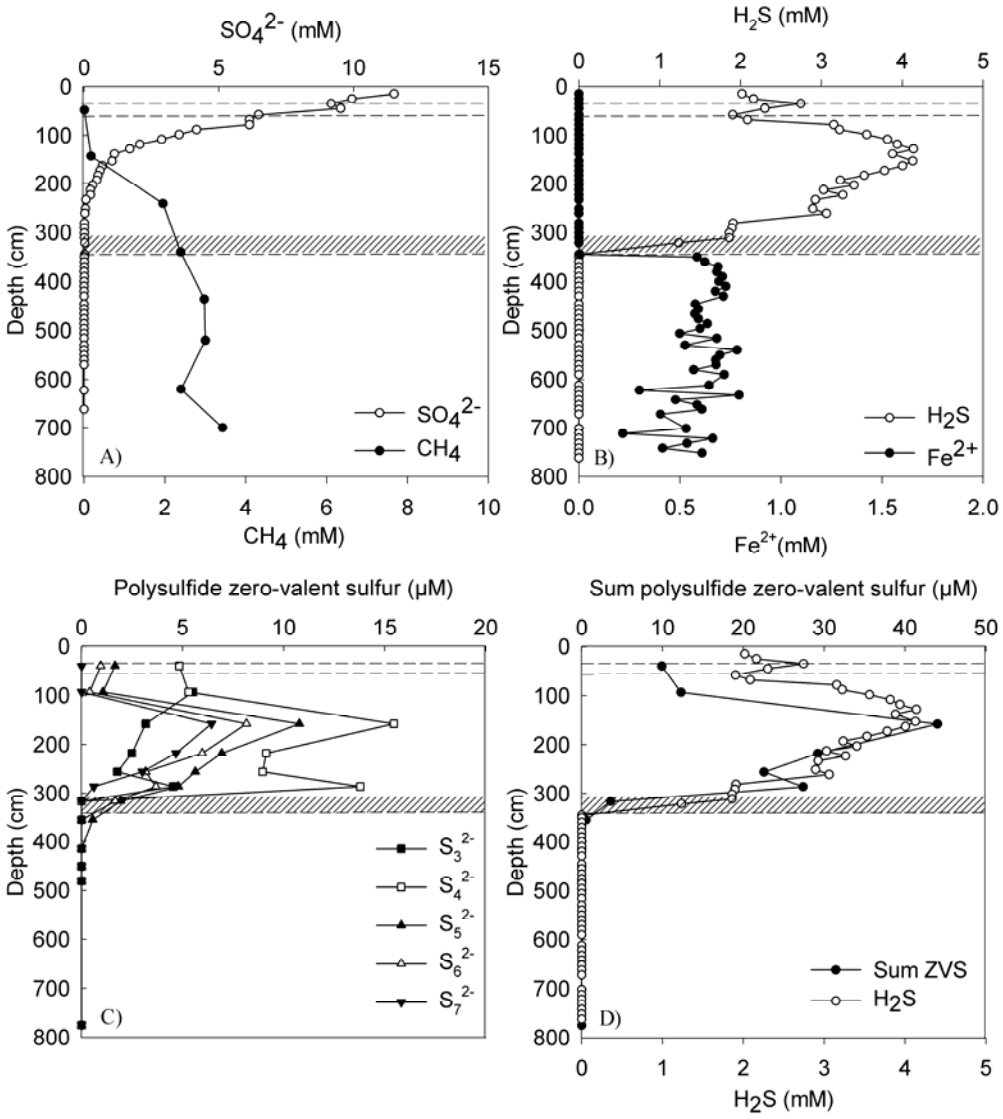
SO4 2- (mM)
CH4 (mM)
Depth (cm)
SO4 2-
CH4
A)
H2S (mM)
Fe2+(mM)
H2S
Fe2+
B)
Polysulfide zero-valent sulfur (µM)
S3 2-
S4 2-
S5 2-
S6 2-
S7 2-
C)
Sum polysulfide zero-valent sulfur (µM)
Sum ZVS
H2S
D)

Fig. 3

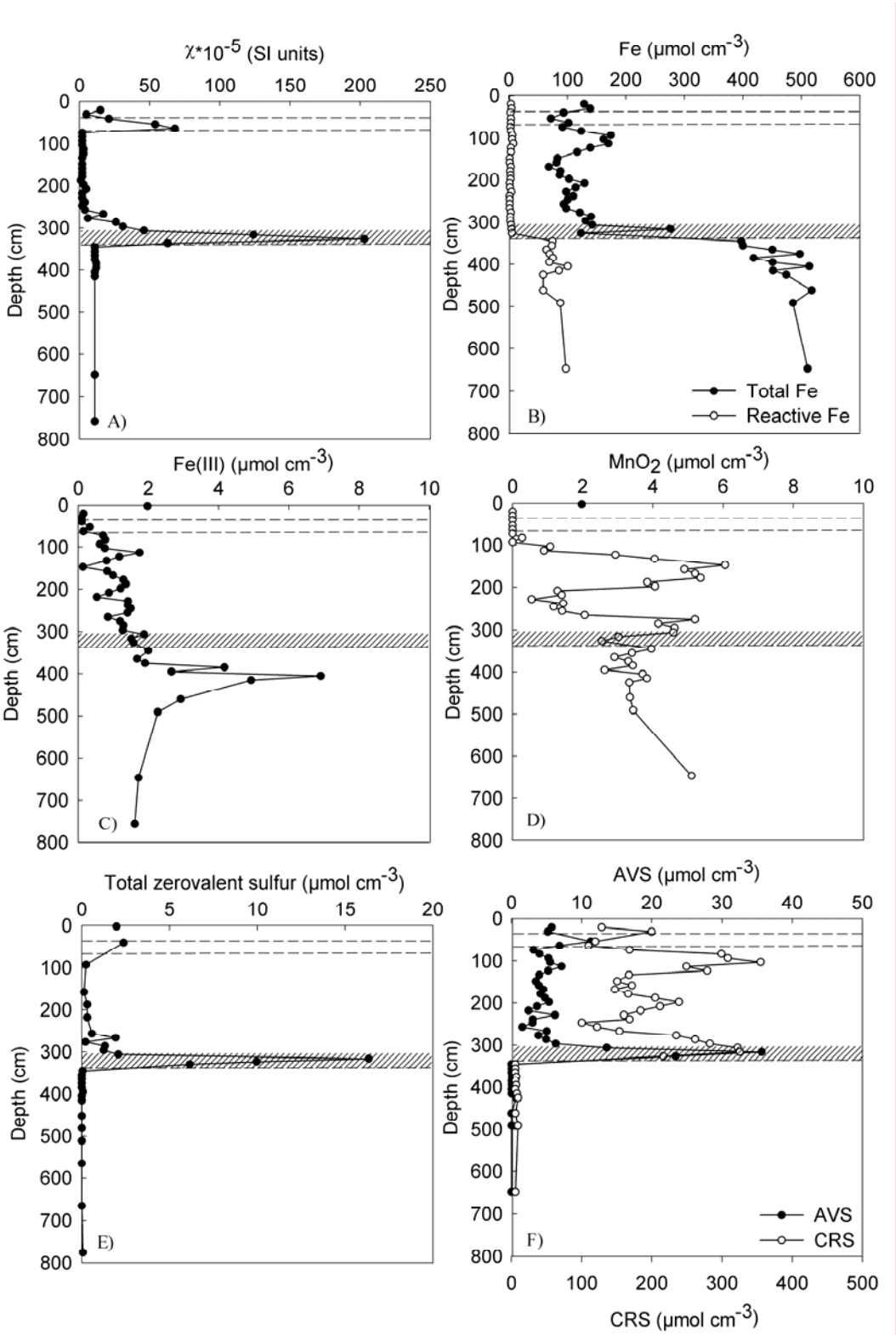
χ*10-5 (SI units)
Depth (cm)
A)
Fe (μmol cm-3)
Total Fe
Reactive Fe
B)
Fe(III) (μmol cm-3)
C)
MnO2 (μmol cm-3)
D)
Total zerovalent sulfur (μmol cm-3)
E)
AVS (μmol cm-3)
CRS (μmol cm-3)
AVS
CRS
F)

Fig. 4

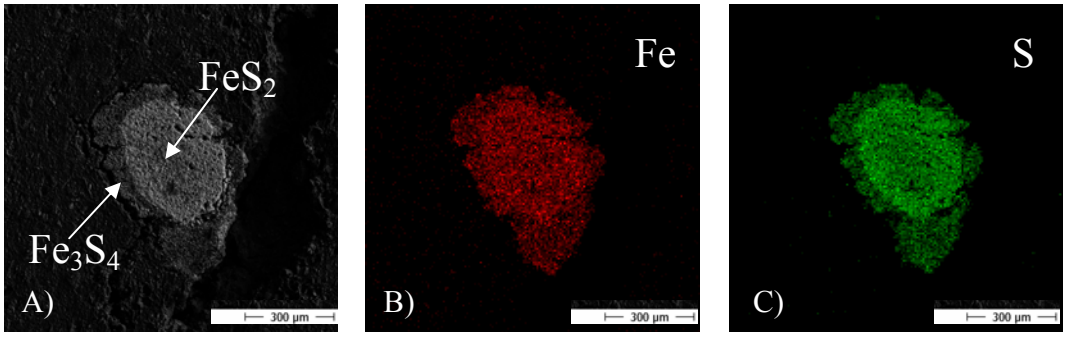

Fig. 5

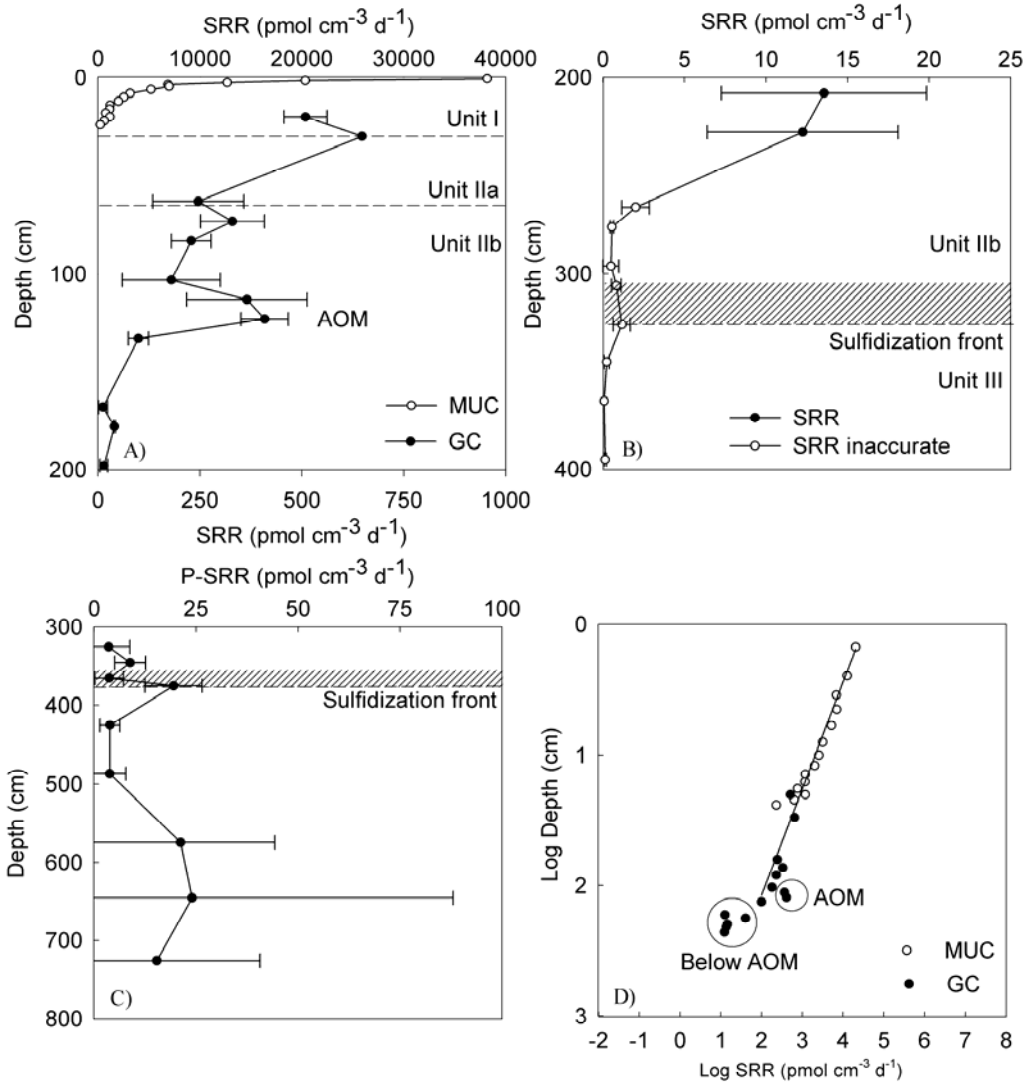
SRR (pmol cm-3 d-1)
Depth (cm)
Unit I
Unit IIa
Unit IIb
AOM
MUC
GC
A)
SRR (pmol cm-3 d-1)
Unit IIb
Sulfidization front
Unit III
SRR
SRR inaccurate
B)
P-SRR (pmol cm-3 d-1)
Sulfidization front
C)
Log Depth (cm)
AOM
Below AOM
MUC
GC
D)
Log SRR (pmol cm-3 d-1)

Chapter 6

Phosphate geochemistry, mineralization processes, and *Thioploca* distribution in shelf sediments off central Chile

Lars Holmkvist*[a], Esther T. Arning[b,c], Kathrin Küster-Heins [d], Verona Vandieken[a,e], Jörn Peckmann[c], Matthias Zabel[d] and Bo Barker Jørgensen[a,f]

[a]*Max Planck Institute for Marine Microbiology, D-28359 Bremen, Germany*

[b]*GFZ German Research Centre for Geosci. Telegrafenberg, D-14473 Potsdam, Germany*

[c]*MARUM – Center for Marine Environmental Sciences, University of Bremen, D-28359 Bremen, Germany*

[d]*Department of Geosciences, University of Bremen, D-28334 Bremen, Germany*

[e]*University of Southern Denmark, Institute of Biology, DK-5230 Odense M, Denmark*

[f]*Center for Geomicrobiology, University of Aarhus, DK-8000 Aarhus C, Denmark*

Keywords: Chile; *Thioploca*; phosphorus; hydroxyapatite, phosphate release

*Corresponding author

E-mail address: LHT@teknologisk.dk, Tel.: +45 72 20 23 95

Abstract

Sediments underlying the major costal upwelling systems of the world oceans are hot-spots of modern formation of hydroxyapatites, often associated with benthic communities of large, nitrate-accumulating, sulfur bacteria. We studied the association between phosphate release, organic phosphorus mineralization, and dense communities of the filamentous sulfur bacteria, *Thioploca* spp., on the continental shelf off central Chile during the austral summer when high phytoplankton productivity and anoxic bottom water prevailed. Freshly deposited phytodetritus stimulated extremely high sulfate reduction rates, which supported a large *Thioploca* community of up to 100 g biomass per m^2. Effective bacterial sulfide uptake kept the sulfide concentration low, which enabled the accumulation of free iron, thus demonstrating intensive iron reduction concurrent with sulfate reduction. Phosphate released to the pore water reached 100-300 μM peak concentrations within the uppermost 0-5 cm and phosphate was lost to the overlying anoxic water column. The large phosphate release was not directly related to the presence of *Thioploca* but rather the result of a high deposition and mineralization rate of fresh organic detritus. Although the pore water was super-saturated with respect to hydroxyapatite, this mineral fraction could only be identified as a minor P-component in the sediment. Most solid-phase phosphate was bound to iron.

1. Introduction

The mineralization of freshly deposited phytoplankton detritus and other organic material in marine sediments triggers regeneration of phosphate, which is required for the long-term marine productivity (Froelich et al., 1988; Garber, 1984; Ruttenberg and Berner, 1993). A part of the deposited phosphorus (P) is buried in the sediment rather than being released again to the water column. For example, in the Gulf of St. Lawrence, the Eastern Canadian shelf and slope, the Chesapeake Bay, and the Portuguese continental margin it was found that only 20-30% of the total P in the surface sediment was remobilized to the overlying water (Anschutz et al., 1998). In the much shallower Aarhus Bay (Denmark), 65-71% of the annually settled P returned to the water column (Jensen et al., 1995).

Several mechanisms are known by which P is retained in the sediment: a) burial of organic phosphate, b) adsorption of phosphate onto clay particles and iron oxyhydroxides, c) formation of finely dispersed inorganic precipitates and d) the formation of inorganic P-rich deposits such as phosphorites (hydroxyapatite). The release of phosphate from the sediment to the bottom water depends strongly on adsorption-desorption processes in the surface sediment (Krom and Berner, 1981; Yamada and Kayama, 1987). Yet, phosphate bound to for example iron oxides is potentially a mobile pool of P which can be released to the bottom water when sediments become anoxic and iron oxides are reduced (Anschutz et al., 1998; Sundby et al., 1992). A correlation was observed between sulfate reduction and the phosphate release from a surface sediment in Aarhus Bay (Denmark) (Mortensen et al., 1993). This was interpreted as chemical reduction of iron oxides by sulfide, which then caused the release of phosphate.

The formation of hydroxyapatite, or more specifically the precipitation of francolite ($[Ca, Na, Mg]_{10}[PO_4]_{6-}x[CO_3]_xF_y[F, OH]_2$), is a major sink in the global P budget of marine sediments since hydroxyapatite is one of the most abundant minerals containing phosphate (Ruttenberg, 1992). Hydroxypatite commonly forms in marine shelf areas with strong coastal upwelling and oxygen minimum zones, such as off the coast of southwest Africa or on the upper continental slope off Peru and Chile (Birch et al., 1983). The concentrating mechanism that leads to super-saturation of pore water with respect to hydroxyapatite and its subsequent precipitation in the sediment is still not clear. It has been suggested that the release of regenerated, organically bound phosphate or of phosphate adsorbed to iron minerals close to the sediment-water interface can trigger the formation of authigenic hydroxyapatite (Froelich et al., 1988; Jahnke et al., 1983). Alternatively, it was proposed in a recent study from the upwelling region off Namibia that the large sulfur bacteria, *Thiomargarita namibiensis*, are able to release phosphate to the pore water in concentrations high enough to trigger hydroxyapatite precipitation (Schulz and Schulz, 2005).

The motivation for the present study was the observation that high pore water phosphate concentrations and rich benthic communities of large sulfur bacteria (e.g. *Thioploca* spp. and/or *Beggiatoa* spp.) often co-occur in sediments underlying the oxygen minimum zone along the Pacific coast of Chile and Peru. Intense seasonal upwelling takes place on the continental shelf during the austral spring and summer. Cold and nutrient rich water is transported up into the euphotic zone and stimulates extremely high productivity of phytoplankton (Ahumada et al., 1983; Peterson et al., 1988). This upwelling region is also the habitat of dense populations of large, colorless, filamentous

sulfur bacteria, *Thioploca* spp., which are involved in the cycling of the nitrogen, carbon, and sulfur (Fossing et al., 1995). In order to explore a possible connection between these sulfur bacteria and the precipitation of hydroxyapatite, we combined the study of pore water and solid phase geochemistry with experimental measurements of anaerobic mineralization rates and the quantification of *Thioploca* bacteria at two stations off the Bay of Concepción, Central Chile.

2. Materials and Methods

2.1. Sampling

Sediment was collected on board the R/V *Kay Kay* just outside the Bay of Concepción at Station 7 (St. 7) and in the adjacent shelf area at Station 18 (St. 18) (Fig. 1, Table 1) on January 17 and 24, 2006. The water depths were 36 m at St. 7 and 93 m at St. 18. The bottom water oxygen concentration was below detection (<2 μM) at both stations while the temperature ranged from 10.5º to 11.2°C (Table 1). Sediment cores of 10 cm diameter were obtained using a multiple corer (MUC). The cores were immediately stoppered without headspace and stored at near in situ temperature on board the vessel. Bottom water samples were taken from some MUC cores for the measurement of oxygen and phosphate.

2.2. Pore water extraction and solid phase sampling

Sediment cores collected on January 17 were processed within two days after retrieval, whereas cores collected on January 24 were processed within a few hours after retrieval. Pore water was extracted directly from the cores using rhizon soil moisture samplers (Rhizosphere Research Products, Wageningen, The Netherlands). The rhizons consist of a 2 mm thick and 5 cm long, porous tube of an inert polymer with a pore size of 0.1 μm. The rhizons were gently pushed into pre-drilled 3 mm holes in the MUC core liner at 1 cm depth intervals in the upper 10 cm, at 2 cm intervals at 10-20 cm, and at 5 cm intervals at 20-30 cm. Pore water (ca 4-5 ml) was extracted by connecting each rhizon to the vacuum of a disposable 10 mL syringe. Pore water extraction started at the top to avoid pore water displacement in the core. Bottom water samples were taken from each

core before pore water extraction. The first ~0.5 mL of the extracted pore water was discarded to ensure that the collected pore water had not been exposed to air. Sub-samples for the determination of dissolved sulfide and sulfate were fixed by mixing 1 mL of pore water with 0.1 mL 1% Zn chloride. The rest of the pore water extracted from each depth interval (ca 3 mL) was acidified with 0.1 mL 10% HCl for later determination of phosphate, dissolved iron, manganese, calcium, fluoride and ammonium. Acidification prevented the oxidation of dissolved iron and enabled samples to be purged with N_2 to remove sulfide before the determination of phosphate.

Sub-samples for solid phase analyses were taken in sub-cores of 50 mm in diameter from the same MUC core as the pore water samples. Sub-cores were sectioned into 1 cm sections within the upper 10 cm of the sediment, 2 cm sections at 10-20 cm depth, and 5 cm sections at 20-30 cm depth. Sediment from each depth was collected in a plastic bag and immediately frozen.

2.3. Pore water analysis

The following analyses were done spectrophotometrically (Shimadzu UV 1202): Phosphate was determined with the molybdenum blue method as modified by Murphy and Riley (1962). Dissolved iron (Fe(II)) was measured according to Stookey (1970) with Ferrozine (1 g L^{-1} in 50 mM HEPES buffer, pH 7) and the absorbance read at 562 nm. Dissolved sulfide was determined on Zn-preserved pore water by the methylene blue method and read at 670 nm (Cline, 1969). Ammonium was determined according to Grasshoff et al. (1999) and read at 630 nm.

Sulfate was analyzed by non-suppressed ion chromatography (100 µl injection volume, Waters, column IC-Pak^{TM}, 50 × 4.6 mm) . The eluant was 1 mM isophthalate buffer in 10% methanol, adjusted to pH 4.5 with saturated Na borohydrate and the flow rate was 1.0 mL min^{-1}. Fluoride was measured by anion chromatography on a Dionex DX500 with an electrochemical detector ED40 (Dionex Corporation, Sunnyvale, CA, USA). Dissolved calcium and manganese were measured by inductively coupled plasma atomic emission spectrometry (Perkin Elmer Optima 3300 RL).

2.4. Solid phase iron and sulfur extraction

AVS (acid volatile sulfide = dissolved sulfide + Fe monosulfides) and CRS (chromium-reducible sulfur = mostly pyrite + elemental S) were determined on thawn sediment samples by the two-step acidic Cr-(II) method (Fossing and Jørgensen, 1989). The volatilized and trapped sulfide was determined by the methylene blue method (Cline, 1969). For solid phase ferric iron (Fe(III)) determination, sediment was extracted with 0.5 M HCl for 1 h at room temperature and the HCl-extracts were analyzed for Fe(II) with Ferrozine and for total iron (Fe(II) + Fe(III)) with Ferrozine + 1% (w/v) hydroxylamine hydrochloride. Total reactive iron in the sediment was extracted with dithionite-citrate-acetic acid (Canfield, 1989). Solid manganese oxides were measured on the same dithionite extracts by flame atomic absorption spectrometry (Perkin Elmer, Atomic Absorption Spectrometer 3110).

2.5. Sequential solid phase phosphate extraction

For the solid-phase speciation of P we used a five-step sequential extraction scheme according to Ruttenberg (1992), as modified by Schenau and Lange (2000). The extracted fractions were: biogenic apatite (Step 1), iron-bound phosphate (Step 2), authigenic hydroxyapatite (Step 3), residual inorganic phosphate (Step 4), and organic-bound phosphate (Step 5). Dried and ground sediment (~125 mg), was washed with 25 mL 2 M NH_4Cl (pH 7) (Step 1), 25 mL citrate dithionite buffer (pH 7.5) (Step 2), 25 mL 1 M Na-acetate (pH 4) (Step 3), 25 mL 1 M HCl (Step 4), and 25 mL 1 M HCl after ignition at 550°C (Step 5). Sediment was rinsed successively with 25 mL 2 M NH_4Cl and demineralized water after the second and third extraction step to prevent re-adsorption of phosphate. All extracted solutions, except iron-bound phosphate (step 2), were measured spectrophotometrically according to Strickland and Parsons (1972). Iron-bound phosphate was measured using an inductively coupled plasma atomic emission spectrometer ICP-AES (Perkin Elmer Optima 3000). During the first five-step sequential extraction of solid phase P the sediment was washed once with NH_4Cl (Step 1) for 16 hours. A second extraction of solid phase P was at St. 7, in which the NH_4Cl treatment (Step 1) was divided into ten 4 h extractions, each with new NH_4Cl solution. This was done in order to increase the recovery (the amount of P extracted out of the total P pool). The recovery of the first extraction was about 77%, but we were able to increase the recovery up to 93% in the second extraction. A more detailed description of the P extraction method (SEDEX) is given in Küster-Heins et al. (2009, in prep).

2.6. Sulfate reduction rates

Sulfate reduction rates were determined using the whole-core $^{35}SO_4^{2-}$ incubation method (Jørgensen, 1978). From each station three Plexiglas sub-cores of 26 mm diameter were taken from the same MUC core and injected with radiotracer (~200 kBq per injection) at 1 to 2 cm depth intervals. The injected cores were incubated for 6 h in the dark at the in situ temperature of ca 10°C. Sulfate reduction was terminated by sectioning the sediment cores, fixing the sections with 20 mL of 20% (w/v) Zn acetate, and freezing. The samples were treated by cold chromium distillation after Kallmeyer et al. (2004). In order to examine the potential reoxidation of sulfide during incubation we incubated a time series for 0.75, 3, 4 and 6 h using four sub-cores taken from St. 18 on January 24.

2.7. Sediment characteristics and Thioploca biovolume determination

The sediment water content (mL g^{-1}), density (g cm^{-3}) and porosity (mL cm^{-3}) were determined from different depths of St. 7 and 18. The water content was determined from the weight loss after drying at 60°C until constant weight was achieved. The density was determined as the wet weight per cm^{-3} which also allowed the calculation of porosity. Freeze dried samples for the determination of total organic C and N were pre-treated with HCl, dried again, and analyzed using a CNS analyzer (Fisons^{TM} Na1500 elemental analyzer).

For *Thioploca* biomass determination, sub-cores were taken from the MUC cores with Plexiglas tubes of 36 mm diameter and stored at 11°C for up to 3 days. The sediment was extruded from the sub-cores and placed on a slightly tilted Plexiglas plate. In order to expose the *Thioploca* sheaths, the sediment between the sheaths was carefully

washed away with seawater from a squirt bottle, starting at the bottom of the core. The number of exposed *Thioploca* sheaths was then counted after consecutive segments of 1 cm of sediment had been washed away. In this way, the number of sheaths throughout the sub-cores was counted at 1 cm depth intervals. Randomly chosen sheaths at each depth were inspected under the microscope to count the number of trichomes and measure their diameter. The number of sheaths per square centimeter multiplied by the average number of trichomes per sheath and the diameter of the trichomes gave the biovolume of trichomes per sediment volume at a given depth (mm^3 biovolume cm^{-3} ~ mg biomass cm^{-3}). According to diameter, the *Thioploca* filaments are referred to as *T. chileae* (12-20 μm wide) or *T. araucae* (30-43 μm wide) (Jørgensen and Gallardo, 1999).

2.8. Polyphosphate in Thioploca cells

For the detection of polyphosphate inclusions in *Thioploca* under the light microscope, intact filaments were randomly collected at St. 7 and 18 and immersed for 30-60 seconds in a solution containing 0.3 % toluidine blue in 0.5 % acetic acid. The filaments were then washed and inspected under the light microscope in 0.5 % acetic acid (Schulz and Schulz, 2005).

2.9. Modeling of pore water data

The fluxes of ammonium and phosphate were determined by one dimensional diffusion modeling: Flux = φ D dC/dz, where φ is the porosity, D is the diffusion coefficient, and dC/dz is the concentration gradient in the pore water. Values of D at the in situ

temperature of ca 10°C were 12.9×10^{-6} cm^2 s^{-1} for NH_4^+ and 5.5×10^{-6} cm^2 s^{-1} for $H_2PO_4^-$ /HPO_4^{2-}, taking the pK_2=7.2 into account and assuming a sediment pH of 7.4.

In order to test whether the pore water chemistry would facilitate a spontaneous precipitation of minerals such as hydroxyapatite or iron sulfides in the sediment, the pore water data were modeled using the computer program PHREEQC (U.S. Geol. Survey). Modeling was done by calculating the saturation index with respect to the mineral phase, whereby thermodynamic information on super-saturation, sub-saturation, or equilibrium with respect to potential mineral phases was registered. For the calculations, mean seawater concentrations was assumed for some conservative elements (Cl: 0.546, Na: 0.469, Mg: 0.053, K: 0.01 [mol/l])).

For hydroxyapatite, the pore water compositions at St. 7 and 18 were chosen for modeling from selected sediment depths where phosphate peaks could be observed. The selected depths at St. 7 were the 5-6 and the 3-4 cm depth zones in the cores collected on January 17 and 24, respectively. At St. 18, the 2-3 and 3-5 cm depth zones were chosen in the cores collected on January 17 and 24, respectively. In addition, modeling was also done at St. 7 on January 24 in the 12-13 cm depth interval.

3. Results

3.1. Description of sediment

The porosity of the surface sediment at 0-1 cm depth was high at both stations, exceeding 0.95 mL cm^{-3}, and decreased to <0.85 mL cm^{-3} at 20-25 cm depth (data not shown). At the surface of all the sampled cores there was a layer of fluffy organic material above a distinct black horizon of varying thickness. The sulfidic sediment below was dark brown.

The concentrations of organic carbon in the sediment cores expressed in percent dry weight are shown in Table 2. At both stations, the content of organic carbon was highest within the uppermost 1 cm sediment and ranged from 3.9 to 5.4% at St. 7 and 3.3 to 5.1% at St. 18. The concentrations of organic carbon below 1 cm depth decreased slightly and stayed relatively constant with values in the range of 2.4 to 3.7% at both stations. The depth distributions of total organic carbon and nitrogen expressed in molar C/N ratios are also shown in Table 2. Low C/N ratios, as observed within the upper 0-2 cm of the sediment at both stations, indicate the presence of freshly deposited organic detritus, which formed the fluff layer. The C/N ratios at St. 7 increased from 7.2 to 8.7 at the surface to 11 at 28 cm depth. At St. 18 the C/N ratio was 8.0-9.3 at the surface and increased to >10 below 15 cm depth. A more detailed description of the sediment geochemistry is given by Thamdrup and Canfield (1996).

3.2. Thioploca

Large colorless filamentous sulfur bacteria, *Thioploca* spp. or *Beggiatoa* spp., formed a loose mat or fur-like coat on the surface of the sediment cores collected just outside the Bay of Concepción (St. 7) and on the nearby shelf (St. 18).

On the sediment surface of cores sampled at St. 7 on January 17, the fluff layer was <1 cm thick while the black horizon was 1-2 cm. In the fluff layer, large free-living sulfur bacteria, presumably of the genus *Beggiatoa* (Teske et al., 1999), were abundant (biomass not determined), together with a low biomass of filaments in common sheaths, *Thioploca araucae*. *T. araucae* were sparse and scattered in the upper 7 cm with a depth-integrated biovolume of 0.17 mm^3 cm^{-2} (Fig. 2 A). In contrast, a large population of *T. araucae* occurred at St. 7 on January 24 (Fig. 2 B). The *Thioploca* filaments stretched 2-4 cm up into the bottom water and gave the sediment the appearance of a fur coat. Below the visible *Thioploca* mat there was a conspicuous black horizon of 3-5 cm thickness. The biovolume of *T. araucae* decreased from 2.56 mm^3 cm^{-3} at 0-1 cm to 0.19 mm^3 cm^{-3} at 8-9 cm depth. Trichomes in sheaths were found down to 15 cm depth. The depth-integrated biovolume was very large, 10.6 mm^3 cm^{-2}, the largest found in any of the investigated sediment cores. The large difference in biomass on sampling dates one week apart must be due to heterogeneous population distribution rather than to growth.

St. 18 sediment collected on January 17 contained both *T. araucae* and *T. chileae*, whereas only *T. araucae* was found in the core sampled on January 24. The upper 3 cm of the core from January 17 consisted of fluffy organic material over a black horizon of 1 cm thickness. On top of the fluffy material, there was a few mm thick layer exclusively of *Thioploca*. The largest bacterial density was 0.58 mm^3 cm^{-3} at 0-2 cm depth, dropping to 0.007 mm^3 cm^{-3} at 14-15 cm depth (Fig. 2 C). The total biovolume was 2.57 mm^3 cm^{-2}. In the core sampled on January 24, *Thioploca* filaments were detected down to 20 cm and the total biovolume was 3.93 mm^3 cm^{-2} (Fig. 2 D).

In the *Thioploca* filaments from the two stations, no intracellular polyphosphate granules could be observed microscopically upon staining with toluidine blue. Plenty of elemental sulfur globules were observed in all filaments.

3.3. Sulfate reduction

Sulfate concentrations decreased monotonously with depth at both stations and ranged from 25-29 mM at the sediment surface to 23-25 mM at 25 cm depth (data not shown). Very high rates of sulfate reduction, 1000-1500 nmol cm^{-3} d^{-1}, were measured in the top 0-1 cm of the sediment at St. 7 and St. 18 (Fig. 3 A and B). Below 1 cm, the rates dropped steeply to 100-200 nmol cm^{-3} d^{-1} at 3 cm and then decreased more gradually down to the bottom of the cores.

3.4. Sulfur and iron in pore water and sediment

The depth profiles of sulfide and iron in the pore water at St. 7 and 18 are presented together in Fig. 4 A to D, as they show highly complementary distributions. Very narrow peaks in sulfide were found in most cores in the top 1 or 2 cm. At St. 7 on January 17, the sulfide peak was particularly broad, covering 0-15 cm, and the concentration was very high, up to 800 μM H_2S. Dissolved iron was below detection. On January 24 at St. 7, sulfide and iron displayed sharp, alternating peaks at 2 and 4 cm depth, respectively, and coexisted in the depth interval of 2-10 cm. At St. 18 on both sampling dates, sulfide had a narrow peak in the top 0-1 cm, low concentrations down to 10 cm, coinciding with the zone of free iron, and was not detectable below 10 cm. Iron reached 90 and 160 μM in the pore water on the two dates. The sulfide concentrations deeper than 10 cm were all

below detection except of the core collected at St. 7 on January 17 where sulfide reached >20 cm depth.

Precipitation of iron monosulfides was expected in the upper 10-15 cm of the sediment because of the co-occurrence of sulfide and dissolved iron in the pore water. Acid volatile sulfide (AVS) was present throughout the cores at concentrations, which scattered mostly below 10-20 μmol cm^{-3} at St. 7 and below 5-10 μmol cm^{-3} at St. 18 (Table 2). The highest concentrations of AVS corresponded to dark horizons visible at the top of the cored sediment. Chromium reducible sulfur (CRS) which consists mostly of pyrite (FeS_2) and elemental sulfur (Zopfi et al., 2008), exhibited a steady increase with depth at both stations, with concentrations ranging from 13 μmol cm^{-3} in the upper 2 cm to >200 μmol cm^{-3} at 25 cm (Table 2).

The distribution of Fe(III) in the sediment at St. 7 and 18 is shown in Table 2. In all of the cores, there was a peak in Fe(III) within the upper 10 cm of the sediment. There was a large difference in concentrations between the two sampling dates, in particular at St. 7, probably due to lateral heterogeneity of the sediment.

Manganese concentrations in the pore water were low, between 0.5 and 2 μM, at both stations, with highest values occurring around 5 cm depth (data not shown). The concentrations of solid phase manganese in the sediment were also low, <0.2 μmol cm^{-3} (Table 2). This is consistent with the highly reducing conditions in the sediment which enable the escape of Mn^{2+} to the overlying seawater and thereby its loss from the sediment.

3.5. Ammonium in pore water

The ammonium profiles showed high net ammonium production in the uppermost 10 cm, despite a considerable difference in concentration between the two stations. At St. 7, ammonium peaked with up to 1.3 mM at 5-10 cm depth and dropped below that depth on both sampling dates. At St.18, ammonium increased gradually with depth and reached 2.8 and 1.6 mM on the two sampling dates (Fig. 5 A and B).

3.6. Phosphate in pore water and sediment

Distinct peaks of free phosphate in the pore water showed that a net release of phosphate from the bound phases occurred within the upper 10 cm of the sediment at both St. 7 and 18 (Fig. 6 A and B, respectively; Table 1). At St. 7, the peak concentrations were 130 μM at 6-7 cm and 218 μM at 3-4 cm depth on the two sampling dates (Fig. 6 A). At St. 18, peak concentrations were 320 μM at 2-3 cm and 235 μM at 3-4 cm depth (Fig. 6 B). The concentrations of phosphate below 10 cm decreased gradually (St. 7) or remained constant (St. 18).

Figs. 7 show results from the sequential extraction of solid phase phosphate in sediment at both stations, except of the results on biogenic apatite (Step 1) and residual inorganic phosphate (Step 4) since these concentrations were low and not relevant for the present study. The depth distribution of organic-bound phosphate was similar between St. 7 and 18. Relatively higher concentrations were observed in the upper 10 cm (>0.4 g kg^{-1} dry sediment), whereas lower and more constant concentrations were observed beneath this depth (Fig. 7 A and B). At St. 18, the concentration reached 1.5 g kg^{-1} dry sediment at 1 cm.

The depth distribution of iron-bound phosphate differed strongly between St. 7 and 18 (Fig. 7 C and D). At St. 7, the concentration was about 2 g kg^{-1} dry sediment and generally increased with depth (Fig. 7 C). At St. 18, the concentration decreased steeply from 5.6 g kg^{-1} dry sediment at 0-1 cm depth to 0.9 g kg^{-1} dry sediment at 25-30 cm (Fig. 7 D).

The amount of phosphate from authigenic hydroxyapatite determined from the first extraction procedure was very low at all depths examined at St. 7 and 18 (≤0.1 g kg^{-1} dry sediment, Fig. 7 E and F). In particular within the upper 12 cm of the sediment at St. 7, there was apparently no detectable phosphate present as authigenic hydroxyapatite (Fig. 7 E). At St. 18, the amount of phosphate extracted from authigenic hydroxyapatite varied between 0.00 and 0.02 g kg^{-1} dry sediment (Fig. 7 F). Results from the second extraction procedure at St. 7 showed that especially within the upper 10 cm quite significant amounts of phosphate did in fact occur in hydroxyapatite (Fig. 7 E). The maximum concentration of phosphate extracted from authigenic hydroxyapatite was 0.19 g kg^{-1} dry sediment and the concentrations scattered with depth.

The major fraction of phosphate from the first extraction at St. 7 was bound to ferric iron (69-85%, data not shown). The iron-bound phosphate also made up the largest fraction, 39 to 55%, by the second extraction procedure which was performed only at St. 7 (data not shown). The second largest fraction extracted from the first procedure was organic-bound phosphate, with higher fractions in the upper 12 cm of the sediment (15-29%) compared to 12-15 cm depth (<13%) (data not shown). The remainder of the extracted phosphate (biogenic phosphate, authigenic phosphate, and residual inorganic phosphate) made up ≤6 % at any depth (data not shown). At St. 18, the iron-bound phosphate from

the first extraction also accounted for the largest fraction particularly in the upper 18 cm of the sediment (64-76 %, data not shown). The organic-bound phosphate also made up a large fraction at St. 18, ranging from 10% at 1-2 cm depth to 23% at 10-12 cm (data not shown). Below 18 cm, biogenic apatite accounted for 41-51%. The fractions authigenic hydroxyapatite and residual inorganic phosphate were <4%.

3.7. Calcium and fluoride in pore water

The pore water concentrations of calcium were 10 mM at the sediment surface and generally decreased slightly with depth at both at St. 7 and 18 (data not shown). Scattered, lower (St. 7) or higher (St. 18) values relative to the monotonous trend were observed only on the second sampling date and may be an artifact.

The measured pore water concentrations of fluoride were generally low and scattered with concentrations <11 μM at St. 7 and <32μM at St. 18 on both sampling dates (data not shown). Highest concentrations were found in the upper 15 cm, probably due to a downward diffusion from the water column (Froelich et al., 1983).

4. Discussion

4.1. Thioploca populations

Quantification of the *Thioploca* populations and their depth distribution at two stations showed a common pattern but also distinct differences. In sediments with a well established *Thioploca* community, the density of sheaths and trichomes was highest at the sediment surface and decreased with depth in a quasi-exponential manner. At St. 18, on the middle of the continental shelf, the total population size and depth distribution were very similar between two consecutive sampling times. At St. 7, in contrast, at the mouth of the Bay of Concepción, the *Thioploca* showed a spotty distribution with dense populations of 3-4 times higher biomass than at St. 18, alternating with sediment with few and scattered *Thioploca*. This heterogeneous distribution was confirmed by further core samples taken at St. 7 for which only a qualitative evaluation of the population size was made. The heterogeneous distribution turned out to be a most helpful experiment by nature as it allowed a comparison of the sediment geochemistry with and without a large *Thioploca* population.

A previous study from 1994 of *Thioploca* biovolume from St. 7 showed a much higher biomass density of 12 mm^3 cm^{-3} in the top 0-1 cm of the sediment (Schulz et al., 1996). (For comparison, a biomass of 12 mm^3 cm^{-3} corresponds to a population density of $>10^{10}$ 1 μm^3 size bacteria per mL of sediment). This total depth-integrated biomass was very similar to the present *Thioploca*-rich St. 7 sample, indicating that these gliding bacteria had probably migrated up to the sediment surface in the earlier study. We do not know the cause of population heterogeneity at St. 7. It seems that, due to the very high sulfate reduction rates, *Thioploca* are barely able to keep the sulfide concentration

down to a level, which they can tolerate. When they succeed, they establish very high population densities due to the high energy supply. When they do not succeed, they either migrate to the sediment surface or the population dies out. Earlier studies from St. 7 and 18 show that the populations may vary strongly over the seasons in response to the availability of sulfide or to the adverse effect of oxygen (Schulz et al., 2000). As oxygen was not present in the bottom water at either of the sampling stations at both sampling dates (Table 1), the maximum density of *Thioploca* near the sediment surface probably reflected a requirement for access to nitrate, which they take up from the water column and use as an electron acceptor (Zopfi et al., 2001).

A comparison of the depth profiles of dissolved sulfide and iron among the sediment cores collected at St. 7 and 18 on different dates reveals the impact of the sulfide oxidizing *Thioploca* on pore water composition (Fig. 4). Only the sediment collected at St. 7 on January 17, which had few and scattered *Thioploca*, showed a large peak of sulfide and near-zero free iron in the pore water. In the three other cores with abundant *Thioploca*, sulfide was low and scattered, apart from the top 1 to 2 cm of sediment which consisted of fresh detritus with extremely high sulfate reduction rates (Fig. 3). Instead, dissolved iron peaked in the upper 3-5 cm, just below the surface sulfide peak, with concentrations up to 90-190 μM (Fig. 4).

4.2. Mineralization of organic matter

Sulfate and iron reduction played the major role in the anaerobic mineralization of organic matter within the upper 10-20 cm of the sediment as has been previously noted by Thamdrup and Canfield (1996). Manganese reduction was apparently of minor

importance as the concentration of manganese oxides was low. Furthermore, measurements of free Mn^{2+} show that reduced manganese in the pore water was low, <10 µM, probably because it was lost to the overlying seawater (Zopfi et al., 2008).

Sulfate reduction rates at St. 7 and 18 were similar, with extremely high rates near the sediment surface and a steep decrease with depth. The total depth integrated sulfate reduction rates (∑ 0-21 cm: 33 and 29 mmol m^{-2} d^{-1} at St. 7 and 18, respectively) were in the lower range of previous data from the shelf off Concepción (27 to 56 mmol m^{-2} d^{-1}) (Thamdrup and Canfield, 1996). Importantly, the time course experiments of sulfate reduction indicated that, in the upper 0-10 cm of the sediment, about 25-50% of the radiolabeled sulfide produced from $^{35}SO_4^{2-}$ was reoxidized during the 6 hours of incubation. This shows how dynamic the sulfur cycling is in the *Thioploca* inhabited sediment.

The pore water data for free sulfide and iron showed steep and complimentary profiles, which indicated a competition between sulfate and iron reduction and a rapid reaction between produced sulfide and solid phase or dissolved iron. In all cores from the two stations, sulfate reduction and free sulfide concentrations were very high in the organic fluff layer of the top 0-1 cm (Fig. 3 and 4). In the cores with abundant *Thioploca*, free sulfide dropped steeply below 1 cm and was low down to 10-15 cm, i.e. in the sediment where most of the *Thioploca* biomass occurred. Only in the St. 7 core with very few *Thioploca* did free sulfide remain high throughout the top 15 cm of sediment (Fig. 4 A). This indicates that both iron reduction and sulfate reduction co-occur in the sediment and that the sulfide uptake by *Thioploca* shifts the balance between H_2S and Fe^{2+} net accumulation to allow the appearance of excess Fe^{2+}. In the sediment

without *Thioploca*, the high sulfide production rate presumably exceeds iron reduction to the effect that liberated Fe^{2+} is immediately precipitated by H_2S. A recent study by Zopfi et al. (2008) concluded that the major part of the sulfide removal within these sediments was due to chemical oxidation with Fe(III) rather than to uptake by *Thioploca*. Modeling of the H_2S and Fe^{2+} data with PHREEQCi software indicated that the complementary distributions of the two species are controlled by precipitation as the pore water was supersaturated with respect to FeS and mackinawite in horizons where both were detected.

The distinct peaks of Fe^{2+} at 3-5 cm depth in Fig. 4 B-D show that iron reduction rates are very high in the top 10 cm. However, it remains unclear whether the iron reduction is a bacterial process or due to reaction of Fe(III) species with sulfide produced from sulfate reduction (Thamdrup and Canfield, 1996). Iron-reducing bacteria may compete favorably with sulfate reduction for suitable organic substrates, provided that highly reactive Fe(III), such as poorly crystalline iron hydroxides, are available in sufficient amounts (Lovley and Phillips, 1987). This might be the case in approximately the first 5 cm of sediment below the fluff layer where the high net production of Fe^{2+} took place. The predominance of iron reduction in the upper 5 cm might also explain the subsurface maxima of sulfate reduction observed at 3-8 cm depth in several individual sub-cores from St. 7 and 18.

4.3. Thioploca and phosphate

The major part of the *Thioploca* biovolume in the investigated sediment cores occurred within the upper 5 cm (71 to 84%) where also high pore water concentrations of

phosphate were measured. Furthermore, the largest and steepest pore water phosphate peak was found in the core that contained the largest *Thioploca* biomass and the smallest phosphate peak was observed in the core with very few *Thioploca* (Fig. 2 and 7). A positive correlation between the occurrence of large sulfide oxidizing bacteria, sulfate-reducing bacteria, and the enrichment of phosphate in pore water was observed also in sediments off Chile, Peru, and Namibia (Arning et al., 2008). We therefore considered whether the high phosphate concentrations might be due to phosphate release from *Thioploca* in the same way as the large sulfur bacteria, *Thiomargarita namibiensis*, were found to release phosphate into the pore water of a Namibian sediment (Schulz and Schulz, 2005). The observation from St. 7, where a distinct phosphate peak existed in sediments with abundant *Thioploca* as well as in sediments with only few *Thioploca*, showed, however, that phosphate release from these bacteria could not explain the whole phosphate enrichment in the pore water (Fig. 6 A).

The physiological rationale for phosphate release by *Thiomargarita namibiensis* seems to be their use of polyphosphate as energy storage in the cells. Schulz and Schulz (2005) proposed that phosphate may be taken up by *Thiomargarita* under energetically favourable oxic conditions and released again under anoxic conditions because the cells need to spend energy for the uptake of organic substrates for growth. In contrast to *Thiomargarita*, however, *Thioploca* thrives under anoxic or low-oxic conditions and the large populations partly die off when oxic water covers the continental shelf in years of El Niño (Schulz and Jørgensen, 2001). It was recently demonstrated that marine *Thioploca* can have a high rate of aerobic respiration under low-oxic conditions (Høgslund et al., 2009), so it is not clear whether the die-off is due to oxygen or to the

lack of sulfide caused by low primary productivity and low organic sedimentation during El Niño.

We searched for polyphosphate inclusions in the *Thioploca* filaments from St. 7 and St. 18 by staining with toluidine blue, but with negative results. Although this staining technique may not detect very small inclusions, our current conclusion is that the *Thioploca* populations studied did not contain significant amounts of polyphosphate, which could have been a source of pore water phosphate. A series of experiments, using purified bundles of *Thioploca* filaments, showed that under the experimental conditions of alternating oxygen, sulfide, or acetate no phosphate release from the bacteria could be detected. Neither could an uptake of external, ^{33}P-labeled phosphate be detected in cell inclusions by using microautoradiography (Høgslund et al., 2009).

Results from the sequential solid phase phosphate extractions showed that only very low concentrations of authigenic hydroxyapatite were present at St. 7 and 18, even when the more efficient extraction procedure was applied ($\leq$0.19 g kg^{-1} dry sediment, Fig. 7 E). For comparison, hydroxyapatite concentrations $\geq$50 g kg^{-1} dry sediment were found in the Namibian sediment by Schulz and Schulz (2005), who concluded that, *Thiomargarita namibiensis*, were responsible for the precipitation of hydroxyapatite, providing a mechanism to explain the common coincidence of large sulfur bacteria and phosphogenesis in modern sediments and in the geological past. The observations that (1) peak concentrations of phosphate in the present study did not correlate with *Thioploca* bacteria and (2) very low hydroxyapatite concentrations were found together with high *Thioploca* biovolumes suggest that the formation of authigenic

hydroxyapatite in or near the Bay of Concepción was not directly related to the presence of *Thioploca* bacteria.

Nonetheless, formation of hydroxyapatite, would have been expected to occur within the upper 10 cm of the sediment at either St. 7 or 18 owing to the high pore water concentrations of phosphate, calcium and fluoride. The measured phosphate concentrations were high and within the same range (≤ 300 μM) as in the study by Schulz and Schulz (2005) in sediment from Namibia where hydroxyapatite precipitation did take place. The pore water concentrations of calcium were generally constant with depth in all of the investigated Chilean cores. Hence, there were indications of calcium removal due to the precipitation of hydroxyapatite. Fluoride exhibited peak concentrations within the upper 10 cm of the sediment, but the concentrations were low and did not allow conclusions about the formation of hydroxyapatite, in the sediment.

Modeling of the pore water data reveal that formation of hydroxyapatite should theoretically occur. At both St. 7 and 18, the saturation index of hydroxyapatite (0.23 to 3.16) indicated super-saturation with regard to the pore water constituents involved in the formation of hydroxyapatite. The PHREEQCi model calculations further demonstrated that only pore water concentrations of phosphate below 35 μM result in concentrations below saturation.

The present study was performed during a mid-summer period with anoxia in the bottom waters due to upwelling, which therefore likely caused a transient enhanced release of phosphate to the pore water. During the austral autumn and winter the bottom waters near and in the Bay of Concepción are generally more oxic, and a lower release of phosphate to the pore water could thus be expected. In summary, we therefore propose

that high pore water concentrations of phosphate were only a temporary phenomenon associated with the oxygen minimum and high summer productivity and that these peak concentrations did not lead to a long-term accumulation of hydroxyapatite.

4.4. Remobilization of phosphate to the pore water

The present study indicates that the high concentrations of pore water phosphate were a result of organic matter mineralization and reduction of Fe(III) rather than a release of phosphate from *Thioploca*. In particular, the highest phosphate concentrations were situated right underneath the fluffy detritus layer, implying that phosphate was remobilized from the mineralization of newly settled organic matter (e.g. dead phytoplankton). This was also indicated by the overall decrease in the content of organic-bound phosphate, which was in particular observed from the surface to the bottom of the core from St. 18 on January 24 (Fig. 8 B).

Phosphate exhibited peak concentrations in the pore water at 3-6 cm depth with steep gradients leading up to the sediment surface and with less steep gradients downwards. The upward gradients indicate a diffusive loss of phosphate into the anoxic water column. The downward gradients below the concentration peaks points to a sub-surface sink for phosphate. We modeled these phosphate fluxes for the four coring occasions and thereby calculated the net phosphate release in the top 10 cm of the sediment.

At Station 7, the upwards fluxes to the sediment surface were 0.17 and 0.27 mmol $H_2PO_4^-$ m^{-2} d^{-1} on the two sampling occasions, while the downwards fluxes below the phosphate peak were 0.04 and 0.06 mmol $H_2PO_4^-$ m^{-2} d^{-1}. Thus, out of a net phosphate

release of 0.21 and 0.33 mmol $H_2PO_4^-$ m^{-2} d^{-1}, 19% and 18% was bound below the phosphate peak while the majority, 81% and 82%, was lost by diffusion to the overlying water column. At Station 18 the upwards fluxes were higher, 0.55 and 0.59 mmol $H_2PO_4^-$ m^{-2} d^{-1} on the two sampling occasions while the downwards fluxes were 0.08 and 0.05 mmol $H_2PO_4^-$ m^{-2} d^{-1}. Thus, out of the net phosphate release of 0.63 and 0.64 mmol $H_2PO_4^-$ m^{-2} d^{-1}, 13% and 8% was bound below the phosphate peak while the majority, 87% and 92%, was lost by diffusion to the overlying water column.

These rates of net phosphate release can be compared with the net mineralization of organic matter through sulfate reduction. At Station 7 on January 24, the depth-integrated sulfate reduction in the uppermost 0-10 cm was 29 mmol SO_4^{2-} m^{-2} d^{-1}, which corresponds to the mineralization of ca 58 mmol Corg m^{-2} d^{-1}, given a simple stoichiometry of $SO_4^{2-} + 2CH_2O + 2H^+ \rightarrow H_2S + 2CO_2 + 2H_2O$. By comparison with the net phosphate release at this station and date, the apparent C:P ratio of mineralization was 58:0.33 or 175:1. At Station 18 on January 24 the depth-integrated sulfate reduction in the uppermost 0-10 cm was 26 mmol SO_4^{2-} m^{-2} d^{-1}which corresponds to the mineralization of ca 52 mmol Corg m^{-2} d^{-1}. By comparison with the net phosphate release, the apparent C:P ratio of mineralization was 52:0.64 or 81:1. An expected Redfield ratio of elemental composition would lead to a ratio of 106:1 by the mineralization of fresh phytodetritus. This comparison indicates that the release of phosphate was either lower or higher than expected, assuming stoichiometrically balanced decomposition of freshly deposited phytodetritus as the main phosphate source. The degradation of aged, phosphate-depleted detritus might be the cause of the higher

C:P ratio, whereas phosphate mobilization during the reduction of Fe(III) might release ferric iron-bound phosphate (Fig. 7 B) and thereby cause the lower C:P ratio.

The loss of ammonium by diffusion to the overlying water column at Station 7 on January 24 was 2.22 mmol m^{-2} d^{-1}while the maximum downwards flux below the ammonium peak was -2.15 mmol NH_4^+ m^{-2} d^{-1}. The total net ammonium release was 4.36 mmol NH_4^+ m^{-2} d^{-1}. The resulting apparent stoichiometry of carbon to nitrogen mineralization was thus 58:4.36 or 13:1, which is somewhat more N-depleted than the mean C:N composition of ca 10:1 in the organic matter at the depth of maximum ammonium release (Table 2). The ratio of ammonium to phosphate release was 4.36: 0.33 or 13:1, which indicates a N:P ratio somewhat below the Redfield ratio of 17:1. At Station 18, the ammonium fluxes were even much lower, which appears to be in contrast to the steep phosphate gradients. A more accurate stoichiometric analysis will require further studies, including the bound and adsorbed ammonium and phosphate pools.

Conclusion

In the present study, we combined the study of pore water and solid phase geochemistry with sulfate reduction rates and biomasses of *Thioploca* bacteria at two stations off the Bay of Concepción (Chile), in order to explore a possible connection between these sulfur bacteria and the precipitation of hydroxyapatite. Our results indicate that the sediment at both stations leaked phosphate to the anoxic water column during the summer season. Apparently, the large sulfur bacteria, *Thioploca* spp., did not contribute to this net phosphate release and hydroxyapatite formation did not appear to be an important sink for phosphate at the time and location of our study.

Acknowledgements

We thank the entire Thioploca-team from January 2006 in Dichato for stimulating cooperation. In particular, we thank Ariel Gallardo and his Chilean colleagues at the Dichato station and the *Kay Kay* crew for all their help and enthusiasm. Kirsten Imhoff, Martina Meyer and Andrea Schipper are thanked for logistic help with the equipment. We thank Caroline Slomp from Utrecht University (The Netherlands) for help in interpretation of the P data. The study was financed by the Max Planck Society, and the Excellence Cluster MARUM, Bremen of the Deutsche Forschungsgemeinschaft.

References

Ahumada, B.R., Rudolph, A.G. and Martinez, M.V., 1983. Circulation and fertility of waters in Concepción Bay. Estuarine, Coastal and Shelf Science 16, 95-105.

Anschutz, P., Zhong, S., Sundby, B., Mucci, A. and Gobeil, C., 1998. Burial efficiency of phosphorus and the geochemistry of iron in continental margin sediments. Limnol. Oceanogr. 43, 53-64.

Arning, E.T., Birgel, D., Schulz-Vogt, H., Holmkvist, L., Jørgensen, B., Larson, A. and Peckmann, J., 2008. Lipid Biomarker Patterns of Phosphogenic Sediments from Upwelling Regions. Geochim Cosmochim Acta 25, 69-82.

Birch, G.F., Thomson, J., McArthur, J.M. and Burnett, W.C., 1983. Pleistocene phosphorites off the west coast of South Africa. Nature 302, 601-603.

Canfield, D.E., 1989. Reactive iron in marine sediments. Geochimica et Cosmochimica Acta 53, 619-632.

Cline, J.D., 1969. Spectrophotometric determination of hydrogen sulfide in natural waters. Limnology and Oceanography 14, 454-458.

Fossing, H., Gallardo, V.A., Joergensen, B.B., Huettel, M., Nielsen, L.P., Schulz, H., Canfield, D.E., Forster, S., Glud, R.N., Gundersen, J.K., Kuever, J., Ramsing, N.B., Teske, A., Thamdrup, B. and Ulloa, O., 1995. Concentratin and transport of nitrate by the mat-forming sulphur bacterium Thioploca. Nature 374, 713-715.

Fossing, H. and Jørgensen, B.B., 1989. Measurement of bacterial sulfate reduction in sediments: Evaluation of a single-step chromium reduction method. Biogeochemistry 8, 205-222.

Froelich, J., Kim, K.H., Jahnke, R., Burnett, W.C., Soutar, A. and Deakin, M., 1983. Pore water fluoride in Peru continental margin sediments: uptake from seawater. Geochim. Cosmochim. Acta 47, 1605-1612.

Froelich, P.N., Arthur, M.A., Burnett, W.C., Deakin, M., Hensley, V., Jahnke, R., Kaul, L., Kim, K.H., Roe, K., Soutar, A. and Vathakanon, C., 1988. Early diagenesis of organic matter in Peru continental margin sediments: Phosphorite precipitation. Marine Geology 80, 309-343.

Garber, J.H., 1984. Laboratory study of nitrogen and phosphorus remineralization during decomposition of coastal plankton and seston. Estaurine, Coastal and Shelf science 18, 685-702.

Grasshoff, K., Kremling, K. and Ehrhardt, M., 1999. Methods of Seawater Analysis, third ed. Wiley, New York, 1-600 pp.

Høgslund, S., Revsbech, N.P., Kuenen, J.G., Jørgensen, B.B., Gallardo, V.A., Van de Vossenberg, J., Nielsen, J.L., Holmkvist, L., Arning, E. and Nielsen, L.P., 2009. Physiology and behaviour of marine Thioploca. The ISME journal 3, 647-657.

Jahnke, R.A., Emerson, S.R., Roe, K.K. and Burnett, W.C., 1983. The present day formation of apatite in Mexican continental margin sediments. Geochim Cosmochim Acta 47, 259-266.

Jensen, H.S., Mortensen, P.B., Andersen, F.O., Rasmussen, E. and Jensen, A., 1995. Phosphorus cycling in a coastal marine sediment, Aarhus Bay, Denmark. Limnology and Oceanography 40, 908-917.

Jørgensen, B.B., 1978. A comparison of methods for the quantification of bacterial sulfate reduction in coastal marine sediments. III. Estimation from chemical and bacteriological field data. Geomicrobiology Journal 1, 49-64.

Jørgensen, B.B. and Gallardo, V.A., 1999. *Thioploca* spp.: filamentous sulfur bacteria with nitrate vacuoles. FEMS Microbiology Ecology 28, 301-313.

Kallmeyer, J., Ferdelman, T.G., Weber, A., Fossing, H. and Jørgensen, B.B., 2004. A cold chromium distillation procedure for radiolabeled sulfide applied to sulfate reduction measurements. Limnology and Oceanography: Methods 2, 171-180.

Krom, M.D. and Berner, R.A., 1981. The diagenesis of phosphorus in a nearshore marine sediment. Geochimica et Cosmochima Acta 45, 207-216.

Lovley, D.R. and Phillips, E.J.P., 1987. Competitive mechanisms for inhibition of sulfate reduction and methane production in the zone of ferric iron reduction in sediments. Applied and Environmental Microbiology 53, 2636-2641.

Mortensen, P.B., Jensen, H.S., Rasmussen, E.K. and Thamdrup, B., 1993. Seasonal variation in P-pools, porewater SRP and P-release in a coastal marine sediment. Hydrobiologia 253, 101-102.

Murphy, J. and Riley, J.P., 1962. A modified single solution method for the determination of phosphate in natural waters. Anal. Chim. Acta 27, 31-36.

Peterson, W.T., Arcos, D.F., McManus, G.B., Dam, H., Bellantoni, D., Johnson, T. and Tiselius, P., 1988. The nearshore zone during coastal upwelling: Daily variability and coupling between primary and secondary production off central Chile. Prog. Oceanog. 20, 1-40.

Ruttenberg, K.C., 1992. Development of a sequential extraction method for different forms of phosphorus in marine-sediments. Limnol. Oceanogr 37, 1460-1482.

Ruttenberg, K.C. and Berner, R.A., 1993. Authigenic apatite formation and burial in sediments from non-upwelling, continental margin environments. Geochim. Cosmochim. Acta 57, 991-1007.

Schenau, S. and Lange, G., 2000. A novel chemical method to quantify fish debris in marine sediments. Limnol. Oceanogr 45, 963-971.

Schulz, H.N. and Jørgensen, B.B., 2001. Big bacteria. Annu. Rev. Microbiol. 55, 105-137.

Schulz, H.N., Jørgensen, B.B., Fossing, H.A. and Ramsing, N.B., 1996. Community structure of filamentous, sheath-building sulfur bacteria, Thioploca spp., off the Coast of Chile. Applied and Environmental Microbiology 62, 1855-1862.

Schulz, H.N. and Schulz, H.D., 2005. Large sulfur bacteria and the formation of phosphorite. Science 307, 416-418.

Schulz, H.N., Strotmann, B., Gallardo, V.A. and Joergensen, B.B., 2000. Population study of the filamentous sulfur bacteria Thioploca spp. off the Bay of Concepcion, Chile. Marine Ecology Progress Series 200, 117-126.

Stookey, L.L., 1970. Ferrozine - a new spectrophotometric reagent for iron. Analytical Chemistry 42, 779-781.

Strickland, J.D.H. and Parsons, T.R., 1972. A practical handbook of sea-water analysis 2nd Edition Fish. Res. Bd., Canada, 311pp pp.

Sundby, B., Gobeil, C. and Silverberg, N., 1992. The phosphorus cycle in coastal mar-sedimentsine. Limnol. Oceanogr 37, 1129-1145.

Teske, A., Sogin, M.L., Nielsen, L.P. and Jannasch, H.W., 1999. Phylogenetic relationships of a large marine Beggiatoa. System. Appl. Microbiol. 22, 39-44.

Thamdrup, B. and Canfield, D.E., 1996. Pathways of carbon oxidation in continental margin sediments off central Chile. Limnology and Oceanography 41, 1629-1650.

Yamada, H. and Kayama, M., 1987. Distribution and disolution of several forms of phosphorus in coastal marine sediments. Oceanol. Acta 10, 311-321.

Zopfi, J., Böttcher, M. and Jørgensen, B., 2008. Biogeochemistry of sulfur and iron in Thioploca-colonized surface sediments in the upwelling area off central chile. Geochim Cosmochim Acta 72, 827-843.

Zopfi, J., Kjaer, T., Nielsen, L.P. and Joergensen, B.B., 2001. Ecology of *Thioploca* spp.: Nitrate and sulfur storage in relation to chemical microgradients and influence of *Thioploca* spp. on the sedimentary nitrogen cycle. Applied and Environmental Microbiology 67, 5530-5537.

Figure legends

Fig. 1

Map of the study area, Bay of Concepción with location of coring sites “St. 7” and “St. 18”.

Fig. 2

Biomass of *Thioploca* bacteria from (A) St. 7 17.01.06, (B) St. 7 24.01.06, (C) St. 18 17.01.06 and (D) St. 18 24.01.06.

Fig. 3

Sulfate reduction rates measured experimentally using $^{35}SO_4^{2}$ in the sediment cores at (A) St. 7 24.01.06 and (B) St. 18 24.01.06. Error bars show standard deviation of triplicate measurements.

Fig. 4

Hydrogen sulfide and dissolved iron in pore water from (A) St. 7 17.01.06, (B) St. 7 24.01.06, (C) St. 18 17.01.06 and (D) St. 18 24.01.06.

Fig. 5

Ammonium in pore water from (A) St. 7 the 17.01.06 and 24.01.06 and (B) St. 18 the 17.01.06 and 24.01.06.

Fig. 6

Phosphate in pore water from (A) St. 7 the 17.01.06 and 24.01.06 and (B) St. 18 the 17.01.06 and 24.01.06.

Fig. 7

Depth distributions of organic-bound phosphate in sediment from (A) St. 7 24.01.06 and (B) St. 18 24.01.06, phosphate bound to ferric iron from (C) St. 7 24.01.06 and (D) St. 18 24.01.06 and phosphate in hydroxyapatite from (E) St. 7 24.01.06 and (F) St. 18 24.01.06.

Table 1. Positions of Station 7 and 18 sampled on January 17 and 24, 2006, and data of bottom water.

Station	Sampling date	Position	Depth (m)	Temp. (°C)	Oxygen (µM)	Phosphate (µM)
St. 7	17th of January	36°36.388' S, 73°00.625' W	36	11.2	0	6.5
	24th of January	36°36.168' S, 73°00.658' W	36	10.8	0	3.6
St. 18	17th of January	36°31.259' S, 73°08.014' W	93	10.5	0	20.3
	24th of January	36°30.818' S, 73°07.765' W	93	10.6	0	3.6

Table 2. Solid phase chemical compositions in sediment of Station 7 and 18 determined in January 2006.

Station 7

Depth (cm)	TOC (%)		C/N (mol mol^{-1})		AVS (μmol cm^{-3})		CRS (μmol cm^{-3})		Fe(III) (μmol cm^{-3})		MnO_2 (μmol cm^{-3})	
	17.01	24.01	17.01	24.01	17.01	24.01	17.01	24.01	17.01	24.01	17.01	24.01
0.5	3.9	5.4	8.7	7.2	6.7	0.1	53.3	12.6	6.4	7.2	0.01	0.02
1.5	3.2	3.2	9.2	8.8	3.7	6.9	101.6	44.8	6.1	8.8	0.12	0.08
2.5	2.9	2.7	9.9	9.9	11.2	2.7	99.3	57.0	10.5	8.8	0.16	0.15
3.5	2.7	2.9	9.8	10.0	3.9	8.0	70.4	54.0	6.2	12.5	0.16	0.15
4.5	3.0	2.9	9.5	9.9	10.9	7.4	94.5	81.9	7.5	3.5	0.12	0.14
5.5	n.d.	n.d.	n.d.	n.d.	19.3	4.1	56.1	30.8	9.4	2.0	0.08	0.13
6.5	n.d.	n.d.	n.d.	n.d.	10.5	9.9	49.6	55.0	7.9	4.5	0.08	0.11
7.5	n.d.	n.d.	n.d.	n.d.	8.6	12.3	74.7	44.0	10.4	3.6	0.09	0.13
8.5	n.d.	n.d.	n.d.	n.d.	12.9	16.2	96.6	84.1	13.7	0.4	0.13	0.16
9.5	2.8	2.7	10.0	10.1	19.3	10.6	122.2	83.4	16.4	n.d.	0.12	0.16
11	n.d.	n.d.	n.d.	n.d.	11.4	0.8	116.8	48.1	7.9	3.5	0.14	0.15
13	n.d.	n.d.	n.d.	n.d.	3.1	4.2	91.1	96.3	3.5	15.7	0.16	0.15
15	2.8	2.6	10.4	10.2	9.4	7.8	128.4	127.1	0.0	4.3	0.21	0.18
17	n.d.	n.d.	n.d.	n.d.	16.4	6.3	128.0	116.7	12.1	1.6	0.16	0.17
19	2.8	2.7	10.4	10.7	15.7	5.0	113.6	118.5	8.8	5.7	0.20	0.20
22.5	2.6	2.5	10.7	11.1	15.9	0.9	118.5	173.7	7.0	8.2	0.20	0.18
27.5	2.3	n.d.	11.1	n.d.	n.d.	n.d.	218.7	n.d.	10.3	n.d.	0.20	n.d.

Station 18

Depth (cm)	TOC (%)		C/N (mol mol^{-1})		AVS (µmol cm^{-3})		CRS (µmol cm^{-3})		Fe(III) (µmol cm^{-3})		MnO_2 (µmol cm^{-3})	
	17.01	24.01	17.01	24.01	17.01	24.01	17.01	24.01	17.01	24.01	17.01	24.01
0.5	5.1	3.3	8.0	9.3	0.3	8.3	17.9	35.5	2.6	n.d.	0.10	0.09
1.5	3.7	3.4	9.3	9.5	0.2	0.4	17.6	29.9	1.5	3.0	0.10	0.14
2.5	3.4	3.3	9.8	9.6	1.0	2.2	43.1	43.5	5.8	6.7	0.17	0.14
3.5	3.5	3.4	9.6	9.6	0.5	1.6	42.3	50.5	7.0	9.9	0.18	0.13
4.5	3.5	3.4	9.6	9.7	1.5	0.6	48.9	11.1	11.9	5.6	0.14	0.12
5.5	n.d.	n.d.	n.d.	n.d.	2.9	8.2	27.2	54.3	7.6	11.9	0.12	0.14
6.5	n.d.	n.d.	n.d.	n.d.	16.2	7.1	53.6	62.9	8.6	10.9	0.13	0.13
7.5	n.d.	n.d.	n.d.	n.d.	4.1	3.0	49.1	57.8	6.2	9.7	0.15	0.12
8.5	n.d.	n.d.	n.d.	n.d.	3.3	1.3	54.0	53.9	6.9	10.4	0.13	0.14
9.5	3.3	3.2	9.6	9.8	1.6	0.1	43.3	26.7	8.1	4.8	0.14	0.12
11	n.d.	n.d.	n.d.	n.d.	0.0	0.9	40.8	71.2	4.1	8.9	0.12	0.15
13	n.d.	n.d.	n.d.	n.d.	1.5	1.2	83.5	75.6	8.1	10.2	0.13	0.12
15	2.8	2.8	10.3	10.4	1.3	1.5	73.5	69.0	11.5	12.8	0.16	0.15
17	n.d.	n.d.	n.d.	n.d.	2.3	6.0	67.0	71.6	2.3	8.5	0.19	0.17
19	2.6	2.6	10.3	10.2	2.4	4.7	93.9	69.6	3.3	6.9	0.14	0.15
22.5	2.5	2.4	10.2	10.1	2.8	1.6	104.0	102.7	5.3	11.0	0.16	0.14
27.5	n.d.	n.d.	n.d.	n.d.	3.4	n.d.	122.4	n.d.	4.3	n.d.	0.21	n.d.

Fig. 1

Fig. 2

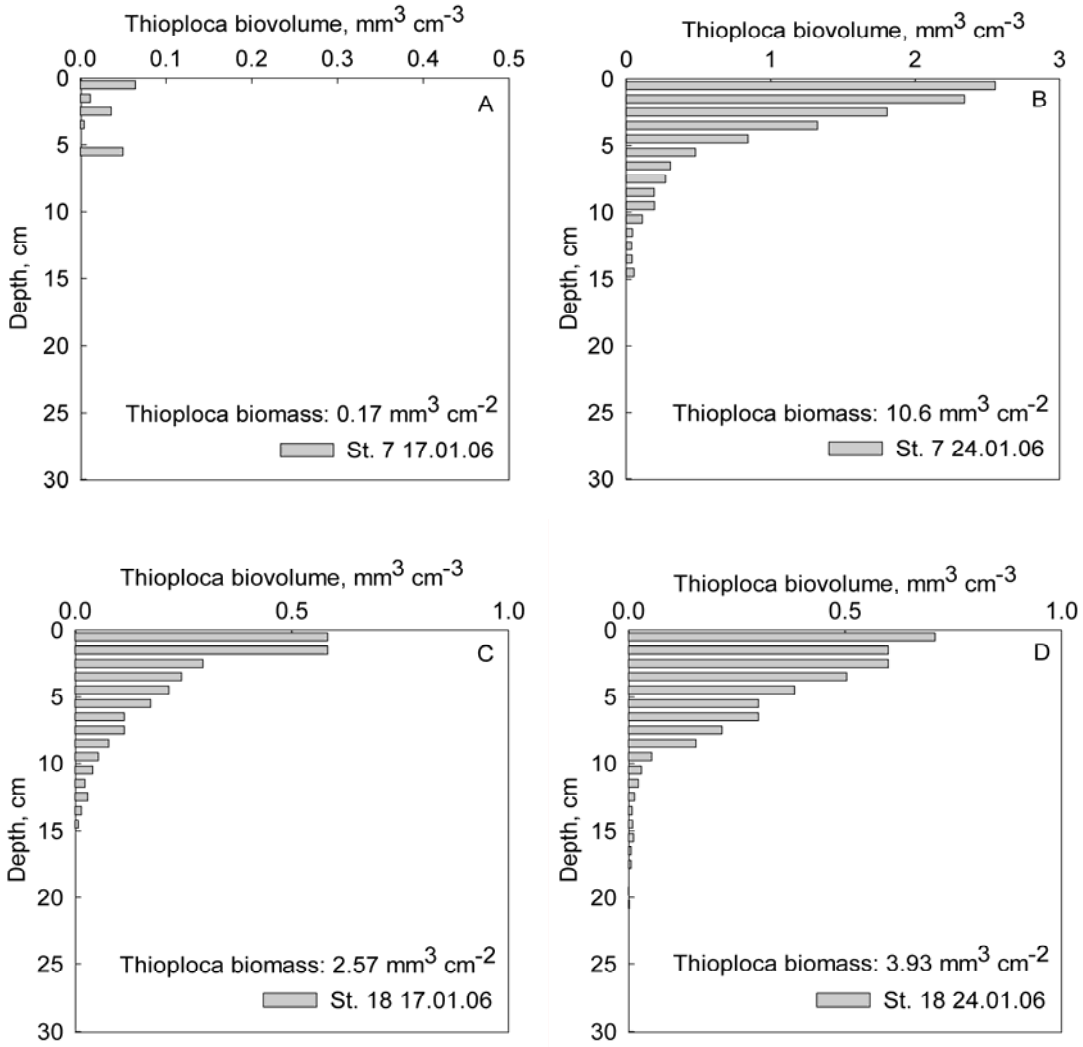
Thioploca biovolume, mm3 cm-3
Depth, cm
A
Thioploca biomass: 0.17 mm3 cm-2
St. 7 17.01.06
B
Thioploca biomass: 10.6 mm3 cm-2
St. 7 24.01.06
C
Thioploca biomass: 2.57 mm3 cm-2
St. 18 17.01.06
D
Thioploca biomass: 3.93 mm3 cm-2
St. 18 24.01.06

Fig. 3

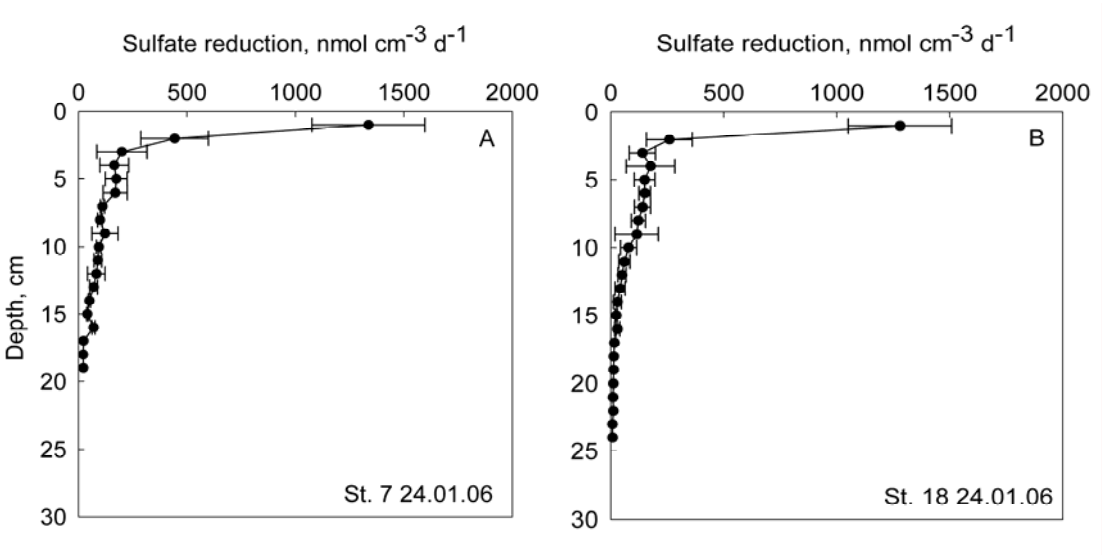
Sulfate reduction, nmol cm-3 d-1
0
500
1000
1500
2000
Depth, cm
0
5
10
15
20
25
30
A
St. 7 24.01.06
Sulfate reduction, nmol cm-3 d-1
B
St. 18 24.01.06

Fig. 4

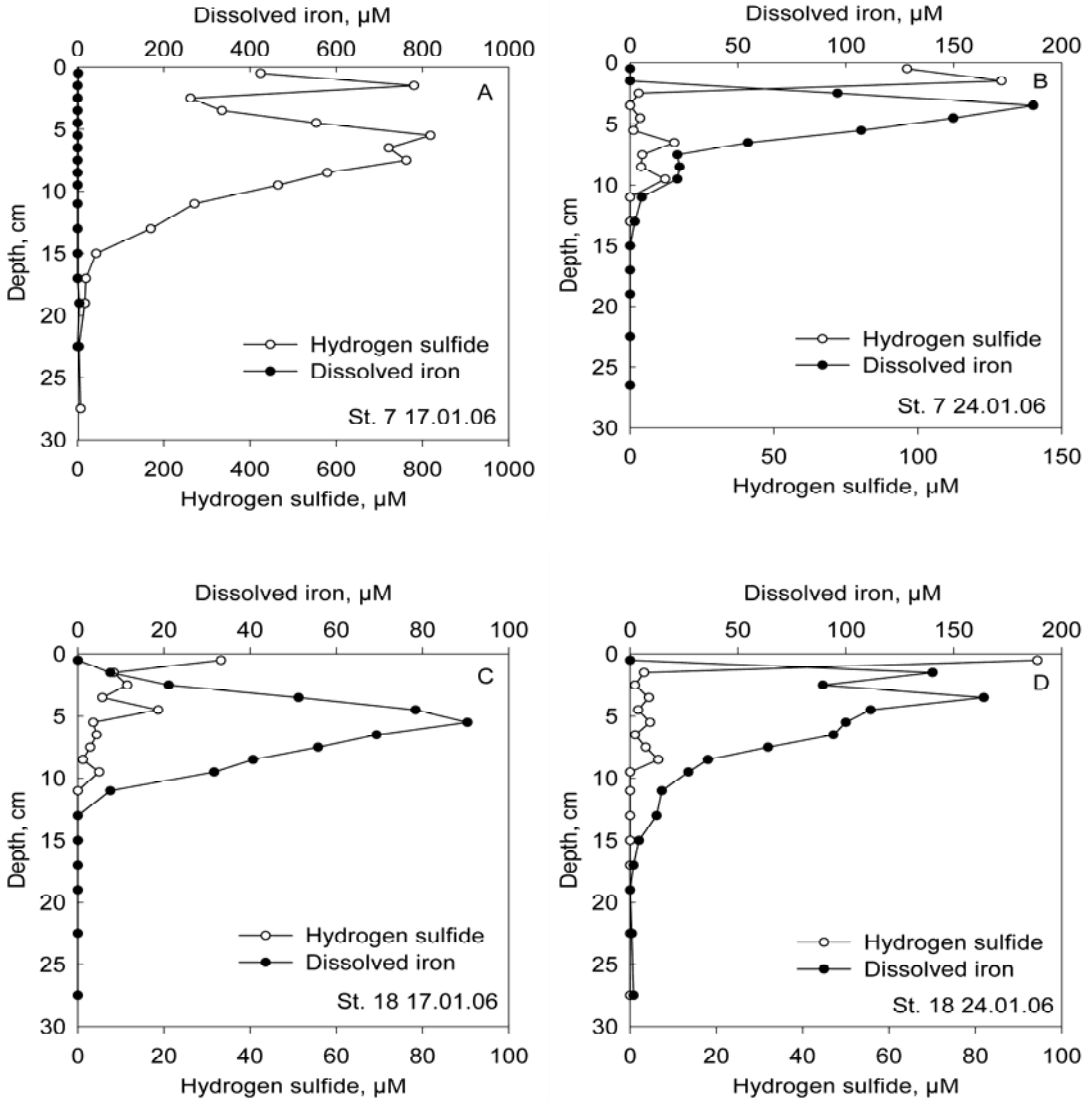
Dissolved iron, μM
Depth, cm
Hydrogen sulfide, μM
Hydrogen sulfide
Dissolved iron
A
St. 7 17.01.06
B
St. 7 24.01.06
C
St. 18 17.01.06
D
St. 18 24.01.06

Fig. 5

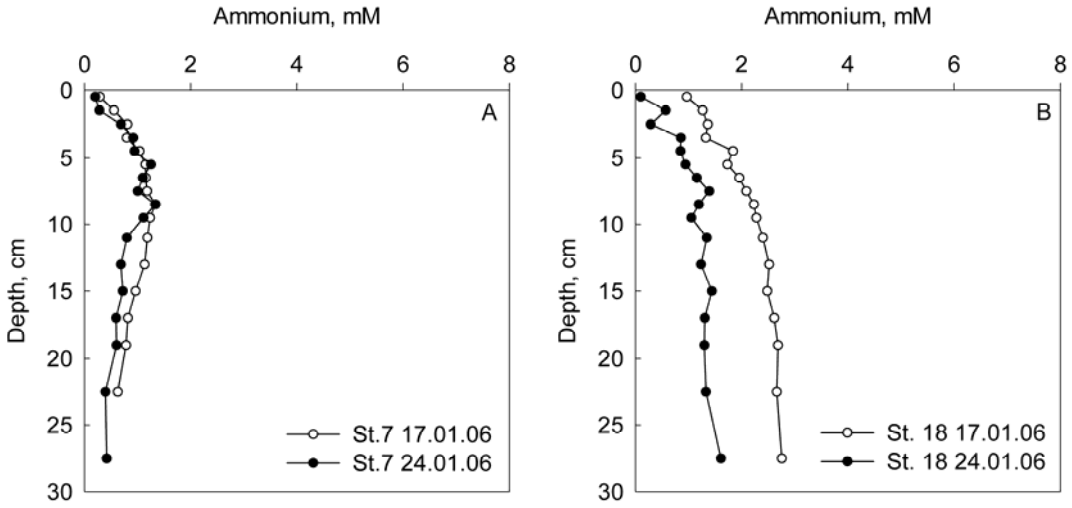
Ammonium, mM
0
2
4
6
8
Depth, cm
0
5
10
15
20
25
30
A
St.7 17.01.06
St.7 24.01.06
Ammonium, mM
B
St. 18 17.01.06
St. 18 24.01.06

Fig. 6

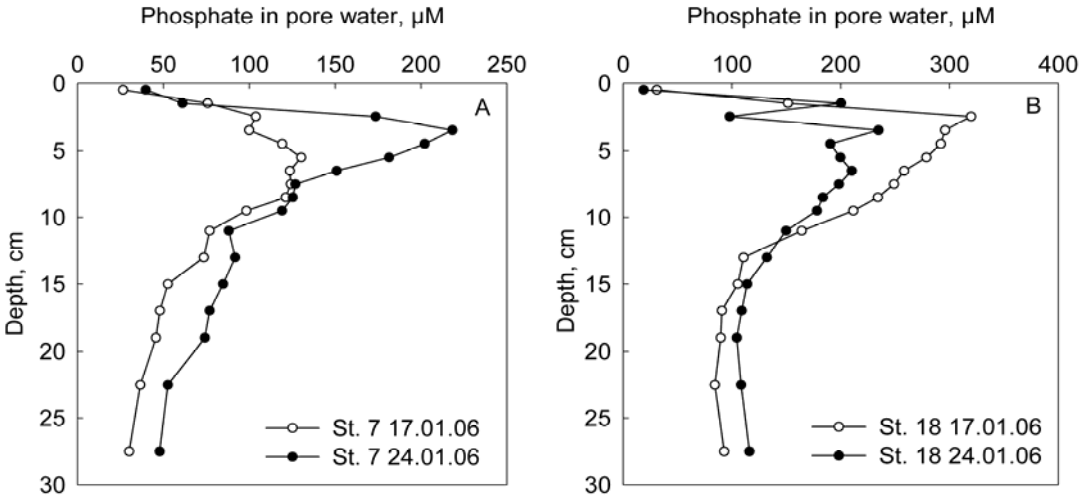
Phosphate in pore water, µM
0
50
100
150
200
250
Depth, cm
0
5
10
15
20
25
30
A
St. 7 17.01.06
St. 7 24.01.06
Phosphate in pore water, µM
0
100
200
300
400
Depth, cm
0
5
10
15
20
25
30
B
St. 18 17.01.06
St. 18 24.01.06

Fig. 7

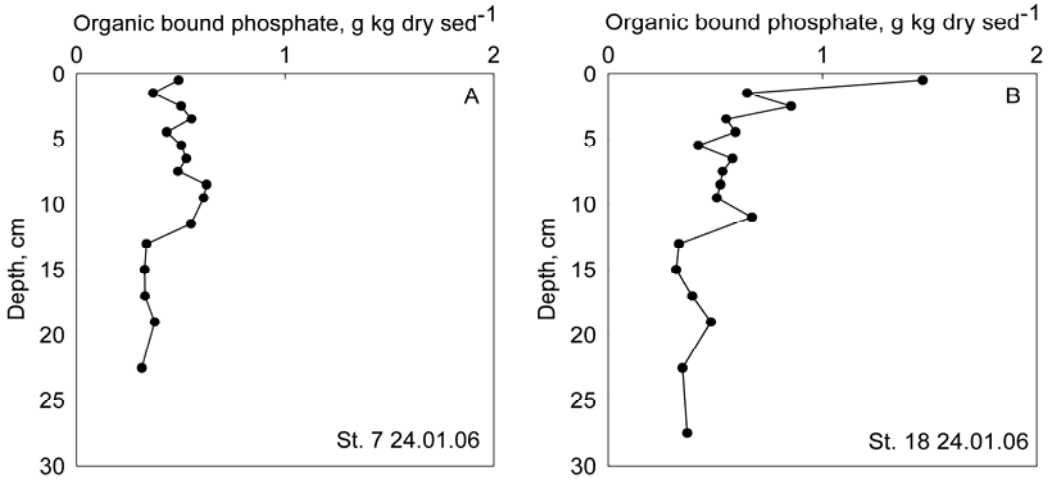
Organic bound phosphate, g kg dry sed-1
0
1
2
Depth, cm
0
5
10
15
20
25
30
A
St. 7 24.01.06
Organic bound phosphate, g kg dry sed-1
0
1
2
Depth, cm
0
5
10
15
20
25
30
B
St. 18 24.01.06

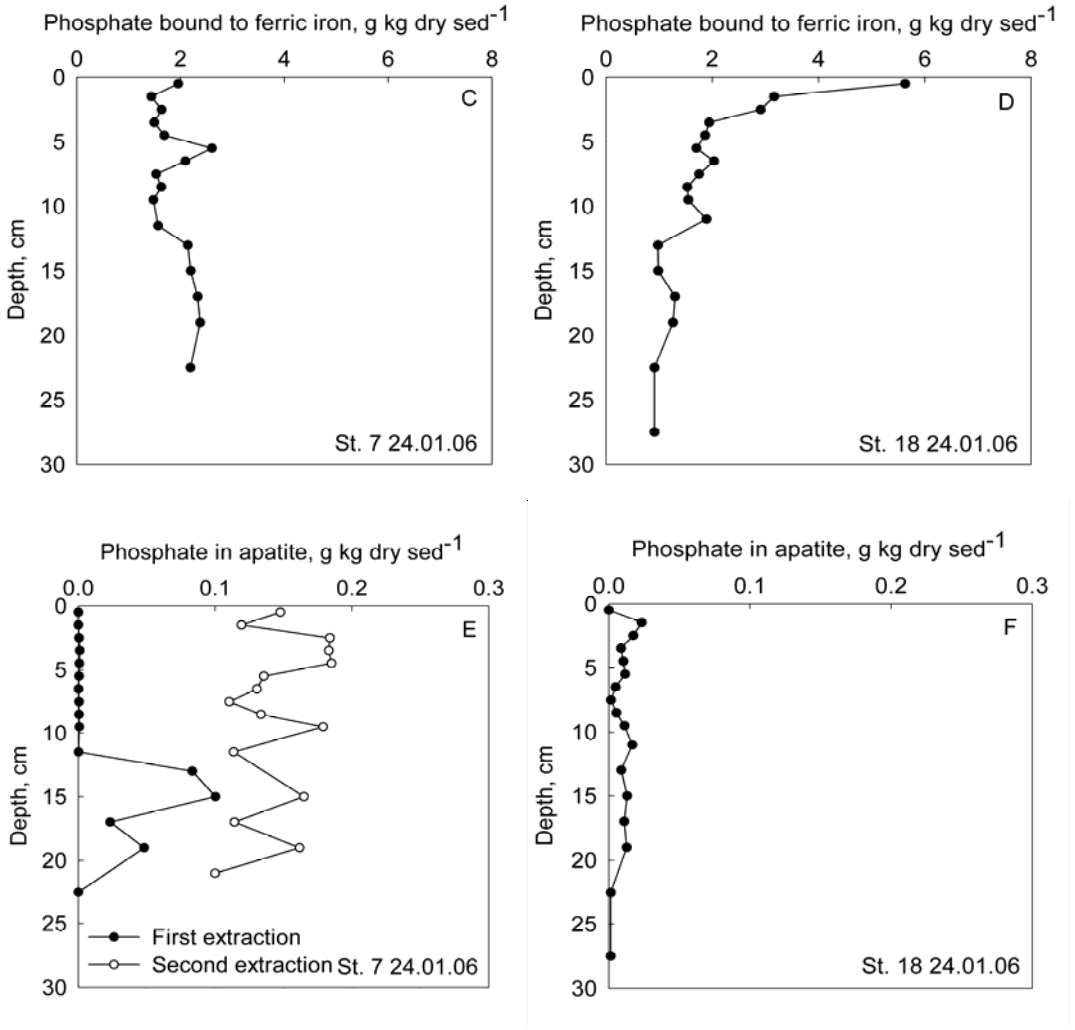
Phosphate bound to ferric iron, g kg dry sed-1
Depth, cm
C
St. 7 24.01.06
Phosphate bound to ferric iron, g kg dry sed-1
D
St. 18 24.01.06
Phosphate in apatite, g kg dry sed-1
E
First extraction
Second extraction
St. 7 24.01.06
Phosphate in apatite, g kg dry sed-1
F
St. 18 24.01.06

Chapter 7

Co-author publications

7.1 Regulation of anaerobic methane oxidation in sediments of the Black Sea

Knab, N. J.; Cragg, B. A.; Hornibrook, E. R. C.; Holmkvist, L.; Pancost, R. D.; Borowski, C.; Parkes, R. J.; Jørgensen, B. B.

Biogeosciences, Volume 6, Issue 8, 2009, pp.1505-1518

Abstract. Anaerobic oxidation of methane (AOM) and sulfate reduction (SRR) were investigated in sediments of the western Black Sea, where upward methane transport is controlled by diffusion. To understand the regulation and dynamics of methane production and oxidation in the Black Sea, rates of methanogenesis, AOM, and SRR were determined using radiotracers in combination with pore water chemistry and stable isotopes. In the Danube Canyon and the Dnjepr palaeo-delta AOM did not consume methane effectively and upwards diffusing methane created an extended sulfate-methane transition zone (SMTZ) that spread over more than 2.5 m and was located in brackish and limnic sediment. Measurable AOM rates occurred mainly in the lower part of the SMTZ, sometimes even at depths where sulfate seemed to be unavailable. The inefficiency of methane oxidation appears to be linked to the paleoceanographic history of the sediment, since in all cores methane was completely oxidized at the transition from the formerly oxic brackish clays to marine anoxic sediments. The upward tailing of methane was less pronounced in a core from the deep sea in the area of the Dnjepr Canyon, the only station with a SMTZ close to the marine deposits. Sub-surface sulfate reduction rates were mostly extremely low, and in the SMTZ were even lower than AOM rates. Rates of bicarbonate-based methanogenesis were below detection limit in two of the cores, but $\delta^{13}C$ values of methane indicate a biogenic origin. The most $\delta^{13}C$- depleted isotopic signal of methane was found in the SMTZ of the core from the deep sea, most likely as a result of carbon recycling between AOM and methanogenesis.

7.2 Lipid Biomarker Patterns of Phosphogenic Sediments from Upwelling Regions

Esther T. Arning; Daniel Birgel; Heide N. Schulz-Vogt b; Lars Holmkvist; Bo Barker Jørgensen; Alyssa Larson; Jörn Peckmann

Geomicrobiology Journal, Volume 25, Issue 2 March 2008, pages 69 - 82

Abstract. Sediments of upwelling regions off Namibia, Peru, and Chile contain dense populations of large nitrate-storing sulfide-oxidizing bacteria, *Thiomargarita*, *Beggiatoa*, and *Thioploca*. Increased contents of monounsaturated C_{16} and C_{18} fatty acids have been found at all stations studied, especially when a high density of sulfide oxidizers in the sediments was observed. The distribution of lipid biomarkers attributed to sulfate reducers ($10MeC_{16:0}$ fatty acid, *ai*-$C_{15:0}$ fatty acid, and mono-*O*-alkyl glycerol ethers) compared to the distribution of sulfide oxidizers indicate a close association between these bacteria. As a consequence, the distributions of sulfate reducers in sediments of Namibia, Peru, and Chile are closely related to differences in the motility of the various sulfide oxidizers at the three study sites. Depth profiles of mono-*O*-alkyl glycerol ethers have been found to correlate best with the occurrence of large sulfide-oxidizing bacteria. This suggests a particularly close link between mono-*O*-alkyl glycerol ether-synthesizing sulfate reducers and sulfide oxidizers. The interaction between sulfide-oxidizing bacteria and sulfate-reducing bacteria reveals intense sulfur cycling and degradation of organic matter in different sediment depths.

7.3 Physiology and behaviour of marine *Thioploca*

Signe Høgslund, Lars Peter Nielsen, Niels Peter Revsbech, Bo Barker Jørgensen, Victor Ariel Gallardo, Jack van de Vossenberg, Jeppe Lund Nielsen, Lars Holmkvist, Ester Arning, Gijs Kuenen

The ISME Journal (2009) 3, 647–657

Abstract

Large vacuolated marine sulphur bacteria of the genus *Thioploca* were studied to address unresolved questions of their oxygen, sulphur, nitrate, phosphorus, and carbon metabolism and their behaviour. In laboratory experiments, *Thioploca* had an aerobic metabolism 5 with an oxygen uptake rate of 1760 μmol O_2 dm^{-3} biovolume h^{-1}, equivalent to 4.4 nmol O_2 min^{-1} mg^{-1} protein. When high ambient sulfide concentrations (~200 μM) were present, a sulfide uptake of 6220 ± 2230 μmol H_2S dm^{-3} h^{-1}, (Mean ± SEM, n = 4) was measured. This sulfide uptake rate was six times higher than the oxidation rate of elemental sulphur by oxygen or nitrate, thus indicating a rapid sulphur accumulation by *Thioploca*. *Thioploca* reduce nitrate to ammonium and we found that dinitrogen was not produced, neither through denitrification nor through anammox activity. Polyphosphate storage was not detectable by microautoradiography in physiological assays or by staining and microscopy. Carbon dioxide fixation increased when nitrate and nitrite were externally available and when organic carbon was added to incubations. Sulfide addition did not increase carbon dioxide 15 fixation, indicating that *Thioploca* use excess of sulfide to rapidly accumulate sulphur rather than to accelerate growth. This is interpreted as an adaptation to infrequent high sulphate reduction rates in the seabed. The physiology and behaviour of *Thioploca* are summarized and the adaptations to an environment, dominated by infrequent oxygen availability and periods of high sulfide abundance, are discussed.

7.4 Sulfate-reducing bacteria in marine sediment (Aarhus Bay, Denmark): abundance and diversity related to geochemical zonation

Leloup, Julie; Fossing, Henrik; Kohls, Katharina; Holmkvist, Lars; Borowski, Christian; Jørgensen, Bo Barker

Environmental Microbiology, Volume 11, Number 5, May 2009, pp. 1278-1291(14)

Abstract. In order to better understand the main factors that influence the distribution of sulfate-reducing bacteria (SRB), their population size and their metabolic activity in high- and low-sulfate zones, we studied the SRB diversity in 3- to 5-m-deep sediment cores, which comprised the entire sulfate reduction zone and the upper methanogenic zone. By combining EMA (ethidium monoazide that can only enter damaged/dead cells and may also bind to free DNA) treatment with real-time PCR, we determined the distributions of total intact bacteria (16S rDNA genes) and intact SRB (dsrAB gene), their relative population sizes, and the proportion of dead cells or free DNA with depth. The abundance of SRB corresponded in average to 13% of the total bacterial community in the sulfate zone, 22% in the sulfate-methane transition zone and 8% in the methane zone. Compared with the total bacterial community, there were relatively less dead/damaged cells and free DNA present than among the SRB and this fraction did not change systematically with depth. By DGGE analysis, based on the amplification of the dsrA gene (400 bp), we found that the richness of SRB did not change with depth through the geochemical zones; but the clustering was related to the chemical zonation. A full-length clone library of the dsrAB gene (1900 bp) was constructed from four different depths (20, 110, 280 and 500 cm), and showed that the dsrAB genes in the near-surface sediment (20 cm) was mainly composed of sequences close to the Desulfobacteraceae, including marine complete and incomplete oxidizers such as Desulfosarcina, Desulfobacterium and Desulfococcus. The three other libraries were predominantly composed of Gram-positive SRB.

7.5 Quantification of Prokaryotic Gene Expression in Shallow Marine Subsurface Sediments of Aarhus Bay, Denmark

Joel Kostka, M. Humphrys, L. Holmkvist, B.B. Jørgensen

In prep.

Abstract. Due to limited resources for microbial growth, the shallow subsurface can serve as an ideal natural laboratory for the deep biosphere that has the advantage of being more easily accessible. Despite the global significance of the shallow subsurface, the microbiology of these environments is in its infancy. There is as yet no consensus on the predominant, "metabolically-active" microbial groups that catalyze biogeochemical cycles in situ. The objective of this study was to develop a molecular proxy for the metabolic activity of sulfate-reducing prokaryotes in the subsurface. This molecular proxy can be applied to the quantification of active sulfate-reducing prokaryotes in oil reservoirs and oil field systems.

The community abundance and diversity of mRNA transcripts directly related to sulfate-reducing prokaryotes were investigated using geochemical and molecular techniques in marine subsurface sediments of Aarhus Bay, Denmark. Using geochemical techniques, determinations of sediment geochemistry, porewater chemistry, and sulfate reduction rates were performed on subsamples from sediment cores to 5 m below the sediment surface. Molecular analysis of the dissimilatory (bi) sulfite reductase (dsrAB) mRNA transcripts and 16S rRNA were performed by reverse transcription real time quantitative PCR and traditional cloning and sequencing.

The distribution of dsrAB transcripts was directly linked to both sulfate reduction rates and rRNA content. Additionally, quantitative analysis of dsrAB gene transcripts indicated the presence of active sulfate reduction at 465 cm below the sediment-water interface, where high methane concentrations persist in regions of near sulfate depletion.

These data illustrate an abundance of active bacteria in zones of high sulfate reduction and a marked decrease in zones of low sulfate reduction rates. Substantiated by geochemical and rRNA analysis, the analysis of mRNA gene transcripts serves as a versatile molecular proxy for the study of sulfate-reducing communities in marine subsurface sediments.

Chapter 8

8.1 Perspectives ad outlook

The major goal of the present project was to understand whether sulfate is generated by reoxidation of sulfide throughout the sulfate and methane zones of marine sediments on the continental shelves, which might explain the abundance of active sulfhate- reducers deep below the main sulfate zone. In order to reach this goal, geochemical investigations of carbon, sulfur and iron species were performed in relation to the activity and distribution of sulfate-reducing bacteria, in sediment obtained from Aarhus Bay (Denmark), the Baltic Sea and the Black Sea.

From the beginning of the project, it was the plan to collect sediment samples especially from within the bay of Aarhus, because this area is well-investigated and because the sediment cores could be retrieved relatively easy. The very first sediment cores were collected from the Baltic Sea and Aarhus Bay in 2004. However, these cores were not nearly long enough as sulfide could still be detected in the pore water at the bottom of the cores (i.e. the cores did note penetrate below the sulfidization front). Overall, trial and errors on these first cores lasted more than one year, but gave valuable and detailed insight into the different analytical techniques that were used later on when sampling of more suited cores was carried out. It was especially the potential sulfate reduction rate measurements, as well as optimization of the sulfur and iron extraction techniques that was practizied on the cores.

In September 2006, long gravity cores from the Arkona Basin (Baltic Sea) were sampled for the project. However, these cores were not suited for potential sulfate reduction rate experiments either, since the pore water was found to contain sulfate in mM concentrations throughout the sediment column. In spite of this, a detailed study was performed on these cores, because the sediment zonation was extreme, i.e. they contained a distinct black sulfidization front and a sharp transition to an orange-brown sediment layer below. The results obtained from the Arkona Basin have helped to shed light onto the many differences between reduced and non-reduced sediment layers. This knowledge was important for the later interpretation of the results from Aarhus Bay and Black Sea.

The Aarhus Bay cores were retrieved in March 2007. The gravity corer on board the MS *Henry* was adjusted so that sediment below the sulfidization front could be sampled. The subsequent analysis of the gravity cores were intiated immediately after the cores were sampled and the analyses went smooth. In May 2006, 10 m long gravity cores were retrieved from the Black Sea, in order to investigate if active sulfate reducers were present also much deeper below the sulfidization front.

The methods that were used to examine the iron and sulfur species in sediment and pore water from the marine sites described above were a combination of well-established techniques that were optimized to the sampled cores, together with more new and advanced methods such as the detection of polysulfides. Much effort was put into optimization of already existing methods with the one purpose of detecting iron and sulfur species at lower concentrations and thus to obtain accurate depth profiles. For example, it was extremely important for the overall outcome of the project to achieve reliable sulfate data especially near the detection limit of the method (from the non-suppressed ion chromatography technique), as the sulfate concentrations below the SMTZ were generally low. This was done by using the right sample dilutions, standards, columns on the ion chromatography etc. Further, the cold chromium distillation technique was used to destill the radioactive samples for sulfate reduction rate measurements instead of the hot distillation, since this method is more sensitive in detecting low radioactive counts. Another example was the use of the rhizone soil moisture samplers for pore water extractions instead of pore water squeezing under N_2 pressure. We found that the rhizone extraction yielded higher and more consistent and reproducible data for reactive pore water species such as H_2S or Fe^{2+} that are highly sensitive to oxygenation.

The results of this study confirm the importance of sulfate reduction in marine sediments and there are many obvious aspects and ways by which the study could be improved and future studies could begin. To better understand sulfate reduction within sub-surface sediments and reoxidation of sulfide to sulfate, coordinated research in a variety of disciplines (e.g. geology, chemistry and biology) is necessary. Below are listed some bullet points with suggestions on how to optimize the data set and/or how to continue the study, and many more could be added:

- A goal of the study was to include as many relevant biogeochemical analyses on the sampled sediment cores as possible, in order to fully investigate the geochemistry of iron and sulfur species along with the sulfate reduction rates. A detailed sampling program was thus developed suited for each sampling so that a number of different analyses could be effitively carried out on the few cores that were collected from each marine site. Still, the study from Aarhus Bay did not include data on elemental sulfur, thiosulfate and polysulfides, because the focus of this study was on the sulfate reduction rates. However, including most of the known analyses on several gravity cores is both very time-consuming and expensive. Thus, future studies should perhaps try to carry out a detailed sampling program on selected depth zones if most of the know methods for iron and sulfur speciation should be applied. For example, it could be interesting to do a detailed investigation of the sulfidization front alone, in order to accurately investigate this interesting zone where a number of complex redox reaction occurs. The study from Aarhus Bay, for instance, revealed that the potential sulfate reduction rates were elevated within the sulfidization front. Whether this was due to an artefact or a stimulated sulfate reduction rate owing to a higher production of sulfate from reoxidation of sulfide need to be studied. Such a study would probably shead light on how pyrite is formed as well as oxidation of sulfur species.

- The concentration depth profiles of iron and sulfur species in pore water and sediment obtained from the three different marine sites (Aarhus Bay, Baltic Sea and Black Sea) exhibited differences as well as similarities. For instance, elemental sulfur peaked within the sulfidization front of both the Arkona Basin and the Black Sea, dissolved iron accumulated below this front in all of the investigated sites and sulfide peaked at all sites above the sulfidization front. However, the different concentration levels of these species has not been compared. It could be interesting to examine these differences in relation to availability of organic carbon, iron oxide concentrations, rates of AOM, etc. in order to search for overall trends theat controls sulfidization processes on the shelves. Such a study would require more data from other marine sites and perhaps also computer modelling.

- A more precise detection method for measuring concentrations of sulfate is obviously needed in order to obtain more reliable sulfate reduction rate data as well as to obtain a sulfate concentration profile that lies closer to the "truth". This method should preferentially be able to detect sulfate at concentrations below 50µM (the detection limit of the in chromatography) independently of the high concentrations of chloride. In this study, we also tried to detect lower sulfate concentrations by the use of a sulfate-electrode, but without success, due to the high concentrations of chloride. It is likely that sulfate could be measured down to a concentration of 1 µM using an ion chromatograph.

- Another improvement of the study that could support the argument of sulfide reoxidation with iron oxides would be to apply a method that better detect and quantify all the different Fe(III) containing minerals with a higher precition than the chemical extractions. For example, the use of Mössbayer Absorption Spectroscopy for identification of iron-containing minerals could be applied. Further, investigations of the crystallography of the iron oxides present within the sub-surface sediment is also of importance, since more crystalline iron oxides

generally tend to react slower with sulfides compared to more amorphous minerals. This is an area that needs to be investigated more.

- Further studies on how the sulfate-reducing communities below the SMTZ may be adapted to the low levels of sulfate. Strains of sulphate-reducers isolated from sub-surface sediments could be tested for their use of substrates. Such studies would also include more molecular studies on the strains of organisms that are present.

This study extends the database quantifying anaerobic carbon mineralization pathways, with focus on sulfate reduction, in continental shelves by looking at the sub-surface sediment layers. Most of the obtained pore water and sediment profiles as well as the sulfate reduction rates determined within the upper 2 m sediment of Aarhus Bay, the Black Sea and the Arkona Basin (Baltic Sea) are generally within the concentration range of earlier studies (see references above). However, the pore water and sediment concentrations of sulfur and iron species as well as the sulfate reduction rates measured below the SMTZ in the present study are relatively new and future studies will be able to compare these result with future studies, but also verify that the ranges of the concentrations as well as the rates are consistent. In addition to the activity measurements of sulfate reduction in sub-surface sediments, future studies also need to include rate measurement of other groups of microorganisms, i.e. methanogens, iron-reducing prokaryotes, fermenters etc., in order to obtain a more complete picture of the anaerobic carbon mineralization processes within sub-surface sediment. This knowledge could give new insight into the many redox processes that exist within marine sediments and probably lead to the discovery of new reactions.

8.2 References

Aller RC (1990) Bioturbation and manganese cycling in hemipelagic sediments. *Phil. Trans. R. Soc. Lond.*, **331,** 51-68.

Aller RC (1994) The sediment Mn cycle in Long Island Sound: Its role as intermediate oxidant and the influence of biotrubation, O_2, and Corg flux on diagenetic reaction balances. *Journal of Marine Research*, **52,** 259-295.

Aller RC, JE Mackin and RT Cox (1986) Diagenesis of Fe and S in Amazon inner shelf muds: apparent dominance of Fe reduction and implications for the genesis of ironstones. *Continental Shelf Res.*, **6,** 263-289.

Aller RC and PD Rude (1988) Complete oxidation of solid phase sulfides by manganese and bacteria in anoxic marine sediments. *Geochimica et Cosmochimica Acta*, **52,** 751-765.

Andrèn E, T Andrèn and G Sohlenius (2000) The Holocene history of the southwestern Baltic Sea as reflected in a sediment core from the Bornholm Basin. *Boreas*, **29,** 233-250.

Bak F and H Cypionka (1987) A novel type of energy metabolism involving fermentation of inorganic sulphur compounds. *Nature*, **326,** 891-892.

Bak F and N Pfennig (1987) Chemolithotrophic growth of *Desulfovibrio sulfodismutans* sp. nov. by disproportionation of inorganic sulfur compounds. *Arch. Microbiol.*, **147,** 184-189.

Bak F and N Pfennig (1991) Microbial sulfate reduction in littoral sediment of Lake Constance. *FEMS Microbiol. Ecol.*, **85,** 31-42.

Barnes RO and ED Goldberg (1976) Methane production and consumption in anoxic marine sediments. *Geol.*, 297-300.

Berner RA (1967) Thermodynamic stability of sedimentary iron sulfides. *Amer. J. Sci.*, **265,** 773-785.

Berner RA (1970) Sedimentary pyrite formation. *Amer. J. Sci.*, **268,** 1-23.

Berner RA (1981) A new geochemical classification of sedimentary environments. *J. Sedimentary Petrology*, **51,** 359-365.

Berner RA (1984) Sedimentary pyrite formation: An update. *Geochimica et Cosmochimica Acta*, **48,** 605-615.

Björck S (1995) A review of the history of the Baltic Sea, 13.0-8.0 ka BP. *Quaternary International*, **27,** 19-40.

Bloomquist RG (1977) Chemical characteristics of interstitial water from the Southern Baltic Sea. *Ph.D. Thesis, University of Stockholm*, 111p.

Boetius A, K Ravenschlag, CJ Schubert, D Rickert, F Widdel, A Gieseke, R Amann, BB Joergensen, U Witte and O Pfannkuche (2000) A marine microbial consortium apparently mediating anaerobic oxidation of methane. *Nature*, **407,** 623-626.

Boettcher ME, BK Khim, A Suzuki, M Gehre, UG Wortmann and HJ Brumsack (2004) Microbial sulfate reduction in deep sediments of the Southwest Pacific (ODP Leg 181, Sites 1119-1125): evidence from stable sulfur isotope fractionation and pore water modeling. *Marine Geology*, **205,** 249-260.

Boettcher ME and A Lepland (2000) Biogeochemistry of sulfur in a sediment core from the west-central Baltic Sea: Evidence from stable isotopes and pyrite textures. *Journal of marine Systems*, **25,** 299-312.

Boettcher ME, H Schale, B Schnetger, K Wallmann and HJ Brumsack (2000) Stable sulfur isotopes indicate net sulfate reduction in near-surface sediments of the deep Arabian Sea. *Deep-Sea Research II*, **47,** 2769-2783.

Borowski WS, CK Paull and WI Ussler (1997) Carbon cycling within the upper methanogenic zone of continental rise sediments: An example from the methane-rich sediments overlying the Blake Ridge gas hydrate deposits. *Marine Chemistry*, **57,** 299-311.

Boulegue J, CJ Lord and TM Church (1982) Sulfur speciation and associated trace metals (fe, cu) in the pore water of great marsh, Delaware. *Geochim. Cosmochim. Acta*, **46,** 453-464.

Burdige DJ and KH Nealson (1986) Chemical and microbiological studies of sulfide-mediated manganese reduction. *Geochemical J.*, **4,** 361-387.

Canfield DE (1989) Reactive iron in marine sediments. *Geochimica et Cosmochimica Acta*, **53,** 619-632.

Canfield DE and RA Berner (1987) Dissolution and pyritization of magnetite in anoxic marine sediments. *Geochimica et Cosmochima Acta*, **51,** 645-659.

Canfield DE, BB Jørgensen, H Fossing, R Glud, J Gundersen, NB Ramsing, B Thamdrup, JW Hansen, LP Nielsen and POJ Hall (1993) Pathways of organic carbon oxidation in three continental margin sediments. *Marine Geology*, **113,** 27-40.

Canfield DE and R Raiswell (1991). Pyrite formation and fossil preservation. In: Allison, PA and DEG Briggs. Taphonomy: Releasing the date locked in the fossil record.,. Topics of Geobiology, Plenum Press, New York. 9. p337-387.

Canfield DE, R Raiswell and S Bottrell (1992) The reactivity of sedimentary iron minerals toward sulfide. *American Journal of Science*, **292,** 659-683.

Canfield DE and B Thamdrup (1994) The production of S-34-depleted sulfide during bacterial disproportionation of elemental sulfur. *Science*, **266,** 1973-1975.

Canfield DE, B Thamdrup and S Fleischer (1998) Isotope fractionation and sulfur metabolism by pure and enrichment cultures of elemental sulfur-disproportionating bacteria. *Limnology and Oceanography*, **43,** 253-264.

Chadwell SJ, D Rickard and GW Luther III (1999) Electrochemical evidence for pentasulfide complexes with Mn^{2+}, Fe^{2+}, Co^{2+}, Ni^{2+}, Cu^{2+} and Zn^{2+}. *Aquatic Geochemistry*, **5,** 29-57.

Champ DR, J Gules and RE Jackson (1979) Oxidation-reduction sequences in ground water flow systems. *Canadian Journal of Earth Science*, **16,** 12-23.

Claypool GE and KA Kvenvolden (1983) Methane and other hydrocarbon gases in marine sediment. *Annual Review of Earth and Planetary Science*, **11,** 299-327.

Cline JD and FA Richards (1969) Oxygenation of hydrogen sulfide in seawater at constant salinity, temperature, and pH. *Environ.Sci.Techn.*, **3,** 838-843.

Coleman ML, DB Hedrick, DR Lovley, DC White and K Pye (1993) Reduction of Fe(III) in sediments by sulphate-reducing bacteria. *Nature*, **361,** 436-438.

Coleman ML and R Raiswell (1995) Source of carbonate and origin of zonation in pyritiferous carbonate concretions: Evaluation of a dynamic model. *American J. Sci.*, **295,** 282-308.

Coolen MJL, H Cypionka, AM Sass, H Sass and J Overmann (2002) Ongoing modification of Mediterranean Pleistocene sapropels medisted by prokaryotes. *Science*, **296,** 2407-2410.

D´Hondt S, BB Jørgensen, DJ Miller, A Batzke, R Blake, BA Cragg, H Cypionka, GR Dickens, TG Ferdelman, KU Hinrichs, NG Holm, R Mitterer, A Spivack, G Wang, B Bekins, B Engelen, K Ford, G Gettemy, SD Rutherford, H Sass, CG Skilbeck, IW Aiello, G Guèrin, CH House, F Inagaki, P Meister, T Naehr, S Niitsuma, RJ Parkes, A Schippers, DC Smith, A Teske, J Wiegel, CN Padilla and JLS Acosta (2004) Distributions of microbial activities in deep subseafloor sediments. *Science*, **306,** 2216-2221.

Dos Santos Afonso M and W Stumm (1992) The reductive dissolution of iron (III) (hydr) oxides by hydrogen sulfide. *Langmuir*, **8,** 1671-1676.

Ehrlich HL (1987) Manganese oxide reduction as a form of anaerobic respiration. *Geomicrobiol. J.*, **5,** 423-431.

Elsgaard L and BB Jørgensen (1992) Anoxic transformations of radiolabeled hydrogen sulfide in marine and freshwater sediments. *Geochimica et Cosmochimica Acta*, **56,** 2425-2435.

Fairbanks RG (1989) A 17,000-year glacio-eustatic sea level record: influence of glacial melting rates on the Younger Dryas event and deep-ocean circulation. *Nature*, **342,** 637-642.

Ferdelman TG (1994) Oceanographic and geochemical controls on sulfur diagenesis in coastal environments. Ph.D. Thesis, University of Delaware, 140p.

Field CB, MJ Behrenfeld, JT Randerson and P Falkowski (1998) Primary production of the biosphere: Integrating terrestrial and oceanic components. *Science*, **281,** 237-240.

Finster K, W Liesack and B Thamdrup (1998) Elemental sulfur and thiosulfate disproportionation by *Desulfocapsa sulfoexigens* sp. nov., a new anaerobic bacterium isolated from marine surface sediment. *Applied and Environmental Microbiology*, **64,** 119-125.

Föllmi KB (1996) The phosphorus cycle, phosphogenesis and marine phosphate rich deposits. *Earth Science Reviews*, **40,** 55-124.

Fossing H (1995). 35S-Radiolabeling to probe biogeochemical cycling of sulphur. In: Vairavamurthy, MA and MAA Schoonen. Geochemical transformations of sedimentary sulphur. ACS symposium Series 612, American chemical society, Washington DC. p 348-364

Fossing H and BB Jørgensen (1990) Oxidation and reduction of radiolabeled inorganic sulfur compounds in an estuarine sediment, Kysing Fjord, Denmark. *Geochimica et Cosmochimica Acta*, **54,** 2731-2742.

Fossing H, B Thamdrup and BB Jørgensen (1992). Sulfur, iron, and manganese cycling in the sea floor of Aarhus Bay. In: Havforskning Fra Miljøstyrelsen, Aarhus.

Froelich PN, GP Klinkhammer, ML Bender, NA Luedtke, GR Heath, D Cullen, P Dauphin, D Hammond and B Hartman (1979) Early oxidation of organic matter in pelatic sediments of the eastern equatorial Atlantic: Suboxic diagenesis. *Geochimica et Cosmochimica Acta*, **43,** 1075-1090.

Fütterer DK (2000). The solid phase of marine sediments. In: Schulz HD and M Zabel. Marine Geochemistry, Springer, Berlin, Heidelberg, p1-25.

Gingele FX and T Leipe (1997) Clay mineral assemblages in the western Baltic Sea: recent distribution and relation to sedimentary units. *Marine Geology*, **140,** 97-115.

Habicht KS and DE Canfield (2001) Isotope fractionation by sulfate-reducing natural populations and the isotopic composition of sulfide in marine sediments. *Geology*, **29,** 555-558.

Habicht KS, L Salling, B Thamdrup and DE Canfield (2005) Effect of low sulfate concentrations on lactate oxidation and isotope fractionation during sulfate reduction by *Archaeoglobus fulgidus* strain Z. *Appl Environ Microbiol*, **71,** 3770-3777.

Haese RR (2000). The reactivity of iron. In: Schulz HD and M Zabel (2006). Marine Geochemistry, Springer, Berlin, Heidelberg, p233-261.

Henrichs SM, Reeburgh and W S (1987) Anaerobic mineralization of marine sediment organic matter: Rates and the role of anaerobic processes in the oceanic carbon economy. *Geomicrobiol. J.*, **5,** 191-237.

Heyer J, U Berger and R Suckow (1990) Methanogenesis in different parts of a brackish water ecosystem. *Limnologica*, **20,** 135-139.

Houmark-Nielsen M (1987) Pleistocene stratigraphy and glacial history of the central part of Denmark. *Bulletin of the Geological Society of Denmark*, **36,** p189.

Houmark-Nielsen M (2003) Signature and timing of the Kattegat Ice Stream: onset of the LGM-sequence at the south western margin of the Scandinavian Ice Sheet. *Boreas*, **32,** 227-241.

Howarth RW (1979) Pyrite: Its rapid formation in a salt marsh and its importance in ecosystem metabolism. *Science*, **203,** 49-51.

Howarth RW (1984) The ecological significance of sulfur in the energy dynamics of salt marsh and coastal marine sediments. *Biogeochem.*, **1,** 5-27.

Iversen N and BB Jørgensen (1985) Anaerobic methane oxidation rates at the sulfate-methane transition in marine sediments from Kattegat and Skagerrak (Denmark). *Limnol. Oceanogr.*, **30,** 944-955.

Jacobsen R and D Postma (1994) In situ rates of sulfate reduction in an aquifer (Rømø, Denmark) and implications for the reactivity of organic matter. *Geology*, **23,** 1103-1106.

Jahnke RA (1990) Early diagenesis and recycling of biogenic debris at the seafloor, Santa Monica Basin, California. *J. Mar. Res.*, **48,** 413-436.

Jensen JB and O Bennike (2009) Geological setting as background for methane distribution in Holocene mud deposits, Århus Bay, Denmark. *Continental Shelf Res.*, **29,** 775-784.

Jensen JB, O Bennike, W Lemke and A Kuijpers (2004) The Storebælt gateway to the Baltic. *Geological Survey of Denmark and Greenland Bulletin*, **7,** 45-48.

Jørgensen B (1988) Ecology of the sulphur cycle: oxidative pathways in sediments. *Symp. Soc. Gen. Microbiol.*, **42,** 31-63.

Jørgensen B (1990) A thiosulfate shunt in the sulfur cycle of marine sediments. *Science*, **249,** 152-154.

Jørgensen BB (1979) A theoretical model of the stable sulfur isotope distribution in marine sediments. *Geochimica et Cosmochimica Acta*, **43,** 363-374.

Jørgensen BB (1982) Mineralization of organic matter in the sea bed-the role of sulphate reduction. *Nature*, **296,** 643-645.

Jørgensen BB (1990) The sulfur cycle of freshwater sediments: Role of thiosulfate. *Limnology and Oceanography*, **35,** 1329-1342.

Jørgensen BB and F Bak (1991) Pathways and microbiology of thiosulfate transformations and sulfate reduction in a marine sediment (Kattegat, Denmark). *Applied and Environmental Microbiology*, **57,** 847-856.

Jørgensen BB, M Bang and TH Blackburn (1990) Anaerobic mineralization in marine sediments from the Baltic-Sea-North-Sea transition. *Marine Ecology-Progress Series*, **59,** 39-54.

Jørgensen BB, ME Boettcher, H Lueschen, LN Neretin and II Volkov (2004) Anaerobic methane oxidation and a deep H_2S sink generate isotopically heavy sulfides in Black Sea sediments. *Geochimica et Cosmochimica Acta*, **68,** 2095-2118.

Jørgensen, BB and DC. Nelson (2004) Sulfide oxidation in marine sediments: Geochemistry meets microbiology, In: J. P. Amend, K. J. Edwards, and T. W. Lyons (eds.) Sulfur Biogeochemistry - Past and Present. Geological Society of America, p36-81.

Kao SJ, CS Horng, AP Roberts and KK Liu (2004) Carbon-sulfur-iron relationships in sedimentary rocks from southwestern Taiwan: influence of geochemical environment on greigite and pyrrhotite formation. *Chemical Geology*, **203,** 153-168.

Kepner Rj and J Pratt (1994) Use of fluorochromes for direct enumeration of total bacteria in environmental sample: past and present. *Microbiol. Rev.*, **58,** 603-615.

King GM (1990) Effects of added manganic and ferric oxides on sulfate reduction and sulfide oxidation in intertidal sediments. *FEMS Micobiology Ecology*, **73,** 131-138.

Knab NJ, BA Cragg, ERC Hornibrook, L Holmkvist, C Borowski, RJ Parkes and BB Jørgensen (2008) Regulation of anaerobic methane oxidation in sediments of the Black Sea. *Biogeosciences Discussions*, **5,** 2305–2341.

Knittel K, T Loesekann, A Boetius, R Kort and R Amann (2005) Diversity and distribution of methanotrophic Archaea at cold seeps. *Applied and Environmental Microbiology*, **71,** 467-479.

Kögler F and B Larsen (1979) The West Bornholm basin in the Baltic Sea: Geological structure and Quaternary sediments. *Boreas*, **8,** 1-22.

König I, M Drodt, E Suess and A Trautwein (1997) Iron reduction through the tan-green color transition in deep-sea sediments. *Geochimica et Cosmaochimica Acta*, **61,** 1679-1683.

Kostka JE and GW Luther (1994) Partitioning and speciation of solid-phase iron in salt-marsh sediments. *Geochimica et Cosmochimica Acta*, **58,** 1701-1710.

Kostka JE and GWI Luther (1995) Seasonal cycling of Fe in saltmarsh sediments. *Biogeochemistry*, **29,** 159-181.

Kostka JE and KH Nealson (1995) Dissolution and reduction of magnetite by bacteria. *Environmental Science & Technology*, **29,** 2535-2540.

Kostka JE, JW Stucki, KH Nealson and J Wu (1996) Reduction of structural Fe(III) in smectite by a pure culture of *Shewanella Putrefaciens* strain MR-1. *Clays and Clay Minerals*, **44,** 522-529.

Kostka JE, B Thamdrup, RN Glud and DE Canfield (1999) Rates and pathways of carbon oxidation in permantently cold Arctic sediments. *Marine Ecology Progress Series*, **180,** 7-21.

Laier T and JB Jensen (2007) Shallow gas depth-contour map of the Skagerak-western Baltic Sea region. *Geo-Mar Lett*, **27,** 127-141.

Leloup J, A Loy, NJ Knab, C Borowski, M Wagner and BB Jørgensen (2007) Diversity and abundance of sulfate-reducing microorganisms in the sulfate and methane zones of a marine sediment, Black Sea. *Environmental Microbiology*, **9,** 131-142.

Leslie BW, DE Hammond, WM Berelson and SP Lund (1990) Diagenesis in anoxic sediments from the California continental Borderland and its influence on iron, sulfur, and magnetite behavior. *Journal of Geophysical Research*, **95,** 4453-4470.

Llobet-Brossa E, R Rabus, ME Boettcher, M Koenneke, N Finke, A Schramm, RL Meyer, S Groetzschel, R Rossello-Mora and R Amann (2002) Community structure and activity of sulfate-reducing bacteria in an intertidal surface sediment: a multi-method approach. *Aquatic Microbial Ecology*, **29,** 211-226.

Lovley DR (1991) Dissimilatory Fe(III) and Mn (IV) Reduction. *Microbiological Reviews*, **55,** 259-287.

Lovley DR and EJP Phillips (1987) Competitive mechanisms for inhibition of sulfate reduction and methane production in the zone of ferric iron reduction in sediments. *Applied and Environmental Microbiology*, **53,** 2636-2641.

Lovley DR and EJP Phillips (1994) Novel processes for anaerobic sulfate production from elemental sulfur by sulfate-reducing bacteria. *Applied and Environmental Microbiology*, **60,** 2394-2399.

Luther GW (1991) Pyrite synthesis via polysulfide compounds. *Geochimica et Cosmochimia Acta*, **55,** 2839-2849.

Luther III GW, TG Ferdelman, JE Kostka, EJ Tsamakis and TM Church (1991) Temporal and spatial variability of reduced sulfur species and porewater parameters in salt marsh sediments. *Biogeochemistry*, **14,** 57-88.

Luther III GW, AE Giblin and R Varsolona (1985) Polarographic analysis of sulfur species in marine porewaters. *Limnology and Oceanograph*, **30,** 727-736.

Luther III GW, B Glazer, SF Ma, R Trouwborst, BR Shultz, G Druschel and C Kraiya (2003) Iron and sulfur chemistry in a stratified lake: Evidence for iron-rich sulfide complexes. *Aquatic Geochemistry*, **9,** 87-110.

Mandernack KW and BM Tebo (1993) Manganese scavenging and oxidation at hydrothermal vents and in vent plumes. *Geochimica et Cosmaochimica Acta*, **57,** 3907-3923.

Martens CS and RA Berner (1974) Methane production in the interstitial waters of sulfate-depleted marine sediments. *Science*, **185,** 1167-1169.

Moeslund L, B Thamdurp and BB Jørgensen (1994) Sulfur and iron cycling in a coastal sediment: Radiotracer studies and seasonal dynamics. *Biogeochemistry*, **27,** 129-152.

Moros M, W Lemke, A Kuijpers, R Endler, JB Jensen, O Bennike and F Gingele (2002) Regressions and transgressions of the Baltic basin reflected by a new high-resolution deglacial and postglacial lithostratigraphy for Arkona Basin sediments (western Baltic Sea). *Boreas*, **31,** 151-162.

Moses CO, DK Nordstrom, JS Herman and AL Mills (1987) Aqueous pyrite oxidation by dissolved oxygen and by ferric iron. *Geochimica et Cosmochimica Acta*, **51,** 1561-1571.

Myers CR and KH Nealson (1988) Microbial reduction of manganese oxides: Interactions with iron and sulfur. *Geochimica et Cosmochimica Acta*, **52,** 2727-2732.

Nealson K (1983) Microbial reduction of manganese and iron. *biomineralization and Biological Metal accumulation*, 459-479.

Neretin LN, ME Boettcher, BB Jørgensen, II Volkov, H Lueschen and K Hilgenfeldt (2004) Pyritization processes and greigite formation in the advancing sulfidization front in the upper pleistocene sediments of the Black Sea. *Geochimica et Cosmochimica Acta*, **68,** 2081-2093.

Neretin LN, II Volkov, AG Rozanov, TP Demidova and AS Falina (2006). Biogeochemistry of the Black Sea anoxic zone with a reference to sulphur cycle. In: Past and present water column anoxia. L. N. Neretin. Springer, Dordrecht, Netherlands, p69-104.

Neumann G (1981) Lagerungsverhältnisse spät- und postglazialer Sedimente im Arkona-Becken. Ph.D. Thesis, Institut für Meereskunde, Warnemünde, Germany, *unpublished*.

Oda H and M Torii (2004) Sea-level change and remagnetization of continental shelf sediments off New Jersey (ODP Leg 174A): magnetite and greigite diagenesis. *Geophysical Journal International*, **156,** 443-458.

Oenema O (1990) Pyrite accumulation in salt marshes in the Eastern Scheldt, southwest Netherlands. *Biogeochem.*, **9,** 75-98.

Orphan VJ, KU Hinrichs, WI Ussler, CK Paull, LT Taylor, SP Sylva, JM Hayes and EF DeLong (2001) Comparative analysis of methane-oxidizing archaea and sulfate-reducing bacteria in anoxic marine sediments. *Applied and Environmental Microbiology*, **67,** 1922-1934.

Parkes RJ, BA Cragg, SJ Bale, JM Getliff, K Goodman, PA Rochelle, JC Fry, AJ Weightman and SM Harvey (1994) Deep bacterial biosphere in Pacific Ocean sediments. *Nature*, **371,** 410-413.

Parkes RJ, BA Cragg and P Wellsbury (2000) Recent studies on bacterial populations and processes in subseafloor. *Hydrogeology Journal*, **8,** 11-28.

Pedersen, SAS & KS Petersen (1997) Djurslands Geologi. Danmarks og Grønlands Geologiske Undersøgelse, + includ. geol. Map, 96p.

Pedersen K (2000) Exploration of deep intraterrestrial microbial life: current perspectives. *FEMS Microbiol Lett*, **185,** 9-16.

Pinet, PR (1996) Invitation to Oceanography, 3rd ed. St. Paul, MN: West Publishing Co.

Postma D and R Jakobsen (1996) Redox zonation: Equilibrium constraints on the Fe(III)/SO_4-reduction interface. *Geochimica et Cosmochimica Acta*, **60,** 3169-3175.

Poulton SW and DE Canfield (2005) Development of a sequential extraction procedure for iron: implications for iron partitioning in continentally derived particulates. *Chemical Geology*, **214,** 209-221.

Poulton SW, MD Krom and R Raiswell (2004) A revised scheme for the reactivity of iron (oxyhydr)oxide minerals towards dissolved sulfide. *Geochimica Et Cosmochimica Acta*, **68,** 3703-3715.

Pyzik AJ and SE Sommer (1981) Sedimentary iron monosulfides: kinetics and mechanism of formation. *Geochimica et Cosmochimica Acta*, **45,** 687-698.

Raiswell R and RA Berner (1985) Pyrite formation in euxinic and semi-euxinic sediments. *American Journal of Science*, **285,** 710-724.

Raiswell R and DE Canfield (1996) Rates of reaction between silicate iron and dissolved sulfide in Peru Margin sediments. *Geochimica et Cosmochimica Acta*, **60,** 2777-2787.

Raiswell R, DE Canfield and RA Berner (1994) A Comparison of iron extraction methods for the determination of degree of pyritisation and the recognition of iron-limited pyrite formation. *Chemical Geology*, **111,** 101-110.

Reeburgh WS (1983) Rates of biogeochemical processes in anoxic sediments. *Ann. Rev. Earth Planet. Sci.*, **11,** 269-298.

Reynolds RL, ML Tuttle, CA Rice, NS Fishman, JA Karachewski and DM Sherman (1994) Magnetization and geochemistry of greigite-bearing cretaceous strata, North-Slope Basin, Alaska. *American Journal of Science*, **294,** 485-528.

Rickard DT (1975) Kinetics and mechanism of pyrite formation at low temperatures. *American Journal of Science*, **275,** 636-652.

Rickard DT and GW Luther III (1997) Kinetics of pyrite formation by the H_2S oxidation of iron (II) monosulfide in aqueous solutions between 25 and 125 degrees Celsius: The mechanism. *Geochemica et Cosmochimica Acta*, **61,** 135-147.

Roberts AP and GM Turner (1993) Diagenetic formation of ferrimagnetic iron sulfide minerals in rapidly deposited marine-sediments, South-Island, New-Zealand. *Earth and Planetary Science Letters*, **115,** 257-273.

Roberts AP and R Weaver (2005) Multiple mechanisms of remagnetization involving sedimentary greigite (Fe_3S_4). *Earth and Planetary Science Letters*, **231,** 263-277.

Roden EE and J Zachara (1996) Microbial reduction of crystalline Fe(III) oxides: Influence of oxide surface area and potential for cell growth. *Environ. Sci. Technol.*, **30,** 1618-1628.

Rooney-Varga J, R Anderson, J Fraga, D Ringelberg and D Lovley (1999) Microbial communities associated with anaerobic benzene degradation in a petroleum-contaminated aquifer. *Appl. Environ. Microbiol.*, **65,** 3056-3064.

Ruttenberg KC (1992) Development of a sequential extraction method for different forms of phosphorus in marine-sediments. *Limnol. Oceanogr*, **37,** 1460-1482.

Sahm K, BJ MacGregor, BB Jørgensen and DA Stahl (1999) Sulphate reduction and vertical distribution of sulphate-reducing bacteria quantified by rRNA slot-blot hybridization in a coastal marine sediment. *Environmental Microbiology*, **1,** 65-74.

Schenau SJ, CP Slomp and GJ De Lange (2000) Phosphogenesis and active phosphorite formation in sediments from the Arabian Sea oxygen minimum zone. *Marine Geiology*, **169,** 1-20.

Schippers A and BB Jørgensen (2001) Oxidation of pyrite and iron sulfide by manganese dioxide in marine sediments. *Geochimica et Cosmochimica Acta*, **65,** 915-922.

Schippers A and LN Neretin (2006) Quantification of microbial communities in near-surface and deeply buried marine sediments on the Peru continental margin using real-time PCR. *Environmental Microbiology*,

Schippers A, LN Neretin, J Kallmeyer, TG Ferdelman, BA Cragg, RJ Parkes and BB Jørgensen (2005) Prokaryotic cells of the deep sub-seafloor biosphere identified as living bacteria. *Nature*, **433,** 861-864.

Schippers A and W Sand (1999) Bacterial leaching of metal sulfides proceeds by two indirect mechanisms via thiosulfate or via polysulfides and sulfur. *Applied and Environmental Microbiology*, **65,** 319-321.

Schoonen AA, Ed. (2004). Mechanism of sedimentary pyrite formation. In: Sulfur Biogeochemistry - Past and Present. Geological Society of America. p117-134.

Schulz HN and BB Jørgensen (2001) Big bacteria. *Annu. Rev. Microbiol.*, **55,** 105-137.

Schulz HN and HD Schulz (2005) Large sulfur bacteria and the formation of phosphorite. *Science*, **307,** 416-418.

Sinclair J and W Ghiorse (1989) Distribution of aerobic bacteria, protozoa, algae, and fungi in deep subsurface sediments. *Geomicrobiol. J.*, **7,** 15-32.

Smith RL and MJ Klug (1981) Reduction of sulfur compounds in the sediments of a eutrophic lake basin. *Appl. Environ. Microbiol.*, **41,** 1230-1237.

Snowball I and R Thompson (1990) A mineral magnetic study of holocene sedimentation in Lough Catherine, Northern-Ireland. *Boreas*, **19,** 127-146.

Sohlenius G, J Sternbeck, E Andren and P Westman (1996) Holocene history of the Baltic Sea as recorded in a sediment core from the Gotland Deep. *Marine Geology*, **134,** 183-201.

Sørensen J (1982) Reduction of ferric iron in anaerobic, marine sediment and interaction with reduction of nitrate and sulfate. *Applied and Environmental Microbiology*, **43,** 319-324.

Sørensen J and BB Jørgensen (1987) Early diagenesis in sediments from Danish coastal waters: Microbial activity and Mn-Fe-S geochemistry. *Geochimica et Cosmochimica Acta*, **51,** 1583-1590.

Sørensen KB (2004) Archaeal phylotypes in a metal-rich and low-activity deep subsurface sediment of the Peru Basin, ODP Leg 201, Site 1231. *Geobiology*, **2,** 151-161.

Stein L, M La Duc, T Grundl and K Nealson (2001) Bacterial and archaeal populations associated with freshwater ferromanganous micronodules and sediments. *Environ. Microbiol.*, **3,** 10-18.

Strechie C, F Andre, A Jelinowska, P Tucholka, F Guichard, G Lericolais and N Panin (2002) Magnetic minerals as indicators of major environmental change in holocene Black Sea sediments: preliminary results. *Physics and Chemistry of the Earth*, **27,** 1363-1370.

Sweeney RE and IR Kaplan (1973) Pyrite framboid formation: Laboratory synthesis and marine sediments. *Economic Geol.*, **68,** 618-634.

Teske A (2005) The deep subsurface biosphere is alive and well. *TRENDS in Microbiology*, **13,** 402-404.

Thamdrup B (2000). Microbial manganese and iron reduction in aquatic sediments. *Advances in Microbial Ecology*., **16,** 41-84.

Thamdrup B and DE Canfield (1996) Pathways of carbon oxidation in continental margin sediments off central Chile. *Limnology and Oceanography*, **41,** 1629-1650.

Thamdrup B, K Finster, JW Hansen and F Bak (1993) Bacterial disproportionation of elemental sulfur coupled to chemical reduction of iron or manganese. *Applied and Environmental Mecorbiology*, **59,** 101-108.

Thiessen O, M Schmidt, F Theilen, M Schmitt and G Klein (2006) Methane formation and distribution of acoustic turbidity in organic-rich surface sediments in the Arkona Basin, Baltic Sea. *Continental Shelf Research*, **26,** 2469-2483.

Thode-Andersen S and BB Jørgensen (1989) Sulfate reduction and the formation of 35S-labeled FeS, FeS_2, and S^0 in coastal marine sediments. *Limnology and Oceanography*, **34,** 793-806.

Thomsen TR, K Finster and NB Ramsing (2001) Biogeochemical and molecular signatures of anaerobic methane oxidation in a marine sediment. *Applied and Environmental Microbiology*, **67,** 1646-1656.

Troelsen H and BB Jørgensen (1982) Seasonal dynemics of elemental sulfur in two coastal sediments. *Estuarine, Coastal and Shelf Science*, **15,** 255-266.

Vairavamurthy A, WL Orr and B Manowitz (1995). Geochemical transformation of sedimentary sulfur: an introduction. In: Geochemical transformation of sedimentary sulfur. Vairavamurthy A and AA. Schoonen. Washington DC, ACS Symposium, 612p.

Wedepohl KH (1995) The composition of the continental crust. *Geochim Cosmochim Acta*, **59,** 1217-1232.

Westrich JT and RA Berner (1988) The effect of temperature on rates of sulfate reduction in marine sediments. *Geomicrobiology*, **6,** 99-117.

Whitman WB, DC Coleman and PH Wiebe (1998) Prokaryotes: the unseen majority. *Proc. Natl. Acac. Sci*, **95,** 6578-6583.

Widdel F and T Hansen (1992). The dissimilatory sulfate-and sulfur-reducing bacteria. In: The Prokaryotes. Balows A, H Trüper, M Dworkin, W Harder and KH. Schleifer. New York, Springer-Verlag, p583-624.

Williams LA and C Reimers (1983) Role of bacterial mats in oxygen-deficient marine basins and coastal upwelling regimes: preliminary report. *Geology*, 267-269.

Wilms R, B Köpke, H Sass, TS Chang, H Cypionka and B Engelen (2006) Deep biosphere-related bacteria within the subsurface of tidal flat sediments. *Environmental Microbiology*,

Zehnder AJB and TD Brock (1979) Methane formation and methane oxidation by methanogenic bacteria. *J. Bacteriol.*, **137,** 420-432.

Zopfi J, Ferdelman TG and Fossing H (2004). Distribution and fate of sulfur intermediates - sulfite, tetrathionate, thiosulfate and elemental sulfur - in marine sediments. In: Sulfur Biogeochemistry - Past and present. Amend, J., K Edwards and T Lyons, Geological Society of America, Boulder, Colorado. p97-116.